National Library of Canada
Bibliothèque nationale du Canada

Canadian Theses Service
Service des thèses canadiennes

Ottawa, Canada
K1A 0N4

NOTICE

The quality of this microform is heavily dependent upon the quality of the original thesis submitted for microfilming. Every effort has been made to ensure the highest quality of reproduction possible.

If pages are missing, contact the university which granted the degree.

Some pages may have indistinct print especially if the original pages were typed with a poor typewriter ribbon or if the university sent us an inferior photocopy.

Reproduction in full or in part of this microform is governed by the Canadian Copyright Act, R.S.C. 1970, c. C-30, and subsequent amendments.

AVIS

La qualité de cette microforme dépend grandement de la qualité de la thèse soumise au microfilmage. Nous avons tout fait pour assurer une qualité supérieure de reproduction.

S'il manque des pages, veuillez communiquer avec l'université qui a conféré le grade.

La qualité d'impression de certaines pages peut laisser à désirer, surtout si les pages originales ont été dactylographiées à l'aide d'un ruban usé ou si l'université nous a fait parvenir une photocopie de qualité inférieure.

La reproduction, même partielle, de cette microforme est soumise à la Loi canadienne sur le droit d'auteur, SRC 1970, c. C-30, et ses amendements subséquents.

NL-339 (r. 88/04) c

Canada

UNIVERSITY OF ALBERTA

THE COMBINED USE OF PRESSURE-DEPTH AND PRESSURE-ELEVATION PLOTS TO ANALYZE GROUNDWATER FLOW FIELDS

BY

MORRIS D. MACCAGNO

A THESIS
SUBMITTED TO THE FACULTY OF GRADUATE STUDIES AND RESEARCH IN PARTIAL FULFILLMENT OF THE REQUIREMENTS FOR THE DEGREE OF MASTER OF SCIENCE

DEPARTMENT OF GEOLOGY

EDMONTON, ALBERTA
FALL, 1991

National Library of Canada
Bibliothèque nationale du Canada

Canadian Theses Service
Service des thèses canadiennes

Ottawa, Canada
K1A 0N4

The author has granted an irrevocable non-exclusive licence allowing the National Library of Canada to reproduce, loan, distribute or sell copies of his/her thesis by any means and in any form or format, making this thesis available to interested persons.

The author retains ownership of the copyright in his/her thesis. Neither the thesis nor substantial extracts from it may be printed or otherwise reproduced without his/her permission.

L'auteur a accordé une licence irrévocable et non exclusive permettant à la Bibliothèque nationale du Canada de reproduire, prêter, distribuer ou vendre des copies de sa thèse de quelque manière et sous quelque forme que ce soit pour mettre des exemplaires de cette thèse à la disposition des personnes intéressées.

L'auteur conserve la propriété du droit d'auteur qui protège sa thèse. Ni la thèse ni des extraits substantiels de celle-ci ne doivent être imprimés ou autrement reproduits sans son autorisation.

ISBN 0-315-69933-7

Canada

UNIVERSITY OF ALBERTA

RELEASE FORM

NAME OF AUTHOR:	MORRIS D. MACCAGNO
TITLE OF THESIS:	THE COMBINED USE OF PRESSURE-DEPTH AND PRESSURE-ELEVATION PLOTS TO ANALYZE GROUNDWATER FLOW FIELDS
DEGREE:	MASTER OF SCIENCE
YEAR THIS DEGREE GRANTED:	1991

PERMISSION IS HEREBY GRANTED TO THE UNIVERSITY OF ALBERTA LIBRARY TO REPRODUCE SINGLE COPIES OF THIS THESIS AND TO LEND OR SELL SUCH COPIES FOR PRIVATE, SCHOLARLY OR SCIENTIFIC RESEARCH PURPOSES ONLY.

THE AUTHOR RESERVES OTHER PUBLICATION RIGHTS, AND NEITHER THE THESIS NOR EXTENSIVE EXTRACTS FROM IT MAY BE PRINTED OR OTHERWISE REPRODUCED WITHOUT THE AUTHOR'S WRITTEN PERMISSION.

M. Maccagno

100, 4500 16TH AVE NW
CALGARY, ALBERTA
CANADA
T3B 0M6

30 SEPTEMBER, 1991

UNIVERSITY OF ALBERTA
FACULTY OF GRADUATE STUDIES AND RESEARCH

THE UNDERSIGNED CERTIFY THAT THEY HAVE READ, AND RECOMMEND TO THE FACULTY OF GRADUATE STUDIES AND RESEARCH FOR ACCEPTANCE, A THESIS ENTITLED "THE COMBINED USE OF PRESSURE-DEPTH AND PRESSURE-ELEVATION PLOTS TO ANALYZE GROUNDWATER FLOW FIELDS" SUBMITTED BY MORRIS DAVID MACCAGNO IN PARTIAL FULFILLMENT OF THE REQUIREMENTS FOR THE DEGREE OF MASTER OF SCIENCE IN GEOLOGY.

Dr. József Tóth, Supervisor

Dr. Bruce Nesbitt

Dr. Hans-G. Machel

Dr. Peter Steffler

Date: Oct. 1, 1991

À mes grandparents

ABSTRACT

Important conditions of regional groundwater flow may be inferred from pore-pressures in geologic formations. Pore-pressures can be represented both as plots of pressure vs. elevation above a horizontal reference plane, $p(z)$, and pressure vs. depth below the land surface, $p(d)$. Commonly, however, either $p(z)$ or $p(d)$ plots only are used. The study shows, however, that a combined use of $p(z)$ and $p(d)$ plots results in greater yet more constrained hydrogeologic information than can be attained from either plot alone. The study is based on an analysis of theoretical steady-state $p(z)$ and $p(d)$ patterns.

The $p(d)$ -$p(z)$ patterns are analyzed using "gradient" and "intercept" curves. The slope of a gradient curve depends on the vertical hydraulic gradient; z-intercept curves indicate the hydraulic head, while d-intercept curves show the potentiometric depth.

Type $p(d)$-$p(z)$ patterns are identified. They indicate to what degree a groundwater system is topographically-influenced within the boundaries of study. A Type I pattern indicates equal hydraulic and topographic gradients, i.e., an ideally unconfined system. A Type II pattern means the hydraulic gradient is subdued relative to the topographic gradient, i.e., a likely unconfined system. A Type III pattern indicates static groundwater beneath a sloping land surface, i.e., a confined or closed system. The Types IV and V patterns each suggest a source of potential other than, or additional to, topography. The $p(d)$-$p(z)$ method is used to investigate lower Cretaceous hydrostratigraphy in an area of east-central Alberta, Canada.

ACKNOWLEDGEMENTS

Thank you first to my supervisor Dr. József Tóth, Tarok grandmaster, who started the journey and helped along the way. Thanks also to my committee: Dr. Peter Steffler for his perceptive comments, Dr. Hans Machel for his interest and kind words of encouragement, and Dr. Bruce Nesbitt for keeping things under control as Chair. Financial assistance for the work was provided by Energy, Mines and Resources Canada and is gratefully acknowledged.

Thanks to my hydro-colleagues. Claus Otto, who consistently beat me to the laser printer, but provided saki when it was most needed. A toast to Emi for her joy and hospitality. Ben Rostron helped with the modeling and countless other tasks, but could never cheer for the right team. Danny Barson for listening and providing tunes. Liané for her good humour and strength. Al Fryar for his inspirational ways. Thanks are also due to past and near-present students Steve and Joanne, Duke, Kriengsak, Dave, John and Debashis.

Thank you to my parents for providing the opportunity and helping me see it through, and Terry for his caring advice. Special thanks to Kathy who gracefully endured my often unbearable single-mindedness.

TABLE OF CONTENTS

1. INTRODUCTION 1

2. BACKGROUND THEORY AND PRACTICE 3

2.1 Fluid Potential, the Driving Force and Groundwater Flow 3

2.2 Mass Conservation and the Governing Equations of Flow 9

2.3 Theoretical Analysis of Topography-Driven Groundwater Flow 10

2.3.1 Theoretical Results 12

2.4 Unconfined, Confined and Closed Systems:
Scales of Topographic Influence 14

2.5 Pressure-Elevation and Pressure-Depth Plots 15

2.5.1 Background 15

2.5.2 Pressure-Elevation Plots 17

2.5.3 Pressure-Depth Plots 21

2.6 Vertical Pressure Gradients and Linear Regression 23

2.7 Vertical Pressure Gradients and Variable Groundwater Density 24

3. FINITE DIFFERENCE MODELING TO OBTAIN THEORETICAL VERTICAL PRESSURE GRADIENTS 41

3.1 Finite Differences 41

3.2 General Description and Choice of MODFLOW 44

3.3 Geometry of Model Basins 44

3.4 Model Discretization 45

3.5 Flow Simulation 46

3.6 Simulation Output 47

4. RESULTS OF MODELING PRESSURE-DEPTH AND PRESSURE-ELEVATION PATTERNS 52
4.1 Terminology 52
4.2 Method of Investigation 57
4.2.1 Estimation of the Vertical Pressure Gradient 58
4.3 Results of Regional Scale Investigation 59
4.3.1 Effects of Geology 60
4.3.2 Effects of Topography 67
4.4 Results of Local Scale Investigation 69
4.5 Type $p(d)$-$p(z)$ Patterns 72
4.5.1 Analysis 72
4.5.2 Implications 76
4.6 Summary and Synthesis 79

5. FIELD STUDY: ANALYSIS OF GROUNDWATER FLOW IN LOWER CRETACEOUS STRATA, EAST-CENTRAL ALBERTA, CANADA 104
5.1 Introduction 104
5.2 Setting and Scales of Topographic Features 105
5.3 Hydrogeologic Framework 105
5.4 Evaluation of Pressure Data 107
5.5 Method of Investigation 108
5.6 Results 109
5.7 Discussion and Overview of Flow Patterns 118
5.8 Summary and Conclusions 121

6. SUMMARY AND CONCLUSIONS 140

7. REFERENCES 144

APPENDIX A 150

APPENDIX B 177

LIST OF TABLES

Table 2.1 - Representative values of hydraulic conductivity for unconsolidated and consolidated sedimentary rocks (after Domenico and Schwartz, 1990).....40

Table 4.1 - Vertical pressure gradient ($\partial p/\partial d$) and vertical hydraulic gradient ($\partial h/\partial d$) in the homogeneous basin with simple topography.....98

Table 4.2 - Hydraulic head $\bar{h}_{ij}$ and potentiometric depth $\bar{d}_{hij}$ in the homogeneous basin with simple topography.....98

Table 4.3 - Vertical pressure gradient ($\partial p/\partial d$) at sites s_i in basins with an upper aquitard and simple topography.....99

Table 4.4 - Hydraulic head $\bar{h}_{ij}$ and potentiometric depth $\bar{d}_{hij}$ in basins with an upper aquitard and simple topography.....100

Table 4.5 - Potentiometric slope ($\partial h/\partial x$) in basins with an upper aquitard and simple topography.....100

Table 4.6 - Vertical pressure gradient ($\partial p/\partial d$) and vertical hydraulic gradient ($\partial h/\partial d$) in topographically-simple basin with upper and lower aquifers.....101

Table 4.7 - Vertical pressure gradient ($\partial p/\partial d$) and vertical hydraulic gradient ($\partial h/\partial d$) in the homogeneous basin with complex topography.....102

Table 4.8 - Vertical pressure gradient ($\partial p/\partial d$) in the upper and lower aquifers at Areas A and B of the topographically complex basin.....103

Table 4.9 - Hydraulic head ($\bar{h}_i$) and potentiometric depth ($\bar{d}_{hi}$) in the upper aquifer of the topographically complex basin.....103

Table 4.10 - Hydraulic head ($\bar{h}_i$) and potentiometric depth ($\bar{d}_{hi}$) in the lower aquifer of the topographically complex basin.....104

Table 5.1 - General Cretaceous-Devonian stratigraphy and hydrostratigraphy of east-central Alberta [after Hitchon et al., 1989(b), Table 1].....138

Table 5.2 - Representative values of hydraulic conductivity for strata in east and north central Alberta [compiled from Hitchon et al., 1989(a), 1989(b)].....139

LIST OF FIGURES

Fig. 2.1 Relations between the driving force **F**, the gravity force $\mathbf{F_g}$, and the pressure force $\mathbf{F_p}$: (a) $\mathbf{F_p}$ and $\mathbf{F_g}$ are balanced along the vertical, the condition is static and the vertical pressure gradient is hydrostatic; (b) - $\mathbf{F_{pz}} = \mathbf{F_g}$, so that **F** is horizontal and the vertical pressure gradient is hydrostatic; (c) - $\mathbf{F_{pz}} < \mathbf{F_g}$, so that **F** has a downward component and the vertical pressure gradient is subhydrostatic (after Hubbert, 1940, Fig.15).....26

Fig. 2.2 Relations between the hydraulic gradient **grad** *h* and flow **q** in: (a) isotropic, and; (b) anisotropic media (after Hubbert, 1940, Fig. 18).....27

Fig. 2.3 The boundary value problem of topography-driven groundwater flow in a homogeneous, isotropic medium (after Tóth, 1962, Fig. 2.).....28

Fig. 2.4 Patterns of hydraulic head and groundwater flow in homogeneous basins with simple topography (after Tóth, 1962, Fig. 3.).....29

Fig. 2.5 Patterns of hydraulic head and groundwater flow in a homogeneous basin with local topography superimposed on the regional slope of the land (after Tóth, 1963, Figure 2g).....30

Fig. 2.6 Topography-induced patterns of hydraulic head and groundwater flow in heterogeneous basins (after Freeze and Witherspoon, 1967, Figs. 2 and 3).....31

Fig. 2.7 Pressure-elevation pattern for a hydraulically discontinuous, static condition.....32

Fig. 2.8 Pressure-elevation pattern for steady-state horizontal flow in a hydraulically continuous medium.....33

Fig. 2.9 Pressure-elevation pattern for steady-state vertical flow in a hydraulically continuous medium.....34

Fig. 2.10 (a) Static conditions beneath a sloping land surface, (b) the associated pressure-depth relations (adapted from Tóth, 1978, Fig. 9).....35

Fig. 2.11 Patterns of: (a) hydraulic head and flow, and (b) pressure-depth in a homogeneous basin with simple topography (after Tóth, 1979, Fig. 1).....36

Fig. 2.12 Patterns of: (a) hydraulic head and flow, and (b) pressure-depth in a heterogeneous basin with simple topography and a thin, extensive aquitard (after Tóth, 1979, Fig. 2).....37

Fig. 2.13 (a) Horizontal potentiometric surface intercepts sloping land surface, (b) the associated pressure-depth pattern.....38

Fig. 2.14 Regression curve fit through pressure-depth data combined from both wells in Fig. 2.13(a), and curves fit through data from each well. Curve through areally-distributed data underestimates the vertical pressure gradient. Curve through data from single, vertical well graphically represents the vertical pressure gradient.....39

Fig. 3.1 General notation of nodes of a finite difference mesh (after Remson et al., 1971, Fig. 3.2).....49

Fig. 3.2 The finite difference mesh for simple topography.....50

Fig. 3.3 Convention of (a) MODFLOW, and (b) this study for spatial discretization.....51

Fig. 4.1 Types of curves used in the analysis.....81

Fig. 4.2 Basin with homogeneous geology and simple topography. Patterns of (a) hydraulic head and flow, (b) pressure-elevation and, (c) pressure-depth.....82

Fig. 4.3 Basin with simple topography and thick, top aquitard and bottom aquifer. Patterns of (a) hydraulic head and flow, (b) pressure-elevation and, (c) pressure-depth.....83

Fig. 4.4 Basin with simple topography and thin, top aquitard and bottom aquifer. Patterns of (a) hydraulic head and flow, (b) pressure-elevation and, (c) pressure-depth.....84

Fig. 4.5 Basin with simple topography and top aquitard, middle intermediate permeability aquifer, and bottom aquifer. Patterns of (a) hydraulic head and flow, (b) pressure-elevation and, (c) pressure-depth.....85

Fig. 4.6 Basin with simple topography and top and bottom aquifers. Patterns of (a) hydraulic head and flow, (b) pressure-elevation and, (c) pressure-depth.....86

Fig. 4.7 Basin with complex topography and homogeneous geology. Patterns of (a) hydraulic head and flow, (b) pressure-elevation and, (c) pressure-depth.....87

Fig. 4.8 Basin with complex topography and thick, top aquitard. Patterns of (a) hydraulic head and flow, (b) pressure-elevation and, (c) pressure-depth.....88

Fig. 4.9 Patterns of hydraulic head and flow in a topographically complex basin with upper and lower aquifers. Pressures from Areas A and B are used for local-scale analysis.....89

Fig. 4.10 Patterns of (a) pressure-elevation and (b) pressure-depth from the upper aquifer at Area A.....90

Fig. 4.11 Patterns of (a) pressure-elevation and (b) pressure-depth from the upper aquifer at Area B.....91

Fig. 4.12 Patterns of (a) pressure-elevation and (b) pressure-depth from the lower aquifer at Area B.....92

Fig. 4.13 Patterns of (a) pressure-elevation and (b) pressure-depth from the lower aquifer at Area C.....93

Fig. 4.14 Relations between the horizontal hydraulic gradient and the topographic gradient possible for an aquifer at depth beneath a sloping land surface. Case I: the hydraulic and topographic gradients are equal; Case II: the hydraulic gradient is less than the topographic gradient; Case III: the hydraulic gradient is zero; Case IV: the hydraulic gradient is opposed to the topographic gradient; Case V: the hydraulic gradient exceeds the topographic gradient.....94

Fig. 4.15 The *p(d)-p(z)* pattern for Case I, the hydraulic and topographic gradients are equal.....95

Fig. 4.16 The *p(d)-p(z)* pattern for Case II, the hydraulic gradient is less than the topographic gradient.....95

Fig. 4.17 The *p(d)-p(z)* pattern for Case III, the hydraulic gradient is zero.....96

Fig. 4.18 The *p(d)-p(z)* pattern for Case IV, the hydraulic gradient opposes the topographic gradient.....96

Fig. 4.19 The *p(d)-p(z)* pattern for Case V, the hydraulic gradient exceeds the topographic gradient.....97

Fig. 5.1 Location of study region.....124

Fig. 5.2 Topography of study region and locations of Areas A to F from which pressures are taken.....125

Fig. 5.3 Regional hydrostratigraphic section, northeast from Area A to Area C.....126

Fig. 5.4 Regional hydrostratigraphic section, northeast from Area F to Area D.....127

Fig. 5.5 Potentiometric surface maps of (a) the Mannville Aquifer, and (b) the Viking Aquifer [from Hitchon et al., 1989(b), Figure 42(c) and Figure 43(b)].....128

Fig. 5.6 Area A *p(d)-p(z)* pattern.....129

Fig. 5.7 Area B *p(d)-p(z)* pattern.....130

Fig. 5.8 Areas A and B *p(d)-p(z)* pattern.....131

Fig. 5.9 Areas C and B *p(d)-p(z)* pattern.....132

Fig. 5.10 Areas A and D *p(d)-p(z)* pattern.....133

Fig. 5.11 Areas D and E *p(d)-p(z)* pattern.....134

Fig. 5.12 Areas F and E $p(d)$-$p(z)$ pattern.....135

Fig. 5.13 Regional hydraulic section, northeast from Area A to Area C.....136

Fig. 5.14 Regional hydraulic section, northeast from Area F to Area D.....137

1. INTRODUCTION

Pore-pressures are often used to analyze regional groundwater flow. Vertical profiles of pressure can be presented either as graphs of pressure vs. elevation above a horizontal plane of reference, i.e., as *p(z)*; or as pressure vs. depth below the land surface, i.e., as *p(d)*. Important groundwater conditions, for instance its static or dynamic state, are commonly inferred from *p(z)* and *p(d)* plots.

Traditionally, vertical pressure profiles have been expressed as *p(z)* plots. Interpretation of *p(z)* patterns is routinely guided by the assumption of little or no hydraulic continuity between strata within a basin. Patterns of *p(d)*, on the other hand, are often analyzed according to a model of regional hydraulic continuity. Indeed, *p(z)* and *p(d)* plots are not currently used in combination largely because the interpretive frameworks underlying each are fundamentally different.

It appears, however, that the dichotomy between *p(z)* and *p(d)* plot use should not continue. Independently of the hydrogeologic model, each plot has particular properties useful for analysis of groundwater flow fields. At the same time, vertical pressure profiles are non-unique. Different hydraulic conditions can result, for example, in the same *p(z)* pattern. Plots of *p(d)* too are non-unique but in a different way. A combined use of *p(z)* and *p(d)* plots, therefore, is expected to yield greater yet more constrained information than can be attained with either plot alone.

The present study has three main objectives. First, to examine the theoretical properties of, and relations between *p(d)* and *p(z)* plots under varying hydrogeologic conditions. Second, to develop a practical *p(d)-p(z)* method of analyzing groundwater flow. Third, to evaluate the validity and usefulness of the *p(d)-p(z)* technique by applying it to a field situation in which the hydrogeology is already well known.

The necessary theoretical background is presented in Chapter 2. The chapter begins with a review of some fundamental principles of groundwater flow. A rigorous

treatment is attempted since current *p(z)* plot interpretation suffers particularly from misunderstanding of basic concepts. Also described is the treatment of topography-driven flow as a steady-state boundary value problem, which constitutes the theoretical basis for the present study. The latter part of Chapter 2 discusses the properties of *p(z)* and *p(d)* plots and demonstrates how each plot is non-unique. Chapter 3 briefly describes the use of finite differences to solve the relevant boundary value problem.

Presented in Chapter 4 are theoretical *p(z)* and *p(d)* plots derived from numerical modeling. Pressure plots are analyzed from several basinal flow models that differ stratigraphically and topographically. Regrettably lacking at present, however, is a consistent terminology for description of vertical pressure data. Chapter 4, therefore, introduces terms and parameters by which the *p(z)* and *p(d)* patterns can be meaningfully described. The analysis reveals characteristic relations between the nature of a groundwater flow field and the combined *p(d)* -*p(z)* pattern. Type *p(d)*-*p(z)* patterns are identified, and it is concluded that a unique pattern occurs when the flow is topographically-influenced. The results lead to a combined *p(d)*-*p(z)* technique that can be applied generally to the investigation of regional groundwater flow.

In Chapter 5, the *p(d)*-*p(z)* method is applied to a field situation in east-central Alberta. Analyzed is the hydrostratigraphy of the lower Cretaceous-Devonian sequence. The results generally agree with those obtained previously by conventional methods, but it also appears that the combined *p(d)*-*p(z)* technique can provide further insight on the nature of regional hydrogeologic conditions.

2. BACKGROUND: THEORY AND PRACTICE

In this chapter, those aspects of groundwater flow theory relevant to the present work are reviewed, and the properties of *p(z)* and *p(d)* plots are discussed. This review forms the basis for the quantitative analysis of *p(d)* and *p(z)* patterns.

2.1 Fluid Potential, the Driving Force and Groundwater Flow

Associated with every conservative field of groundwater flow is a scalar function called the fluid potential. The fluid potential (Hubbert, 1940) is the mechanical energy of a unit mass of fluid and may be expressed

$$\Phi = gz + \int_{P_0}^{P} \frac{dP}{\rho} + \frac{v^2}{2}, \tag{2.1}$$

where $\Phi = \Phi(x, y, z)$, g is the acceleration due to gravity, z is elevation above a datum, $P = P(x, y, z)$ is the absolute fluid pressure, P_0 is the atmospheric pressure, $\rho = \rho(x, y, z)$ is fluid density, and v is the flow velocity. For groundwater motion, the velocities are usually small and the third term may be neglected. Furthermore, for incompressible and homogeneous fluids, i.e., ρ = const., such as commonly is true for groundwater, equation (2.1) reduces to

$$\Phi = gz + \frac{p}{\rho}, \tag{2.2}$$

where p is the gauge pressure. Dividing equation (2.2) by g, the hydraulic head is obtained

$$h = z + \frac{p}{\gamma}, \tag{2.3}$$

where $\gamma = \rho g$ is the specific weight of the groundwater. In substance, the hydraulic head at a point is the height above datum to which the water will rise in a vertical borehole open to

the subsurface at the point. Since the hydraulic head is directly observable, it is a convenient field measure of the fluid potential.

The first term on the right hand side of equation (2.3) is the elevation head, which represents the energy of the water due to its position in the earth's gravitational field, the second term is the pressure head, the energy due to the ambient pore-pressure. That the fluid potential has both a positional and a pressure component is fundamental to the understanding of groundwater flow (Freeze and Cherry, 1979).

Groundwater moves in response to spatial differences in the fluid potential. In a potential field, surfaces of equal potential may be defined, i.e., $\Phi(x, y, z) = \text{const}$. Normal to an equipotential surface is the force which drives groundwater flow

$$\mathbf{F} = -\,\mathbf{grad}\,\Phi\,. \tag{2.4}$$

The driving force **F** therefore acts in the direction in which the potential, or hydraulic head, decreases most rapidly and its magnitude is the rate of potential decrease in that direction.

The driving force **F** is the sum of the gravitational force $\mathbf{F}_g$ and a pressure force $\mathbf{F}_p$ per unit of mass (Hubbert, 1940),

$$\mathbf{F} = \mathbf{F}_g + \mathbf{F}_p. \tag{2.5}$$

An equivalent form of equation (2.5), expressed in terms of the gradients of the pressure and gravitational potentials, is obtained by substituting (2.2) into (2.4),

$$-\,\mathbf{grad}\,\Phi = -\,\mathbf{grad}\,(gz) - \frac{1}{\rho}\,\mathbf{grad}\,p. \tag{2.6}$$

For most problems the gravity force $\mathbf{F}_g$ can be considered constant in magnitude as well as direction, i.e., vertically downward. The pressure force $\mathbf{F}_p$, however, can have any possible combination of magnitude and direction (Hubbert, 1940). Generally, $\mathbf{F}_p$ is directed upward at some angle from the vertical.

To understand the relations between the groundwater driving force and the vertical pressure gradient, it is important to examine (2.5) and (2.6) in some detail. The discussion is simplified when restricted to two dimensions, as in a vertical plane of x and z coordinates. Consider a small volume element of water submerged in a body of water (Figure 2.1).

In Figure 2.1(a), the pressure force $\mathbf{F}_p$ and gravitational force $\mathbf{F}_g$ are equal in magnitude but opposite in direction. The two forces cancel each other so that the resultant driving force $\mathbf{F}$ is zero. The relation between the pressure and gravitational forces may be written

$$- \mathbf{F}_p = \mathbf{F}_g, \tag{2.7}$$

and (2.5) becomes

$$\mathbf{F} = \mathbf{0}\ , \tag{2.8}$$

which is the zero vector. The expression (2.8) signifies that the driving force $\mathbf{F}$ lacks a component in both the x and z directions. Together, these are the necessary and sufficient conditions for static equilibrium (Beer and Johnston, 1977).

In terms of the gradients of p and gz, the equivalent expression of (2.7) is

$$- \frac{1}{\rho} \mathbf{grad}\ p = \mathbf{grad}(gz), \tag{2.9}$$

or,

$$- \frac{1}{\rho} [\mathbf{i} \frac{\partial p}{\partial x} + \mathbf{k} \frac{\partial p}{\partial z}] = [\mathbf{i} \frac{\partial (gz)}{\partial x} + \mathbf{k} \frac{\partial (gz)}{\partial z}], \tag{2.10}$$

where $\mathbf{i}$ and $\mathbf{k}$ are the unit vectors, directed respectively along the x and z axes. Since in the static case pressure is a function only of elevation, i.e., $p = p(z)$, the horizontal derivatives are zero and (2.10) is simplified,

$$\frac{dp}{dz} = - \gamma. \tag{2.11}$$

In other words, when the pressure and gravitational forces are balanced along the vertical, the vertical rate of pressure change is given by the water's specific weight γ. The vertical pressure gradient is then described as "hydrostatic".

A hydrostatic vertical pressure gradient does not, however, result only from a static condition. Consider Fig. 2.1(b), where the pressure force $\mathbf{F}_p$ is directed arbitrarily away

from the vertical. The vertical component of the pressure force $\mathbf{F}_p$ is $\mathbf{F}_{pz} = \mathbf{k}\, F_{pz}$. For this case, the magnitude of this vector component of the pressure force $\mathbf{F}_{pz}$ is equal to the magnitude of the gravitational force $\mathbf{F}_g$. Here too, as in Fig. 2.1(a), the vertical component forces are vertically balanced, i.e., the vertical resultant force acting on the fluid element is zero. The relation may be written

$$- \mathbf{F}_{pz} = \mathbf{F}_g . \tag{2.12}$$

Yet in this case the condition is dynamic since the total driving force $\mathbf{F}$ is non-zero. Lacking a vertical component, the driving force $\mathbf{F}$ is horizontal.

Written in terms of the vertical pressure gradient, equation (2.12) is

$$- [- \frac{1}{\rho} \mathbf{k} \frac{\partial p}{\partial z}] = - [\mathbf{k} \frac{\partial (gz)}{\partial z}] , \tag{2.13}$$

or,

$$\frac{\partial p}{\partial z} = - \gamma . \tag{2.14}$$

Like the static case previously, the vertical rate of pressure change is equal to the water's specific weight γ also when the driving force is horizontal. A hydrostatic vertical pressure gradient, therefore, is necessary but not sufficient for the static condition. In other words, the most that can be said when a vertical pressure gradient is hydrostatic is that the driving force $\mathbf{F}$ lacks a vertical component.

To determine with pressures whether a horizontal component of $\mathbf{F}$ also is absent, i.e., if there is no flow at all, the analysis must be extended to two dimensions. This point is illustrated later, in conjunction with the use of pressure-elevation plots.

For now, consider Fig. 2.1(c), where again the pressure force $\mathbf{F}_p$ is directed from the vertical. Yet unlike previously, the magnitude of the vertical pressure component $\mathbf{F}_{pz}$ is less than the magnitude of the gravitational force $\mathbf{F}_g$,

$$- \mathbf{F}_{pz} < \mathbf{F}_g , \tag{2.15}$$

so that the resultant force $\mathbf{F}$ has a vertical as well as a horizontal component. For the vertical pressure gradient, (2.15) is expressed

$$\frac{\partial p}{\partial z} < -\gamma. \tag{2.16}$$

Thus a vertical pressure gradient that is less than hydrostatic, i.e., "subhydrostatic", results in an impelling force **F** with a downward component.

It can similarly be shown that when the magnitude of $\mathbf{F}_{pz}$ exceeds that of $\mathbf{F}_g$, the driving force **F** will have an upward component. In such a case, the vertical pressure gradient is "superhydrostatic", i.e.,

$$\frac{\partial p}{\partial z} > -\gamma. \tag{2.17}$$

Partial derivatives are required in all but the static case since pressure is generally a function of horizontal as well as vertical position, i.e., in two dimensions $p = p(x, z)$.

Relating the driving force to porous medium flow requires consideration of the rock and fluid properties which influence the motion. For macroscopic groundwater flow these parameters are embodied in the hydraulic conductivity,

$$K = k\frac{\rho g}{\mu}, \tag{2.18}$$

where k is the intrinsic permeability of the rock and μ is the dynamic viscosity of the fluid. The intrinsic permeability k is inversely proportional to the resistance of the medium to shear stresses, i.e., to flow. Typical values of hydraulic conductivity K for both consolidated and unconsolidated sedimentary rocks are provided in Table 2.1.

The value of hydraulic conductivity K in a stratum may be dependent on both the position and direction of measurement. Assuming a homogeneous fluid, if K varies with position the stratum is heterogeneous, otherwise it is homogeneous; if K varies with direction the formation is anisotropic, otherwise it is isotropic (Freeze and Cherry, 1979). Whereas the flow in isotropic media is always normal to the equipotential surfaces, i.e., in the direction of **F**, the same is not generally true of anisotropic formations.

The hydraulic conductivity relates the fields of flow and force through Darcy's law. In its most general form Darcy's law may be written

$$\mathbf{q} = \bar{\mathbf{K}} \cdot \mathbf{F} = - \bar{\mathbf{K}} \cdot \mathbf{grad}\ h, \tag{2.21}$$

where **q** is the vector of macroscopic flux of water, $\bar{\mathbf{K}}$ is the second rank symmetric tensor of hydraulic conductivity, and **F** = - **grad** h is the hydraulic gradient (Bear, 1988). The hydraulic conductivity is a tensor $\bar{\mathbf{K}}$ when the principal axes of anisotropy, the three mutually normal directions containing the maximum and minimum values of hydraulic conductivity, do not coincide with the Cartesian axes. For instance, a force **F** in the x direction may generate components of flow in the directions y and z (de Marsily, 1986). If the principal axes of anisotropy coincide with the x, y and z directions, equation (2.21) may be written (Freeze and Cherry, 1979),

$$q_x = - K_x \frac{\partial h}{\partial x}, \tag{2.22}$$

$$q_y = - K_y \frac{\partial h}{\partial y},$$

$$q_z = - K_z \frac{\partial h}{\partial z},$$

where K_x, K_y and K_z are the hydraulic conductivities in the directions x, y and z. When a formation is isotropic, the hydraulic conductivity is a scalar, i.e., $K = K(x, y, z)$, and Darcy's law reduces to

$$\mathbf{q} = K\,\mathbf{F} = - K\ \mathbf{grad}\ h\,. \tag{2.23}$$

Equation (2.23) indicates that when a rock is isotropic, the directions of force and flow coincide.

In an isotropic formation, therefore, the vertical sense of groundwater motion can be inferred directly with a vertical pressure gradient. For instance, the vertical pressure gradient $\partial p/\partial z$ may be calculated from formation water pressures measured along a vertical, as in a bore hole. The determined rate of pressure change can then be compared with the water's specific weight γ, as calculated from measured values of water density ρ. If the vertical pressure gradient is superhydrostatic the flow has an upward component; if it is subhydrostatic the flow has a downward component; if the vertical pressure gradient is

hydrostatic a vertical component is absent. For anisotropic strata, the relation of vertical flow to the vertical pressure gradient is more complex and not considered in this work.

2.2 Mass Conservation and the Governing Equations of Flow

The concepts of this section form the basis for the mathematical modeling of steady-state groundwater motion. The law of conservation of matter for groundwater flow requires that the difference between the rates of mass flow into and out of any unit control volume of rock be equal to the time rate of change of fluid mass stored within the volume. The equation of continuity expresses the conservation law (Freeze and Cherry, 1979),

$$\frac{\partial(\rho q_x)}{\partial x} + \frac{\partial(\rho q_y)}{\partial y} + \frac{\partial(\rho q_z)}{\partial z} = -\frac{\partial(\rho n)}{\partial t} \quad , \tag{2.24}$$

where n is the porosity and t is time. For steady-state flow, there is no storage and the right hand side of equation (2.24) is zero. For homogeneous and incompressible groundwater, also the density ρ is eliminated so that (2.24) becomes

$$\frac{\partial q_x}{\partial x} + \frac{\partial q_y}{\partial y} + \frac{\partial q_z}{\partial z} = 0 \quad \text{or} \quad \text{div } \mathbf{q} = 0 \, . \tag{2.25}$$

where div is the divergence operator. Physically, div $\mathbf{q} = 0$ means that the mass flux of water entering the control volume is the same as that leaving it.

When the flow is through isotropic but heterogeneous media, the form of Darcy's law (2.23) is substituted into (2.25) to give Richard's equation (Freeze, 1969),

$$\text{div } (K \, \mathbf{grad} \, h) = 0 \, . \tag{2.26}$$

For homogeneous media, continuity is expressed by Laplace's equation,

$$\text{div } (\mathbf{grad} \, h) = 0 \quad \text{or} \quad \nabla^2 h = 0 \, . \tag{2.27}$$

Richard's and Laplace's equations are the governing equations of steady-state groundwater motion through heterogeneous and homogeneous isotropic media, respectively. Knowing the geometry of, and the distribution of hydraulic conductivity in a flow domain, as well as the conditions of hydraulic head at the domain's boundaries, a mathematical model of the flow can be formulated. Such a model is called a boundary value problem. The solution of a steady-state boundary value problem yields the spatial distribution of hydraulic head, which allows lines of equal head, i.e., equipotentials, to be contoured. Normal to the equipotentials are flow lines, and the pattern of groundwater flow is determined.

2.3 Theoretical Analysis of Topography-Driven Groundwater Flow

Steady-state topography-driven groundwater motion can be investigated theoretically. Tóth (1962, 1963) first formulated the representative boundary value problem. Solving the problem analytically, he analyzed the effects of varying basin depth and water table configuration in basins of homogeneous hydraulic conductivity. The investigation was extended by Freeze and Witherspoon (1966, 1967), who numerically modeled the flow in heterogeneous and anisotropic basins.

Consider the flow domain presented in Figure 2.3. The land surface has a water divide and a slightly sloping valley bottom, each trending parallel to the y axis. The steeper descent of the land is normal to valley axis. Components of flow generated parallel to the valley are assumed negligible compared to those generated normal to it. This assumption allows the problem to be reduced to two dimensions. The topography has mirror symmetry about the hill crest and valley floor (Fig. 2.3).

Due to an assumed sufficiency of areal precipitation, the mean position of the water table closely coincides with the land surface. The problem can thus be treated as a steady-state one.

The flow domain is bounded above by the water table, along the sides by hydraulic no-flow boundaries, and along its base by an effectively impermeable stratum. To obtain the hydraulic head distribution within the domain, the conditions at the four boundaries must be defined.

Consider first the water table. By definition, the water table is a surface in the saturated zone upon which the pressure is atmospheric, i.e., $p = 0$. Therefore, from

equation (2.2), the hydraulic head at any point on the water table, h_w, is equal to the point's elevation above datum. By designating the water table's position a function of the horizontal distance x from the valley axis, the water table's hydraulic heads can be expressed generally as $h_w = f(x)$, which is the upper boundary condition.

For the two vertical boundaries, the heads at points of the same elevation on either side of a boundary will be equal, because of topographic symmetry. Thus, vertical hydraulic divides occur beneath the hill and the valley, across which flow does not occur. As for the final boundary condition, a slightly permeable formation is assumed along the base. For the sake of mathematical simplicity this lower stratum is called impermeable, although it is shown by Freeze and Witherspoon (1967) that the solution does not much differ whether the layer is slightly permeable or absolutely impermeable. Since groundwater does not flow across the basal and vertical boundaries, the normal derivatives of head are zero, i.e., $\partial h/\partial n = 0$, which expresses generally the three remaining boundary conditions.

The boundary value problem for the heterogeneous, isotropic case can thus be stated:

$$\text{div } (K \, \mathbf{grad} \, h) = 0$$

$$h_w = f(x) \qquad x_0 \le x \le x_s, \quad z = z_w \tag{2.28}$$

$$\frac{\partial h}{\partial x} = 0 \qquad x = 0, \quad z_0 \le z \le z_w$$

$$\frac{\partial h}{\partial x} = 0 \qquad x = x_l, \quad z_0 \le z \le z_w$$

$$\frac{\partial h}{\partial z} = 0 \qquad x_0 \le x \le x_s, \quad z = 0$$

Tóth (1962, 1963) used the separation of variables to obtain a solution for a rectangular approximation of the domain, Freeze and Witherspoon (1966) applied a finite difference technique.

In addition to the balance of water mass implicit in the governing equation, the boundary value problem includes a requirement of the energy balance (Tóth, 1962). Groundwater motion will not occur if the water table is horizontal because, by definition in a conservative field, there can be no hydraulic gradient. The energy available to drive the flow is provided solely by the water table relief. In a gravitational system, therefore, a value of head can be no larger than the highest elevation and no less than the least elevation of the water table, i.e., the heads are between the limiting values implicit in the first boundary condition above.

2.3.1 Theoretical Results

Results of Tóth (1962, 1963)

Among the parameters considered by Tóth were the ratio of a basin's depth to its lateral extent and the local relief of the water table.

The patterns of potential and flow in basins with the same water table slope and lateral extent, but different depth, are shown in Figure 2.4. Since the water table relief is the same in each basin, the available energy is equal.

In both basins of Fig. 2.4, flow is downward beneath the hill, horizontal beneath median elevations, and upward beneath the valley. According to the sense of motion relative to the water table, these are called "recharge", "midline" and "discharge" areas, respectively. The hydraulic heads decrease downward, are constant with depth, and increase downward from recharge to midline to discharge area.

Comparing Figs. 2.4(a) and 2.4(b), increasing the basin depth causes more extensive vertical flow. In Fig. 2.4(b), the deep basin, a larger proportion of the energy is consumed by vertical motion. The horizontal hydraulic gradient at depth is therefore much less than at the water table. By contrast, it is uniform across much of the shallow basin.

Hierarchal systems of groundwater flow are developed when a basin has complex topography, i.e., local topographic relief is imposed on a regionally sloping water table. An example is provided in Figure 2.5. A "local" system contains the ensemble of flow paths extending from a local water divide to an adjacent stream valley. If one or more

topographic highs are between the recharge and discharge areas of a set of flow paths, a system is "intermediate", whereas if the water enters at the regional topographic high and leaves at the regional low, the system is "regional". The flow is active in a local system and sluggish in a regional system. Quasi-stagnant zones are developed where systems of different order converge. Furthermore, comparing Fig. 2.5 with Fig. 2.4(b), the slight hydraulic gradient near the base results only from the regional topography, and appears unaffected by the local relief.

Results of Freeze and Witherspoon (1966, 1967)

Freeze and Witherspoon focussed on the effects of subsurface permeability contrast. The effect of introducing a layer of low permeability over one of high permeability is illustrated by comparing Figure 2.6(a) with Fig. 2.4(b). The flow in the aquitard is predominantly vertical while in the aquifer it is largely horizontal. As the permeability contrast increases, Figure 2.6(b), the hydraulic gradient increases in the aquitard and decreases in the aquifer. Although the spacing between the equipotentials in the aquifer of Fig. 2.6(b) may suggest near-stagnant conditions, application of Darcy's law would indicate a higher specific discharge here than in the aquifer of Fig. 2.6(a).

Generally for this type of stratified permeability distribution, large volumes of water are transmitted vertically across an aquitard and horizontally in an aquifer. In contrast, when an aquifer overlies an aquitard, Figure 2.6(c), the flow pattern does not substantially change from the homogeneous case. Rather, the equipotentials in the aquifer meet the aquitard's surface normally, as if it were the basal boundary.

Like in the homogeneous case, local flow systems are generated when the topography is complex, Figure 2.6(d). The depth and extent of the local systems are, however, largely restricted to the upper aquitard so that the hydraulic gradient in the lower aquifer is only slightly influenced by the local hills and valleys, and reflects mainly the regional topographic relief.

While the details of the head distribution in topography-driven regimes are influenced by basin geometry and contrasting permeability, certain general features are consistently observed. These include the downward and upward flow, respectively, beneath topographic highs and lows, the lateral flow across the middle areas, and the comparatively high hydraulic gradient near the water table and lower gradient at depth. On the other hand, if another source of basinal fluid potential were present, there would be no

reason to expect this general pattern. Observation of the pattern in a basin, for instance by fluid parameters such as pore-pressure which are related to the energy distribution, thus provides compelling evidence for topography-driven flow (Tóth, 1978).

2.4 Unconfined, Confined and Closed Systems: Scales of Topographic Influence

Many of the above mentioned flow features are consistent with both unconfined and confined systems (Freeze and Witherspoon, 1967). An unconfined system is one in which "the potential distribution ... is affected by the potential distribution of the water table in the overlying rocks", while in a confined system the "the potential distribution is not affected by the overlying water table" (Domenico, 1972, p.176).

The unconfined or confined nature of a system depends on the scale of topographic features under consideration. For instance, the hydraulic gradient in the lower aquifer of the topographically complex, stratified basin in Fig. 2.6(d) is largely uninfluenced by the local variations in water table elevation. Locally, then, this aquifer is confined. The existence at all of the basal hydraulic gradient is, however, due to the regional water table relief. Regionally, the aquifer is unconfined. In the homogeneous, topographically complex basin, Fig. 2.5, the potential pattern near the base is similarly influenced only by the regional slope of the water table. Confinement appears therefore dependant not on heterogeneity, but rather on the spatial scale of investigation.

In a thermodynamic sense, groundwater systems may be classified as "open" or "closed" (Domenico, 1972). An open system exchanges matter and energy with its surroundings. A property of open systems is that a dynamic equilibrium may be established so that a balance is struck between the quantities of matter and energy entering and leaving the system. Opposed to this are closed systems which exchange neither matter nor energy with their surroundings. Closed systems, on the other hand, strive towards maximum entropy until a static equilibrium is attained (Domenico, 1972).

Gravitational systems, whether unconfined or confined, may be considered as types of open system. Both unconfined and confined systems exchange matter and energy with the larger hydrologic system. Meteoric water enters the subsurface hydrologic system at recharge areas and is eventually discharged, either directly back to the land or cross-formationally into other systems. For closed systems at equilibrium, by contrast, there is neither recharge nor discharge. Even for a closed system not at equilibrium, it appears that

the matter and energy are transferred only in one direction, rather than exchanged. Examples of closed hydrogeologic systems include compactional or thermal systems (Kovács, 1978), where fluids are usually expelled upward.

A general hydrogeologic problem is to determine whether a system is open or closed, and to establish the boundary surface between the two types (Kovács, 1978). The energy relations of the types are, however, fundamentally different. In an open system, the hydraulic heads are limited by the maximum and minimum elevations of the water table that belong to the hydraulic continuum. In a closed system at equilibrium, the hydraulic head is constant and may take on any value independently of the water table elevation. Consideration of the energy relations, therefore, appears to be a simple but key step in distinguishing between open and closed systems.

In nature, of course, the distinction will rarely be well-defined. As put by Kovács (1978, p. 42): "... gradual transitions are generally characteristic of any changes in ... Nature, and only the human brain tries to simplify the processes and to describe them by using generalized and deterministic relationships." As will be shown in Chapter 4, a combined use of pressure-elevation and pressure-depth plots, however, may help to identify the dominant nature of a system, i.e., whether it is open, and by what scale of topographic features it is unconfined or confined, or whether it is closed.

2.5 Pressure-Elevation and Pressure-Depth Plots

2.5.1 Background

Pressure-elevation *p(z)* and pressure-depth *p(d)* plots are both used currently but never together, perhaps because the conceptual bases which guide their interpretation are fundamentally opposed. On the one hand is the view that impermeable strata partition a basin into hydraulically isolated systems (Hunt, 1990), on the other the assertion that regional hydraulic continuity is a fundamental property of the rock framework (Tóth, 1990).

To describe the rock framework as hydraulically continuous is to state that the voids are interconnected such that the fluid potential is a continuous function of the spatial coordinates. Hydraulic discontinuity, alternatively, implies surfaces of fluid potential singularity resulting from the absolute impermeability of strata. Choosing between

continuity and discontinuity is critical. If the rock framework is hydraulically continuous, spatial differences in hydraulic head indicate groundwater motion. Across a surface of discontinuity, on the other hand, a hydraulic gradient is undefined and flow cannot be inferred.

In practice, hydraulic head can be characterized as the ratio of an induced change in hydraulic head, or pressure, at a point to an inducing change in head, or pressure, at a distant point (Tóth, 1990). The velocity of pressure disturbance propagation depends on the hydraulic diffusivity, i.e., the hydraulic conductivity over the storativity, of the rock. Practically, therefore, hydraulic continuity depends on the distance and time scales of a problem. For instance at the distances and times of interest to a reservoir engineer, it may be acceptable to assume that a pressure change at one location will not induce a pressure change elsewhere, either because the distance is sufficiently large or the diffusivity small, i.e., the rock is "impermeable". It is quite a different matter, however, to presume the same rock is impermeable at the distances and times required for the basinal analysis of natural groundwater conditions.

The conventional use of pressure-elevation $p(z)$ plots is based on a model of regional hydraulic discontinuity, espoused most recently by Hunt (1990). According to the model, fluid systems are compartmentalized by impermeable strata. Within a compartment, the fluids are static, and the hydraulic heads, or pore-pressures, are not influenced by topography at any scale. Graphical representation of pore-pressure is made relative to a horizontal datum, as a $p(z)$ plot, since use of the land surface as datum is considered only to scatter the data. In other words, the lack of topographic influence is an *a priori* assumption. Furthermore, $p(z)$ patterns which indicate hydraulic head differences are routinely taken as evidence of impermeability rather than flow. Often cited is the argument by Bradley (1975, p.957) that flow would cause the pressures to "equalize to hydrostatic". As demonstrated shortly, the reasoning is invalid if water is exchanged in an open system.

Pressure-depth $p(d)$ plots are often used to identify so-called "abnormal" formation pressures, i.e., pressures at a given depth below the water table unequal to those expected for static conditions in a non-deforming rock framework. Under completely static conditions extending from the water table, the expected pressures are given by

$$p = \gamma d, \tag{2.29}$$

where d is depth below the water table. "Abnormal" pressures are sometimes presented as evidence of impermeability (Hunt, 1990).

In settings where the rock framework is deforming, "abnormal" pressures may be generated by any number of mechanisms. These include compaction disequilibrium (Bredehoeft and Hanshaw, 1968) and thermal expansion of fluids (Sharp, 1983). Dilation of aquitards in response to erosional unloading can induce pressures that are less than hydrostatic (Neuzil and Pollock, 1983; Tóth and Corbet, 1986). The key to the effectiveness of these mechanisms appears to be that the rate of pressure generation exceed the rate of pressure dissipation. Thus rocks of low hydraulic diffusivity are frequently associated with ahydrostatic pressures (Domenico and Schwartz, 1990).

When the rock framework is non-deforming, i.e., "geologically mature", gravitational forces are dominant. The vertical pressure gradients, $\partial p/\partial d$ or $\partial p/\partial z$, and values of pressure associated with topography-driven flow, however, are also generally ahydrostatic (Tóth, 1978, 1979; Senger and Fogg, 1987; Belitz and Bredehoeft, 1989). Numerous theoretical examples of significantly ahydrostatic, or "abnormal", pressures as a condition of dynamic equilibrium in geologically mature basins are provided in Chapter 4.

Tóth (1978) advanced a more systematic, and less descriptive, approach to *p(d)* plot analysis. Topography-influenced pressure distributions, and flow regimes, are thought to be recognized more readily with the land surface as the datum. As employed by Tóth (1978; 1979) *p(d)* plots were used to demonstrate regional hydraulic continuity, and to infer cross-formational groundwater flow. This latter use of *p(d)* plots has been applied by Orr and Kreitler (1985) and Bair (1987a, 1987b) in the Palo Duro Basin of Texas, as well as by Hitchon (1989a, 1989b) and Holysh (1989) in east- and north-central Alberta.

2.5.2 Pressure-Elevation Plots

A pressure-elevation, *p(z)*, plot is illustrated in Figure 2.7. Plotted are pressures determined at points in the right circular cylinder in Fig. 2.7(a). The cylinder is divided at its midsection by an impermeable disc. On both sides of the disc is a homogeneous sand. Inlet tubes, A and B, are on the left and right ends of the cylinder, respectively. Sets of vertical manometer tubes are located at measurement sites s_1 and s_2. In each compartment, a manometer is open to the sand at elevations z_1 and z_2, with the datum as the $z = 0$ horizontal line. Water of specific weight γ is pumped through the inlet tubes until the hydraulic heads are as illustrated.

The hydraulic head at a point is denoted h_{ij} where i = s_1 , s_2 = 1, 2 and j = z_1, z_2 = 1, 2. The pressures p_{ij} are similarly denoted. The pressures p_{ij} are given by

$$p_{ij} = (h_{ij} - z_j)\,\gamma . \tag{2.30}$$

The pressure p_{ij} is the weight per unit area of the water column overlying the point. Since the water is static in each compartment, the pressure changes vertically at a hydrostatic rate, i.e., $dp/dz = -\gamma$.

The pressures p_{ij} measured at the elevations z_1 and z_2 are plotted on the $p(z)$ graph illustrated in Fig. 2.7(b). A line joins points measured from along a vertical, as for instance that which connects the points from site s_1. The slope of this line represents the vertical pressure gradient beneath the site. Since the water is static the slope is hydrostatic, i.e. (Sec. 2.1), $dp/dz = -\gamma$. Actually the slope as portrayed on the graph is $(-\gamma)^{-1}$, but to avoid unnecessary complication a hydrostatic slope will be henceforth referred to as γ. The same procedure is followed to construct a line joining pressures measured along s_2. Again, the vertical pressure gradient is γ.

Dahlberg (1982) notes an important property of $p(z)$ plots, namely that the hydraulic head at a point is indicated. The technique is to project a line of slope γ through the point to the $p = 0$ axis. The value of z at the intercept equals the hydraulic head at the point.

To illustrate, consider the point (p_{11}, z_1) in Fig. 2.7(b), through which a line with slope γ is extrapolated to the $p = 0$ axis. Letting (p_{1j}, z_j) be the coordinates of any other point on the line, an equation of the line is

$$(z_1 - z_j) = -\frac{1}{\gamma}(p_{11} - p_{1j}) . \tag{2.31}$$

When made to intercept the z-axis at the point $(0, h_{1j})$, the line may be expressed

$$(h_{1j} - z_j) = \frac{p_{1j}}{\gamma} , \tag{2.32}$$

or rearranging in terms of the z-intercept,

$$h_{1j} = z_j + \frac{p_{1j}}{\gamma} \quad , \tag{2.33}$$

which is the hydraulic head at the point (p_{11}, z_1) and, indeed all other plotted points which may fall on this line.

Similarly for the hydraulic heads beneath site s_2,

$$h_{2j} = z_j + \frac{p_{2j}}{\gamma} \quad . \tag{2.34}$$

Because the hydraulic head at s_1 is larger than at s_2, the intercept of the curve from site s_1 is greater than the intercept from site s_2, i.e., $h_{1j} > h_{2j}$. The sense and magnitude of the head difference between the compartments, therefore, is indicated on the $p(z)$ plot by the z-intercepts of curves with hydrostatic slope.

An important point is that two types of curves may be constructed. One joins vertically measured pressures and represents the vertical pressure gradient $\partial p/\partial z$; the other has slope γ and gives the hydraulic head at a point. In Fig. 2.7(b), vertically-constant hydraulic head is shown by the first curve type, while a horizontal head difference is indicated by the latter. It would be erroneous, however, to interpret this head difference as flow since the cylinder is hydraulically discontinuous.

Nevertheless, Dahlberg (1982) recognizes that the same p(z) pattern as in Fig. 2.7(b) can result from horizontal, steady-state flow. As an example, consider Figure 2.8(a) in which the impermeable disc is replaced with slightly permeable clay. The sand has hydraulic conductivity K_S and the clay has $K_C = 1/8\ K_S$. Water enters the cylinder at A and leaves at B. The specific discharges at A and B are equal and constant. The flow is held so that the heads h_{ij}, denoted as previously, are the same as in Fig. 2.7(a). By arbitrarily designating a head decline of 1 unit across each sand,the head drop across half the distance of the clay is 4 units. Illustrated in the upper portion of Fig. 2.8(a) is a gentle hydraulic gradient through the sand and a steep one through the clay.

The associated $p(z)$ plot is illustrated in Fig. 2.8(b). Plotted points from along the vertical at each site are joined by a line. The slope of the line from each site s_1 and s_2 is again equal to γ. Now, however, the slopes are hydrostatic because flow is horizontal. Curves of slope γ may also be extrapolated through the points to the $p = 0$ axis. Again, the z-intercepts indicate the relative values of hydraulic head h_{ij}. These heads h_{ij} are the same

as previously. The pattern of *p(z)* points in Fig. 2.8(b) is thus precisely that observed in Fig. 2.7(b).

A *p(z)* pattern like that in Fig. 2.8(b), therefore, has two equally possible but opposite interpretations. One static and hydraulically discontinuous, the other dynamic and continuous. The *p(z)* plot alone cannot tell which alternative is most probable. Given the ingrained tendency of some to characterize shales as "impermeable", however, the first interpretation seems more likely to be chosen.

Despite their ambiguity, *p(z)* plots can nevertheless indicate vertical hydraulic gradients and point values of head. They should not be altogether discarded. Instead, a way of demonstrating hydraulic continuity, used conjunctively with *p(z)* plots, appears needed. As demonstrated in Chapter 4, this may be provided by *p(d)* plots.

A final example is intended to clarify the distinction between the two *p(z)* curve types. In Figure 2.9(a) the cylinder now stands upright. The hydraulic gradient is like that in Fig. 2.8, but the water flows upward. The measured pressures and heads, respectively, are p_j and h_j where $j = z_1, z_2, z_3, z_4 = 1, 2, 3, 4$.

The p(z) graph is presented in Fig. 2.9(b). Representing the vertical pressure gradient, the first curve type links the vertically-measured points. Examples of such curves are in the sands. The upper and lower ends of these curves are extended to the boundary with the clay. Within the clay, a line joins with those in the upper and lower sand. Estimates of the slopes of these curves are estimates of the vertical pressure gradient $\partial p/\partial z$. Within the sands, the slopes are slightly superhydrostatic because of upward flow. Within the clay, the slopes are more greatly superhydrostatic because of the steeper vertical hydraulic gradient.

For the second curve type, lines of slope γ are projected through each point to the $p = 0$ axis. As previously, the heads h_j are given by the $p = 0$ intercepts, i.e.,

$$h_j = z_j + \frac{p_j}{\gamma} \quad . \tag{2.35}$$

The intercepts (Fig. 2.9b) show that $h_1 > h_2 > h_3 > h_4$. Consistently with the vertical pressure gradient, upward flow is indicated. In essence, the first curve type gives the sense of the vertical hydraulic gradient, whereas the second yields point values of head.

2.5.3 Pressure-Depth Plots

A fundamentally different approach to the analysis of pore-pressures was advanced by Tóth (1978, 1979). The pressures are interpreted to exist in a unified flow field rather than in isolated compartments. According to this view, topography-driven flow results in distinct basinal pore-pressure distributions which are more readily recognized when the land surface is the datum, as in a *p(d)* plot.

Tóth (1978, 1979) investigated a number of conceptual basins, one of a static condition, and others of topography-driven flow. The cases illustrated in Figures 2.10 to 2.12 are discussed in some detail.

Figure 2.10 shows a case of static water in an aquifer beneath a sloping land surface. The water has specific weight γ. Referring to Fig. 2.10(a), wells are located on the land surface at sites s_i where i = 1, 2. At each site, pressures are p_{ij} at the elevations z_j, j = 1, 2. The depth to a point is designated d_{ij}, where henceforth i = s_1, s_2 = 1, 2 and j = z_1, z_2 = 1, 2. At a site s_i the land surface elevation is z_{oi}. The hydraulic head in the aquifer is constant, thus subscripts are unnecessary and $h_{ij} = h$. Evidently, the topography exerts no influence on the hydraulic head, or pressures, in the aquifer.

The result of plotting these points on a *p(d)* graph is illustrated in Fig. 2.10(b). As with a *p(z)* plot two different types of curve are useful. One type is drawn by connecting points from along the vertical at a site. In Fig. 2.10(b) such curves beneath each site have a hydrostatic slope, i.e., $(\gamma)^{-1}$, because the water is static. Like with a *p(z)* plot the curve indicates simply that the head is vertically constant.

A second curve type is drawn by projecting a line of hydrostatic slope through a point to the depth, i.e., $p = 0$, axis. For a given point, the resulting intercept is denoted d_{hi}. It can be shown that the value of the intercept d_{hi} is the difference between the land surface elevation vertically above the point, z_{oi}, and the hydraulic head h of the point,

$$d_{hi} = (z_{oi} - h). \tag{2.36}$$

In other words, the intercept gives the depth to the potentiometric surface, or the "potentiometric depth". Since the potentiometric depth is variable in Fig. 2.10(a), the curves in Fig. 2.10(b) are spread apart. More precisely, the potentiometric depth is indicated greater at site s_2 than at site s_1, i.e., $d_{h2} > d_{h1}$

As with a $p(z)$ plot, the graphical determination of the potentiometric depth d_{hi} is valid also when there is vertical flow, so long as a hydrostatic slope is used in the extrapolation. At the same time, the use of a hydrostatic slope does not imply a static condition. A slope other than hydrostatic simply cannot be used, because the resulting $p = 0$ intercept would have no meaning, graphically or physically. Again, therefore, a curve which joins vertical pressures must be distinguished from an extrapolated curve of slope γ. The former has significance for the vertical hydraulic gradient, the latter for the potentiometric depth.

Tóth (1978, 1979) also analyzed cases, illustrated in Figures 2.11 and 2.12, where the pressures are influenced by the regional scale topographic relief, i.e., the flow systems are regionally unconfined. For each basin, curves are constructed from pressures along the vertical within the recharge, midline and discharge areas. Across each basin the position of the water table is assumed to coincide with the land surface. The water table, by definition, is the surface where $p = 0$. Therefore, the $p(d)$ curves begin at the origin, i.e., $p = 0$ where $d = 0$.

The case of a homogeneous basin with simple topography is given in Fig. 2.11. From the recharge to discharge areas the $p(d)$ curves are generated at the sites s_i, where i = 1, 2, 3, respectively. Beneath the site s_2, at the midline, the flow is entirely horizontal and the pressure increases linearly with depth at a hydrostatic rate. For the site s_1, at the recharge area, the pressure increases with depth at a less than hydrostatic rate, indicating downward flow, whereas at s_3, the discharge area, the rate greater than hydrostatic signifies upward flow. The curves in these areas are not linear. With increased depth their slopes approach hydrostatic. This response occurs because the hydraulic gradient both decreases and becomes more horizontal with depth. Thus, particularly near the bottom of the basin, the value of pressure is ahydrostatic, i.e., $p \neq \gamma \cdot d$ [Sec. 2.5.1], at the same time that the vertical pressure gradient is hydrostatic, i.e., $\partial p/\partial d = \gamma$.

Illustrated in Figure 2.12 is a basin of simple topography with a thick, areally extensive aquitard. The flow is largely horizontal in the upper and lower aquifers as well as in the central regions of the aquitard. Strong vertically-oriented flow occurs through the aquitard near the basin's lateral boundaries. At site s_2 the flow is horizontal at all depths so that the vertical pressure gradient is hydrostatic. Similarly, through both aquifers at sites s_1 and s_3 the slopes are nearly hydrostatic. Across the aquitard, however, the slopes are markedly ahydrostatic because of the steep vertical hydraulic gradient. The pressures in the

lower aquifer, particularly beneath the recharge and discharge areas, are thus substantially ahydrostatic.

From the theoretical analysis Tóth (1978, 1979) concluded that in a regionally unconfined flow field, the *p(d)* curves are symmetrically arranged about the origin of the *p(d)* plot, such that the vertical pressure gradient $\partial p/\partial d$ increases with decreasing topographic elevation.

A shortcoming of *p(d)* plots, however, is that the general pattern of curves in a dynamic case can sometimes be difficult to distinguish from a static case. The difficulty increases with depth in stratified basins since the hydraulic gradient tends generally to decrease.

The above point is illustrated with reference to Figure 2.13, which is like Fig. 2.10 but the horizontal potentiometric surface now crosses the sloping land surface. The change is effected on the *p(d)* plot, Fig. 2.13(b), by a downward translation of the plot's origin. The vertical pressure gradients remain hydrostatic, but the negative value of the site s_1 depth-intercept d_{h1} and the positive site s_2 depth-intercept d_{h2} indicate that the heads are greater and less than the land surface elevation, respectively. Comparing Fig. 2.13(b) alongside the lower portions of the curves in Fig. 2.12(b), a similarity is apparent: in both cases the vertical pressure gradients are effectively hydrostatic at all sites, and in both cases the curves are arranged symmetrically about the origin. Presented with a *p(d)* plot like that in Fig 2.13(b), it would be difficult to tell if the horizontal hydraulic gradient is subdued or altogether absent.

Of course the fundamental difference between Figs. 2.12 and 2.13 is that a topography-induced hydraulic gradient exists in the one case and not the other. The difference could be revealed indirectly by solving for h at the different sites with the relation (2.36), but a far simpler and potentially more revealing method is to concurrently analyze a *p(z)* graph constructed from the same set of data. As discussed earlier, *p(z)* plots aptly reveal lateral head differences. More of this is discussed in Chapter 4.

2.6 Vertical Pressure Gradients and Linear Regression

Orr and Kreitler (1985) raise a concern regarding the validity of fitting a regression curve through-spatially distributed *p(d)* data to estimate the vertical pressure gradient. The *p(d)* curves from the theoretical models in Figs. 2.11 and 2.12 are from vertical pressure

measurements. By definition, such a curve represents the vertical pressure gradient and its slope can be used to infer vertical motion. A curve derived from data spread in two or three dimensions, strictly speaking, is no longer a vertical pressure gradient. Thus, using it to infer vertical motion is not rigorously valid.

For instance, consider the *p(d)* plot in Figure 2.14, which is like that in Fig. 2.13(b) but a regression curve is fit through the combined data from both sites. The regression relation minimizes the values of pressure and passes diagonally through the points. If the slope of the regression line were taken as the vertical pressure gradient, vertical flow would be inferred when it is not occurring. Furthermore, the $p = 0$ intercept of the line does not indicate the potentiometric depth. Orr and Kreitler (1984) provide numerous examples which clearly demonstrate the invalidity of applying regression analysis to spatially-distributed points in order to estimate the vertical pressure gradient.

On the other hand, as observed by Orr and Kreitler (1984), the correct vertical pressure gradient is obtained from data within a single vertical well, as should be from physical considerations. Such a distribution of measurements in practice is unfortunately rare. In mathematics, a method has probably been developed by which a single-dimensional functional relation, i.e., pressure as a vertical function of depth, can be estimated from a multi-dimensional distribution of variables, i.e., pressure measurements scattered laterally as well as vertically, but it is not known to the writer. Without such a technique, it appears that only pressure measurements from along a vertical can be used to safely estimate the vertical pressure gradient.

The above argument applies as well to *p(z)* plots.

2.7 Vertical Pressure Gradients and Variable Groundwater Density

A final point needs to be raised regarding the usefulness of *p(d)*, and *p(z)*, plots to indicate vertical flow in variable density groundwater systems. Whereas it is not strictly valid to use equivalent freshwater heads to detect vertical flow in density-stratified systems (Lusczynsi, 1961), an upward or downward sense of motion can be detected independently of hydraulic head with the use of vertical pressure gradients (Tóth, 1978; Bair, 1987b). In cases of density-stratified formation water, the use of vertical pressure gradients has therefore an advantage over techniques which use hydraulic heads.

Bair (1987a), citing Wilton and Picking (1985), provides an expression for determining the vertical hydraulic gradient in a variable-density flow regime,

$$\frac{\partial h}{\partial z} = \frac{1}{\gamma}\left(\frac{\partial p}{\partial z} - \gamma_a\right) \tag{2.37}$$

where γ_a is the average specific weight of formation water between variable density regimes.

The hypothetical cases presented in Chapter 4 assume a constant density of 1.000 kg/m^3 for the water. For constant water density, equation (2.37) reduces to

$$\frac{\partial h}{\partial d} = \frac{1}{\gamma}\frac{\partial p}{\partial d} - 1 \quad \text{or} \quad \frac{\partial h}{\partial z} = -\frac{1}{\gamma}\frac{\partial p}{\partial z} - 1\,, \tag{2.38}$$

so that the vertical hydraulic gradient $\partial h/\partial d$ or $\partial h/\partial z$ can be calculated from the vertical pressure gradient.

Oberlander (1989) contends that when the groundwater is sufficiently heterogeneous, fluid density and fluid pressure must both be known spatially to properly determine the three-dimensional driving force. It may be anticipated that a combined use of *p(d)* and *p(z)* plots may prove to be particularly useful in variable density fluid regimes.

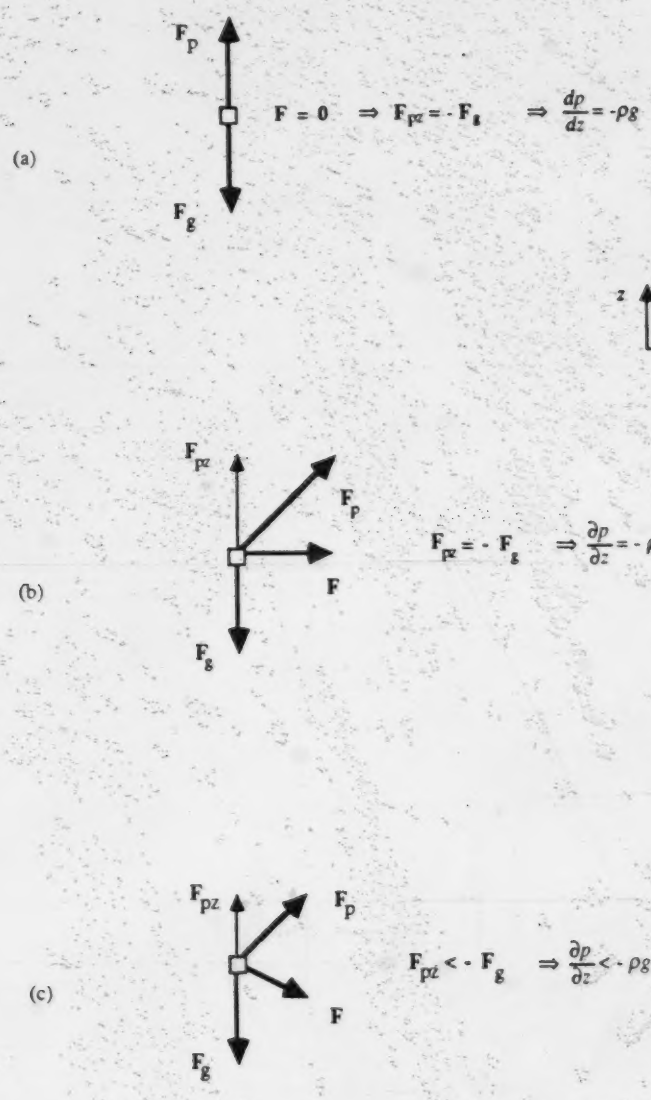

Fig. 2.1 Relations between the driving force **F**, the gravity force $\mathbf{F_g}$, and the pressure force $\mathbf{F_p}$: (a) $\mathbf{F_p}$ and $\mathbf{F_g}$ are balanced along the vertical, the condition is static and the vertical pressure gradient is hydrostatic; (b) $-\mathbf{F_{pz}} = \mathbf{F_g}$, so that **F** is horizontal and the vertical pressure gradient is hydrostatic; (c) $-\mathbf{F_{pz}} < \mathbf{F_g}$, so that **F** has a downward component and the vertical pressure gradient is subhydrostatic (after Hubbert, 1940, FIG. 15).

(a)

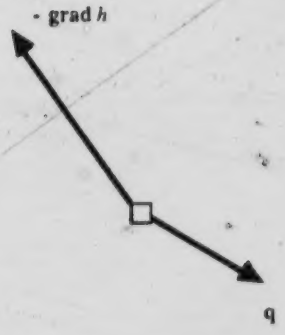

(b)

Fig. 2.2 Relations between the hydraulic gradient **grad** h and flow **q** in: (a) isotropic, and; (b) anisotropic media (after Hubbert, 1940, FIG. 18).

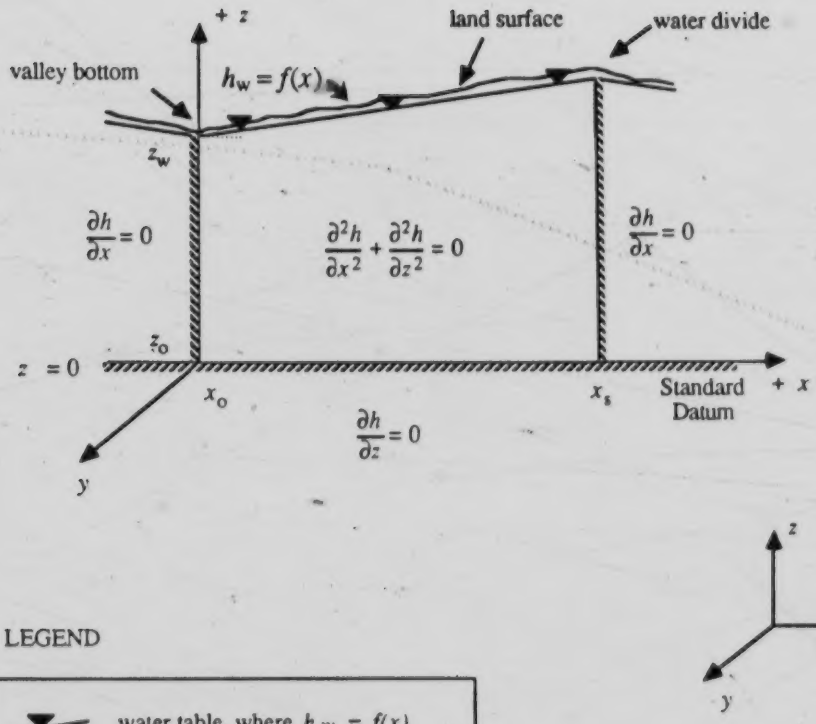

Fig. 2.3 The boundary value problem of topography-driven groundwater flow in a homogeneous, isotropic medium (after Tóth, 1962, Fig. 2.).

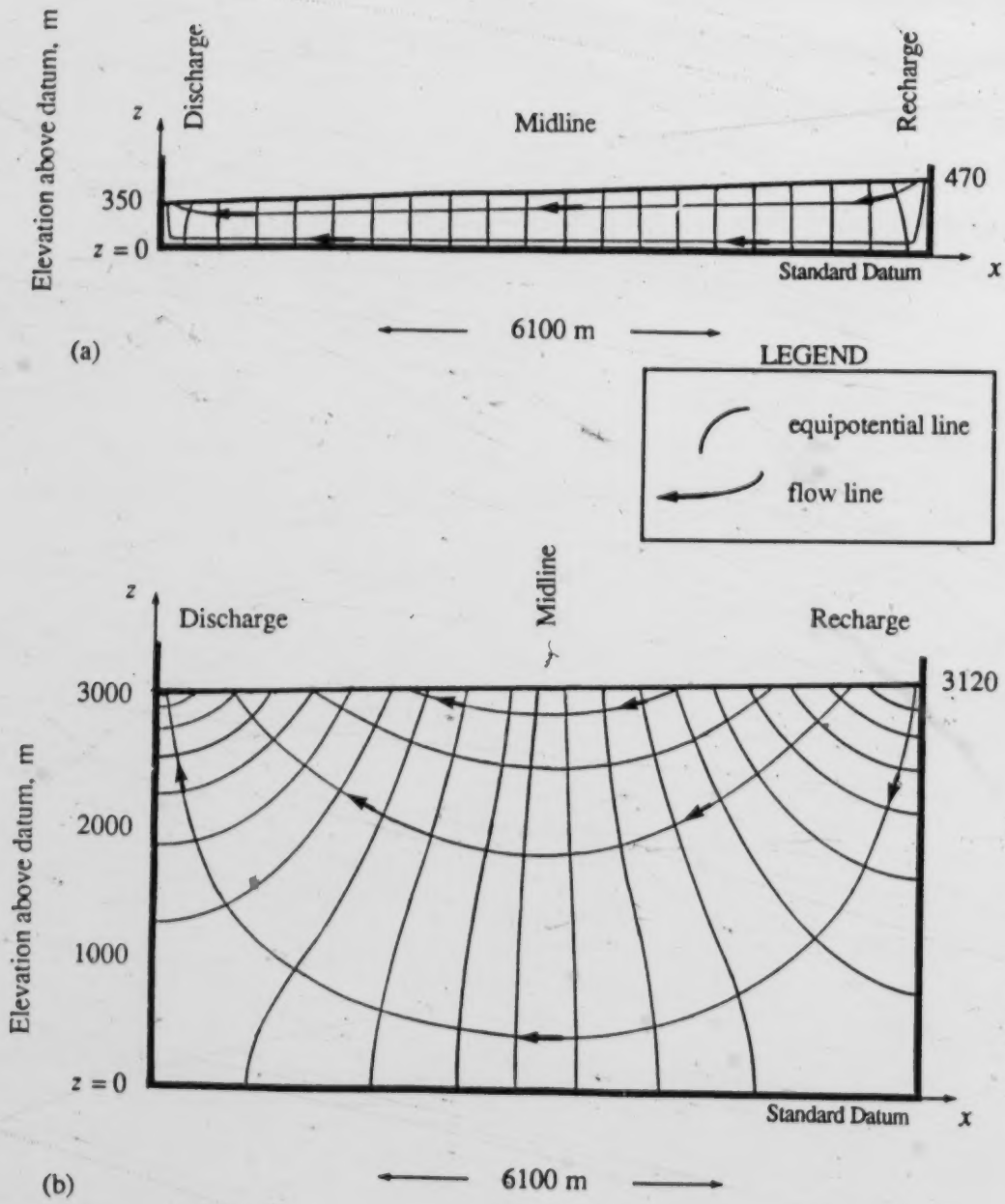

Fig. 2.4 Patterns of hydraulic head and groundwater flow in homogeneous basins with simple topography (after Tóth, 1962, Fig. 3.).

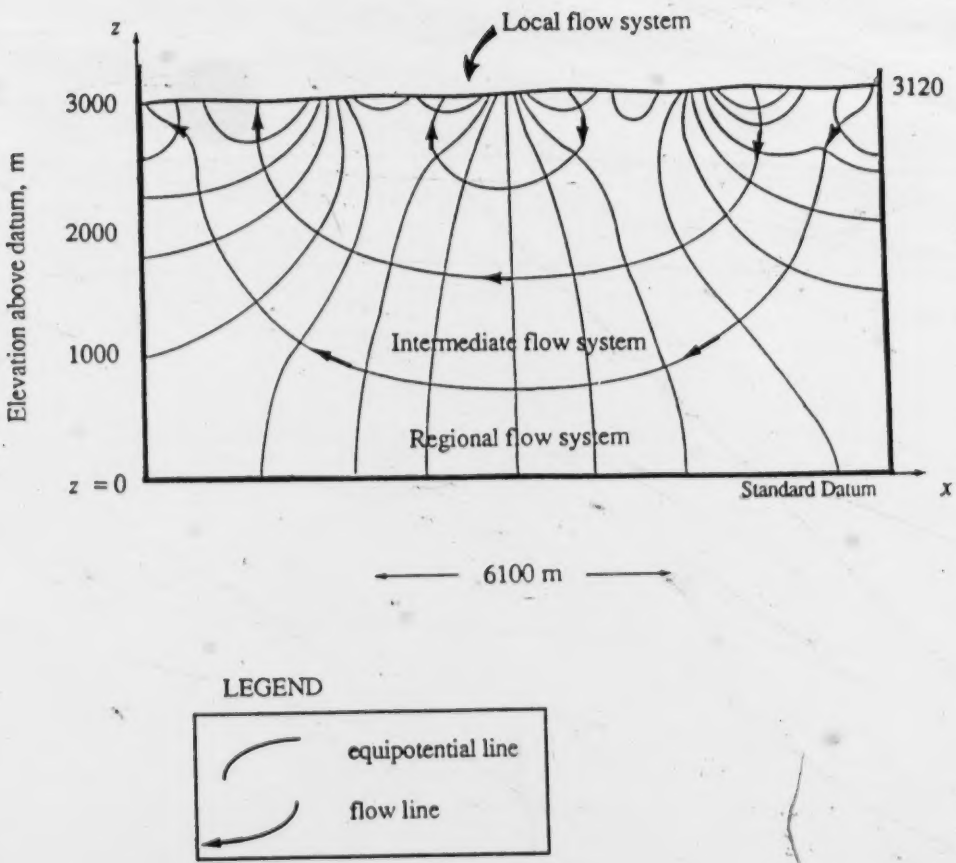

Fig. 2.5 Patterns of hydraulic head and groundwater flow in a homogeneous basin with local topography superimposed on the regional slope of the land (after Tóth, 1963, Figure 2g).

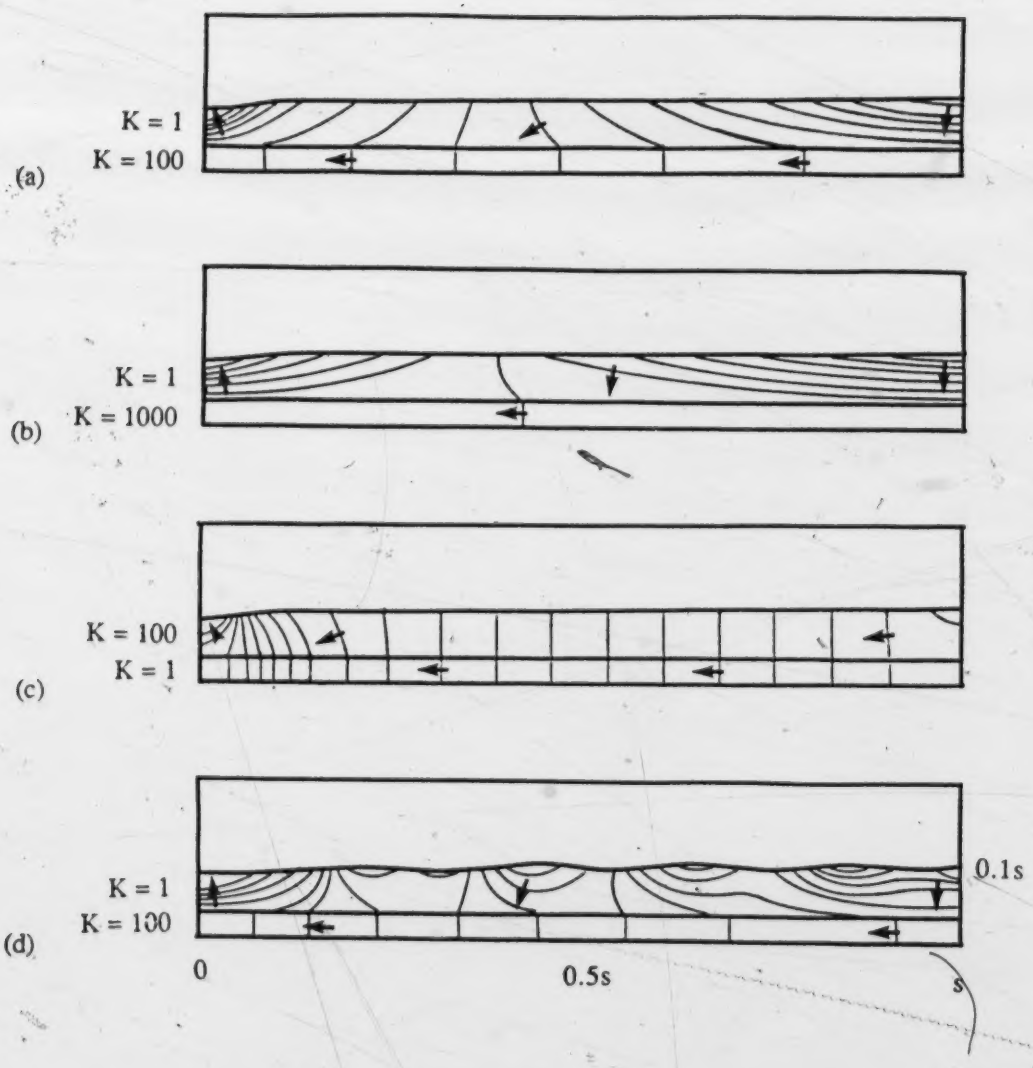

Fig. 2.6 Topography-induced patterns of hydraulic head and groundwater flow in heterogeneous basins (after Freeze and Witherspoon, 1967, Figs. 2 and 3).

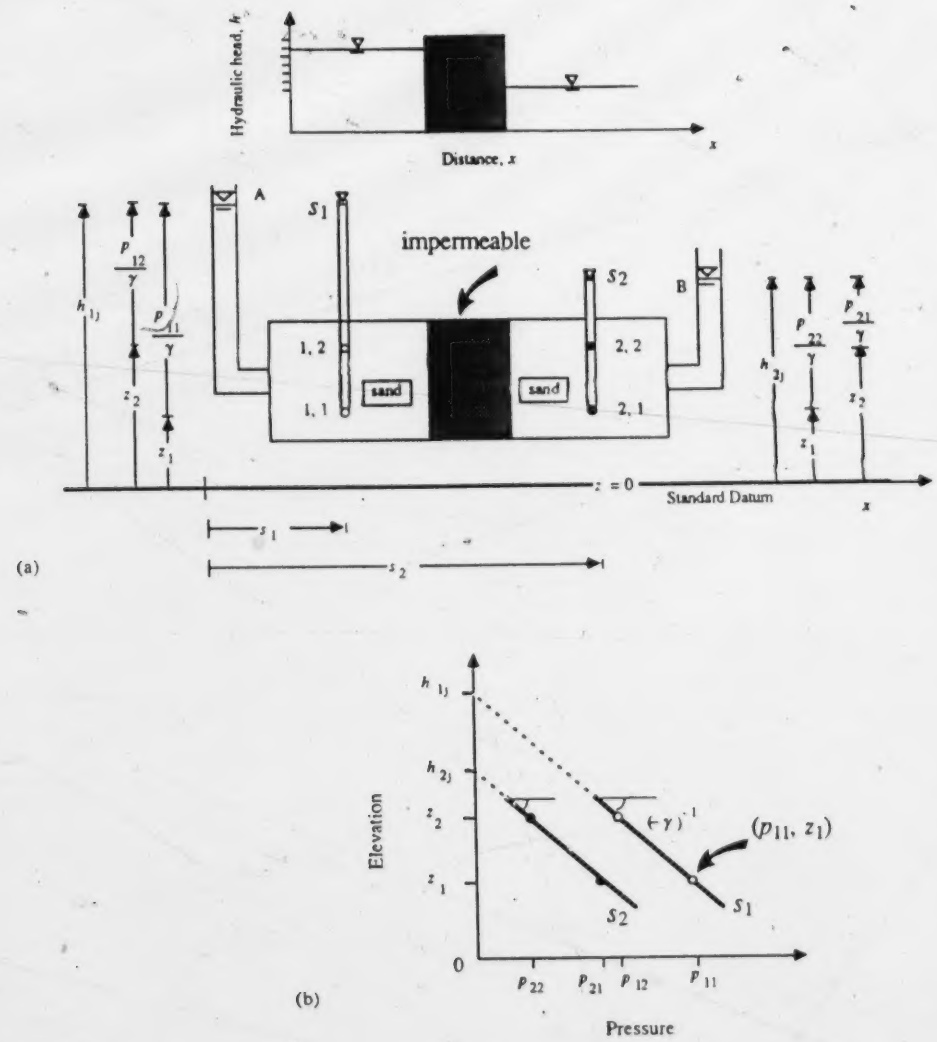

Fig. 2.7 Pressure-elevation pattern for a hydraulically discontinuous, static condition.

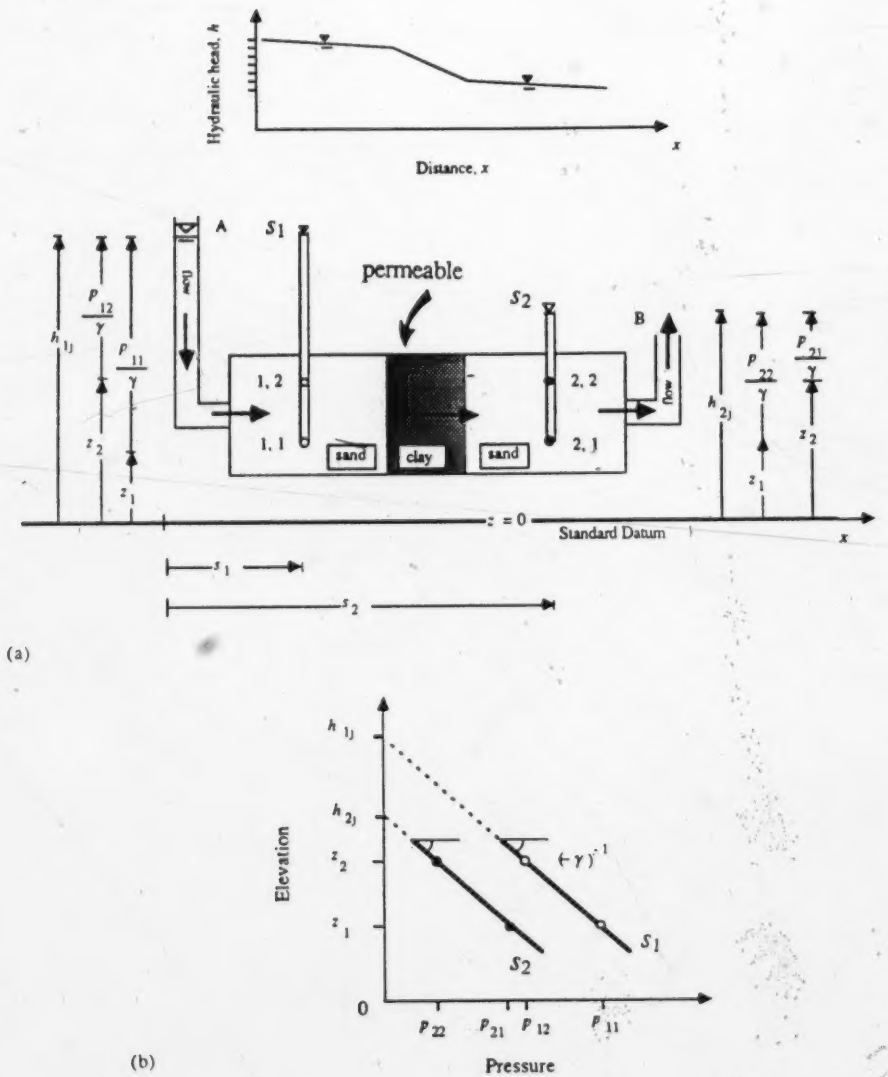

Fig. 2.8 Pressure-elevation pattern for steady-state horizontal flow in a hydraulically continuous medium.

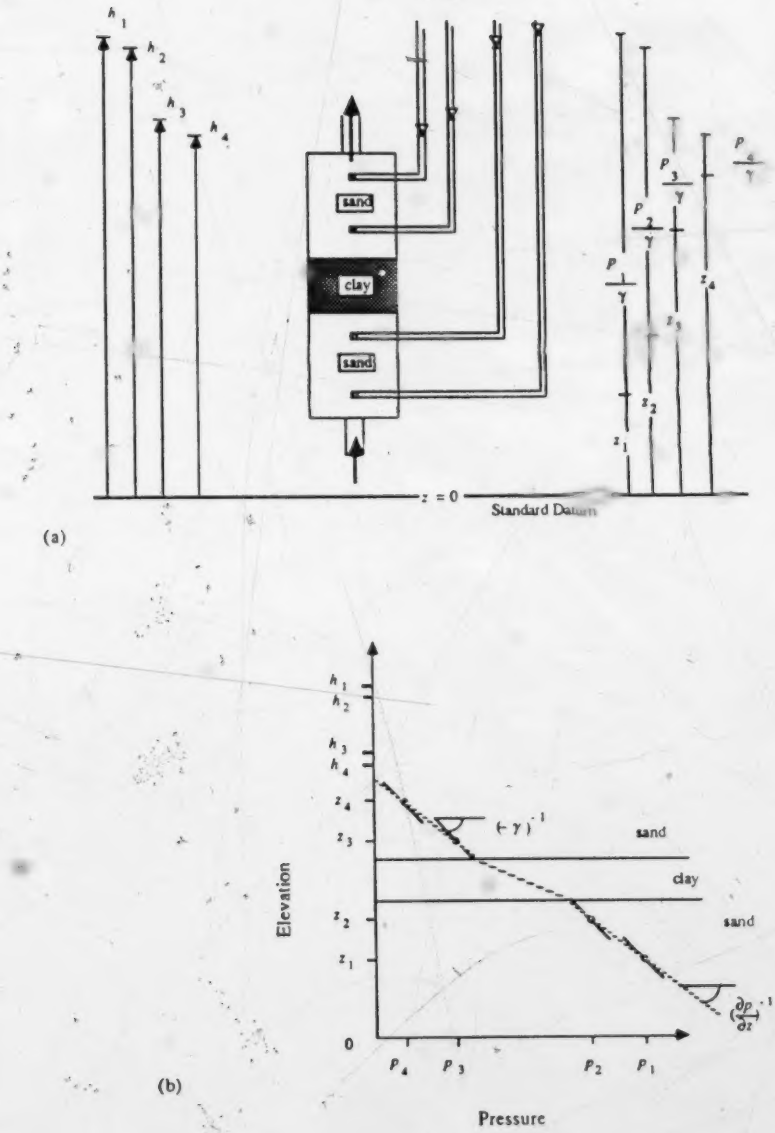

Fig. 2.9 Pressure-elevation pattern for steady-state vertical flow in a hydraulically continuous medium.

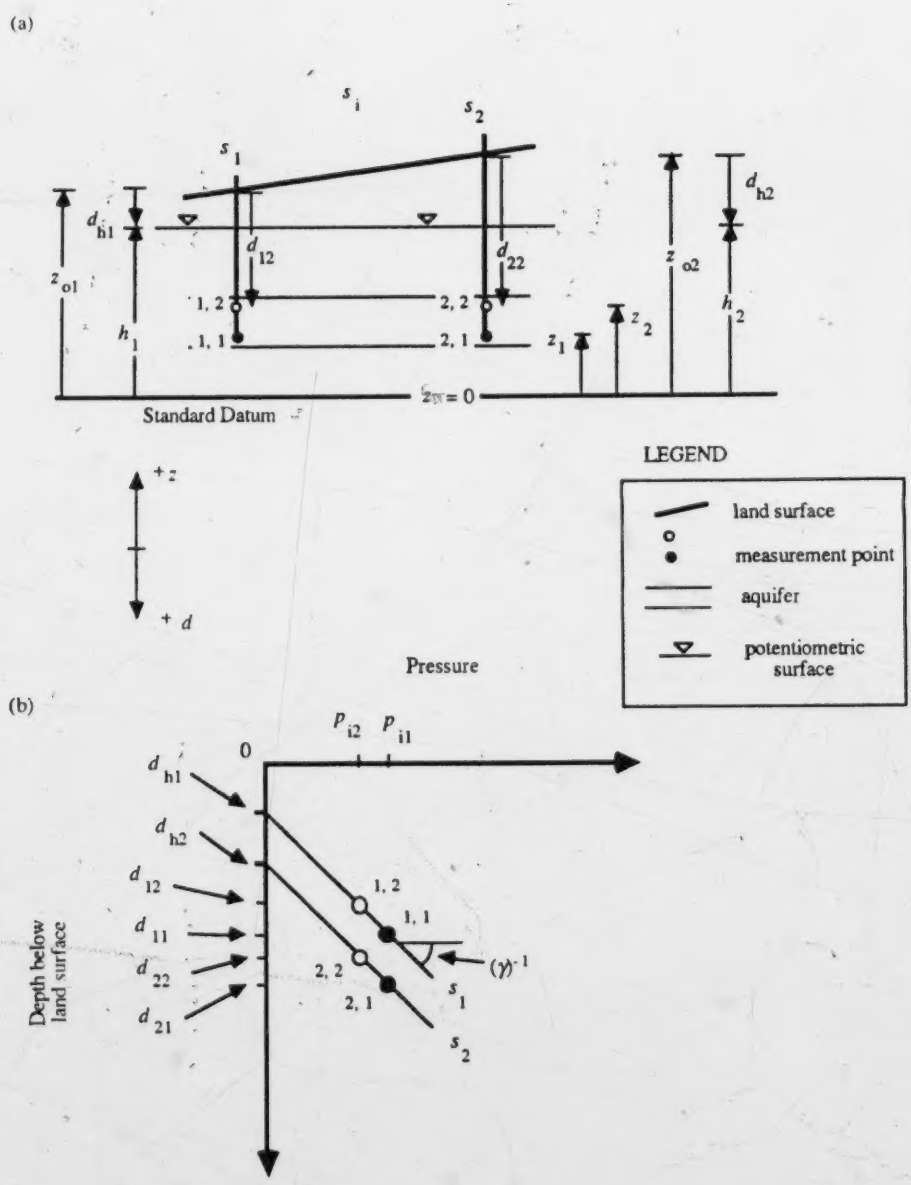

Fig. 2.10 (a) Static conditions beneath a sloping land surface, (b) the associated pressure-depth relations (adapted from Tóth, 1978, Fig. 9).

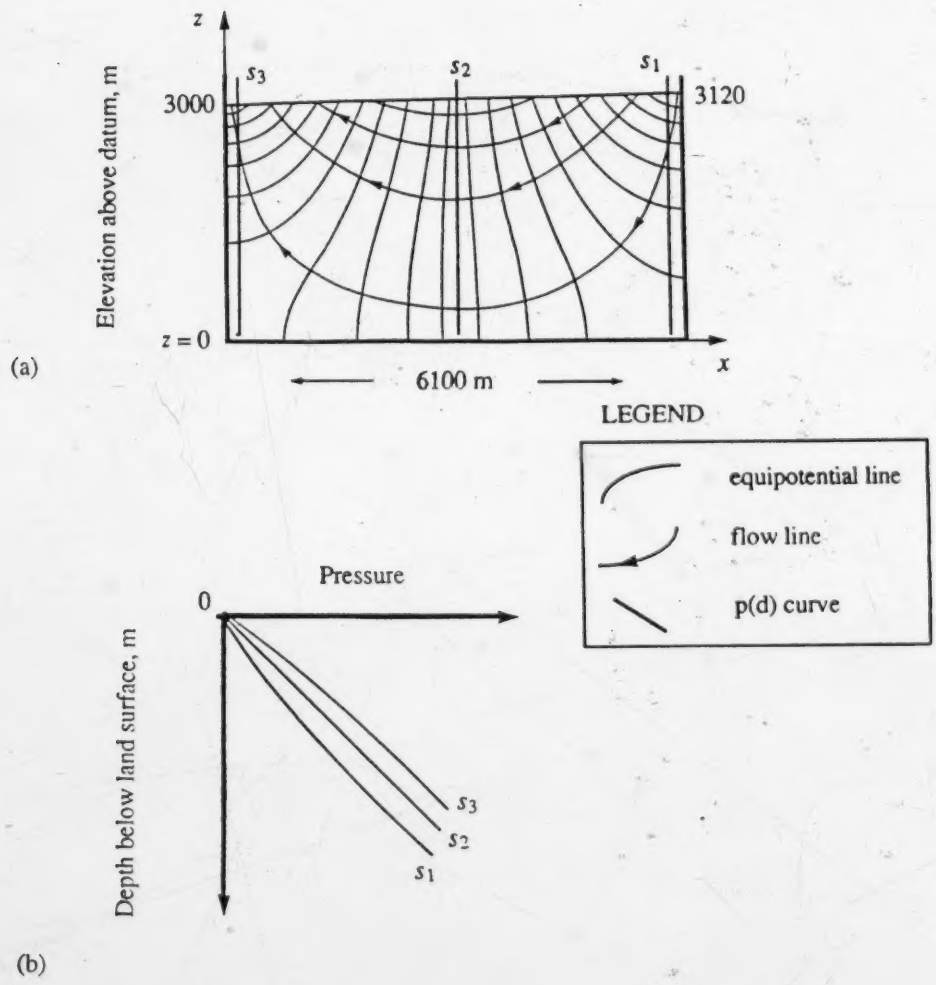

Fig. 2.11 Patterns of: (a) hydraulic head and flow, and (b) pressure-depth in a homogeneous basin with simple topography (after Tóth, 1979, Fig. 1).

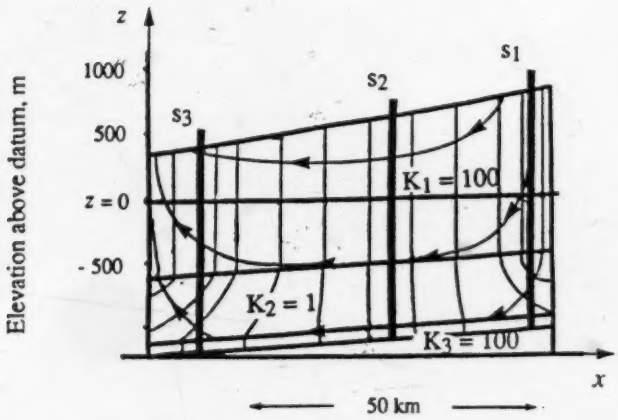

(a)

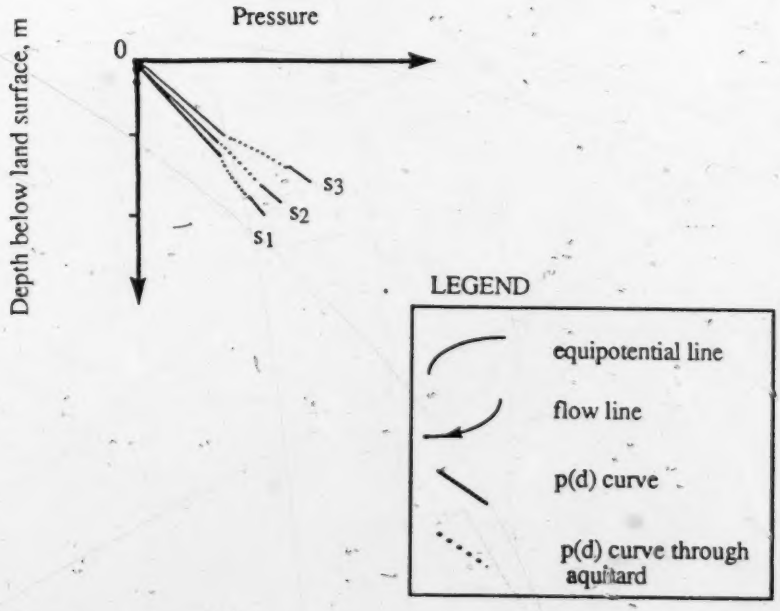

(b)

Fig. 2.12 Patterns of: (a) hydraulic head and flow, and (b) pressure-depth in a heterogeneous basin with simple topography and a thin, extensive aquitard (after Tóth, 1979, Fig. 2).

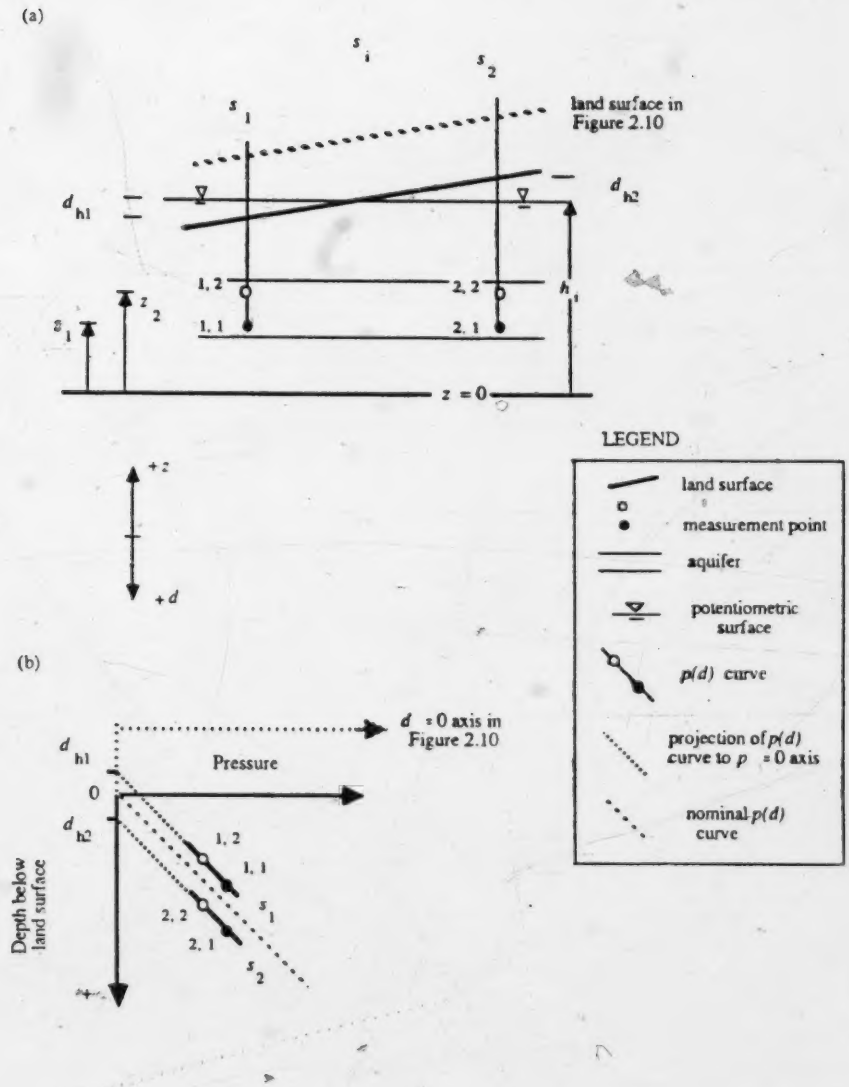

Fig. 2.13 (a) Horizontal potentiometric surface intercepts sloping land surface, (b) the associated pressure-depth pattern.

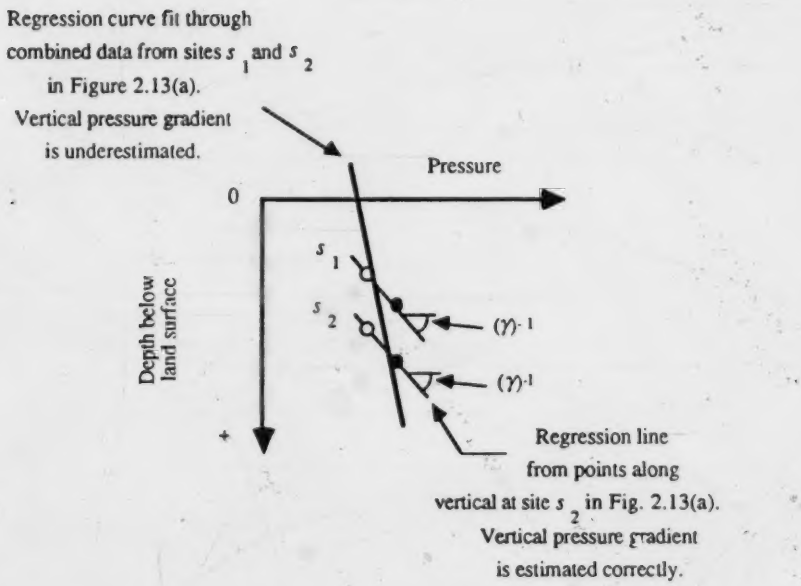

Fig. 2.14 Regression curve fit through pressure-depth data combined from both wells in Fig. 2.13(a), and curves fit through data from each well. Curve through areally-distributed data underestimates the vertical pressure gradient. Curve through data from single, vertical well graphically represents the vertical pressure gradient.

Table 2.1 - Representative values of hydraulic conductivity K for unconsolidated and consolidated sedimentary rocks (after Domenico and Schwartz, 1990)

Material	Hydraulic conductivity (m/s)
UNCONSOLIDATED ROCKS	
Gravel	$3 \cdot 10^{-4}$ - $3 \cdot 10^{-2}$
Coarse sand	$9 \cdot 10^{-7}$ - $6 \cdot 10^{-3}$
Medium sand	$9 \cdot 10^{-4}$ - $5 \cdot 10^{-4}$
Fine sand	$2 \cdot 10^{-7}$ - $2 \cdot 10^{-4}$
Silt	$1 \cdot 10^{-9}$ - $2 \cdot 10^{-5}$
Till	$1 \cdot 10^{-12}$ - $2 \cdot 10^{-6}$
Clay	$1 \cdot 10^{-11}$ - $4.7 \cdot 10^{-9}$
CONSOLIDATED SEDIMENTARY ROCKS	
Karst and reef limestone	$1 \cdot 10^{-6}$ - $2 \cdot 10^{-2}$
Limestone, dolomite	$1 \cdot 10^{-9}$ - $6 \cdot 10^{-6}$
Sandstone	$3 \cdot 10^{-10}$ - $6 \cdot 10^{-6}$
Siltstone	$1 \cdot 10^{-11}$ - $1.4 \cdot 10^{-8}$
Salt	$1 \cdot 10^{-12}$ - $1 \cdot 10^{-10}$
Anhydrite	$4 \cdot 10^{-13}$ - $2 \cdot 10^{-8}$
Shale	$1 \cdot 10^{-13}$ - $2 \cdot 10^{-9}$

3. FINITE DIFFERENCE MODELING TO OBTAIN THEORETICAL VERTICAL PRESSURE GRADIENTS

In the theoretical analysis of the properties of *p(z)* and *p(d)* patterns, a finite difference model was employed. The model simulates the hydraulic head distribution associated with steady-state, gravity-driven groundwater flow. The flow is modeled in basins of different topographic configurations and stratified permeability distributions. The simulation output consists of the hydraulic head at discrete points of the flow domain. These data permit the generation of *p(z)* and *p(d)* plots, as well as the construction of vertical sections of hydraulic head which are used in the analysis of the pressure gradient patterns. In this chapter, the general method of finite differences is discussed briefly, as are the implementation and output of the chosen code.

3.1 Finite Differences

The general idea of the finite difference method is to approximate a continuous differential equation with algebraic difference equations at each of a finite number of points in a problem domain (Remson et al., 1971). By superimposing a grid of orthogonal lines parallel to the coordinate axes, the problem domain is discretized spatially into rectilinear cells. Within a cell the rock and fluid properties are assumed constant. At the central point or "node" of an interior cell the unknown head is expressed by the ratios of head differences over finite distances to adjacent nodes, with coefficients given by the known parameters, including the rock and fluid parameters and the boundary conditions.

The finite difference approximation of Richard's equation [Section 2.2] in two-dimensions can be obtained either mathematically by a Taylor series expansion of $h = h(x, y, z)$ about the independent variables (Remson et al., 1971), or physically by consideration of Darcy's law and formulation of the equation of continuity for grid cells (McDonald and Harbaugh, 1988). The result in either case is the same.

The approximation of derivatives by differences is illustrated by considering the interior node P of the rectangular grid shown in Figure 3.1. Let the coordinates of P be (x_i, z_j) where $x_i = i\Delta x$ for i = 0, 1, 2, ..., n, and $z_j = j\Delta z$ for j = 0, 1, 2, ..., m. The head $h(x_i, z_j)$ at P is denoted by h_{ij}. At P a finite difference approximation of the first partial derivative of h with respect to x is (Remson et al., 1971)

$$\frac{\partial h_{ij}}{\partial x} \approx \frac{h_{i+1,j} - h_{i-1,j}}{2\Delta x} . \qquad (3.1)$$

Similarly, the partial derivative of h with respect to z is approximated by

$$\frac{\partial h_{ij}}{\partial z} \approx \frac{h_{i,j+1} - h_{i,j-1}}{2\Delta z} . \qquad (3.2)$$

The first term on the left of Richard's equation can be written

$$\frac{\partial}{\partial x}\left[K(x,z)\,\frac{\partial h_{ij}}{\partial x}\right] \approx \frac{K_{i+1/2,j}\left(\frac{h_{i+1,j} - h_{i,j}}{2\Delta x}\right) - K_{i-1/2,j}\left(\frac{h_{i,j} - h_{i-1,j}}{2\Delta x}\right)}{\Delta x} , \qquad (3.3)$$

and the second term as

$$\frac{\partial}{\partial z}\left[K(x,z)\,\frac{\partial h_{ij}}{\partial z}\right] \approx \frac{K_{i,j+1/2}\left(\frac{h_{i,j+1} - h_{i,j}}{2\Delta z}\right) - K_{i,j-1/2}\left(\frac{h_{i,j} - h_{i,j-1}}{2\Delta z}\right)}{\Delta z} , \qquad (3.4)$$

where $K_{i+1/2,j}$ is the average value of hydraulic conductivity K between $(x_{i+1,j})$ and $(x_{i,j})$, and defined similarly are $K_{i-1/2,j}$, $K_{i,j+1/2}$, $K_{i,j-1/2}$.

Adding (3.3) and (3.4) and equating to zero yields the finite difference approximation of Richard's equation,

$$\frac{1}{\Delta x^2}\left[K_{i+1/2,j}\,(h_{i+1,j} - h_{i,j}) - K_{i-1/2,j}\,(h_{i,j} - h_{i-1,j})\right] +$$

$$\frac{1}{\Delta z^2}\left[K_{i,j+1/2}\,(h_{i,j+1} - h_{i,j}) - K_{i,j-1/2}\,(h_{i,j} - h_{i,j-1})\right] = 0 . \qquad (3.5)$$

For the heterogeneous, isotropic case $K_{i,j+1/2} = K_{i+1/2,j} = K_{i-1/2,j} = K_{i,j-1/2} = K_{i,j}$ and (3.5) is simplified (Freeze, 1969),

$$\frac{1}{\Delta x^2}[K_{i,j}(h_{i+1,j} - 2h_{i,j} + h_{i-1,j})] +$$

$$\frac{1}{\Delta z^2}[K_{i,j}(h_{i,j+1} - 2h_{i,j} + h_{i,j-1})] \qquad (3.6)$$

With the head h_{ij} as the unknown, equation (3.6) is formulated for each internal node of a flow region. The known parameters are the nodal spacing, the hydraulic conductivities, and the hydraulic heads specified at the water table. A system of n equations in n unknown heads with coefficients determined by the known parameters is written for the n interior nodes. In matrix form, the system of equations is

$$[\mathbf{A}]\{h\} = \{f\}, \qquad (3.7)$$

where [**A**] is the matrix of the known coefficients, $\{h\}$ is the vector of the unknown heads and $\{f\}$ is the vector of heads specified at the boundaries.

Solution of (3.7) is mathematically simple by direct methods, e.g., Gaussian elimination, but computationally expensive for large matrices. To improve efficiency, numerous iterative and combined iterative-direct methods of solution have been devised. Briefly, an "iteration" consists of computing the hydraulic heads h_{ij} node by node in a regular manner across the grid using the assigned or most recently computed heads from neighboring nodes. After successive iterations the calculated heads tend more closely to the final values. The "residual" is the difference in head at a given node from one iteration to the next. The "convergence criterion" is the specified head change at any given node to be tolerated for an acceptable solution. When all residuals are less than the convergence criterion, a numerical solution to (3.7) is found and iteration stops.

Among the iterative-direct solution methods, the strongly implicit procedure (SIP), the one chosen for this study, is considered to converge fastest for problems of steady-state flow in heterogeneous or anisotropic media (Remson et al., 1971). In short, the procedure consists of finding a matrix [**B**] which is "close" to [**A**] above such that the matrix [**A** + **B**] can be decomposed into upper and lower triangular matrices, which are more amenable to direct solution (Wang and Anderson, 1982). Detailed discussion of SIP is found in McDonald and Harbaugh (1988) and Remson et al. (1971).

3.2 General Description and Choice of MODFLOW

The finite difference code MODFLOW (McDonald and Harbaugh, 1988) is a descendent of a widely-employed groundwater flow model developed by Trescott, Pinder and Larson (1976). The program is written in FORTRAN 77. Put to its most general use, MODFLOW can solve three dimensional boundary value problems in the diffusion equation. Of relevance to this study, MODFLOW can also solve problems in Richard's equation. As discussed in Section 2.3, the accompanying boundary conditions are those identified by Tóth (1962, 1963).

MODFLOW is structured of a main code and numerous independent subroutines grouped into optional "packages", summoned according to the needs of a solution. The packages invoked for the present study are the "basic", the "block-centered flow", and the "SIP" packages. Implementation of the packages is described shortly.

MODFLOW was selected for the following reasons. First, the modular structure of the program is particularly suited to sensitivity analysis of permeability distribution. Second, the program is well-documented and well-used, so that a minimum of internal programming errors can be expected. Last, the wide lateral extent of the modeled basins made attractive the capability of a rectangular grid, since a square grid would result in an unnecessarily large number of nodes.

3.3 Geometry of Model Basins

The basins in this study share the same ratio 1: 20 of mean depth to lateral extent, as measured from the water table to the basal boundary and between the major hydraulic divides. The ratio was chosen from examination of the regional topography and depth to the basement in the Western Canada Sedimentary Basin. From major water shed divides to the valleys of large rivers the distance is generally on the order of 40 km, and the thickness of Phanerozoic strata across the middle portions of the basin is 2 km (Porter et al., 1982).

A simple and a complex topography are considered. MODFLOW demands that units of length be specified so that the regional high is assigned an elevation of 1200 m above the standard datum surface, defined at the basal no-flow boundary, and the elevation of the valley bottom is 800 m. The mean depth from land surface to basement is therefore

1000 m. From the major topographic high to the low, the distance is 20 km. Thus, referring to Figure 3.2, the simple topography slopes linearly at -20 m/km or -0.02. The complex topography has four pairs of smaller-scale hills and valleys superimposed on the regional slope. An example of this configuration is given in Chapter 4. This local relief is approximated by linear segments having slopes of -0.05217 and 0.01217.

3.4 Model Discretization

The same grid is used for all simulations in which the topography is the same, even if permeability distribution is changed. There were two constraints to the grid discretization. First, a high degree of precision was desirable for the analysis of vertical pressure variation; second, a maximum of three hydrostratigraphic units were to be allowed for a given simulation. These factors restricted the vertical separation between nodes, which in turn limits the horizontal separation.

Considering the first factor, too large a vertical distance between nodes was feared to render invisible small but important changes in the value of the vertical pressure gradient. On the other hand, too small a separation is expensive and yields little quantitative improvement of results. A 20 m vertical distance between nodes was thought reasonable.

To accommodate a maximum of three different strata, boundaries of possible hydrostratigraphic units are at elevations of 300 m and 600 m (Fig. 3.2). Thus, for a three layer case, a lower and a middle stratum distinguished by their contrasting permeabilities each has a thickness of 300 m, while the upper formation bounded by the land surface has variable thickness. Alternatively, a two layer case is specified, for instance, by making the permeability of lower and middle units equal.

Relatively large head gradients are expected at stratigraphic boundaries with a large permeability contrast. Generally associated with these rapid head changes are difficulties in convergence. Convergence is facilitated if the mesh is made finer. To increase the rate of convergence, the vertical distance between nodes in these areas is reduced from 20 m to 10 m (Fig. 3.2). The maximum number of nodes along the vertical is 72.

The vertical node separation necessitates a similarly narrow spacing in the horizontal, since the finite difference approximation becomes less precise as the ratio of width to length of cells departs from unity. Although a square mesh is ideal, in this study it would generate a prohibitively large number of nodes, given both the relatively broad

lateral extent of a basin and the small vertical distance between nodes. Instead, a rectangular grid is used. As an upper restraint on cell geometry , solutions are considered unreliable when the ratio of width to length of cells exceeds 1:100 (de Marsily, 1986). In trial simulations of a homogeneous basin, the horizontal distance between nodes was initially 1000 m but this was too coarse since the resulting equipotential pattern consisted simply of a series of vertical lines. The distance was decreased to 500 m and then 100 m. Comparing these meshes, it appeared that the 100 m grid gave a sufficiently improved solution to justify its use for the actual simulations. The resulting grid for the cases of simple topography is illustrated in Fig. 3.2.

3.5 Flow Simulation

The parameters needed for the modeling are supplied to the "basic", "block-centered", and "SIP" packages. An example of these data, either entered manually or generated by programs written independently of MODFLOW, is provided in Appendix A.

In the basic package the simulation is designated as steady-state, the numbers of rows and columns of the mesh are specified, and each cell is designated either as "constant" head, no-flow, or "variable" head, i.e., corresponding respectively to cells at the water table, at the vertical and basal boundaries, and in the interior. Head values at the water table and the initial heads of the interior nodes are also assigned here. The programs written to generate these water table and starting heads are included in Appendix A.

Cell geometry as well as formation transmissivity are required by the block-centered flow package. For a given simulation, a stratum is assigned one of four hydraulic conductivities ranging from $K = 10^{-7}$ m/s to $K = 10^{-10}$ m/s, and differing incrementally by an order of magnitude. The high and low values are reasonable ones for consolidated sandstone and shale respectively (Freeze and Cherry, 1979). As well, the high value of K is within an order of magnitude of those determined (Hitchon et al., 1989a, 1989b) from drillstem tests for the lower Mannville Group strata in north and east central Alberta ($K = 6.7 \cdot 10^{-8}$ m/s), while the lower value corresponds well with that of the Joli Fou shales ($K = 1.4 \cdot 10^{-10}$). The vertical pressure distributions associated with these strata are analyzed in Chapter 5.

The convention of MODFLOW for spatial discretization is illustrated in Figure 3.3(a). Vertical discretization is in terms of "layers" and the horizontal discretization is by

"rows" and "columns". For two practical reasons this convention was not followed. First, the maximum number of "layers" is 80 and it was not initially known whether this number would be sufficient. Second, the entry of cell dimension and hydraulic conductivity data is very cumbersome and repetitious under this convention, since the layers are treated as if they define individual strata and their conductivities must be specified layer by layer. Instead, the flow was modeled in a single layer of rows and columns, with the rows parallel to the x-axis and the columns parallel to the z-axis, Fig. 3.3(b).

The convention chosen one way or another does not affect the solution, since the eventual values of head are relative to a common "horizontal" datum and the gravitational force is embodied in the expression of head itself. Thus the solution obtained in a flow domain defined by rows and columns in a single layer is the same as that determined in a region defined by layers and columns in a single row, so long as the spatial and geometrical relations between the "horizontal" datum and the head values at a boundary are the same.

In choosing this convention, however, the program requires that the thickness of the layer be given implicitly as a transmissivity. Thus hydraulic conductivities are entered indirectly. A constant "layer" thickness of $b = 20$ m was assumed, transmissivities T were calculated from the hydraulic conductivities by the relation $T = Kb$, and these were supplied to the code. More detailed description of the requirements of simulation are in McDonald and Harbaugh (1988). A program for generating transmissivities is provided in Appendix A.

Once the finite difference equations have been formulated, the SIP package solves the system of equations. The maximum number of iterations for convergence was set at 350 and a $1.0 \cdot 10^{-5}$ m convergence criterion was specified (Appendix A). In general about 150 iterations were needed to arrive at a solution.

3.6 Simulation Output

Output was channelled into three files. A first, voluminous one generated automatically by MODFLOW summarizes the input parameters for each cell, i.e., width, length and hydraulic conductivity, as well as the final values of head. An example of this file is in Appendix A. A second file, generated by modification of the MODFLOW code, contains heads h_{ij} at x_i and z_j node coordinates. These data were read as input to the

program SURFACE II (Sampson, 1975), which contoured the heads and generated the hydraulic sections.

The solution for the homogeneous basin was verified by comparison of the equipotential distribution with those determined by Tóth (1962) and Freeze (1969) for similar basins. A more general measure of the validity of a solution is a summation of the difference between inflow and outflow of each cell. For most of the simulations this measure of mass balance was zero, as ideally it should be for steady-state flow. The maximum difference was 0.03 m^3/s.

A third file contains the elevations z_j along distances x_i, the depths d_{ij} of nodes below the land surface, and the pressures p_{ij}. From this file the *p(z)* and *p(d)* plots are constructed. The pressures p_{ij} were calculated by

$$p_{ij} = (h_{ij} - z_j)\rho g \ , \tag{3.8}$$

where a specific weight, or hydrostatic pressure gradient, ρg = 9.80665 kPa/m was specified. Many examples of the hydraulic sections and the *p(z)* and *p(d)* plots are found in Chapter 4.

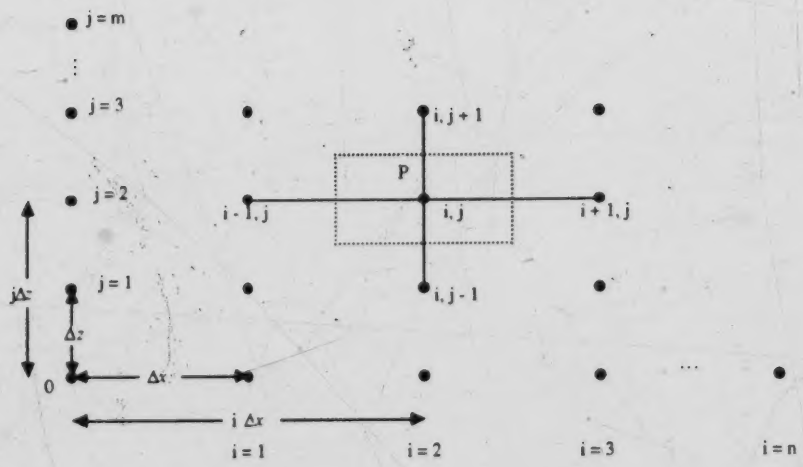

Fig. 3.1 General notation of nodes of a finite difference mesh (after Remson et al., 1971, Fig. 3.2).

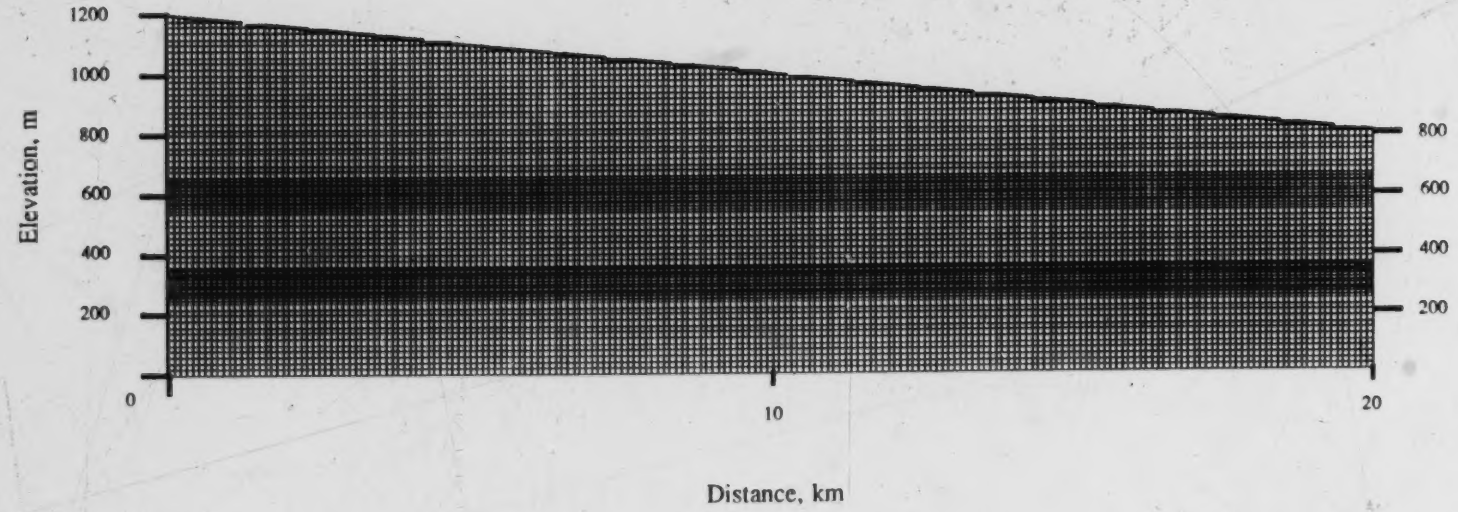

Fig. 3.2 The finite difference mesh for simple topography.

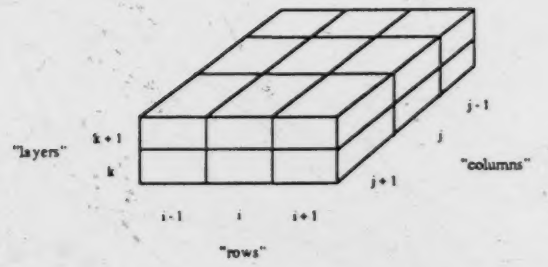

(a)

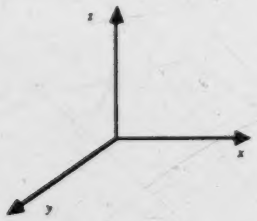

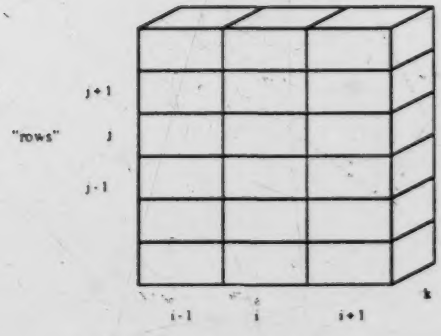

(b)

Fig. 3.3 Convention of (a) MODFLOW, and (b) this study for spatial discretization.

4. RESULTS OF MODELING PRESSURE-DEPTH AND PRESSURE-ELEVATION PATTERNS

Presented in this chapter are the *p(d)* and *p(z)* plots derived from models of topography-induced steady-state, basinal flow of groundwater. The calculated pressure data are analyzed in terms of the values and gradients of hydraulic head. The analysis reveals characteristic relations between the nature of a groundwater flow field, i.e., the magnitude and direction of the hydraulic gradient, and the associated *p(d)* -*p(z)* pattern. A distinct *p(d)*-*p(z)* pattern emerges when the groundwater motion is influenced by the topography. The results lead to a combined *p(d)*-*p(z)* technique that can be applied generally to the investigation of basinal groundwater flow.

4.1 Terminology

The literature of subsurface pore-pressures, unfortunately, is replete with similar terms sharing poorly defined meanings. To facilitate discussion of the results, the following terms are herein defined.

pore-pressure, formation-fluid pressure, formation pressure: at a point in a fluid occupying void space in rock beneath the land surface, the normal force per unit area acting on an infinitesimal plane situated at the point. In this study, the fluid is water.

vertical pressure gradient: the vertical rate of pore-pressure change. From Section (2.1), it is the vertical component $\partial p/\partial d = -\partial p/\partial z$ of the pressure gradient **grad***p*, where $p = p(x, y, z)$. The vertical pressure gradient is the actual rate of pressure change, not the nominal rate of a static condition.

hydrostatic can describe either a pore-pressure or a vertical pressure gradient. A pressure is hydrostatic at a point if it equals the normal force per unit area, i.e., the weight, exerted by a column of water that extends vertically from that point to the overlying water table,

$$p = \gamma d \quad \text{and} \quad p = \gamma(z_o - z), \tag{4.1}$$

where γ is the water's specific weight, d is depth below the water table, z_0 is the elevation of the water table relative to a horizontal datum, and z is the elevation. A hydrostatic pressure means that the hydraulic head h equals the elevation of the vertically overlying water table, i.e., $h = z_0$.

A vertical pressure gradient is hydrostatic if it equals the water's specific weight γ [Sec. 2.1]. A vertical pressure gradient can be hydrostatic either when the water is static,

$$\frac{dp}{dd} = -\frac{dp}{dz} = \gamma, \tag{4.2}$$

in which case the derivatives are normal since $p = p(z)$, i.e., the pressure only varies vertically; or when the groundwater driving force is horizontal,

$$\frac{\partial p}{\partial d} = -\frac{\partial p}{\partial z} = \gamma, \tag{4.3}$$

in which case the derivatives are partial since $p = p(x, y, z)$, i.e., the pressure also varies horizontally. A hydrostatic vertical pressure gradient indicates not the total absence of a groundwater driving force, but only the lack of a vertical force component.

superhydrostatic can similarly describe either a pressure or a vertical pressure gradient. A pressure is superhydrostatic when greater than the weight of the overlying water column,

$$p > \gamma d = \gamma (z_0 - z) . \tag{4.4}$$

A superhydrostatic pressure means that the hydraulic head at a point exceeds the elevation of the vertically overlying water table, i.e., $h > z_0$.

A vertical pressure gradient is superhydrostatic when greater than the water's specific weight,

$$\frac{\partial p}{\partial d} = -\frac{\partial p}{\partial z} > \gamma . \tag{4.5}$$

A superhydrostatic vertical pressure gradient means that the groundwater driving force has an upward component [Sec. 2.1].

subhydrostatic can also be applied either to a pressure or a vertical pressure gradient, such that,

$$p < \gamma d = \gamma (z_o - z) , \tag{4.6}$$

or,

$$\frac{\partial p}{\partial d} = - \frac{\partial p}{\partial z} < \gamma, \tag{4.7}$$

respectively. A subhydrostatic pressure indicates that the head at a point is less than the elevation of the vertically overlying water table, i.e., $h < z_o$. A subhydrostatic vertical pressure gradient signifies a downward force component.

nominal *p(d)* curve (Tóth, 1978; 1979): the representation of equation (4.1) on a *p(d)* graph, i.e., of the vertical rate of pressure increase in a column of static water with given density. A nominal *p(d)* curve allows easy visual comparison of actual pressure values and vertical pressure gradients, and in turn values and gradients of head, with those expected for static water.

In this study the elevations of the land surface and the water table are assumed to coincide, and by definition $p = 0$ at the water table. Therefore, a nominal *p(d)* curve will intercept a plot's origin regardless of basinal topography. Nominal *p(z)* curves can also be constructed, but are cumbersome since a different curve will occur for each difference in water table elevation, i.e., the $p = 0$ intercepts will vary.

gradient curve: a curve on a *p(d)* or *p(z)* plot which joins pressures along a vertical. The slope of a gradient curve is the graphical representation of the vertical pressure gradient, $\partial p/\partial d = - \partial p/\partial z$. Description of the slope as "superhydrostatic", "hydrostatic" or "subhydrostatic" indicates the vertical sense of the driving force. From the vertical pressure gradient $\partial p/\partial d$, the vertical hydraulic gradient $\partial h/\partial d$ can be determined [Sec. 2.7],

$$\frac{\partial h}{\partial d} = \frac{1}{\gamma} \frac{\partial p}{\partial d} - 1 . \tag{4.8}$$

Similarly, the vertical hydraulic gradient $\partial h/\partial z$ can be determined from a *p(z)* gradient curve.

intercept curve: a curve on a *p(z)* or *p(d)* plot, the slope of which is given by the specific weight γ of the groundwater. An intercept curve is projected through a point *(p, z)* or *(p, d)* to the $p = 0$ axis of a *p(z)* or *p(d)* plot, respectively.

According to each plot are "elevation-intercept" and "depth-intercept" curves. An elevation-intercept curve is given by

$$h = z + \frac{p}{\gamma}, \tag{4.9}$$

The *z*-intercept *h* on a *p(z)* plot is the hydraulic head or potentiometric elevation at a point of elevation *z* [Section 2.5.2]. A depth-intercept curve is given by

$$d_h = d - \frac{p}{\gamma}. \tag{4.10}$$

The *d*-intercept d_h on a *p(d)* plot is the difference between the vertically overlying water table elevation and the hydraulic head at a point, i.e., $d_h = (z_o - h)$, or the depth to the water column risen from depth *d*, or simply, the potentiometric depth [Section 2.5.3].

Analogously with individual points, a *z*-intercept or *d*-intercept curve can be extrapolated through the mean point $(\bar{p}, \bar{z})$ or $(\bar{p}, \bar{d})$ of a set of pressure measurements. These curves are respectively,

$$\bar{h} = \bar{z} + \frac{\bar{p}}{\gamma} \quad \text{and} \quad \bar{d}_h = \bar{d} - \frac{\bar{p}}{\gamma}, \tag{4.11}$$

where,

$$\bar{p} = \frac{1}{n}\sum_{i=1}^{n} p_i, \quad \bar{z} = \frac{1}{n}\sum_{i=1}^{n} z_i \quad \text{and} \quad \bar{d} = \frac{1}{n}\sum_{i=1}^{n} d_i, \tag{4.12}$$

and n is the number of pressure measurements. The intercept $\bar{h}$ on a *p(z)* plot is the mean hydraulic head of the set and the intercept $\bar{d}_h$ on a *p(d)* plot is the mean potentiometric depth. These mean curves are useful for handling a large number of points. An alternative is to apply regression analysis which, however, yields curves useful neither in slope nor $p = 0$ intercept [Sec. 2.6].

position: the location of an intercept curve with reference to the location of any other intercept curve. Additionally, for a *p(d)* plot, the position of a *d*-intercept curve can be described with respect to the nominal *p(d)* curve.

Position is used to compare hydraulic head values, absolutely in the case of *z*-intercept curves, and relative to the head along the water table in the case of *d*-intercept curves. For example, if the pressures of a *d*-intercept curve are all superhydrostatic, the *d*-intercept curve's position can be described as superhydrostatic. In turn, it follows that the associated hydraulic heads exceed the water table elevation.

For the lack of a better term, "underpressured" is also used to describe the relative positions of *z*- and *d*-intercept curves.

underpressured: If the pressures of one *z*-intercept curve are less than those of another one at points of similar elevation, the position of the former is described as "underpressured" with respect to the latter. Similarly, if the pressures of one *d*-intercept curve are less than those of another at points of similar depth, the former is relatively "underpressured".

Perhaps an illustration would help. Consider the hypothetical *p(z)* and *p(d)* plots in Figure 4.1, which are constructed with measurements from an areally extensive aquifer saturated by water of constant density. One set of measurements is from beneath an Area A bounded on the land surface and another set is from Area B, the areas being separated by some lateral distance.

At one particular site s_1 in Area A, pressures are known at two points along a vertical. Gradient curves of *p(d)* and *p(z)*, which reflect the actual rate of vertical pressure variation, are constructed by joining the two points. Compared to the slope of the nominal *p(d)* curve, the slope of the *p(d)* gradient curve is subhydrostatic, thus indicating a downward force.

Intercept curves are constructed by determining the mean points ($\bar{p}$, $\bar{z}$) and ($\bar{p}$, $\bar{d}$) for each area. A line of hydrostatic slope is then projected through each mean point to the p = 0 axis of a plot. On the *p(d)* plot, with respect to the nominal *p(d)* curve, the position of the *d*-intercept curve from Area A is subhydrostatic, whereas the *d*-intercept curve from Area B is superhydrostatic. Additionally, the *d*-intercept curve from Area A is underpressured with respect to that from Area B. On the *p(z)* graph, the area B *z*-intercept curve is underpressured relative to the area A *z*-intercept curve.

Two essential curve types, gradient and intercept, are used extensively below. Vertical hydraulic gradients are analyzed with gradient curves whereas hydraulic heads and lateral hydraulic gradients are analyzed with intercept curves. Gradient curves are not used to determine hydraulic head, since their slopes are not necessarily hydrostatic. Instead, intercept curves are required. That an intercept curve has hydrostatic slope does not imply that vertical flow is absent. Rather, the computation of head demands a hydrostatic slope. Generally speaking, the need to define gradient and intercept curves arises from the distinction between a gradient of a scalar function and a value of a scalar function.

4.2 Method of Investigation

For the analysis, a hydrostratigraphic unit with hydraulic conductivity of $K = 10^{-8}$ m/s or $K = 10^{-7}$ m/s is considered an aquifer, whereas one with a hydraulic conductivity of 10^{-10} m/s is an aquitard.

The *p(z)* and *p(d)* plots are analyzed by the slopes of gradient curves and positions of intercept curves. Gradient curves of *p(z)* and *p(d)* are constructed for aquitards as well as aquifers at various sites within a basin. The method of determining these slopes is described shortly.

Intercept curves are computed with equation (4.11), but only from data within an aquifer, since large vertical head changes generally occur within aquitards. Large vertical hydraulic gradients are better left characterized by gradient curves. Graphically-determined hydraulic heads $\bar{h}$ and potentiometric depths $\bar{d}_h$ are presented on the elevation and depth axes of the *p(z)* and *p(d)* plots, respectively.

First analyzed are curves from sites separated by a regional scale of distance followed by curves from a local scale.

4.2.1 Estimation of the Vertical Pressure Gradient

The vertical pressure gradient beneath a measurement site is estimated by the method of least squares. Assuming a linear pressure change, the functional relation between pressure and depth within a formation can be expressed as

$$p_k = \alpha\, d_k + \beta\ , \tag{4.13}$$

where p_k is the value of pressure at depth d_k , α is the actual vertical pressure gradient to be estimated, β is the p-intercept which value is dependent on α, and the subscript (k = 1, 2, ..., n) refers to the n vertical points within a formation.

Statistically, as well as functionally, the pressure is treated as the dependent variable and depth as the independent variable, so that error in pressure is the quantity to be minimized. This use of regression is fundamentally different from that described earlier [Sec. 2.6] since only data obtained along a single vertical are used.

It should be stated, however, that estimation of the parameters of a functional relation, e.g., the slope α, is not generally a valid use of least squares. This use is questionable even where two-dimensional spatial relations are not a consideration, since the regression relation and the functional relation do not usually coincide (Lindley, 1947; Williams, 1959; Kendall and Stuart, 1967). Briefly, regression analysis is reserved for the evaluation of a statistically significant relation between variables. If such a relation is found, the value of the dependent variable may then be predicted or estimated at a given value of the independent variable, i.e., the pressure p_k at depth d_k is predicted. Although the terms "dependent" and "independent" are entrenched in regression analysis, causality between variables is not to be inferred (Williams, 1959).

In the case of a functional relation, on the other hand, a relationship among the variables is already known. The matter of interest is instead the estimation of a parameter, i.e., the slope α. That is, pressure is known to increase with depth but the rate of increase is in question. The techniques of determining the regression and functional relations also differ: the former takes into account only the error variance of the dependent variable, and the independent variable is assumed to be measured without error, whereas the latter takes considers the error variances of both variables. Detailed discussion of the distinction between the regression and functional relations is provided by Lindley (1947), Williams

(1959), Kendall and Stuart (1967) and, as applied to problems in physical geography, by Mark and Church (1979).

Importantly, the functional and regression relations do coincide when the independent variable is measured without error (Lindley, 1947). For the numerical models, at least, the depths and elevations are known precisely whereas the heads and in turn the pressures are subject to some small truncation error. Moreover, the $p(d)$ and $p(z)$ relations at a measurement site are one-dimensional, so that the problem of estimating the vertical pressure gradient from spatially distributed data, if it is possible to do so, is set aside. Therefore, subject to these constraints, the estimation of a vertical pressure gradient with linear regression is valid.

Detailed description of the theory and practice of linear regression is given by Williams (1959) and Draper and Smith (1967).

4.3 Results of Regional Scale Investigation

The results of plotting the pressures from laterally separated measurement sites are provided in Figures 4.2 to 4.8. As measured horizontally from a basin's left boundary, the sites are at s_1 = 50 m, s_2 = 10050 m, and s_3 = 19950 m, near the regional topographic high, the geographic midline and the regional topographic low, respectively. Pressure data at a site are grouped vertically. The vertical intervals are z_j where j =1 is from elevations 0 $\leq z_1 <$ 300 m, j = 2 is from 300 m $\leq z_2 <$ 600 m, and j = 3 is from 600 m $\leq z_3 \leq z_o$. Analyzed, then, are the gradient and intercept curves associated with a particular interval at a particular site.

The curves presented on the plots are gradient curves. Intercept curves are not shown since the inclusion of the two curve types would cause unnecessary clutter. For qualitative purposes, gradient curves within aquifers are sufficiently close to hydrostatic to allow their use as intercept curves. Nevertheless, the slopes of gradient curves and the graphically-determined potentiometric elevations $\bar{h}$ and potentiometric depths $\bar{d}_h$ are tabulated. The intercept of a z-intercept curve for a vertical interval at a site is denoted $\bar{h}_{ij}$ where henceforth i = s_1, s_2, s_3 = 1, 2, 3, and j = z_1, z_2, z_3. The intercept of a d-intercept curve is similarly denoted $\bar{d}_{h\,ij}$.

The vertical and horizontal scales of the hydraulic profiles (Figs. 4.2 to 4.8) are equal. There is a 20 m difference between equipotential lines. The relative head along an

equipotential is appraised by the elevation at which it intercepts the land surface, where the pressure is zero and thus $h = z_0$. Flow directions are indicated by arrows normal to the equipotentials. The spacing between equipotentials is inversely proportional to the magnitude of the hydraulic gradient.

First the effects of geology in basins with simple topography and then the effects of complex topography are examined.

4.3.1 Effects of Geology

The effects of different permeability distributions are illustrated in Figs. 4.2 to 4.6. In all cases, the topographic gradient is - 0.02.

Figure 4.2

Fig. 4.2(a) shows a basin with a linearly sloping land surface and homogeneous rock framework. Groundwater motion is predominantly horizontal in a single system. Indicated by the equipotential pattern is a horizontal, indeed total, hydraulic gradient which is nearly equal to the slope of the land surface. Adjacent to the basin margins, apparently weak vertical flow components are revealed by slight deflections of the equipotentials. Nowhere, however, does the hydraulic head at depth differ from that at the water table by more than 20 m. The vertical flow causes slight decreases of the horizontal hydraulic gradient at greater depth.

On the *p(z)* plot, Fig. 4.2(b), the pressure is zero at the land surface elevation of a site. Associated with each site is a distinct curve, widely separated from another. The downward rate of pressure increase appears similar for each site. By contrast, on the *p(d)* plot, the curves begin at the origin and are positioned closely together. Since the flow is horizontal at site s_2, this curve may be used as the nominal one. As may be seen on the *p(d)* plot, the slope is subhydrostatic at the recharge site s_1 and superhydrostatic at the discharge site s_3.

The slopes at sites s_1 and s_3 change along the vertical. The variation is most clearly observed in Table 4.1, which presents the estimated vertical pressure gradients for the upper z_3, middle z_2 and basal z_1 intervals. At sites s_1 and s_3 the slopes are most ahydrostatic along the upper interval z_3 and tend to hydrostatic with depth. This result was observed by Tóth (1978, 1979) and is a consequence of the flow in gravity-driven systems

being most vertical and the hydraulic gradient largest at shallow depths near the hydraulic divides.

Broadly across the central portion of the basin, as at site s_2, hydrostatic slopes would be observed, yet nowhere are the conditions static. Instead, flow occurs in all parts of the basin and is intensive horizontally.

On the *p(z)* plot, the curves are positioned such that the one from the site s_3 is underpressured relative to the site s_2 curve, which in turn is underpressured with respect to the one from site s_1. Following a curve to its z intercept, the hydraulic head is indicated to decrease laterally from about 1200 m at the recharge site s_1 to 800 m at the discharge site s_3. More precise hydraulic head estimates are provided in Table 4.2, by the intercepts $\bar{h}_{ij}$ of the z-intercept curves. For the basal interval z_1, the relative values of these are such that $\bar{h}_{31} < \bar{h}_{21} < \bar{h}_{11}$. Thus on the *p(z)* plot, the lateral sense of flow is indicated qualitatively by the sense of underpressuring of the *p(z)* curves, and quantitatively by the intercepts $\bar{h}_{ij}$.

Use of the intercepts $\bar{h}_{i1}$ can be taken a step further, to estimate the horizontal hydraulic gradient. Over the 19900 m distance from sites s_1 to s_3, the estimated horizontal hydraulic gradient is $-1.89 \cdot 10^{-2}$ along the basal interval. As expected from the cross-section, Fig. 4.2(a), the hydraulic gradient at depth is decreased relative to the topographic gradient, i.e., $-2.00 \cdot 10^{-2}$.

On the *p(d)* plot, Fig. 4.2(b), the position of the site s_1 curve for the basal interval z_1 is slightly subhydrostatic whereas that of the site s_3 is slightly superhydrostatic. These positions are observed because the hydraulic heads are marginally below the land surface at the recharge area, while above it at the discharge area [Fig. 4.2(a)]. The potentiometric depths for the basin's bottom are quantified by the intercepts $\bar{d}_{hi1}$ (Table 4.2). As expected from the hydraulic head relations, the intercepts for the sites s_1 and s_3 are such that $\bar{d}_{h11} > 0$ and $\bar{d}_{h31} < 0$. The d-intercept curves thus indicate generally downward groundwater motion from the land at site s_1, and upward flow to the land at site s_3. The positions of a d-intercept curves relative to nominal, therefore, reveal the general sense of vertical flow relative to the land surface.

As with the *p(z)* plot, analysis of the d-intercepts can be extended to two dimensions. Note that the *p(d)* curves are serried so that the differences between the intercepts $\bar{d}_{hi1}$ are only about 10 m. Laterally across the basin, then, the potentiometric depth remains nearly constant. Now, for the potentiometric depth to be constant while the land is sloping, it must mean that the potentiometric surface slopes at the same angle as the

land surface. In other words, the two surfaces must be parallel since the distance between them, i.e., the potentiometric depth, is constant.

Remember, by contrast, that if the potentiometric surface is horizontal, while the land surface is sloping, i.e., the two surfaces are no longer parallel, the potentiometric depth will vary across a basin [Sec. 2.5.3]. Correspondingly, the *p(d)* curve spacing will be relatively large, since it is an expression only of the topographic relief. Returning to Fig. 4.2, it appears that when the horizontal hydraulic gradient is nearly equal to the topographic gradient, the result is closely spaced *p(d)* curves.

Finally, it should be noted of the basal *p(d)* curves that the s_1 curve is subtly underpressured with respect to the s_2 curve, which is underpressured relative to the one from s_3. This relative sense of underpressuring of *p(d)* curves is the opposite of that which the same curves take on the *p(z)* plot. Graphically, it may be considered that an exchange of the relative positions has occurred from one plot to another.

Figures 4.3 to 4.5

Each basin has an aquitard overlying a basal aquifer. The hydraulic gradient in an aquitard is largely vertical, except at the small area of a hydraulic midline. Within an aquifer, the hydraulic gradient is predominantly horizontal. From the spacing of equipotentials, much of the available energy is spent driving the flow through an aquitard and, consequently, the hydraulic gradient in an aquifer is relatively low. Although an aquitard dampens the influence of the topography, the direction of flow remains dictated by the slope of the land.

The *p(z)* and *p(d)* patterns of Figures 4.3 to 4.5 share similar features. In contrast to the homogeneous case previously, the curves from an aquifer are pressed together on the *p(z)* while spread apart on the *p(d)*.

In each basin, the vertical pressure gradient through an aquitard is strongly subhydrostatic and superhydrostatic in the recharge and discharge areas, respectively. These cause the values of pressure to be substantially ahydrostatic in the lower aquifer across much of a basin. For example, on the *p(d)* plot of Fig. 4.4, taking the site s_2 curve to approximate the nominal, pressures in the aquifer at sites s_1 and s_3 are about 2000 kPa less than and 1300 kPa greater than the hydrostatic values, solely because of flow through the aquitard. Pressures are hydrostatic only in the hydraulic midline of each basin.

The vertical pressure gradients in each basin are presented in Table 4.3. Like in the homogeneous case, the slopes differ increasingly from hydrostatic toward a hydraulic divide because of the increasing magnitude of the vertical hydraulic gradient. In these instances, however, the low permeability of an aquitard magnifies the effect. In an aquifer, the slopes are essentially hydrostatic at all the sites due to horizontal flow.

The vertical pressure gradients at sites s_1 and s_3 are now compared among the basins (Table 4.3). The most greatly ahydrostatic slopes are from the basin with the thin aquitard and thick, homogeneous aquifer (Fig. 4.4), while the least are in the basin with the thick aquitard and thin aquifer (Fig. 4.3). The hydraulic conductivities of the aquitards are equal ($K = 10^{-10}$ m/s). The result is perhaps surprising, since it may be expected that a slope would be more ahydrostatic in a thick aquitard. Nevertheless, while the aquitard's thickness decreases, from Fig. 4.3 to Fig. 4.4, the aquifer's thickness increases. The thicker aquifer allows a comparatively larger volume of water to be conveyed through it. To maintain mass balance, the vertical hydraulic gradient through the thin aquitard must be larger so that a greater volume of water may be driven to and from the aquifer. Thus the gradient curves are strongly ahydrostatic. The vertical pressure gradient, therefore, is influenced not only by the properties of the rock framework in itself, i.e., the permeability contrast and thickness, but perhaps foremost, is an expression of the requirement for mass balance.

Illustrated in Figure 4.5 is a three layer case in which the aquitard is underlain by an aquifer of intermediate permeability ($K = 10^{-8}$ m/s) beneath which there is a higher permeability aquifer ($K = 10^{-7}$ m/s). With reference to Table 4.3, the slopes in the $K = 10^{-8}$ m/s z_2 unit are more ahydrostatic than those at the same sites in the $K = 10^{-7}$ m/s z_2 unit of Fig. 4.4. Generally more prevalent vertical flow can be expected in units of lesser permeability, including those considered aquifers.

For the analysis of curve positions, it is convenient to refer to as the "potentiometric slope" the horizontal hydraulic gradient within an aquifer. On the *p(z)* plot of each basin, the s_3 curve is underpressured relative to the s_2 curve which is underpressured relative to the s_1 curve. Like previously, then, the lateral flow from site s_1 to site s_3 is expressed by the sense of *p(z)* curve underpressuring. As well, the intercepts $\bar{h}_{i1}$ from the z_1 interval are such that the $\bar{h}_{31} < \bar{h}_{21} < \bar{h}_{11}$ (Table 4.4). The differences between the intercepts $\bar{h}_{i1}$, however, are now on the order of 30 m rather than the 200 m observed in the homogeneous basin (cf. Tables 4.4 and 4.2).

The potentiometric slopes are estimated from the differences in z-intercepts $\bar{h}_{i1}$. These are about an order of magnitude less than the topographic slope (Table 4.5). The decrease in the potentiometric slope, compared to the homogeneous case, is signified graphically by the narrower spacing of *p(z)* curves.

The potentiometric slope, as indicated by a *p(z)* plot, is greatest in the aquifer of Fig. 4.5(a) and least in Fig. 4.4(a). This observation can be confirmed by comparing the number of equipotentials of each hydraulic section. The Fig. 4.4(b) *p(z)* pattern warns of the possible misinterpretation of actual data. Together, the close positioning of the curves and the essentially hydrostatic vertical pressure gradients suggest near static water. Yet from Darcy's law the specific discharge, which depends not only on the gradient but also on the transmissivity, is almost twice as large in the aquifer of Fig. 4.4(a) as that in Fig. 4.3(a), as noted by Freeze and Witherspoon (1967) for a similar example.

Turning to the positions of the *p(d)* curves, the basal curves from site s_1 are notably subhydrostatic relative to nominal, from site s_2 they are marginally so, and the s_3 curves are substantially superhydrostatic. Quantitatively, the large positive value of an intercept $\bar{d}_{h11}$ at a recharge site s_1 signifies that the aquifer hydraulic head is about 190 m less than the land surface elevation, while at a discharge site s_3 the large negative intercept $\bar{d}_{h31}$ indicates that the head is about 140 m above the land (Table 4.4). The positions of the *p(d)* curves, relative to nominal, thereby reveal strong downward flow from the land to an aquifer at a site s_1 and strong upward flow at a site s_3.

The position of a *p(d)* curve relative to nominal, however, says nothing about the vertical sense of flow within an aquifer itself. For instance, in Fig.4.4(c) the site s_2 curve has a subhydrostatic position whereas the vertical pressure gradient in the aquifer is hydrostatic (Table 4.3). The position indicates a deficiency of head relative to the vertically overlying water table, but does not mean vertical motion within the aquifer. Therefore, while the position allows inference of the general sense of groundwater flow relative to the land within superjacent strata, the slope of a gradient curve is required to analyze the vertical flow within an aquifer.

The *p(d)* curves may also be examined according to their positions relative to each other. Within an aquifer, the recharge site s_1 *p(d)* curve is underpressured with respect to the midline site s_2 curve which is underpressured relative to the s_3 curve. As the land elevation decreases from recharge area to hydraulic midline, so too does the depth to the potentiometric surface. Expressed graphically, from a site s_1 to s_2, the *p(d)* intercept $\bar{d}_{hi1}$

decreases, since the potentiometric surface is nearly horizontal while the land surface is sloping. From site s_2 to s_3 the potentiometric depth continues to decrease, and indeed, becomes negative. Therefore, as the potentiometric surface approaches the horizontal, i.e., the horizontal hydraulic gradient nears zero, the *p(d)* curves become more spread. By contrast, in the homogeneous basin previously, when the horizontal hydraulic gradient approximates the topographic gradient, the *p(d)* curves are close together.

The above outlined sense of underpressuring of the *p(d)* curves is opposite to the sense of underpressuring of the *p(z)* curves. As in the homogeneous basin, the curves exchange positions from one type of plot to the other. The exchange of the curve positions is therefore a characteristic feature of the combined *p(d)* and *p(z)* patterns from the two types of basins, i.e., homogeneous and stratified. By contrast, however, the *p(z)* curves in the homogeneous basin are widely spaced and the *p(d)* curves are serried (Fig. 4.2), whereas the *p(z)* curves in a stratified basin are serried and the *p(d)* curves are spread apart (e.g., Fig. 4.3). While the styles of flow differ, largely by the magnitude of the horizontal hydraulic gradient, the common feature of both basin types is that the flow is driven laterally toward decreasing potentiometric depth by the topographic relief.

Figure 4.6

Figure 4.6(a) illustrates the equipotential pattern when an aquitard of hydraulic conductivity $K = 10^{-10}$ m/s, is positioned between an upper and lower aquifer, each with $K = 10^{-7}$ m/s. As previously, the flow is predominantly horizontal in an aquifer whereas it has a strong vertical component in the aquitard. The horizontal hydraulic gradient in the upper aquifer is approximately equal to the topographic gradient, while that in the lower aquifer is somewhat less.

Over much of the basin, the vertical hydraulic gradient changes markedly across the upper and lower aquitard boundaries. On the *p(z)* and *p(d)* plots, these changes in magnitude give rise to the three-slope forms of the gradient curves at sites s_1 and s_3. Within the upper and lower aquifers the slopes at sites s_1 and s_3 are nearly hydrostatic. Through the aquitard at site s_1, the slope is notably subhydrostatic, indicating strong recharge from the upper aquifer to the lower one, while the superhydrostatic slope at site s_3 reveals strong upward flow. At site s_2, the slope is approximately hydrostatic throughout the basin's depth. The vertical pressure gradients are provided in Table 4.6.

The behavior of the slope points to the fallacy in the frequently made assumption that a sharp change in the vertical pressure gradient indicates impermeability. Indeed, the cross-formational flux is directly dependent on the magnitude of the vertical hydraulic gradient, which is linked intrinsically to the vertical pressure gradient. A corollary of the impermeability assumption is that the closer the cross-formational vertical pressure gradient approaches hydrostatic, the greater the hydraulic communication. In Fig. 4.6 the hydraulic conductivity of the aquitard is constant. Yet in moving from site s_1 or s_3 toward the hydraulic midline, the cross-formational vertical pressure gradient approaches hydrostatic, simply because the hydraulic head is vertically constant. In a hydraulically continuous medium, the three-slope form of a vertical pressure gradient is a signature of cross-formational flow.

On a *p(z)* plot, the *z*-intercepts $\bar{h}_{ij}$ can be used to indicate the cross-stratigraphic head difference at a site. For instance at the discharge site s_3, the intercept $\bar{h}_{31}$ for the basal z_1 formation yields a hydraulic head of about 966 m [Fig. 4.6(b)]. At the same site for the upper z_3 interval, the intercept $\bar{h}_{33}$ indicates an 800 m head. The upward flow across the aquitard is thus revealed on the *p(z)* plot by the upward decline in hydraulic head. Following the same technique at site s_1, flow from the upper to the lower aquifer is indicated. Knowing the aquitard thickness, the vertical hydraulic gradients may also be calculated with the *z*-intercepts.

The combined *p(z)* and *p(d)* pattern in Fig. 4.6 summarizes many properties of the intercept curve positions so far observed. Where the horizontal hydraulic gradient is large, as in the upper aquifer of Fig. 4.6 and in the homogeneous basin (Fig. 4.2), the *p(z)* curves are widely separated; where it is slight, as in the lower aquifer of Fig. 4.6 and in the stratified basins previously (Figs. 4.3 to 4.5), the *p(z)* curves are narrowly separated. For equidistant sites, therefore, the degree of *p(z)* curve separation is proportional to the horizontal hydraulic gradient. As for the *p(d)* curves, where they are positioned closely together, as in the upper aquifer of Fig. 4.6 and in the homogeneous basin, the horizontal hydraulic gradient is about the same as the topographic gradient. Where the *p(d)* curve separation is large, as in the lower aquifer of Fig. 4.6 and in the stratified basins, the potentiometric slope is much less than the topographic gradient.

4.3.2 Effects of Topography

The effects of imposing local topographic relief are illustrated in Figures 4.7 and 4.8. The permeability distributions are as in the basins of Figs. 4.2 and 4.3, respectively, i.e., a homogeneous basin and one with a thick upper aquitard ($K = 10^{-10}$ m/s) and thin basal aquifer ($K = 10^{-7}$ m/s). Pressure measurements are again taken at the sites s_1, s_2 and s_3 separated by a regional distance.

Figure 4.7 - Homogeneous basin with complex topography

Relatively deep local flow systems are developed so that the larger basin is partitioned hydraulically into several smaller ones. Because of the local water divides, vertical flow is more prevalent and more intense than is the case of simple topography. The hydraulic gradient is strongest at shallow depth near the steepest slopes of the land surface. Along the basal boundary hydraulic gradient is clearly influenced by local topography, yet the basal groundwater flow is to the major valley because of the regional topographic relief.

The vertical pressure gradients are given in Table 4.7. Although difficult to see on the plots, the slopes are more ahydrostatic than in the simple basin (cf. Tables 4.1 and 4.7). Once again, the most ahydrostatic slopes are nearest the water table, while they approach hydrostatic with depth. Contrary to the simple case, the slopes at site s_2 are also superhydrostatic and indicate upward flow under a vertical hydraulic gradient similar in magnitude to that at site s_3. However, the s_2 curve is from points within a local and the regional flow system, whereas the s_3 curve is entirely in the regional system. Unless a reversal of the vertical sense of flow occurs, it appears that a boundary between flow systems of different order cannot be determined with a gradient curve, since no physical change is associated with the boundary, as noted by Tóth (1963).

The positions of the $p(z)$ intercept curves indicate a decline in hydraulic head from site s_1 to s_3. While the relative positions reveal the sense and magnitude of the lateral head decrease, a number of local head extrema occur between the sites. These would invalidate an inference of direct flow from sites s_1 to s_3, which occurs only along the base. This example, therefore, illustrates that laterally uninterrupted motion should not be concluded from a $p(z)$ pattern when the sites are separated by a distance exceeding the extent of a flow system.

Nevertheless, the overall *p(z)* and *p(d)* patterns in Fig. 4.7 are very similar to those in the simple basin (Fig. 4.2). The distinct, broadly-spaced *p(z)* curves signify a large head decrease across the basin. Simultaneously, the serried *p(d)* curves indicate that this basin-wide head change is similar in magnitude to the regional topographic relief. Thus, while uninterrupted lateral flow cannot be inferred, this combined *p(d)-p(z)* pattern is observed consistently when the basinal head decrease is about the same as the regional change in land surface elevation, i.e., there is hydraulic continuity.

Figure 4.8 - Stratified basin with complex topography

The groundwater motion here is largely vertical in the aquitard and horizontal in the aquifer. The local flow reaches only to shallow depth so that the lower aquifer's hydraulic gradient is unaffected by the local topography (cf. Figs. 4.3 and 4.8).

At this scale of investigation, the local relief induces little difference between this combined *p(d)-p(z)* pattern and that of Fig. 4.3. Although flow within the aquifer is laterally continuous, this cannot be inferred since the coarse resolution of the *p(z)* and *p(d)* plots would leave undetected any local head extrema. Rather than speaking of flow, therefore, the positions of the curves must be interpreted in terms of magnitudes of head changes.

In any case, within the aquifer, the hydrostatic slopes reveal little vertical flow, while a relatively small lateral head decline from recharge site s_1 to discharge site s_3 is indicated by the spreading and sense of underpressuring of the *p(z)* curves. Relative to nominal, approximated by the s_2 curve, the *p(d)* curve positions reveal downward flow from the land surface, i.e., through the aquitard, at site s_1, and upward flow at site s_3. Relative to each other, the *p(d)* curves indicate a decrease in the potentiometric depth from site s_1 to s_3. For the aquifer, the exchange of *p(z)* and *p(d)* curve positions again occurs when the lateral head decline is in the direction of decreasing potentiometric depth.

4.4 Results of Local Scale Investigation

"Local scale" means that the measurement sites are within a local drainage basin. The distance between a local hill and a nearby valley is 3 km. Within a small drainage basin, one measurement site is located near the local topographic high, one near the low, and one near the local midline.

Only the basin in Figure 4.9 is analyzed on a local scale. The basin has complex topography and an aquitard ($K = 10^{-10}$ m/s) positioned between upper and lower aquifers ($K = 10^{-7}$ m/s). Observed are active as well as sluggish local flow in the upper aquifer, and regional flow in the lower aquifer, occurring with and against the local topography.

Sites separated by distances of 1 km are within the Areas "A" and "B" shown in Fig. 4.9. Within an area, sites are denoted s_i where = 1, 2, 3 refers to the lateral location from left to right. The slope of the land surface within Area A is relatively small (0.01217) and is directed oppositely to the direction of the regional slope. Within Area B, on the other hand, the local slope is steeper (-0.05217) and in the direction of the regional topographic decline.

First analyzed are the *p(z)* and *p(d)* plots from Areas A and B in the upper aquifer, followed by the ones from the lower aquifer. The plots are presented in Figures 4.10 to 4.13. The illustrated curves are gradient curves, i.e., they join pressures along a vertical. The gradient curves approximate the *p(z)* and *p(d)* intercept curves, which are not illustrated. Quantitatively, the position of a *z*-intercept and a *d*-intercept curve is anchored by its $p = 0$ intercept, i.e., $\bar{h}$ and $\bar{d}_h$.

Upper Aquifer - Area A

In the upper aquifer of Area A the flow within a local system is from site s_3 to site s_1 (Fig. 4.9). The slight topographic slope generates a weak hydraulic gradient. Recharge occurs at site s_3. Between sites s_1 and s_2 a quasi-stagnant zone is developed, since flow converges from the regional divide and local hill.

The *p(z)* and *p(d)* plots for Area A are illustrated in Figure 4.10. The *p(z)* and *p(d)* patterns are similar in that the curves on both graphs are closely spaced.

The slope of the site s_2 gradient curve is essentially hydrostatic (Table 4.8). The downward flow at site s_3 is indicated by the curve's subhydrostatic slope, especially at higher elevation. The superhydrostatic slope of the site s_1 curve reveals upward flow.

With decreased elevation, the slopes tend to hydrostatic and below an elevation of 950 m, the s_1 and s_2 *p(z)* curves merge. An absence of positional difference on the *p(z)* means a lack of lateral flow. Furthermore, the merging to a hydrostatic slope means the absence of both a vertical and a horizontal hydraulic gradient, i.e., the water is static [Sec. 2.1]. The stagnant zone near the aquitard boundary between sites s_1 and s_2 is thus identified with the *p(z)* plot.

By the *p(z)* curve positions, the hydraulic heads near the water table are seen to decrease from site s_3 to site s_1. By the *z*-intercepts $\bar{h}$, presented in Table 4.9, the horizontal hydraulic gradient between sites s_1 and s_2 is $1.0 \cdot 10^{-4}$ and between s_2 and s_3 it is $8.8 \cdot 10^{-3}$. The narrow spacing between curves is thus a consequence of the low lateral hydraulic gradient.

At shallow depth, the *p(d)* curves also are serried, suggesting a nearly constant potentiometric depth $\bar{d}_h$ from sites s_1 to s_3. In other words, there is little difference between the slope of the land surface and the lateral rate of head variation, as previously in the simple, homogeneous basin (Fig 4.2). The *d*-intercepts $\bar{d}_h$ are presented in Table 4.10. With depth in the static zone, the *p(d)* curves are increasingly separated. Here the spacing is due entirely to the topography.

Upper Aquifer - Area B

At Area B, groundwater motion is from site s_1 to site s_3 under a relatively steep hydraulic gradient (Fig. 4.9). Recharge is at s_1 and discharge at s_3.

The combined *p(z)* and *p(d)* pattern from Area B is illustrated in Figure 4.11. It differs from the previous example chiefly in the greater *p(z)* curve separation, because of the larger horizontal hydraulic gradient. From the intercepts $\bar{h}$ (Table 4.9) the horizontal hydraulic gradient between s_1 and s_3 is about -0.03. The overlying topographic gradient is about -0.05. As previously, the *p(d)* curves are close together. Comparing Figs. 4.10 and 4.11, it is concluded that a narrow spacing of *p(d)* curves is observed regardless of the individual magnitudes of the hydraulic and topographic gradients, so long as the two are similar.

Lower Aquifer - Area B

In the lower aquifer at Area B, the measurements are from a portion of the regional system. The flow from s_1 to s_3 is horizontal. Judging from the equipotential spacing (Fig. 4.9), the potentiometric slope is relatively small.

The *p(z)* and *p(d)* plots are provided in Figure 4.12. The gradient curves, hydrostatic at all locations (Table 4.9), are parallel. On the *p(z)* plot, the lateral flow from site s_1 to site s_3 is indicated. As previously in Fig. 4.10, the narrow spacing of the *p(z)* curves results from the gentle horizontal hydraulic gradient. Unlike Fig. 4.10, the *p(d)* curves in Fig. 4.12 are positioned far apart. More specifically, the relative *p(d)* curve positions indicate that the potentiometric depth decreases from site s_1 to site s_3. By the exchange of curve positions from the *p(z)* to the *p(d)* plot, flow toward decreasing potentiometric depth is indicated. So far, it seems a combined *p(z)* and *p(d)* pattern showing an exchange of curve positions is consistently associated with topography-induced flow. The next example illustrates that the exchange is not observed when a relation between topography and flow is lacking.

Lower Aquifer - Area A

Within Area A the groundwater motion is against the local topography (Fig. 4.9). The hill exerts no effect on the lower aquifer's hydraulic gradient. On a local distance the lower aquifer is confined [Sec. 2.4].

The *p(z)* and *p(d)* patterns are illustrated in Figure 4.13. As in Fig. 4.12, the gradient curves from all sites are hydrostatic (Table 4.8). The relative underpressuring and close spacing of the *p(z)* curves indicate flow from site s_1 to site s_3 under a shallow hydraulic gradient. At the same time, the underpressuring of the *p(d)* curves reveals an increase in potentiometric depth from site s_1 to s_3. Thus flow is toward increasing potentiometric depth. This style of flow, previously unobserved, is expressed by a combined *p(z)* and *p(d)* pattern in which the curves do not exchange positions, also previously unobserved. Whether a lack of positional exchange is always associated with a confined condition is explored in the following section.

4.5 Type *p(d)-p(z)* Patterns

The behavior of the intercept curves, specifically the combination of hydraulic gradient and topography which results in the positional exchange, can be made clearer with reference to the schematic diagram in Figure 4.14.

4.5.1 Analysis

Consider the horizontal aquifer at depth beneath a sloping land surface (Fig. 4.14). Sites are located at s_1 and s_2, where the topographic elevations are z_{o1} and z_{o2}, the land elevation being higher at site s_2. Pressures at sites s_1 and s_2 are denoted p_{ij}, where i = s_1, s_2 = 1, 2 and j = z_1, z_2 = 1, 2. Schematically, a value of pressure is determined by the relation $p_{ij} = (h_{ij} - z_i)\gamma$.

Hypothetical conditions of horizontal flow in the aquifer are effected by changing the potentiometric slope (Fig. 4.14). Five cases are considered: I, the hydraulic gradient is equal to the topographic gradient; II, the hydraulic gradient is less than the topographic gradient but the senses are the same; III, the hydraulic gradient is zero; IV, the senses of the hydraulic and topographic gradients are opposed, and; V, the hydraulic gradient exceeds the slope of topography while the senses are the same. In each case, the hydraulic gradient within the aquifer is uniform and the water's specific weight γ is constant.

Because vertical flow is absent, the gradient and intercept curves coincide. The *z*-intercepts are denoted h_i and the *d*-intercepts are d_{hi}, where i = 1, 2. An intercept is no longer a mean since the hydraulic head is vertically constant. The pressures are plotted on the *p(z)* and *p(d)* graphs illustrated in Figures 4.15 to 4.19, corresponding to the Cases I to V.

Case I - Figure 4.15

Through-flow in the aquifer from site s_2 to s_1 is assumed generated by the land surface relief. The hydraulic gradient is equal to the topographic slope (Fig. 4.14) so that the system is "ideally unconfined". In other words, the aquifer may be considered as in the midline region of a perfectly open basin [Sec. 2.4]. Since the potentiometric and land surfaces are parallel, the potentiometric depth is laterally constant.

The resulting *p(d)-p(z)* pattern is illustrated in Fig. 4.15. The decreasing head from site s_2 to s_1 is expressed by the relative underpressuring of the *p(z)* curves, i.e., the intercepts are $h_2 < h_1$. The constant potentiometric depth causes the *p(d)* curves to be coincidental, i.e., the intercepts are $d_{h2} = d_{h1}$. Ideally unconfined conditions, therefore, result in a combined pattern in which a *p(z)* curve is at each site of different hydraulic head and the *p(d)* curves are overlain.

The pattern of multiple *p(z)* curves and coincidental *p(d)* curves (Fig. 4.15) is independent of the magnitudes of hydraulic head relative to the land elevation, and requires only that the potentiometric and the topographic gradients be equal. For instance, in Fig. 4.15, the potentiometric depth is positive, $d_{hi} > 0$, because the potentiometric surface is below the land surface. On the other hand, if the aquifer's heads were made equal to the overlying land elevation, i.e., $h_1 = z_{o1}$ and $h_2 = z_{o2}$, then the *p(d)* curves would intercept the origin, so that again the *p(d)* curves would be overlain, with $d_{h1} = d_{h2} = 0$. Similarly, if the potentiometric surface was above the land surface, the *p(d)* curves would reveal a constant, negative potentiometric depth, i.e., $d_{hi} < 0$.

Case II - Figure 4.16

The flow is directed, as previously, from beneath higher to lower land elevation but the hydraulic gradient is relatively subdued. This case represents generally "unconfined" conditions, i.e., the hydraulic gradient is generated by topographic relief but is relatively diminished [Sec 2.4]. In other words, as on the cross-section (Fig. 4.14), the senses of the potentiometric and topographic slopes coincide, while the former is less inclined. Because of this relation, the potentiometric depth decreases progressively in the direction of flow (Fig. 4.14).

On both the *p(z)* and *p(d)* plots, Fig. 4.16, a curve is associated with each site. As in Case I, the head decline from site s_2 to s_1 results in the sense of *p(z)* curve underpressuring, i.e., the intercepts remain $h_2 > h_1$. Because of the diminished hydraulic gradient, however, the *p(z)* curves in Fig. 4.16 are closer together. Increased potentiometric depth with higher land elevation causes on the *p(d)* plot the underpressuring of the site s_2 *p(d)* curve, i.e., the intercepts are $d_{h2} > d_{h1}$. Hence, the the combined *p(d)* - *p(z)* pattern shows the exchange of curve positions. The exchange, therefore, indicates that flow from s_2 to s_1 is toward decreasing potentiometric depth.

Similarly to Case I, positional exchange is dependant on the relation of the potentiometric to the topographic gradient, not on the magnitudes of head. For instance, if the heads were generally above the land surface, the potentiometric depth would still decrease, i.e., be increasingly negative, in the flow direction. An example is provided by the behavior of the site s_2 and s_3 curves in the stratified basin of Fig. 4.3, where the heads exceed the land elevation while the potentiometric slope is small.

Case III - Figure 4.17

The hydraulic gradient is zero beneath the sloping land surface. Since the topographic relief induces no groundwater motion, conditions are "static and confined". As indicated by the cross-section, Fig. 4.14, the potentiometric surface is horizontal. Therefore, the difference in potentiometric depth between sites s_1 and s_2 is equal to the associated difference in land surface elevation [Sec. 2.5.3].

The consequent *p(z)* and *p(d)* pattern is illustrated in Fig 4.17. Because of the constant head, the *p(z)* curves are overlain, i.e., the intercepts are $h_2 = h_1$, whereas separate *p(d)* curves result at each site. As previously in Case II (Fig. 4.16), the *p(d)* curve underpressuring is toward increasing land elevation, i.e., the intercepts are $d_{h2} > d_{h1}$. This static situation is, however, easily distinguished from the dynamic by the coincidental *p(z)* curves.

Cases I and III may be considered ideal end-members of topography-influenced groundwater systems. Case I is perfectly unconfined whereas Case III is perfectly static. In reality, neither can be achieved, but rather a range of possibilities is in between. These are variations on Case II.

Among the numerical models, the ideally unconfined *p(d)-p(z)* pattern (Case I) is most closely approached in the homogeneous, simple basin (Fig. 4.2). Nevertheless, in the homogeneous basin, the horizontal hydraulic gradient decreases with depth since energy is expended in vertical flow at the recharge and discharge areas. Near the opposite end of the spectrum is the thick aquifer beneath the aquitard (Fig. 4.4). The associated *p(d)-p(z)* pattern approaches that of the confined, static situation (Case III), but there is nevertheless horizontal flow. In all the topographically-simple basins, then, the flow is like that of Case II, i.e., unconfined, and the result is a positional exchange of curves. To determine if the exchange occurs when the topography is uninfluential, two additional possibilities are analyzed.

Case IV - Figure 4.18

The flow is now from site s_1 to s_2, toward increasing land elevation (Fig. 4.14). The potentiometric and topographic surfaces slope oppositely. Although the topography is uninfluential, there is nevertheless a hydraulic gradient. For the moment, the condition is called "dynamic and confined".

The *p(z)* curves are once again spread apart (Fig. 4.18). Their underpressuring is a result of the head decrease toward site s_2, i.e., the intercepts are $h_2 < h_1$. On the *p(d)* plot the underpressuring is again toward higher land elevation, i.e., the relation is $d_{h2} > d_{h1}$. Under this confined but dynamic condition, the positional exchange is lacking because the flow is toward greater potentiometric depth (Figs. 4.14 and 4.18).

From a numerical example, a combined *p(d)-p(z)* pattern like that in Fig. 4.18 results from regional flow against the locally-increasing land elevation (Fig. 4.13).

Case V - Figure 4.19

Here, the hydraulic gradient is larger than but in the same direction as the topographic gradient (Fig. 4.14). The energy to drive the motion exceeds that which is available from the land surface relief. The potentiometric surface is thus more steeply inclined than the land surface. Putting aside for the moment the energy source, it is clearly not the overlying topography. The condition may be considered as another "confined and dynamic" one.

As previously in Cases II and IV, a *p(z)* and a *p(d)* curve result at each site. Because the head decreases downhill, the *p(z)* curve underpressuring is from site s_2 to s_1, i.e., the intercepts are $h_2 > h_1$. At the same time, the potentiometric depth increases in the direction of flow so that the *p(d)* curve from site s_1 is underpressured, i.e, the relation between the intercepts is $d_{h2} < d_{h1}$. Therefore, positional exchange is absent also in Case V.

It appears that a characteristic of generally unconfined flow is a decrease in potentiometric depth in the direction of flow. Under these circumstances, exemplified by Case II (Fig. 4.14), the *p(d)-p(z)* pattern shows exchanged curve positions. The exchange is not observed when conditions are confined. Positional exchange, therefore, indicates

likely unconfined conditions. In turn, unconfinement signifies hydraulic continuity between the groundwater regime and the overlying topography.

4.5.2 Implications

The positions of the *z*-and *d*-intercept curves are anchored by their intercepts. The preceding results are thereby summarized most readily by the relative values of the intercepts. By comparison of the intercepts, the five general *p(d)-p(z)* patterns and their significance are discussed below.

Type I: $h_2 > h_1$ and $d_{h2} = d_{h1}$ (Fig. 4.15). Manifested graphically as multiple *p(z)* curves and coincidental *p(d)* curves, this pattern indicates a decrease in head under equal hydraulic and topographic gradients, i.e., in the midline region of a perfectly unconfined groundwater regime.

Whether uninterrupted lateral flow can be inferred depends on the scale of resolution. For instance, if distance between sites exceeds the dimension of a flow system, there may be local head extrema. Recognizing this possibility, a Type I pattern nevertheless means a lateral head change generated exclusively by topographic relief. This point is illustrated numerically by the complex, homogeneous basin in Fig. 4.7.

Type II: $h_2 > h_1$ and $d_{h2} > d_{h1}$ (Fig. 4.16). This pattern is revealed by the exchange of curve positions. The exchange indicates a lateral head decrease toward decreased potentiometric depth, which is characteristic of unconfinement, i.e., the hydraulic gradient has the sense of the generative topographic gradient but its magnitude is subdued.

A Type H pattern will also be observed if a larger-scale hydraulic gradient simply coincides with a smaller-scale topographic gradient, without an actual relation between the two. In other words, regional flow beneath a local hill to a depression. From the numerical results, an example is provided in Fig. 4.13 by the motion in the lower aquifer in Area B.

On a regional scale, it appears that a Type II is indicative of topography-induced, basinal flow of groundwater. In the absence of topographic influence, there is no reason to expect the particular combination of hydraulic and topographic conditions implied by the pattern. It is therefore highly improbable that the pattern be observed if either the strata are

impermeable, or the hydraulic gradient has a non-topographic source. The analysis of $p(d)$-$p(z)$ patterns thereby provides a means of testing regional unconfinement. Demonstrating topographic influence, in turn, is one way of providing evidence for hydraulic continuity.

Type III: $h_2 = h_1$ and $d_{h2} > d_{h1}$ (Fig. 4.17). Here the $p(z)$ curves coincide whereas the $p(d)$ curves are separated. The lateral hydraulic gradient is zero, despite the inclined land surface, i.e., static and confined.

Locally, a Type III may be observed at a quasi-stagnant zone, where flow systems are convergent. A modeled example is in Fig. 4.10, from the upper aquifer of the topographically complex basin (Fig. 4.9).

A Type III is significant for a three-dimensional analysis of flow. The pattern, particularly the coincidence of $p(z)$ curves, will be observed if sites are located along the potentiometric strike of a flow system, i.e., measurement points are on the same equipotential surface rather than in the direction of the hydraulic gradient. Such, for instance, can be envisaged in the lower aquifer of a complex basin, e.g., Fig. 4.9, if sites separated by a local distance are positioned normally to the page. The $p(d)$-$p(z)$ pattern would reveal a single $p(z)$ curve and $p(d)$ curves for each site of different topographic elevation. As with a vertical pressure gradient, a Type III pattern indicates only an absence of flow in one direction, but not necessarily a static condition.

Returning to a two-dimensional analysis, the topographic influence even on a regional scale appears to become weaker with depth in stratified basins. Although not modeled, it can be expected in certain geological settings that other sources of potential become dominant [Sec 2.4]. If by such a source, compactional for instance, the hydraulic heads are laterally constant in an aquifer, then a regional Type III pattern may be observed. Large, negative potentiometric depths d_h would at the same time be associated with a compactional regime if the hydraulic heads everywhere exceeded the land surface elevation.

Type IV: $h_2 < h_1$ and $d_{h2} > d_{h1}$ (Fig. 4.19). Indicated graphically by a lack of positional exchange, the pattern occurs because of a head decrease toward increasing potentiometric depth, i.e, a dynamic and confined regime. In Fig. 4.19, the head decreases toward increasing land surface elevation.

A Type IV pattern may be used to determine by what scale of topographic features the hydraulic gradient is influenced. For example, the head in the lower aquifer of Fig. 4.6

is influenced by the regional topography, while it is unperturbed by the introduction of local relief (cf. Figs. 4.6 and 4.9). Local scale plots of $p(z)$ and $p(d)$ from the lower aquifer of the complex situation (Fig. 4.9) exhibit both Type II and Type IV patterns (Figs. 4.12 and 4.14, respectively). The Type II is simply coincidental, as noted previously, whereas the Type IV is a direct indication of confinement, i.e, the local hills and valleys are unimportant to the head distribution.

Observation of a Type IV cannot, however, be extended to mean that the hydraulic regime is altogether uninfluenced by topography. On a regional scale of resolution, the unconfined nature of this lower aquifer would be indicated by a $p(d)$-$p(z)$ pattern similar to that of Fig. 4.6, i.e., Type II.

On the other hand, a regional Type IV pattern suggests a force drawing the groundwater toward topographically high areas. A possible mechanism for this type of flow is the elastic expansion of an aquitard, and concomitant increase in pore volume, in response to the rapid erosion of substantial overburden (Neuzil and Pollock, 1983; Tóth and Corbett, 1986). If a potential sink can be expected beneath higher land elevation, the regional $p(d)$-$p(z)$ patterns are likely to be Type IV.

Type V: $h_2 > h_1$ and $d_{h2} < d_{h1}$ Fig. 4.19. Here again positional exchange is absent, but it results from a rapid head decrease toward decreasing land elevation.

A Type V pattern has not been modeled here. It is known, however, that local reductions in aquifer permeability are accompanied by increases in the horizontal hydraulic gradient in an otherwise uniform flow field (Freeze and Witherspoon, 1967; Tóth and Rakhit, 1989). In a unconfined system, it is easy to envisage how a $p(d)$-$p(z)$ pattern from across a local low permeability zone would indicate a hydraulic gradient exceeding the overlying topographic slope.

A regional Type V pattern may possibly be observed for certain transient groundwater systems. For instance, a head distribution may remain adjusted to a previous topography for geologically-significant lengths of time (Tóth and Millar,1983; England and Freeze (1988). If a previous land surface had greater relief, the extant regional hydraulic gradient may be larger than what can be attributed to the present topography. Expected furthermore in this situation, would be negative potentiometric depths d_h indicating heads above the present land surface.

4.6 Summary and Synthesis

Plots of *p(d)* and *p(z)* derived from models of topography-induced basinal groundwater flow were analyzed. Theoretically, it appears that the combined use of *p(d)* and *p(z)* plots can yield important information on the physical nature of a groundwater regime, beyond those which can be inferred from either method alone.

Vertical pressure distributions plotted as *p(d)* and *p(z)* were analyzed in terms of hydraulic heads and their gradients. For this purpose, intercept and gradient curves were defined. A gradient curve joins vertically measured pressures, and graphically represents the vertical pressure gradient. Whether on a *p(d)* or *p(z)* plot, the slope of a gradient curve indicates the magnitude and sense of the vertical hydraulic gradient. An upward impelling force is signified by a superhydrostatic slope, and a downward force by a subhydrostatic slope. A hydrostatic slope means the absence of a vertical driving force.

Intercept curves are constructed by calculating mean elevations, depths and pressures, and projecting curves of hydrostatic slope through the means to the elevation and depth axes. The resulting *p(z)* curve is a *z*-intercept curve and its intercept is the mean hydraulic head, the *p(d)* curve is a *d*-intercept curve and its intercept indicates the mean potentiometric depth. Intercept curves are analyzed according to their relative positions.

At shallow depth, vertical pressure gradients are increasingly subhydrostatic and superhydrostatic toward recharge and discharge areas. Within an upper aquitard the effect is magnified, so that ahydrostatic slopes occur everywhere but the areally-restricted hydraulic midline. The slopes tend to hydrostatic with increased depth. Within a deep aquifer, the slopes are largely hydrostatic even in recharge and discharge areas.

Interformational flow is indicated by intercept curves. A subhydrostatic *d*-intercept curve indicates a deficiency of head relative to the land surface, and thus generally downward flow; a superhydrostatic one means an excess of head and generally upward flow to the land surface. Independently of the land surface, *z* intercept curves from upper and lower strata show the vertical sense of flow across an intervening aquitard. Intraformational vertical flow cannot, however, be determined with intercept curves since their slopes are necessarily hydrostatic.

The use of intercept curves is naturally extended to two, or even three dimensions. The lateral hydraulic gradient can be analyzed in itself, with *z*-intercepts, and in its relation to the overlying topography, with *d*-intercepts. The underpressuring of *z*-intercept curves indicates the horizontal sense of flow. Between equidistant sites, the spacing between *z*-

intercept curves is proportional to the magnitude of the horizontal hydraulic gradient. When the gradient is zero, the *z*-intercept curves are overlain. For the *d*-intercept curves, the underpressuring is toward increasing potentiometric depth. The degree of coincidence of *d*-intercept curves is dependent on the degree of correspondence between the potentiometric and topographic gradients. When the potentiometric and topographic gradients are equal, the *d*-intercept curves are overlain.

Type *p(d)-p(z)* patterns were identified. A Type I pattern, multiple *z*-intercept curves and a coincidence of *d*-intercept curves, signifies a horizontal hydraulic gradient equal to the topographic gradient, i.e., ideally unconfined conditions. A Type II pattern, an exchange of curve positions, occurs when the hydraulic gradient has the same sense as the topographic gradient but is relatively subdued, i.e., a likely unconfined groundwater regime. A Type III pattern, coincidental *z*-intercepts and multiple *d*-intercepts, indicates a zero hydraulic gradient beneath a sloping land surface, i.e., static and likely confined conditions. The Types IV and V patterns, a lack of positional exchange, both indicate an increase in potentiometric depth in the direction of flow. Respectively, these types occur when the motion is toward higher land surface elevation, and when it is toward lower land elevation under a hydraulic gradient that exceeds the topographic gradient, i.e., confined but dynamic regimes.

Significantly, the positional exchange is observed only for unconfined systems. A combined use of *p(d)* and *p(z)* plots can thereby determine by what scale of topographic. features the hydraulic head distribution is influenced. Identification of a flow regime as topographically-influenced is important. The model of topography-induced flow is theoretically well-founded and its implications for the basinal distributions of energy and matter are broad and far reaching. If need be, demonstration of unconfinement offers a way of providing evidence for regional hydraulic continuity. Once continuity is accepted, spatial differences in hydraulic head must be interpreted in terms of groundwater flow.

The combined *p(d)-p(z)* method appears, therefore, to be a useful instrument for the analysis of regional groundwater flow. Rather than antagonistic, the two plots are complementary. A *p(z)* plot preserves the Cartesian integrity of points so that horizontal hydraulic gradients are easily determined, a *p(d)* plot places the hydraulic gradients in their context with the topographic relief. With either plot, vertical hydraulic gradients can be determined. What remains is to adapt the method to the analysis of actual data, and evaluate its utility under field conditions.

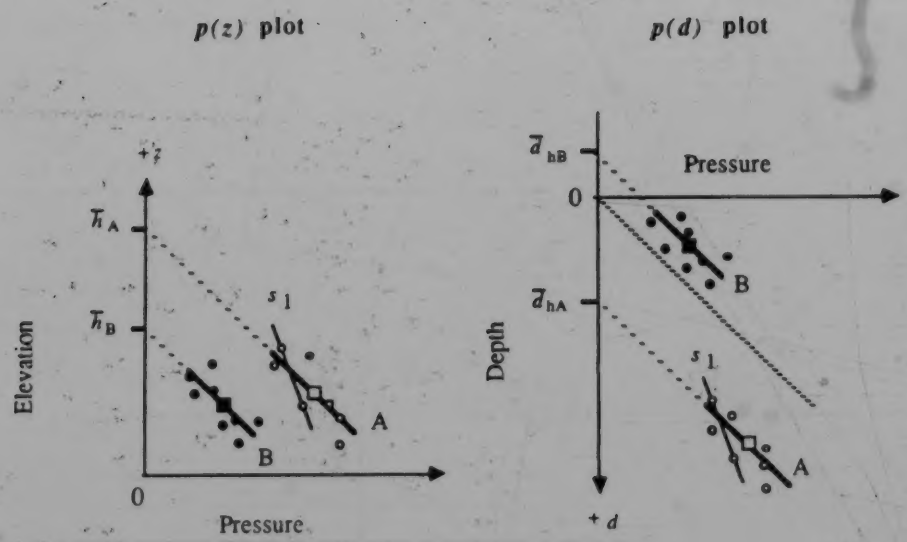

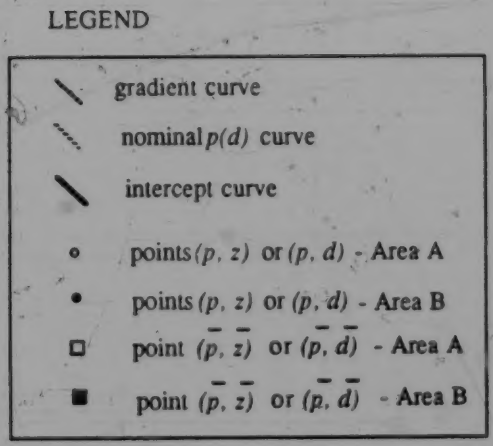
LEGEND
gradient curve
nominal p(d) curve
intercept curve
points (p, z) or (p, d) - Area A
points (p, z) or (p, d) - Area B
point $(\bar{p}, \bar{z})$ or $(\bar{p}, \bar{d})$ - Area A
point $(\bar{p}, \bar{z})$ or $(\bar{p}, \bar{d})$ - Area B

Fig. 4.1 Types of curves used in the analysis.

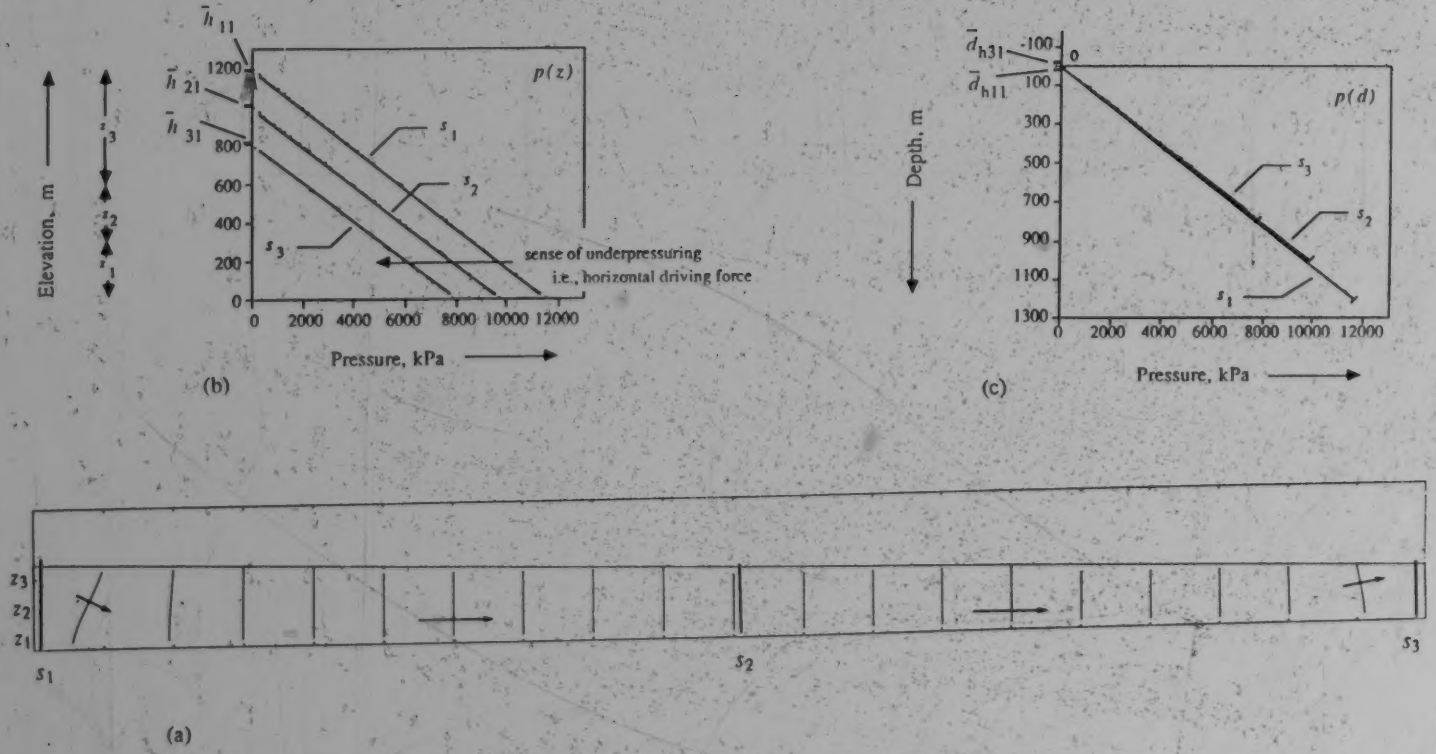

Fig. 4.2 Basin with homogeneous geology and simple topography. Patterns of (a) hydraulic head and flow, (b) pressure-elevation and, (c) pressure-depth.

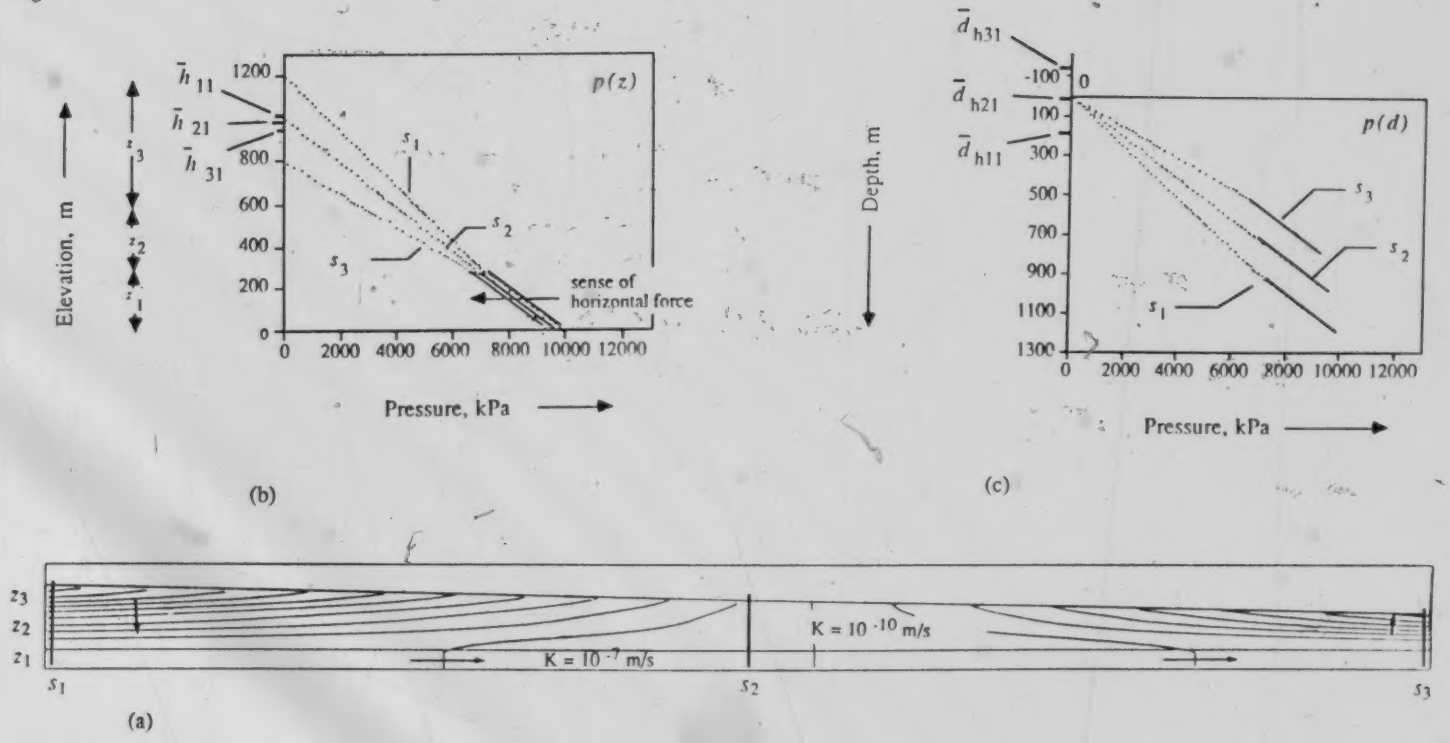

Fig. 4.3 Basin with simple topography and thick, top aquitard and bottom aquifer. Patterns of (a) hydraulic head and flow, (b) pressure-elevation and, (c) pressure-depth.

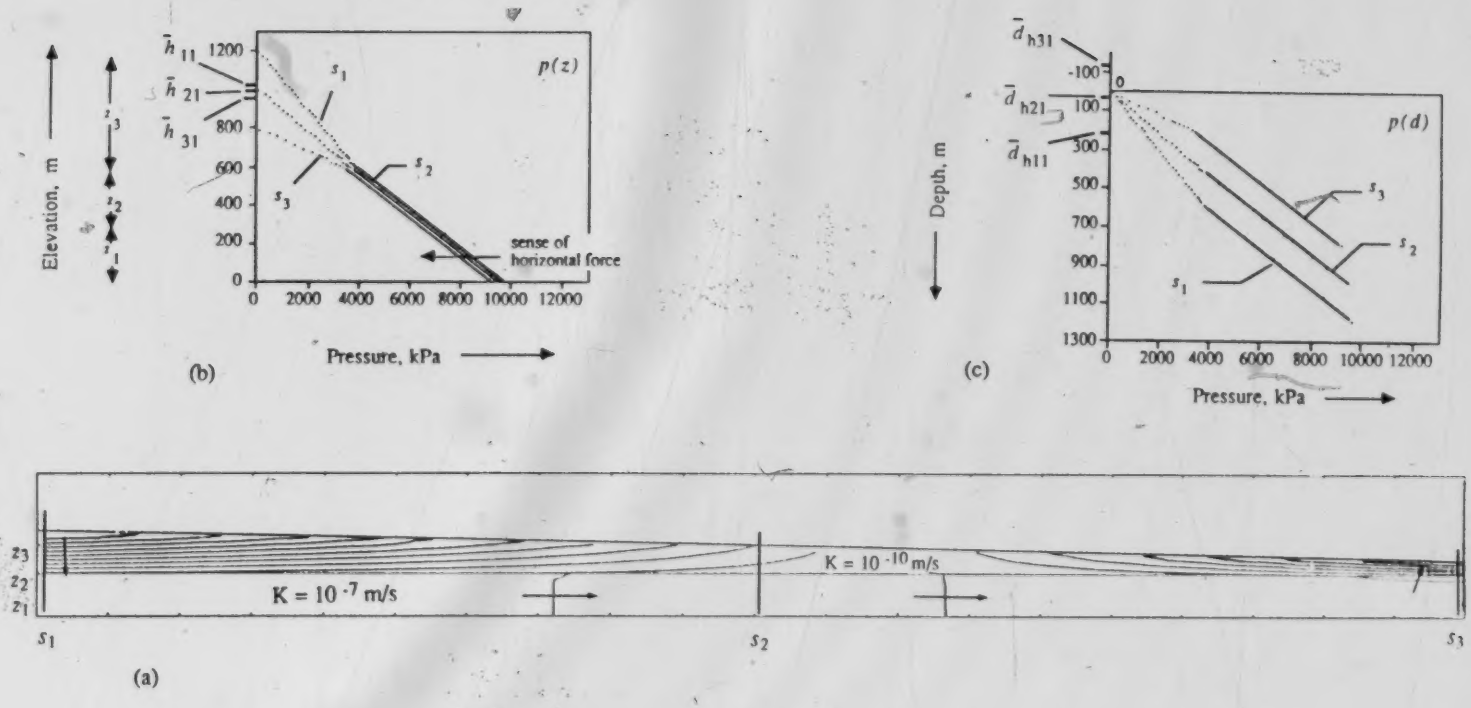

Fig. 4.4 Basin with simple topography and thin, top aquitard and bottom aquifer. Patterns of (a) hydraulic head and flow, (b) pressure-elevation and, (c) pressure-depth.

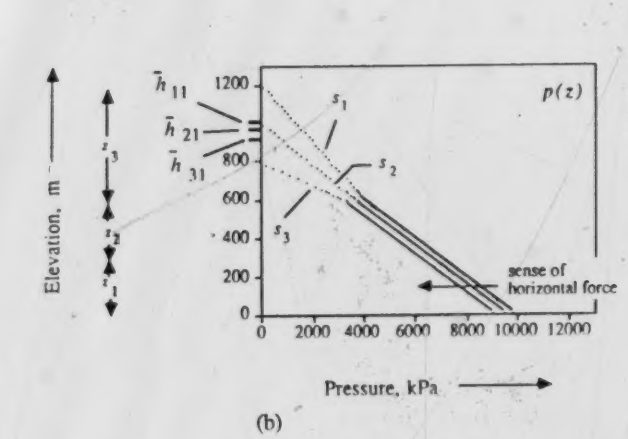

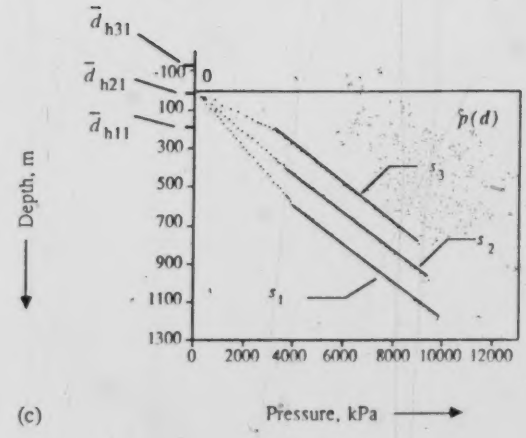

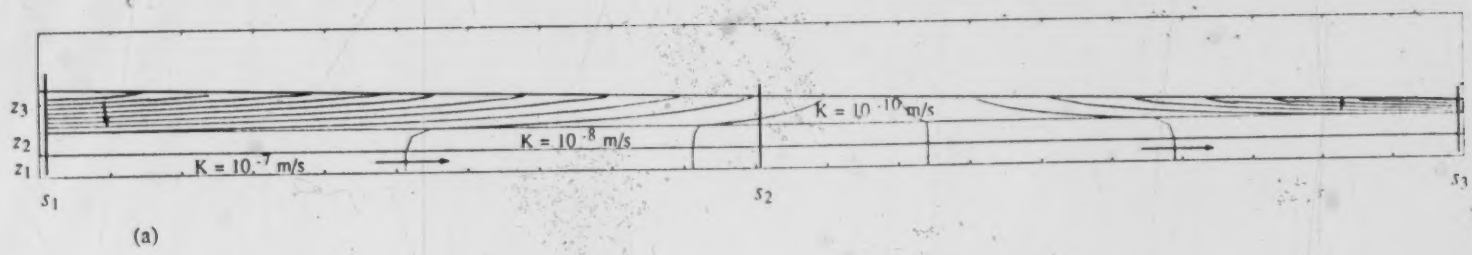

Fig. 4.5 Basin with simple topography and top aquitard, middle intermediate permeability aquifer, and bottom aquifer. Patterns of (a) hydraulic head and flow, (b) pressure-elevation and, (c) pressure-depth.

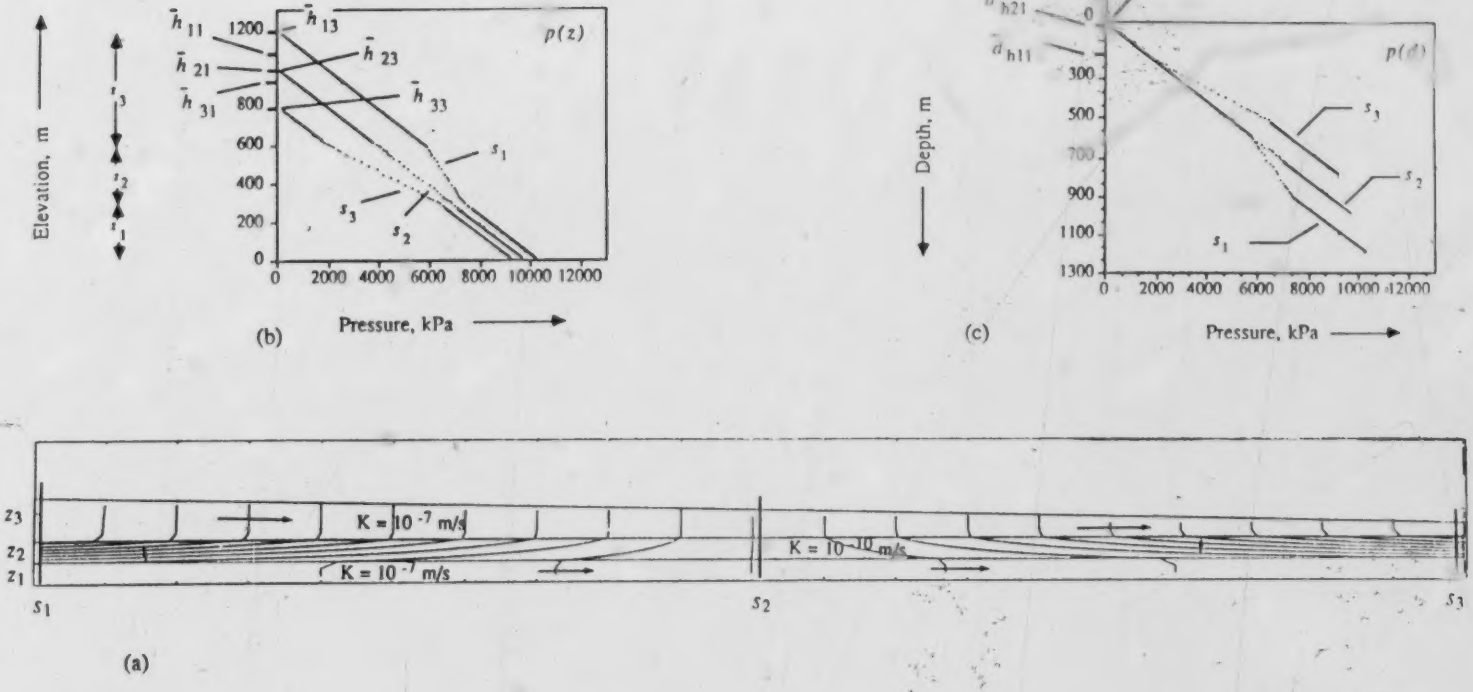

Fig. 4.6 Basin with simple topography and top and bottom aquifers. Patterns of (a) hydraulic head and flow, (b) pressure-elevation and, (c) pressure-depth.

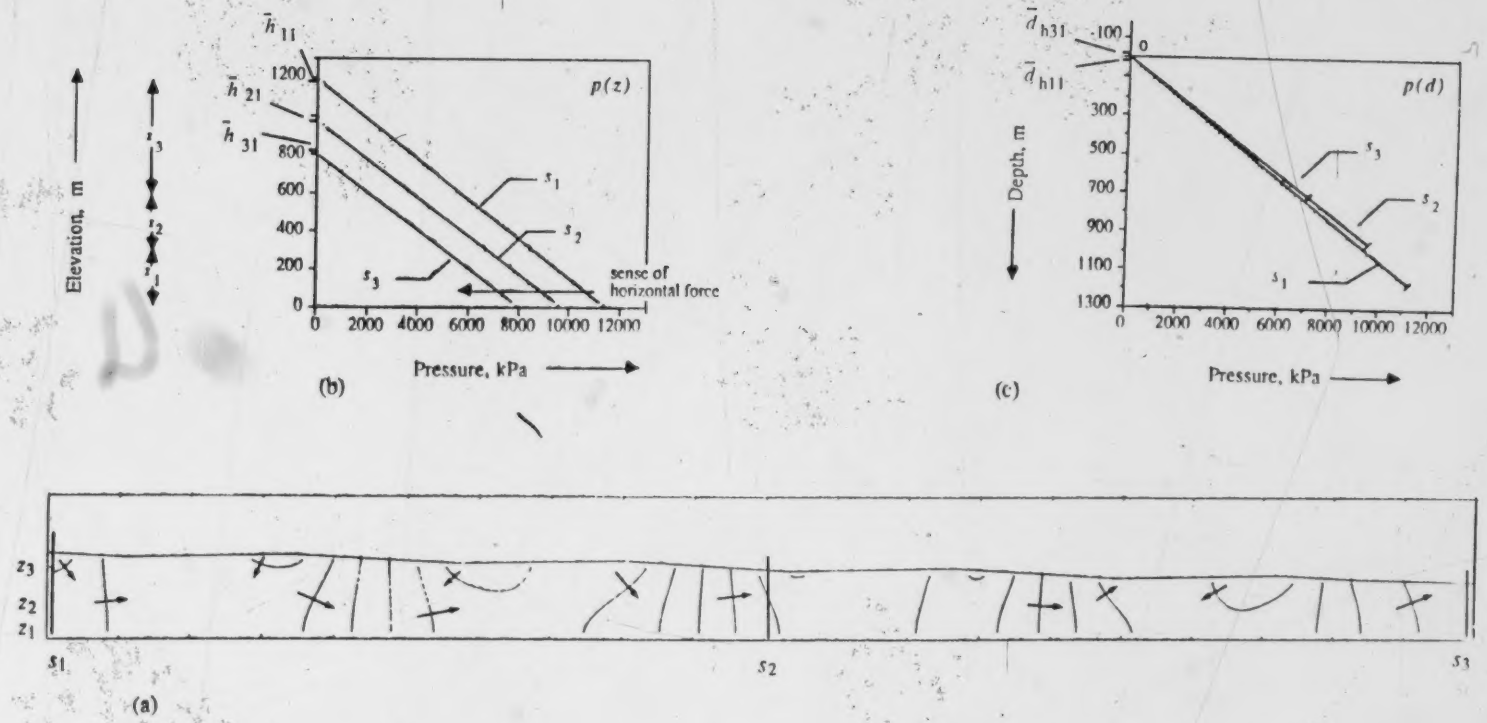

Fig. 4.7 Basin with complex topography and homogeneous geology. Patterns of (a) hydraulic head and flow, (b) pressure-elevation and, (c) pressure-depth.

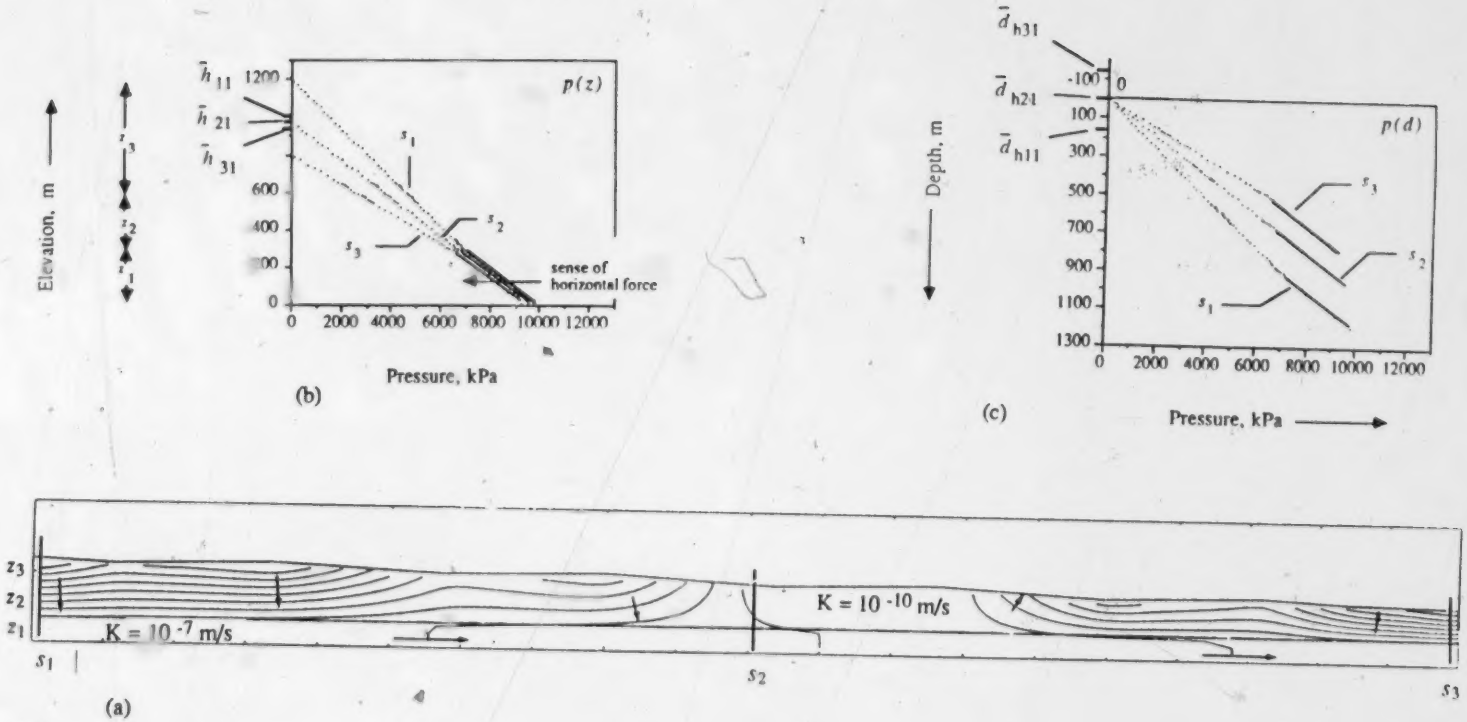

Fig. 4.8 Basin with complex topography and thick, top aquitard. Patterns of (a) hydraulic head and flow, (b) pressure-elevation and, (c) pressure-depth.

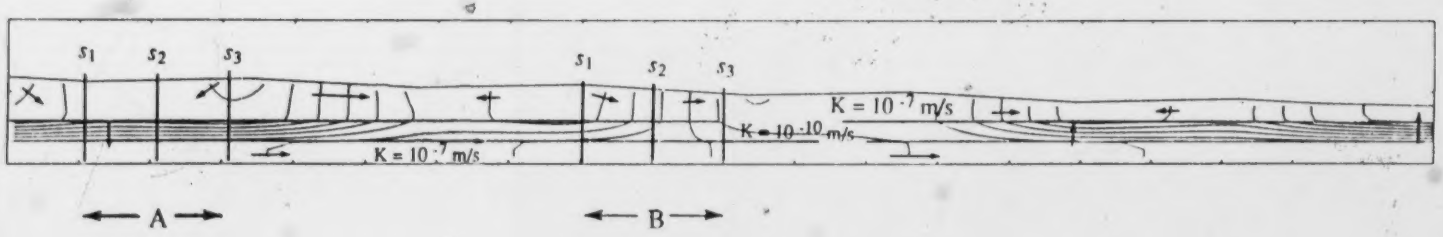

Fig. 4.9 Patterns of hydraulic head and flow in a topographically complex basin with upper and lower aquifers. Pressures from Areas A and B are used for local-scale analysis.

Upper aquifer - Area A

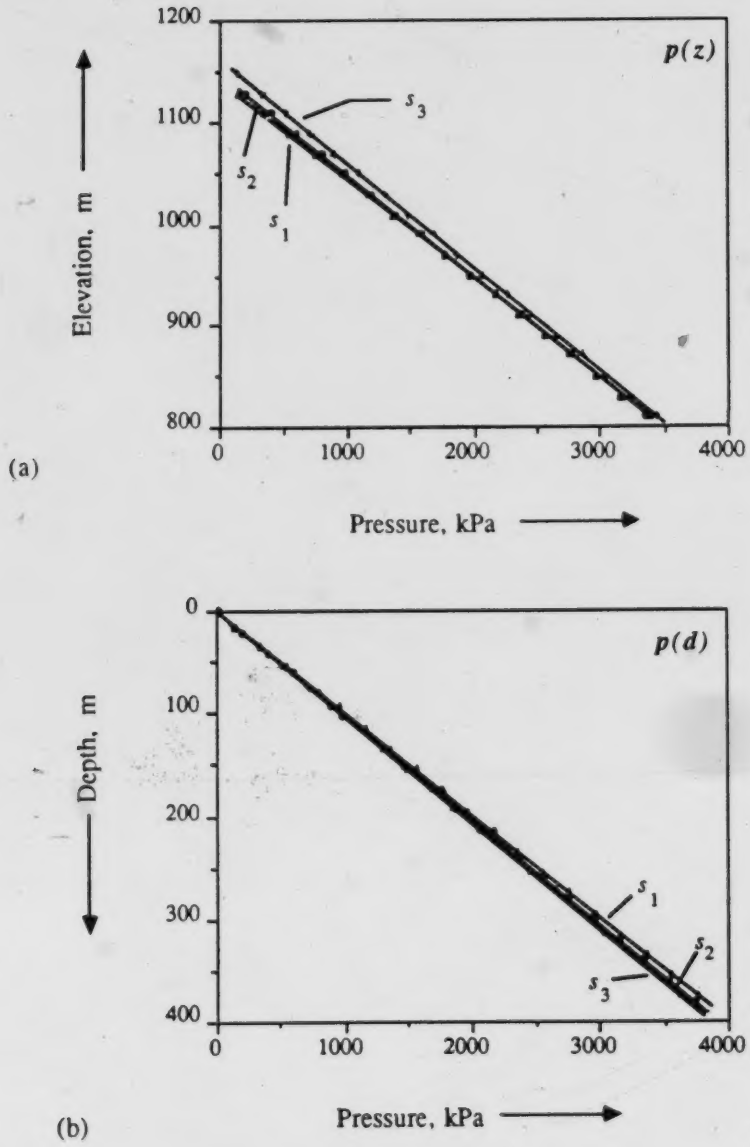

Fig. 4.10 Patterns of (a) pressure-elevation and (b) pressure-depth from the upper aquifer at Area A.

Upper aquifer - Area B

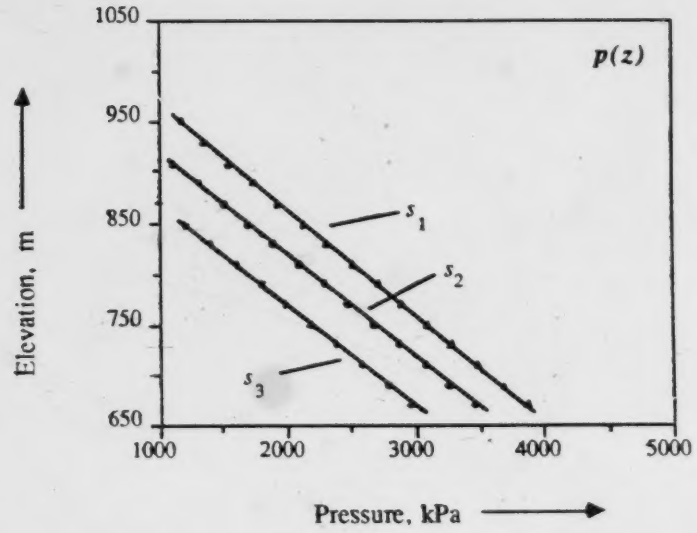

(a)

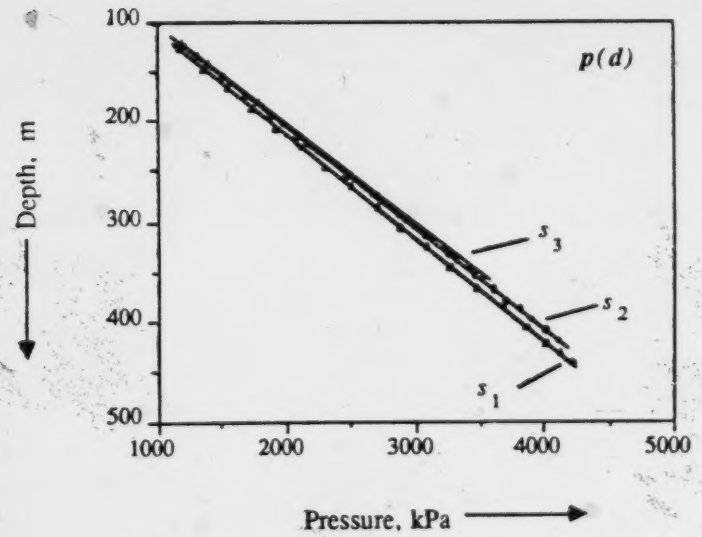

(b)

Fig. 4.11 Patterns of (a) pressure-elevation and (b) pressure-depth from the upper aquifer at Area B.

Lower aquifer - Area B

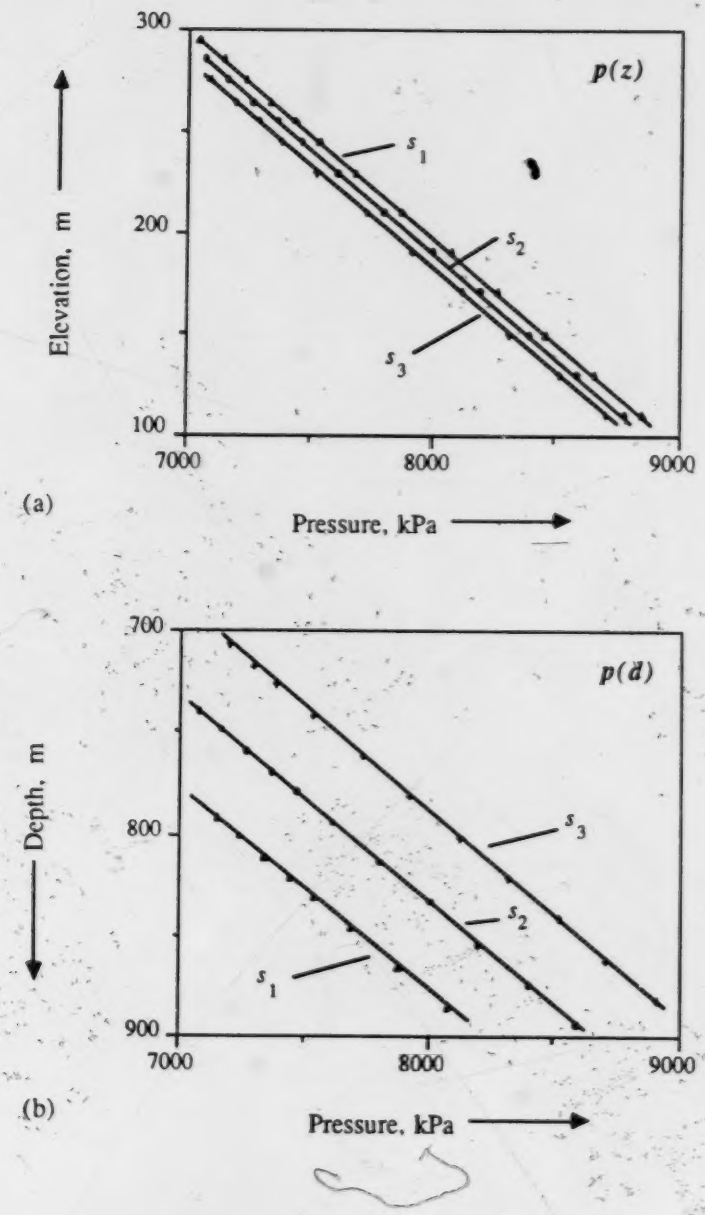

Fig. 4.12 Patterns of (a) pressure-elevation and (b) pressure-depth from the lower aquifer at Area B.

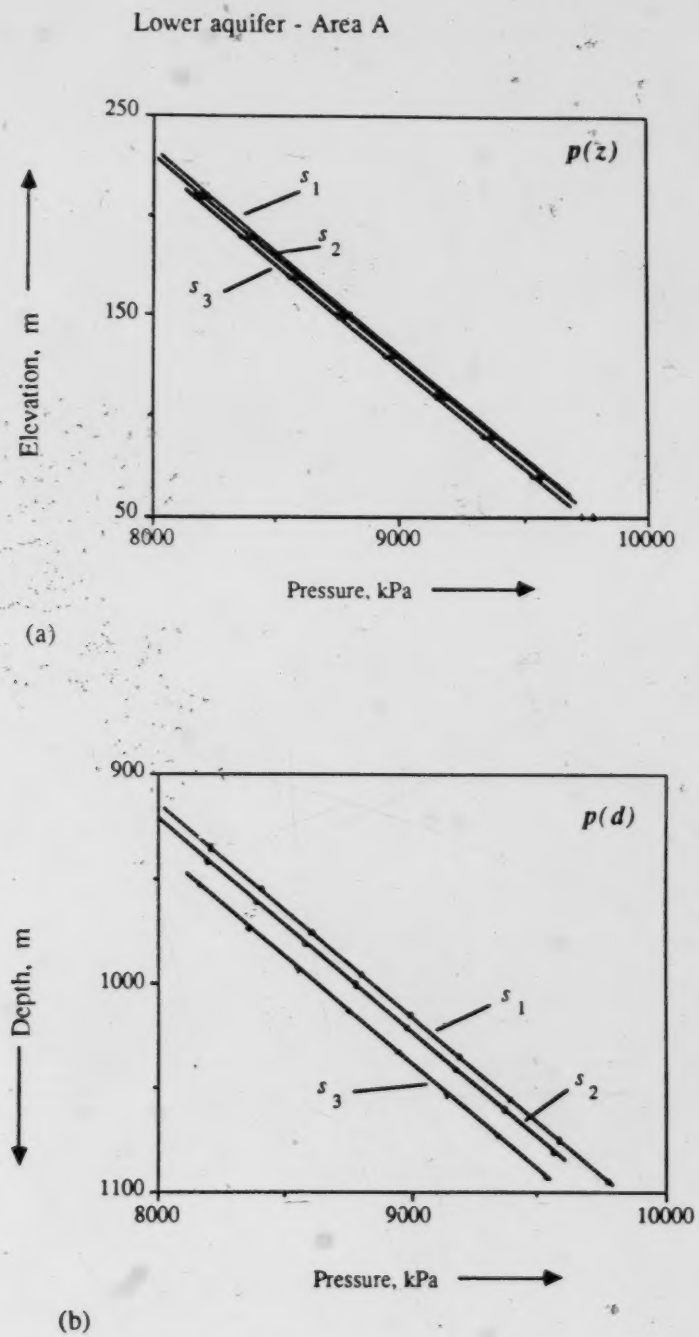

Fig. 4.13 Patterns of (a) pressure-elevation and (b) pressure-depth from the lower aquifer at Area C.

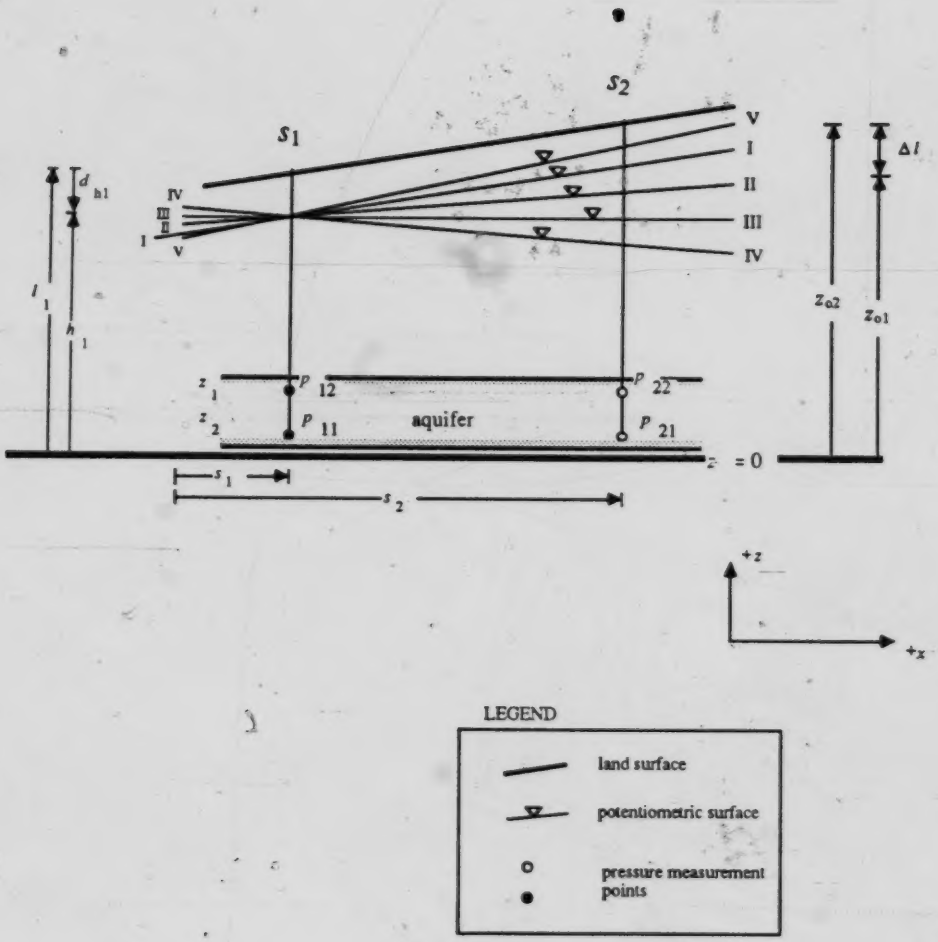

Fig. 4.14 Relations between the horizontal hydraulic gradient and the topographic gradient possible for an aquifer at depth beneath a sloping land surface. Case I: the hydraulic and topographic gradients are equal; Case II: the hydraulic gradient is less than the topographic gradient; Case III: the hydraulic gradient is zero; Case IV: the hydraulic gradient is opposed to the topographic gradient; Case V: the hydraulic gradient exceeds the topographic gradient.

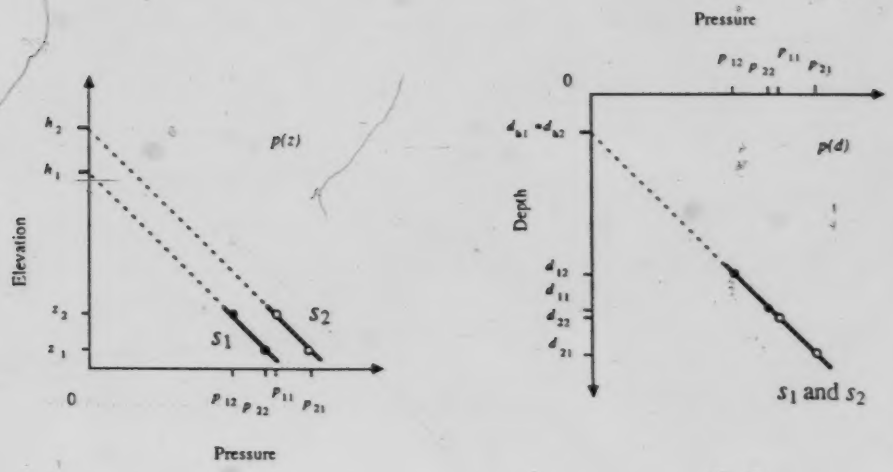

Fig. 4.15 The *p(d)-p(z)* pattern for Case I, the hydraulic and topographic gradients are equal.

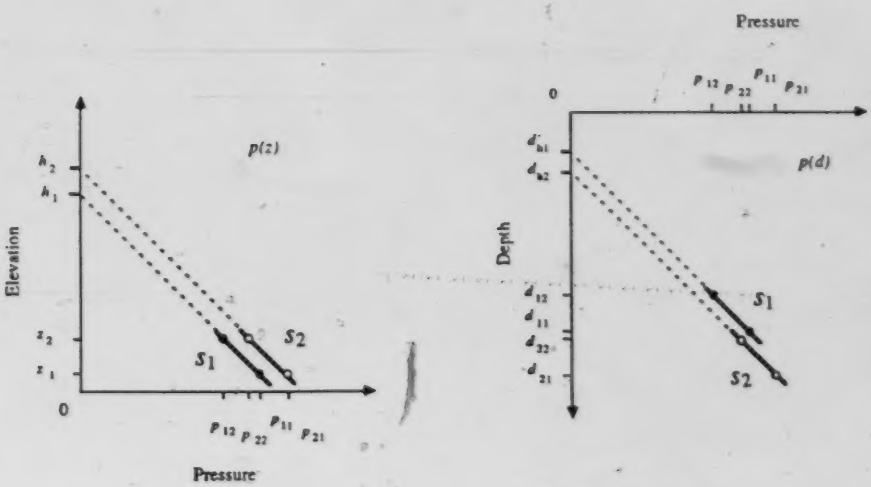

Fig. 4.16 The *p(d)-p(z)* pattern for Case II, the hydraulic gradient is less than the topographic gradient.

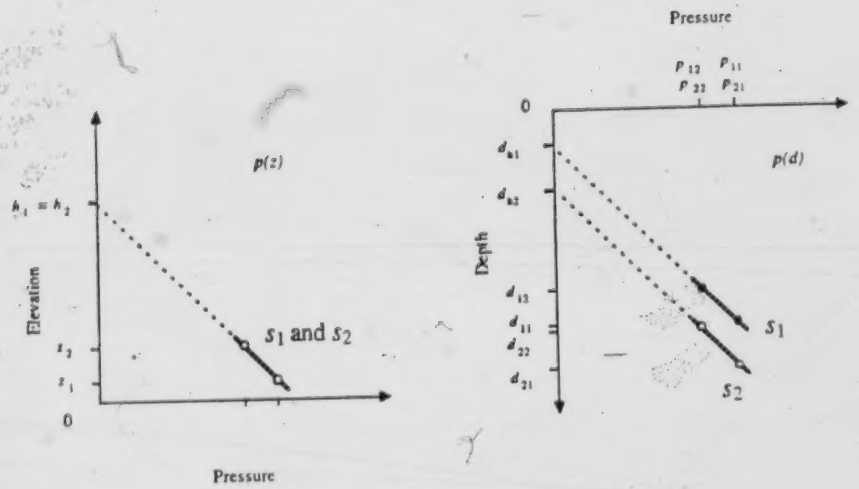

Fig. 4.17 The *p(d)-p(z)* pattern for Case III, the hydraulic gradient is zero.

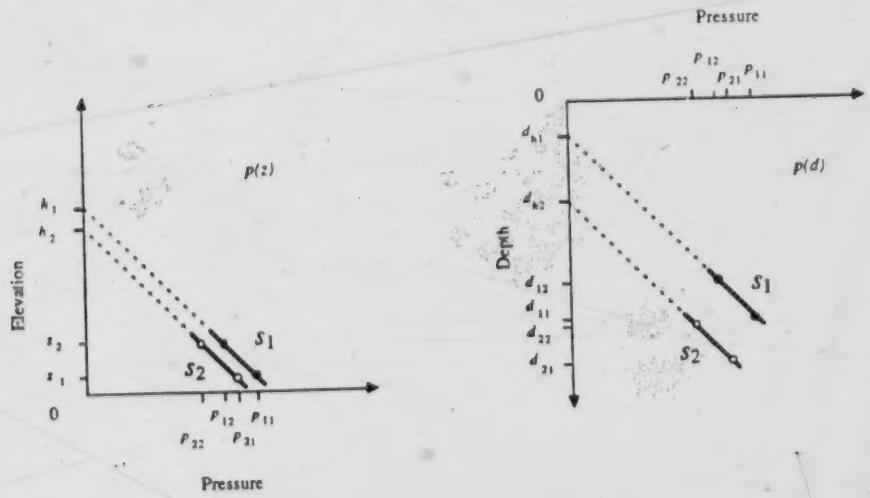

Fig. 4.18 The *p(d)-p(z)* pattern for Case IV, the hydraulic gradient opposes the topographic gradient.

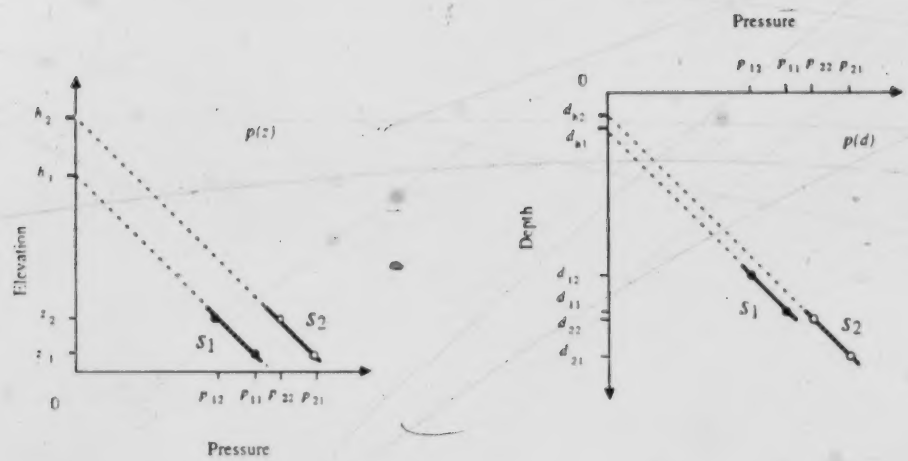

Fig. 4.19 The *p(d)-p(z)* pattern for Case V, the hydraulic gradient exceeds the topographic gradient.

Table 4.1 - Vertical pressure gradient ($\partial p/\partial d$) and vertical hydraulic gradient ($\partial h/\partial d$) in the homogeneous basin with simple topography

	s_1		s_2		s_3	
	$\frac{\partial p}{\partial d}$	$\frac{\partial h}{\partial d}$	$\frac{\partial p}{\partial d}$	$\frac{\partial h}{\partial d}$	$\frac{\partial p}{\partial d}$	$\frac{\partial h}{\partial d}$
z_3	9.60	- 0.020	9.81	0	10.09	0.020
z_2	9.73	- 0.008	9.81	0	9.94	0.013
z_1	9.78	- 0.003	9.81	0	9.85	0.004

Table 4.2 - Hydraulic head $\bar{h}_{ij}$ and potentiometric depth $\bar{d}_{hij}$ in the homogeneous basin with simple topography

	s_1		s_2		s_3	
	$\bar{h}_{1j}$	$\bar{d}_{h1j}$	$\bar{h}_{2j}$	$\bar{d}_{h2j}$	$\bar{h}_{3j}$	$\bar{d}_{h3j}$
z_3	1190.0	8.99	999.0	0	804.4	-3.4
z_2	1183.7	15.30	999.0	0	809.8	-8.8
z_1	1182.6	16.41	999.0	0	811.5	-10.5

Table 4.3 - Vertical pressure gradient ($\partial p/\partial d$) at sites s_i in basins with an upper aquitard and simple topography

	s_1			s_2			s_3		
Figure	4.3	4.4	4.5	4.3	4.4	4.5	4.3	4.4	4.5
z_3	7.69	6.38	6.70	9.59	9.08	9.19	12.97	17.01	16.25
z_2	7.78	9.80	9.78	9.59	9.81	9.80	12.83	9.81	9.87
z_1	9.81	9.81	9.81	9.81	9.81	9.81	9.81	9.81	9.81

Table 4.4 - Hydraulic head $\bar{h}_{ij}$ and potentiometric depth $\bar{d}_{hij}$ in basins with an upper aquitard and simple topography

	Fig. 4.3		Fig. 4.4		Fig. 4.5	
	$\bar{h}_{1j}$	$\bar{d}_{h1j}$	$\bar{h}_{1j}$	$\bar{d}_{h1j}$	$\bar{h}_{1j}$	$\bar{d}_{h1j}$
s_1	1009.7	189.3	992.8	206.2	1011.1	187.9
s_2	984.1	14.9	970.0	29.0	974.5	24.5
s_3	954.8	-153.8	940.8	-139.8	927.8	-126.8

Table 4.5 - Potentiometric slope ($\partial h/\partial x$) in basins with an upper aquitard and simple topography

	Fig. 4.3	Fig. 4.4	Fig.4.5
$\frac{\partial h}{\partial x}$	$-2.76 \cdot 10^{-3}$	$-2.61 \cdot 10^{-3}$	$-4.2 \cdot 10^{-3}$

Table 4.6 - Vertical pressure gradient ($\partial p/\partial d$) and vertical hydraulic gradient ($\partial h/\partial d$) in topographically-simple basin with upper and lower aquifers

	s_1		s_2		s_3	
	$\frac{\partial p}{\partial d}$	$\frac{\partial h}{\partial d}$	$\frac{\partial p}{\partial d}$	$\frac{\partial h}{\partial d}$	$\frac{\partial p}{\partial d}$	$\frac{\partial h}{\partial d}$
z_3	9.68	- 0.01	9.81	0	9.92	0.01
z_2	5.23	- 0.47	9.82	0	14.56	0.48
z_1	9.80	0	9.81	0	9.81	0

Table 4.7 - Vertical pressure gradient ($\partial p/\partial d$) and vertical hydraulic gradient ($\partial h/\partial d$) in the homogeneous basin with complex topography

	s_1		s_2		s_3	
	$\frac{\partial p}{\partial d}$	$\frac{\partial h}{\partial d}$	$\frac{\partial p}{\partial d}$	$\frac{\partial h}{\partial d}$	$\frac{\partial p}{\partial d}$	$\frac{\partial h}{\partial d}$
z_3	9.41	- 0.04	10.03	0.02	10.10	0.03
z_2	9.69	- 0.01	9.93	0.01	9.95	0.01
z_1	9.77	- 0.004	9.85	0.004	9.85	0.004

Table 4.8 - Vertical pressure gradient ($\partial p/\partial d$) in the upper and lower aquifers at Areas A and B of the topographically complex basin

	Area A			Area B		
	s_1	s_2	s_3	s_1	s_2	s_3
upper	9.95	9.82	9.72	9.60	9.80	9.87
lower	9.80	9.80	9.80	9.80	9.80	9.81

Table 4.9 - Hydraulic head ($\bar{h}_i$) and potentiometric depth ($\bar{d}_{hi}$) in the upper aquifer of the topographically complex basin

	s_1		s_2		s_3	
	$\bar{h}_1$	$\bar{d}_{h1}$	$\bar{h}_2$	$\bar{d}_{h2}$	$\bar{h}_3$	$\bar{d}_{h3}$
Area A	1151.2	-5.9	1151.3	- 0.3	1160.1	3.1
Area B	1067.9	8.0	1023.6	0.2	973.3	-1.7

Table 4.10 - Hydraulic head ($\bar{h}_i$) and potentiometric depth ($\bar{d}_{hi}$) in the lower aquifer of the topographically complex basin

	s_1		s_2		s_3	
	$\bar{h}_1$	$\bar{d}_{h1}$	$\bar{h}_2$	$\bar{d}_{h2}$	$\bar{h}_3$	$\bar{d}_{h3}$
Area A	1047.6	97.6	1045.6	105.4	1042.5	120.6
Area B	1013.3	62.7	1005.9	17.9	998.2	-26.5

5. FIELD STUDY: ANALYSIS OF GROUNDWATER FLOW IN LOWER CRETACEOUS STRATA, EAST-CENTRAL ALBERTA, CANADA

5.1 Introduction

The study region is located in east-central Alberta, Canada in townships 50 to 58 and ranges 1 to 18 west of the Fourth Meridian (Figure 5.1). Having been explored intensively for hydrocarbons, the region's geology and hydrogeology already are relatively well understood.

Previous hydrogeological investigations have been conducted by Le Breton (1963), Hitchon et al. (1989b) and Holysh (1989). Le Breton (1963, Figure 14) noted a close similarity between topographic features and the hydraulic head distribution within the upper Cretaceous-Quaternary strata. Hitchon et al. (1989b), analyzing hydrogeologic conditions from the basal Cambrian to the Cretaceous, observed sluggish "regional" groundwater flow to the northeast in the Paleozoic aquifers, and a major hydraulic divide in the Mannville units. West of the hydraulic divide, Mannville flow is against the "regional" topographic decline, and to the east it is apparently influenced by regional- or "intermediate"-scale topography (Hitchon et al., 1989b, Figure 42c). Flow within the Viking aquifer is influenced by intermediate or "local"-scale topography (Hitchon et al., 1989b, Figure 43c). Holysh (1989) also noted northeasterly Mannville flow, and speculated that its waters are discharged at its outcrop in north-central Saskatchewan.

In view of these different types of flow, the region was considered appropriate for a practical test of the *p(d)-p(z)* method. Theoretically, *p(d)-p(z)* analysis can determine the senses and magnitudes of vertical and lateral hydraulic gradients, and can indicate at what scale of topographic features the flow is influenced. The theoretical analysis was conducted, however, from the standpoint that large numbers of precise data are available at locations of choice. Given the limitations of actual data, a *p(d)-p(z)* method is adapted for field study.

The intents of this chapter, therefore, are to demonstrate a practical method of *p(d)-p(z)* analysis, to test the validity of the method by comparing the results with those obtained previously, and to illustrate that the *p(d)-p(z)* technique can provide further insight into the nature of a region's groundwater flow.

5.2 Setting and Scales of Topographic Features

As a consequence of late Tertiary uplift in the Rocky Mountain thrust and fold belt, the land surface of the Western Canada basin is elevated to the west. From the edge of the thrust belt to the Precambrian shield, a distance of roughly 700 km, the land elevation declines from over 1000 m to less than 400 m (Garven, 1989, Fig. 2). This scale of topographic decline will be considered as "basinal". Within the study region itself, important topographic features have resulted from erosional incision by major streams, chiefly the North Saskatchewan River (Figure 5.2). Land surface elevations exceeding 700 m are at the drainage divides between the North Saskatchewan and Vermilion Rivers, while elevations below 520 m are in the North Saskatchewan valley. Distances of about 30 km, termed "regional", separate these major topographic highs from the valleys. On a regional scale, the topography is gently undulating in the central and western portions of the area and rolling in the northeast (Figure 5.3). The "local" topographic features are the minor hills and depressions occurring on the flanks of the regional topographic slopes. A local distance is about 3 km.

5.3 Hydrogeologic Framework

The region is within the Western Canada Sedimentary Basin. The geologic section includes strata from the upper Devonian to the lower Cretaceous (Table 5.1). The Devonian rocks are passive margin marine carbonates and shales, whereas the Cretaceous sediments are an alternating marine-continental assemblage of Cordilleran clastics shed into the foreland basin (Price et al., 1982). Since pressures are available mainly from the lower Cretaceous Mannville Group and Viking Formation, the hydrogeologic analysis focuses on these strata.

A hydrogeologic unit is a stratum or group of strata which function in bulk as either a water-bearing or a water-retarding rock complex relative to the adjacent strata (Tóth, 1978). Generally, strata consisting of sand or carbonate are aquifers, whereas laterally extensive shales are aquitards. The designation of aquifers and aquitards in this study is based on hydraulic conductivities determined by Hitchon et al. (1989b) from drillstem tests, and from literature values (Table 5.2). Seven hydrogeologic units are specified: the Beaverhill Lake Aquifer, the Camrose Aquifer, the Ireton Aquitard, the Mannville Aquifer, the Joli Fou Aquitard, the Viking Aquifer, and the Colorado Aquitard (Table 5.1).

Vertical cross-sections of the hydrostratigraphy are presented in Figures 5.3 and 5.4. The profile in Fig. 5.3 is from the eastern half of the region, whereas the section in Fig. 5.4 is from the west. The section locations are provided in Fig. 5.2. The profiles are approximately normal to the strike of the Cretaceous strata.

The Beaverhill Lake Aquifer is a 200 m thick, areally extensive platform carbonate (Fig. 5.3). The calcareous shales of the Ireton Aquitard stratigraphically overlay the Beaverhill Lake Aquifer. Within the upper Ireton Aquitard is the thin, less than 10 m, Camrose Member Aquifer, a coarsely dolomitized (Stoakes, 1980) carbonate present only in the southwest corner of the study region (Fig. 5.4). About 15 m of the Ireton Aquitard separates the Camrose Member from the overlying Mannville Aquifer. Owing to the southwesterly dip of the Paleozoic strata, the Mannville is atop the Beaverhill Lake Aquifer across the northeastern third of the area, while in the southwest the Mannville Aquifer overlays the Ireton Aquitard (Fig. 5.4). The Ireton Aquitard's thickness varies from zero in the region's eastern portion to about 200 m in the west (Hitchon et al., 1989b).

Upper Devonian Winterburn Group and Mississippian strata were eroded during the Pennsylvanian to middle Jurassic Periods, prior to development of the foreland basin (Porter et al., 1982).

Deposited first on the Paleozoic erosional surface was the Lower Cretaceous Mannville Group, a complicated sequence of interbedded and cross-cutting sands and shales. Putnam (1982) informally divides the Mannville Group into lower, middle and upper formations (Table 5.1). The lower Mannville comprises fine- to coarse-grained sand bodies which filled northwest trending fluvial channels on the Devonian land surface. The channel fill is from tens to hundreds of kilometers in length, several tens of kilometers in width, and up to 70 m in thickness. The middle Mannville consists of sheet sandstones less than 9 m thick but up to several tens of kilometers in area. Coarsening upward from silty shales to fine-grained sandstones, the sheets are truncated by narrow but thick sandstone or shale deposits (Putnam, 1982). Separating the middle and upper Mannville is the Clearwater shale, which increases in thickness to the northwest. The upper Mannville is similarly characterized by sheet- and ribbon-shaped sandstone bodies. Because of the stratigraphically discontinuous nature of its shales and the prevalence of intervening sands and silts, the Mannville Group can be considered in bulk as a complex of "leaky" aquifers (Hitchon et. al., 1989b). The Mannville Aquifer, approximately 150 m thick, occurs throughout the region (Figs. 5.3 and 5.4), and subcrops at low elevation about 200 km northeast of the region (Holysh, 1989).

Blanketing the Mannville Aquifer is the Joli Fou Aquitard, an extensive marine shale about 35 m thick. Overlying the Joli Fou Aquitard is the Viking Aquifer, comprising 4 m thick, ill-delineated sand and conglomerate bodies (Beaumont, 1984). The Viking Formation is difficult to distinguish from the overlying shales of the Colorado Group as it becomes progressively thinner and finer grained to the east (Simpson, 1975). At the same time, in west-central Saskatchewan, both the Joli Fou and Big River Formations (Table 5.1) show a progressive increase in sand content as well as thickness to their eastern subcrop (Simpson, 1975). Eastward, then, it is possible that the Viking and the Joli Fou or Big River Formations function as a single aquifer. Overlying the Viking Aquifer, is the 500 m thick Colorado Aquitard (Hitchon et al., 1989b).

5.4 Evaluation of Pressure Data

Pressures, depths of measurement and kelly bushing (KB) elevations of sites are from drillstem tests (DSTs) on file with the Energy Resources and Conservation Board of Alberta. The pressures were subject to the following selection criteria. First, data were accepted only if the recovered fluid was primarily water, and the column of water exceeded 30 m. DSTs which recovered principally hydrocarbons were rejected since it appears invalid to infer vertical groundwater flow from vertical pressure gradients of different phase fluids. A large volume of recovered water is desirable. It indicates a greater likelihood that the DST-determined pressure is an accurate measure of the actual formation pressure, since either the time of the test has been sufficient for equilibrium, or the hydraulic conductivity is high. The value of 30 m is arbitrary.

From the DSTs which passed this criterion, formation pressures were calculated by the Horner (1961) method, or by stabilized shut-in pressures. Among these DSTs, only a final shut-in pressure which agreed within 3 % of the initial shut-in value was accepted. The agreement of shut-in values eliminates pressures skewed by formation damage or mechanical error. It should be noted, however, that discordant shut-ins may also signify a linear, highly permeable rock body (Reid, 1986). Pressures obtained from DSTs have a precision on the order of ± 1 % of the measured value (Dahlberg, 1982). For instance, a pressure of 4000 kPa is precise to within ± 40 kPa, which translates to about ±4 m of hydraulic head.

The data used in the analysis are provided in Appendix B.

5.5 Method of Investigation

For the theoretical analysis of regional flow, Chapter 4, measurement sites were located at high, median and low land elevations. Moreover, multilevel formation water pressures were considered to be available at each site. With such spatially-distributed data, lateral and vertical hydraulic gradients can be determined and analyzed in relation to the overlying topography. A similar spatial arrangement of data is sought for the field *p(d)-p(z)* analysis. In reality, however, reliable vertical pressures at preferred locations across the area are unavailable. Data are instead collected from selected areas within the study region, which act as the single sites in the theoretical analysis. Vertical and lateral flow are analyzed locally by the pressures within an area. Regional flow is analyzed with the data from adjacent areas.

The selected areas are the six townships, each about 10 km^2, labelled "A" to "F" in Figure 5.2. The locations of Areas A to F were chosen by consideration of the basinal and regional scale topography (Fig. 5.2), together with the Viking and Mannville potentiometric surface maps of Hitchon et al. (1989b). These maps are presented in Figure 5.5.

Trending northwesterly within the Mannville Aquifer, Fig. 5.5(a), is a hydraulic divide (Hitchon et al., 1989b). West of the divide, groundwater flow is southwesterly under a steep hydraulic gradient, east of the divide it is northeasterly under a shallow gradient. The Areas A to F are generally aligned northeasterly to see how the different directions of flow and intensities of hydraulic gradient, and their relations to the overlying topography, are manifested on the associated *p(d)-p(z)* patterns. For instance, the *p(d)-p(z)* pattern that results when flow is against topography, as from Area D to Area F, should be distinguishable from the pattern when motion is toward lower elevation, as from Area A to C. Along the hydraulic divide, on the other hand, the *p(d)-p(z)* pattern combining data from Areas A and D should reveal constant hydraulic head in the Mannville.

From the Viking potentiometric surface map, Fig. 5.5(b), a relationship is apparent between the regional topographic features and the hydraulic head distribution (Hitchon et al., 1989b). At Area A, for example, a potentiometric mound in the Viking coincides with the drainage divide between the North Saskatchewan and Vermilion Rivers. At Area B, near the North Saskatchewan River, the Viking hydraulic heads are lower. The relation of the lateral hydraulic gradient to the regional topographic gradient is analyzed with the *p(d)-p(z)* pattern which includes data from Areas A and B. Elsewhere within the study region,

the relation of hydraulic head to regional topography is examined with data from adjacent areas, as for instance, Areas E and F.

For an aquifer beneath a given area, mean pressures, elevations and depths are calculated. With these means, *z*-intercept and *d*-intercept curves are constructed. To recall, the *z*-intercept $\bar{h}$ is the mean hydraulic head for an aquifer beneath an area, and the *d*-intercept $\bar{d}_h$ is the mean potentiometric depth. A slope $\gamma = 10.19892$ kPa/m (Johnston, 1986) is used for Viking as well as Mannville waters. Where formation water pressures are from along a vertical, i.e., in a single well, slopes of gradient curves are computed to directly analyze vertical flow.

The groundwater flow directions inferred from the *p(d)-p(z)* analysis are used to construct the hydraulic sections illustrated in Figures 5.13 and 5.14. Where the flow in one or more hydrogeologic units appears influenced by similar boundary conditions, a "hydrodynamic zone" is identified. A hydrodynamic zone is " a set of hydrogeologic units, in each member of which the energy and flow are subject to similar factors. The characteristics of the energy and flow distributions in the various units of a hydrodynamic zone are therefore coherent, which constitutes the criterion used in the delimiting of such a zone" (Tóth, 1978, p. 835). From the following results, at least three hydrodynamic zones are identified.

5.6 Results

Area A (Tp. 52 R.8 W4M) - Figure 5.6

The land elevation is about 680 m. Locally, the topography slopes southeasterly to 640 m of elevation (inset map, Fig. 5.6). Only a few pressures are available: one each from the Viking Aquifer and the upper, middle and lower Mannville Aquifer (Fig. 5.5). The methods of analyzing vertical flow within the area are illustrated.

On the *p(z)* plot, the Viking *z*-intercept curve is denoted $\bar{h}_{AV}$ and that for the Mannville is $\bar{h}_{AM}$, where the first subscript indicates Area A and the second denotes the Viking (V) or Mannville (M) Aquifer. Similarly, on the p(d) plot, the Viking *d*-intercept curve is $\bar{d}_{hAV}$ and that for the Mannville is $\bar{d}_{hAM}$. The $p = 0$ axes are not shown on the plots, since the points fall within a narrow range of pressures, and details of the pressure pattern would be lost by including a plot's origin. Instead, the *z*-intercepts, $\bar{h}_{AV} = 555.2$

m and $\bar{h}_{AM}$ = 467.9, and *d*-intercepts, $\bar{d}_{hAV}$ = 119.6 m and $\bar{d}_{hAM}$= 214.7 m, are presented on the left margin of the respective plot. The nominal *p(d)* curve, the hydrostatic one extrapolated from the *p(d)* plot's origin, is also illustrated. The mean hydraulic heads $\bar{h}_{AV}$ and $\bar{h}_{AM}$ are posted for Area A on the hydraulic section (Fig. 5.13).

Relative to the nominal *p(d)* curve, the Viking and Mannville pressures are subhydrostatic, meaning that the hydraulic heads of each aquifer are below the overlying land surface. In the study region, the water table coincides closely with the topography (Le Breton, 1963). It is assumed for the moment that hydraulic continuity exists from the water table to the Viking, i.e., across the intervening Colorado Aquitard. Under this assumption a downward hydraulic head decline across the Colorado Aquitard is indicated both by the subhydrostatic position of the Viking point and by the positive Viking *d*-intercept $\bar{d}_{hAV}$. Downward groundwater flow in the Colorado Aquitard beneath Area A is thus illustrated in the hydraulic section (Fig. 5.13).

With only one pressure in the Viking, vertical flow within the aquifer cannot be analyzed.

The Mannville *p(d)* points are further removed from the nominal *p(d)* curve than the the Viking point. This means that the hydraulic head decreases even more from the Viking to the Mannville Aquifer, i.e., across the Joli Fou Aquitard. The magnitude of the head decline is indicated on the *p(z)* plot by the Viking and Mannville *z*-intercepts $\bar{h}_{AV}$ = 555.2 m and $\bar{h}_{AM}$ = 467.9. Using these values, the difference of Viking and Mannville heads ($\bar{h}_{AV}$ - $\bar{h}_{AM}$) is about 87 m. The Joli Fou Aquitard is about 35 m thick. Assuming the Joli Fou Aquitard is hydraulically continuous, the vertical hydraulic gradient $\Delta h/\Delta z$ across it is about 2.5.

The vertical hydraulic gradient can also be computed with multilevel pressures in a single vertical well. Along the vertical, at site 07-02 (inset map), measurements are in both the Viking and Mannville Aquifers. Using the pressures and elevations at site 07-02 (Appendix B), the vertical pressure gradient is $\Delta p/\Delta z$ = 6.3 kPa/m. This translates to a vertical hydraulic gradient $\Delta h/\Delta z$ = 1.6, which agrees generally with that calculated by the *z*-intercepts. Groundwater flow across the Joli Fou Aquitard is thus illustrated in Fig. 5.13 to have a downward component.

Vertical flow in the Mannville Aquifer is now analyzed. On the *p(z)* plot, the points are increasingly underpressured with decreased elevation. Envisaging *z*-intercept curves through each point, this pattern of underpressuring implies that the heads decrease downward in the Mannville. Yet, the pressures are from well sites about 10 km apart, so

that a lateral head decline from well 07-02 to 16-35 may instead cause the observed *p(z)* point distribution.

The *p(d)* plot does not help to decide whether vertical or lateral flow is predominant. Locally, the land surface is relatively flat so that the datum of the *p(d)* plot also is nearly horizontal. The similar relative positioning of *p(d)* and *p(z)* points observed in Fig. 5.6 is, then, to be expected. Without more pressures, or at least two along a vertical, the cause of the Mannville point positioning cannot be determined with certainty. In the next example, however, a larger number of points provides evidence that vertical flow in the Mannville is the more probable cause.

Area B (Tp. 54 R.4 W4M) - Figure 5.7

The land surface of Area B, near the North Saskatchewan River, has lower elevation than Area A (Figs. 5.2 and 5.13). Within Area B, the land surface declines to the east and southeast from 610 m to 580 m (inset map, Figure 5.6). One pressure is from the Viking, several from the Mannville and one from the Beaverhill Lake Aquifer. The Mannville and Beaverhill Lake are in direct contact since the Ireton Aquitard is absent (Fig. 5.3).

As in Area A, the Viking *p(d)* point is subhydrostatic. The inferred downward flow through the Colorado Aquitard is shown on Fig. 5.13.

Like previously, the Viking and Mannville *z*-intercepts, denoted respectively as $\bar{h}_{BV}$ and $\bar{h}_{BM}$, indicate a substantial vertical head drop across the Joli Fou Aquitard. Shown on the *p(z)* plot and posted on Fig. 5.13, the Viking and Mannville hydraulic heads are $\bar{h}_{BV}$ = 526.7 m and $\bar{h}_{BM}$ = 450.4 m. Across the 35 m thick Joli Fou Aquitard, the vertical hydraulic gradient $\Delta h/\Delta z$ is therefore about 2.2. In general, then, cross-stratigraphic flow in Area B also appears to be from the water table to the Viking and on to the Mannville (Fig. 5.13).

Within the Mannville, there is little difference between the arrangements of the *p(z)* and the *p(d)* points. The points on each plot are clustered closely about the Mannville intercept curve, and such that the relative underpressuring occurs from the upper to the lower Mannville. Although the points are from wells separated laterally, as previously in Fig. 5.6, there are more sites and these are evenly scattered throughout the area (inset map, Fig. 5.7).

The even spatial distribution of measurement points makes the inference of vertical flow in the Mannville more certain. On the *p(z)* plot particularly, if head differences were strictly lateral, then the points would be positioned more or less normally about the curve at all elevations. In other words, some upper Mannville points could be expected to lie below the *z*-intercept curve and some above. Similarly with the lower Mannville. Instead, the downward underpressuring of *p(z)* points implies that the hydraulic head is decreasing downward, regardless of well location. Mannville groundwater flow, therefore, is shown in Fig. 5.13 to have a downward component in Area B, as it likely does in Area A.

At well 13-24, measurements are available at points in the upper and middle Mannville. The vertical hydraulic gradient $\Delta h/\Delta z$ calculated from these points is - 0.05, which signifies upward flow. Perhaps local upward flow occurs near site 13-24, but the indicated head difference is insignificant given the imprecision of DSTs, i.e., it is less than 4 m.

Combined Plots for Areas A and B - Figure 5.8

Illustrated in Fig. 5.8 are the combined pressures from Areas A and B. These data are combined to examine the relation of Viking and Mannville hydraulic heads to the regional land elevation decline, which occurs from the drainage divide at Area A to the North Saskatchewan River near Area B (Figs. 5.2 and 5.13).

Analyzed are the relative positions of the intercept curves from each area. A decrease in Viking hydraulic head from Area A to Area B is indicated by the relative underpressuring of the *p(z)* curves, i.e., the *z*-intercepts are $\bar{h}_{AV}$ = 555.2 m and $\bar{h}_{BV}$ = 526.7 m. On the *p(d)* plot, increased potentiometric depth with higher land elevation is indicated by the relatively underpressured Area A *d*-intercept curve, i.e., the intercepts are $\bar{d}_{hAV}$ = 119.6 m and $\bar{d}_{hBV}$ = 75.9 m. In other words, the Viking *p(d)* and *p(z)* curves have exchanged their relative positions, which from Sec. 4.5 is a Type II *p(d)-p(z)* pattern. The results are summarized,

Viking: $\bar{h}_{AV} > \bar{h}_{BV}$ and $\bar{d}_{hAV} > \bar{d}_{hBV}$, a Type II pattern.

To recall, a Type II pattern (Fig. 4.16) is observed when the hydraulic gradient has the same sense as the topographic gradient but is relatively subdued. Thus shown in the hydraulic section, Fig. 5.13, is a lateral head decline from Area A to Area B accompanied

by a general decrease in the gap between the hydraulic head and the land surface. This relation of head to topography is evidence that the Viking Aquifer is regionally unconfined.

An inversion of intercept curves is observed also for the Mannville Aquifer,

Mannville: $\bar{h}_{AM} > \bar{h}_{BM}$ and $\bar{d}_{hAM} > \bar{d}_{hBM}$, a Type II pattern.

Like in the Viking, then, lateral flow in the Mannville may be topographically-influenced (Fig. 5.13). In contrast to the Viking, the more subdued Mannville hydraulic gradient is indicated by a closer spacing of the Mannville *z*-intercepts, in combination with a wider separation of the *d*-intercepts.

For the Viking Aquifer, the hydraulic head difference between Areas A and B ($\bar{h}_{AV} - \bar{h}_{BV}$) is indicated to be about 28 m. The distance separating the areas is roughly 35 km, so that the lateral Viking hydraulic gradient is about $8.0 \cdot 10^{-4}$. In the Mannville, the lateral hydraulic gradient is approximately $5.0 \cdot 10^{-4}$, which is comparable to the values computed from the potentiometric surface maps of Hitchon et al. (1989b) and Holysh (1989).

The inferred flow toward the river valley may simply be coincidental and unrelated to the topography. The possibility of coincidence is tested with the following *p(d)-p(z)* pattern which combines data from Areas B and C.

Combined Plots for Areas B and C (Tp. 55 R.1 W4M) - Figure 5.9

Area C is across the North Saskatchewan River from Area B (Figs. 5.2 and 5.13). The land surface elevation of Area C increases from 580 m in the southwest to over 650 m in the northeast. If the Viking and Mannville are indeed regionally unconfined, flow may be expected to converge to the valley, southwesterly from Area C to Area B as well as northeasterly from Area A to B.

The Viking *z*-intercepts indicate a hydraulic head decline from Area C to Area B: $\bar{h}_{CV} = 550.1$ m, $\bar{h}_{BV} = 526.7$ m. Viking flow, therefore, is toward the valley (Fig. 5.13). The lateral hydraulic gradient is indicated to be less than the topographic gradient because the potentiometric depth decreases also toward the valley: $\bar{d}_{hCV} = 112.0$ m and $\bar{d}_{hBV} = 75.9$ m. As previously in Fig. 5.8, this is a Type II pattern,

$\bar{h}_{CV} > \bar{h}_{BV}$ and $\bar{d}_{hCV} > \bar{d}_{hBV}$.

Since Type II patterns are observed for both the Areas A-B and B-C plots, which consider the topographic influence from opposite directions, the Viking Aquifer appears to be regionally unconfined. That is, the lateral hydraulic gradient in the Viking is influenced by the regional relief of the water table.

In turn, unconfinement of the Viking Aquifer means that the energy differences imparted by the regional water table relief are transmitted through the Colorado Aquitard. The Colorado Aquitard must, therefore, be hydraulically continuous. Justification is thereby provided for interpreting as downward groundwater flow the previously noted vertical head drops across the Colorado Aquitard (Figs. 5.6 to 5.9).

On the basis of the *p(d)-p(z)* analysis, Fig. 5.13 shows recharge of the Viking Aquifer through the Colorado Aquitard, and lateral Viking flow from the topographically elevated areas toward the North Saskatchewan River.

For the Mannville, the *z*-intercepts are coincidental, $\bar{h}_{CM} \approx \bar{h}_{BM} \approx 451.7$ m. This coincidence implies that the hydraulic head remains constant between Areas C and B. Area C, however, has higher land elevation so that the potentiometric depth is greater. Consequently, its *d*-intercept curve is relatively underpressured, i.e., $\bar{d}_{hCM} = 172.0$ m while $\bar{d}_{hBM} = 149.8$ m. In other words,

$$\bar{h}_{CM} \approx \bar{h}_{BM} \text{ and } \bar{d}_{hCM} > \bar{d}_{hBM},$$

which is a Type III *p(d)-p(z)* pattern (Sec. 4.5; Fig. 4.17). Thus, from Area C to B the Mannville potentiometric surface is horizontal despite the elevated land surface at Area C (Fig. 5.13).

Within Area C itself, the Mannville pressures are neatly aligned along the *z*-intercept curve. The alignment of the points indicates that the hydraulic heads are equal, even though the measurement points are geographically and stratigraphically dispersed. Since lateral as well as vertical head differences are lacking in the Mannville, the groundwater must be static. By contrast, most of the *p(d)* points are widely removed from the *d*-intercept curve. As on the larger scale, between Areas C and B, the *p(d)* point scattering occurs because the hydraulic head is constant while the local land elevation is variable, i.e., a local Type III configuration results.

Indicated, therefore, in Fig. 5.13 is a quasi-stagnant zone in the Mannville. Beneath Area C, the groundwater is static from the upper to at least the lower Mannville. The quasi-stagnant zone extends to the southwest near Area B. The northeasterly extent of

the zone, beyond the study region, is unknown. Corresponding to the quasi-stagnant zone is the Cold Lake Oil Sand Deposit (Hitchon et al., 1989b, Figure 50).

Combined Plots for Areas A and D (Tp. 56 R.10 W4M) - Figure 5.10

Area D is near the North Saskatchewan River (Fig. 5.2), where the land elevation is about 20 m lower than at Area A. In addition, both areas lie along the Mannville hydraulic divide [Fig. 5.5(a)]. If the Viking hydraulic heads are influenced only by the regional topography, they may be expected to decrease from Area A to D. Such a decrease is indicated on the potentiometric surface map Fig. 5.5(b). The Mannville hydraulic heads should, on the other hand, remain constant.

Contrary to expectation, the Viking *p(z)* points indicate a greater hydraulic head beneath Area D: $\bar{h}_{AV} = 555.2$ m while $\bar{h}_{DV} = 583.9$ m. Because the Area D hydraulic head is greater while the land elevation is less, the potentiometric depth at D is less: $\bar{d}_{hCV} = 119.6$ m and $\bar{d}_{hDV} = 63.5$ m. The result is a Type IV *p(d)-p(z)* pattern,

$$\bar{h}_{AV} < \bar{h}_{DV} \text{ and } \bar{d}_{hAV} > \bar{d}_{hDV},$$

which is observed generally when the hydraulic head increases toward lower topography (Sec. 4.5; Fig. 4.18). This pattern in the Viking is not readily explained. Perhaps it is related to the proximity of Area D to the Mannville hydraulic divide. As will be seen shortly, the hydraulic character of both the Viking and Mannville Aquifers changes markedly across the divide.

The Mannville pressures conform to expectation. For both areas, the arrangements of *p(z)* and *p(d)* points are remarkably similar. As in Areas A and B, downward flow beneath Area D is inferred by the downward underpressuring of the *p(z)* points. As well, the coincidence of the *z*-intercepts, $\bar{h}_{AM} \approx \bar{h}_{DM} = 464.6$ m, indicates laterally constant hydraulic head. The greater potentiometric depth at Area A, $\bar{d}_{hAM} = 214.7$ m and $\bar{d}_{hDM} = 188.5$ m, is due then to its higher land elevation, i.e., the elevation effect. A Type III pattern is the result,

$$\bar{h}_{AM} \approx \bar{h}_{DM} \text{ and } \bar{d}_{hAM} > \bar{d}_{hDM},$$

which is expected along potentiometric strike if the topography does not influence the underlying head distribution.

Combined Plots for Areas D and E (Tp. 56 R.10 W4M) - Figure 5.11

Area E is near the Vermilion River, 30 km southwest of Area D (Fig. 5.2). The land surface declines generally from 650 m at Area D to 610 m at E. The Viking potentiometric surface map, Fig. 5.5(b), indicates a closed low at Area E. The potentiometric surface map for the Mannville, Fig. 5.5(a), shows southwesterly flow under a steep hydraulic gradient.

Beneath Area E the Viking and upper Mannville *p(z)* points are hydrostatically aligned. The heads therefore are equal across the Joli Fou Aquitard. Downward, from the upper to middle Mannville the *p(z)* points indicate a large head decrease, and an even greater drop to the lower Mannville.

Because the vertical hydraulic relations have fundamentally changed, it no longer suffices to construct separate intercept curves for the Viking and Mannville Aquifers. Elevation-intercepts are instead computed for the combined Viking-upper Mannville, denoted $\bar{h}_{EV}$, and for each of the middle and lower Mannville, designated as $\bar{h}_{EmM}$ and $\bar{h}_{ElM}$. The Area E *d*-intercepts for the Viking-upper Mannville, middle Mannville, and lower Mannville are similarly symbolized as $\bar{d}_{hEV}$, $\bar{d}_{hEmM}$, and $\bar{d}_{hElM}$.

The lateral hydraulic relations between Areas D and E are analyzed by comparing the *z*- and *d*-intercepts successively from the Viking to the Mannville. The relations are:

Viking: $\bar{h}_{DV} > \bar{h}_{EV}$ and $\bar{d}_{hDV} < \bar{d}_{hEV}$, a Type V pattern,

upper Mannville: $\bar{h}_{DuM} < \bar{h}_{EuM}$ and $\bar{d}_{hDuM} > \bar{d}_{hEuM}$, a Type IV pattern,

middle Mannville: $\bar{h}_{DmM} < \bar{h}_{EmM}$ and $\bar{d}_{hDmM} > \bar{d}_{hEmM}$, a Type IV pattern,

lower Mannville: $\bar{h}_{DlM} > \bar{h}_{ElM}$ and $\bar{d}_{hDlM} > \bar{d}_{hElM}$, a Type II pattern.

The Type V pattern for the Viking indicates a head decrease from Area D to E at a rate exceeding that which can be imparted by the topography. Shown then on Figure 5.14, the hydraulic section for the western portion of the study region, is a Viking potentiometric surface sloping steeply from Area D to Area E. The Type IV patterns of the upper and middle Mannville indicate a head increase toward the decreased land elevation beneath Area E. As illustrated in Fig. 5.14, lateral motion in the upper-middle Mannville continues to be toward the northeast, like previously from Area A to B, and is uninfluenced by the higher

topography beneath Area D. By contrast, the Type II pattern for the lower Mannville signifies a subdued head decline from Area D to E. Given the head distributions in the superjacent strata, however, lower Mannville flow (Fig. 5.14) could hardly be ascribed to topography.

Combined Plots for Areas E and F (Tp. 52 R.16 W4M) - Figure 5.12

From Area E to Area F the land surface elevation increases to about 670 m as a consequence of a broad, southwesterly inclination (Figs. 5.2 and 5.14). The Viking potentiometric surface map, Fig. 5.5(b), indicates increased hydraulic head toward Area F, whereas that for the Mannville, Fig. 5.5(a), shows a southwesterly decline.

As previously in Area E, the *p(z)* plot indicates approximately equivalent Viking and upper Mannville hydraulic heads. In more detail, the Viking-upper Mannville *p(z)* points are arranged such that the underpressuring increases slightly with elevation, perhaps indicating upward groundwater flow. Maintained as previously for Area E is a large head decrease to the lower Mannville. At site 11-10, vertical pressures are available from the middle Mannville and Camrose Member (Appendix B). From these, the vertical hydraulic gradient is $\Delta h/\Delta z \approx 0.6$, indicating downward flow. The hydraulic heads of the lower Mannville and Camrose Member Aquifer appear approximately equal.

A divergence of flow along the vertical may occur in Area F, with upward flow in the Viking-upper Mannville, and downward motion in the middle-lower Mannville. The *p(z)* plot indicates potentially downward flow between the upper-middle Mannville, but the divergence suggests a horizontal hydraulic divide separating the upper and middle Mannville waters (Fig. 5.14).

Intercept curves are constructed for the Viking-upper Mannville, denoted $\bar{h}_{FV}$ and $\bar{d}_{hFV}$, the middle Mannville, $\bar{h}_{FmM}$ and $\bar{d}_{hFmM}$, and the lower Mannville-Camrose Member, $\bar{h}_{FlM}$ and $\bar{d}_{hFlM}$. Using these symbols, the Areas E-F lateral hydraulic relations are summarized,

Viking-upper Mannville: $\bar{h}_{FV} \approx \bar{h}_{EV}$ and $\bar{d}_{hFV} > \bar{d}_{hEV}$, a Type III pattern,

middle Mannville: $\bar{h}_{FmM} < \bar{h}_{EmM}$ and $\bar{d}_{hFmM} > \bar{d}_{hEmM}$, a Type IV pattern,

lower Mannville-Camrose: $\bar{h}_{FlM} < \bar{h}_{ElM}$ and $\bar{d}_{hFlM} > \bar{d}_{hElM}$, a Type IV pattern.

Despite the higher topography, there appears to be a quasi-stagnant zone in the Viking-upper Mannville complex, possibly with some upward flow (Fig. 5.14). In the middle Mannville, the hydraulic head now decreases to the southwest. The lateral sense of middle Mannville flow has thus turned diametrically from the northeasterly flow observed between Areas E and D (Fig. 5.14). In the lower Mannville, the southwesterly flow established previously from Area D is maintained. The lateral motion in the middle and lower Mannville is against the regional slope of topography.

5.7 Discussion and Overview of Flow Patterns

The results substantiate the work of Hitchon et al. [1989(b)], suggesting that a hydraulic divide occurs across the region. On either side of the divide, the hydraulic head distributions and their relations to topography appear fundamentally different. Northeast of the divide, the Viking and Mannville head distributions reflect features of basinal and regional topography. To the southwest, both the Viking and Mannville head patterns appear uninfluenced by topography. Moreover, the head distribution of the Viking-upper Mannville become similar in the southwest, and distinct from the middle-lower Mannville pattern.

It appears that there are three hydrodynamic zones. "Hydrodynamic Zone I" comprises the Viking-Mannville Aquifers northeast of the divide. Southwest of the divide are "Hydrodynamic Zone II" and "Hydrodynamic Zone III". In the southwest, Hydrodynamic Zone II comprises the Viking-upper Mannville and Hydrodynamic Zone III includes the middle-lower Mannville. The flow patterns for these Hydrodynamic Zones, as determined by the *p(d)-p(z)* method, are illustrated in Figs. 5.13 and 5.14. The regional patterns of flow and their possible causes are now discussed.

In Hydrodynamic Zone I, Fig. 5.13, Viking flow converges laterally to the North Saskatchewan River valley from the southwest and northeast, under hydraulic gradients subdued relative to the regional topographic gradients. These conditions imply dependence on topography of flow in the Viking Aquifer. It follows, then, that the Colorado Aquitard is hydraulically continuous. A difficulty with this interpretation, however, is that unlike the numerical models the convergent flow beneath a valley is not accompanied by superhydrostatic pressures. An explanation is provided shortly in conjunction with the head distribution in the Mannville Aquifer.

Vertical flow within the Viking Aquifer could not be determined. However, the downward pressure decrease across the Joli Fou Aquitard indicates a pronounced head drop. Downward flow thus appears to occur both above and below the Viking.

In the western portion of Zone I, i.e., between Areas A and B, the Mannville flow is northeasterly. Further northeast, the head is laterally constant. Vertically within the Mannville, flow also has a downward component, which also decreases to zero in the northeast. A northeastern quasi-static zone is identified by the absence of both lateral and vertical hydraulic gradients (Fig. 5.13). Oil sand deposits coincide with the quasi-stagnant zone.

The subhydrostatic Viking pressures, the downward pressure decrease across the Joli Fou Aquitard and the northeasterly Mannville flow, may all be explained as phenomena related to the "tensiometer effect" (Tóth, 1981). Very briefly, the tensiometer effect occurs when an aquitard overlies a subcropping aquifer, and the subcrop elevation is sufficiently low that the possible discharge at the aquifer subcrop exceeds that which is recharged from the aquitard. To, however, maximize recharge, a large vertical hydraulic gradient is developed in the aquitard; large enough that the pressures in the aquitard decrease with depth. If the elevation of subcrop is below the aquitard-aquifer boundary, negative pressures, i.e., tension, are generated. Vertical pressure gradients in the aquifer are essentially hydrostatic while the pressures are subhydrostatic; superhydrostatic pressures are not developed since the flow is not forced upward through an aquitard (Tóth, 1979, fig. 4). A similar pressure pattern for a system of aquitard recharge and high permeability subcrop discharge was described by Belitz and Bredehoeft (1988).

In the region, the Colorado and Joli Fou Aquitards act as regionally confining layers. The underlying Mannville Aquifer has relatively high transmissivity, and it subcrops near the land surface about 200 km northeast of Zone I. The subcrop elevation is about 350 m. The combination of confining aquitard-high transmissivity aquifer is a causes water to be drawn to the Mannville from above. Water flowing downward through the Joli Fou and Colorado Aquitards loses substantial energy, so that upon reaching the Mannville the hydraulic heads, and pressures, are subhydrostatic. The Mannville hydraulic head, about 450 m (Fig. 5.8), nevertheless exceeds the subcrop elevation. Assuming that the hydraulic head at the subcrop is about equal to its elevation, i.e., 350 m, a lateral hydraulic gradient is established. Thus observed in a portion of Zone I is northeasterly Mannville groundwater flow accompanied by subhydrostatic pressures. By a rough estimation, using a head drop of 100 m over 250 km, this Mannville hydraulic gradient

should be about $5 \cdot 10^{-4}$, which remarkably is the same as that calculated with the *z*-intercepts from Areas A and B.

The Mannville's high transmissivity provides it with the capacity to transport a large volume of water. If the potential subcrop discharge exceeds the aquitard recharge, a large vertical hydraulic gradient can be expected in the Joli Fou Aquitard. This would account for the observed downward decrease in pressure. The large vertical hydraulic gradient may also generate some drawdown in the Viking Aquifer, so that its hydraulic heads are subhydrostatic even where gravitational flow converges. The heads in the Viking Aquifer thus reflect the influences of both regional topography and basinal subcrop discharge in the underlying Mannville.

Similarly, it is conceivable that some of the effects of regional topography are superimposed on the Mannville hydraulic gradient. Such regional topographic influence may explain the Mannville quasi-static zone (Fig. 5.13). Perhaps a southwesterly driving force, subdued because of the Joli Fou Aquitard, is generated beneath Area C, but is opposed by the northeasterly subcrop-driven force. If neither of the opposing forces is dominant, a quasi-static zone would result. Therefore, like the Viking, the Mannville hydraulic head distribution is influenced both by regional topography and subcrop discharge. By the more greatly subhydrostatic pressures and subdued lateral hydraulic gradient, subcrop discharge appears, however, to exercise the greater influence.

Southwest of the divide, although pressures remain subhydrostatic, the nature of the flow changes fundamentally (Fig. 5.14). Two more hydrodynamic zones are recognized.

In Hydrodynamic Zone II, the rate of southwesterly Viking head decline between Areas D and E exceeds the loss in land elevation, a relation unobserved in Zone I. This implies a force other than, or additional to, gravity. At the same time, in the neighborhood of Area E, the Viking and upper Mannville heads have become similar. Farther southwest, between Areas E and F, is a quasi-static zone encompassing the Viking and upper Mannville beneath the elevated land surface. Beneath Area F, there may also be an upward head decline from the upper Mannville to the Viking.

The markedly different head distributions in the middle-lower Mannville justify the delineation of Hydrodynamic Zone III (Fig. 5.14). In Zone III, the lower Mannville head declines southwesterly from Areas D to E, as opposed to the northeasterly flow in Zone I. Near Area E, the middle Mannville head begins also to decrease in a southwesterly direction. This middle-lower Mannville head decline is directed against the topography at any scale. Vertically, the head decreases from the middle to the lower Mannville.

A portion of Zone I flow is indicated in Fig. 5.14, where upper-middle Mannville flow are to the northeast. The boundary between Zones I and III occurs where the northeasterly Mannville flow becomes southwesterly. For the middle Mannville, the boundary is indicated between Areas A and D. In the lower Mannville, the boundary appears to be northeast of Area D. The Zone II - Zone III boundary is defined by a divergence of vertical flow, downward in the middle Mannville and upward or zero in the upper Mannville-Viking. Finally, the Zone I - Zone II boundary appears to coincide with the Joli Fou Shale, since the southwesterly Viking flow no longer appears influenced by a combination of regional topography and Mannville subcrop discharge.

Instead, conditions in Zones II and III appear influenced by non-gravitational mechanisms. The basinal pressure distributions in non-gravitational regimes are not yet well-known, so that only brief speculation on the causes of the observed patterns is possible.

The hydraulic heads in Zone II may reflect elastic rebound of the Colorado shales. In southern Alberta, strata subjacent to the rebounding Colorado show subhydrostatic pressures, upward flow and lateral flow directed irregularly toward higher land surface elevation (Tóth and Corbet, 1986). These are features generally of the head distribution in Zone II. The Clearwater shale, which separates the upper and middle Mannville and increases in thickness to the northwest (Sec. 5.3), may prevent rebound from influencing the middle-lower Mannville heads.

For Zone III, Hitchon et al., (1989b) note the high permeability of the Camrose Member and that the flow in it is westerly toward the Rimbey-Meadowbrook reef trend. It has been suggested that the reef trend acts as a conduit for significant northward flow and subcrop discharge (Hitchon, 1969; Hugo, 1990). Perhaps the southwesterly Zone III flow is focused also toward the reef trend. The viability of this mechanism depends, however, on an uninterrupted head decline to the reef trend, and then across a great distance northward. From the $p(z)$ plot at Area F, it would seem one requirement of such flow is a continuous head decline from a value of 316 m. That the reef is a conduit remains to be demonstrated.

5.8 Summary and Conclusions

A hydrogeological field study of lower Cretaceous strata in east-central Alberta was conducted with the objectives of developing and illustrating a practical method of $p(d)$-$p(z)$

plot analysis. The *p(d)-p(z)* method is used to determine vertical and lateral hydraulic gradients, and to analyze their relations to the overlying topography. Groundwater flow patterns are then inferred from the observed hydraulic gradients. It is believed that the *p(d)-p(z)* method is a practical instrument of analysis which can lead to insight on the patterns and causes of flow.

The field procedure involved the delineation of areas from which *p(z)* and *p(d)* data were obtained. The Areas A to F were chosen from consideration of the regional-scale topography and the Viking and Mannville Aquifer potentiometric surface maps of Hitchon et al. [1989(b)]. Vertical flow was analyzed with pressures plotted from within an area. Plots of *p(d)* were used to determine the vertical sense of motion relative to the water table. Intraformational vertical flow was identified most readily with *p(z)* points, since the spatial, i.e., Cartesian, relations of hydraulic head are more accessible when the datum is horizontal. Lateral flow between areas was analyzed with *z*-intercept and *d*-intercept curves. The curves were constructed for single points within aquifers or groups of points which have vertically similar hydraulic head. Lateral motion and its possible relation to topography were analyzed in terms of the theoretical Types I to V *p(d)-p(z)* patterns defined in Chapter 4.

On the basis of their characteristic head distributions and flow patterns, three hydrodynamic zones were defined. Hydrodynamic Zone I is northeast of the regional hydraulic divide recognized by Hitchon et al. [1989(b)], whereas Zones II and III are southwest of it.

Hydrodynamic Zone I comprises the Viking and Mannville Aquifers. The Viking Aquifer heads decline laterally at a subdued rate and flow converges to a regional topographic low, whereas Mannville Aquifer heads decrease northeasterly and then become laterally-constant. Vertically, the Viking is recharged from the Colorado Aquitard. Flow is downward from the Viking to the Mannville under a substantial vertical hydraulic gradient. Heads generally decline downward in the Mannville, but become vertically-constant to the northeast. By the absence of both lateral and vertical motion, a quasi-static zone is identified in the Mannville. Oil sand deposits are associated with the quasi-stagnant zone. The head distributions of Zone I are influenced by regional topography as well as low elevation subcrop discharge of Mannville waters.

Hydrodynamic Zone II comprises the Viking and upper Mannville. The Viking heads decrease laterally at an accelerated rate toward a regional topographic low and then are constant beneath an inclined land surface. The Viking and upper Mannville heads

become equal, with perhaps some upward flow between the aquifer. Erosional rebound of the Colorado shales may influence the head patterns of Zone II.

Hydrodynamic Zone III includes the middle and lower Mannville. Flow is southwesterly, against regional topography, with downward flow from the middle to lower Mannville. The motion may be directed toward the Rimbey-Meadowbrook reef trend, which has been suggested to act as major conduit for basinal flow.

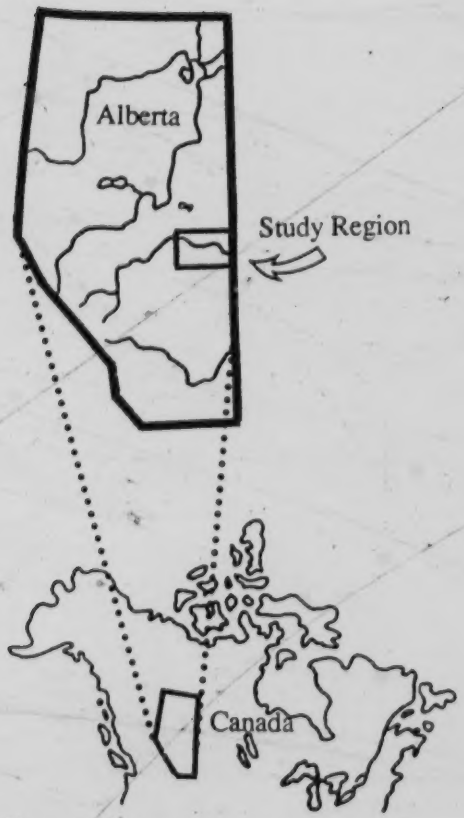

Fig. 5.1 Location of study region.

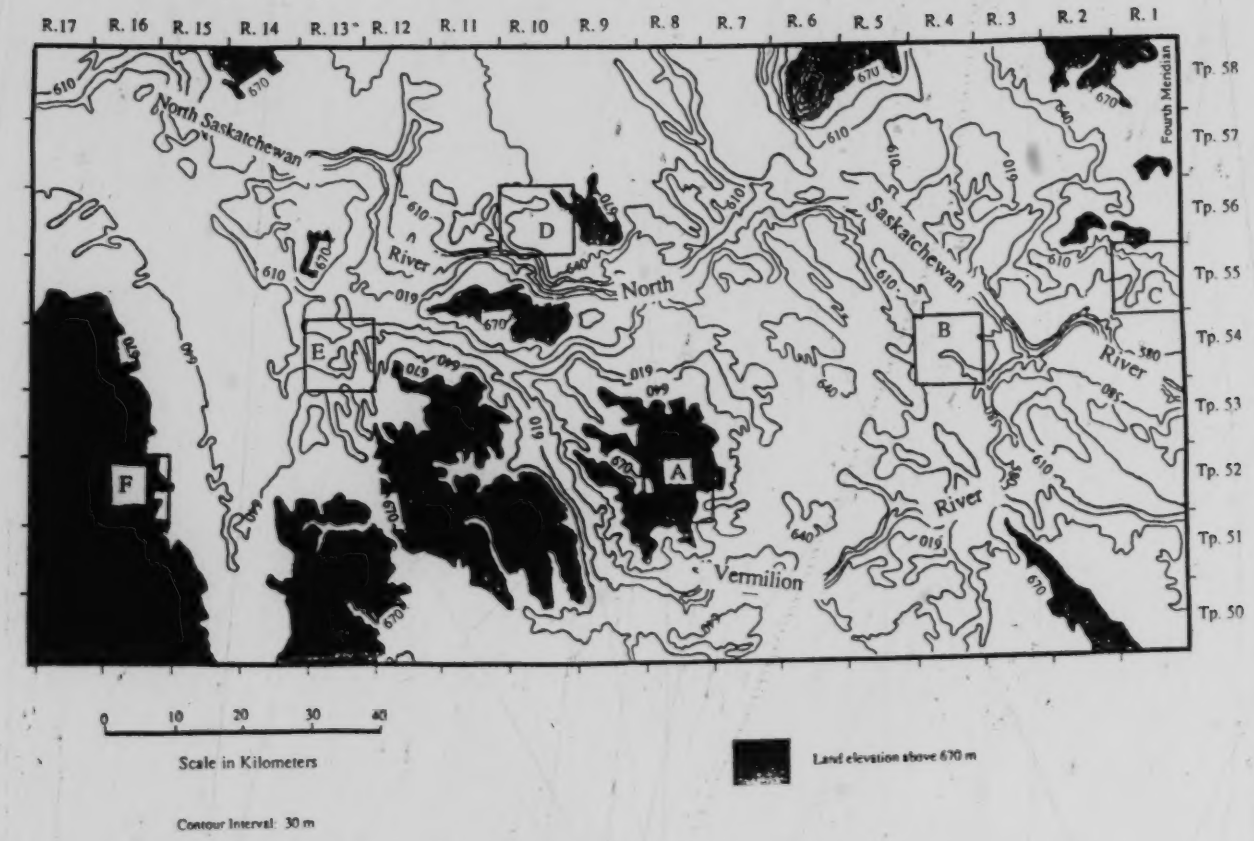

Fig. 5.2 Topography of study region and locations of Areas A to F from which pressures are taken.

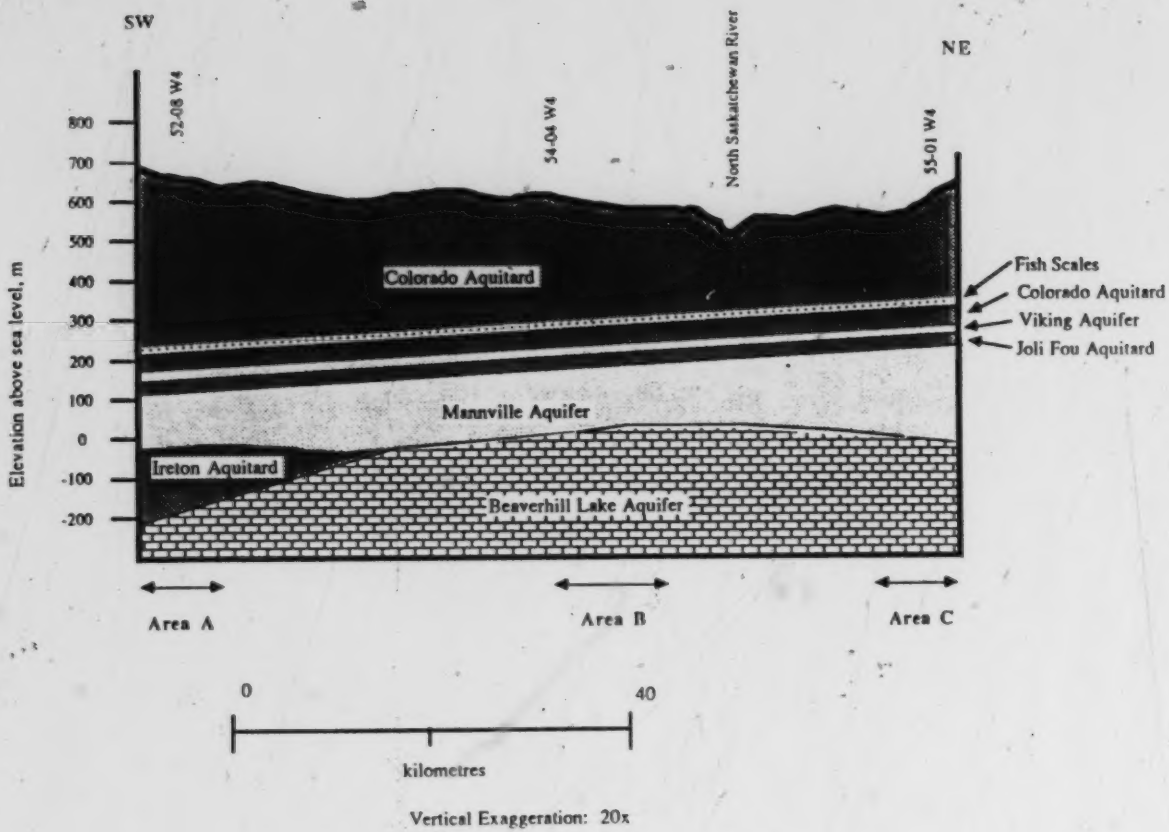

Fig. 5.3 Regional hydrostratigraphic section, northeast from Area A to Area C.

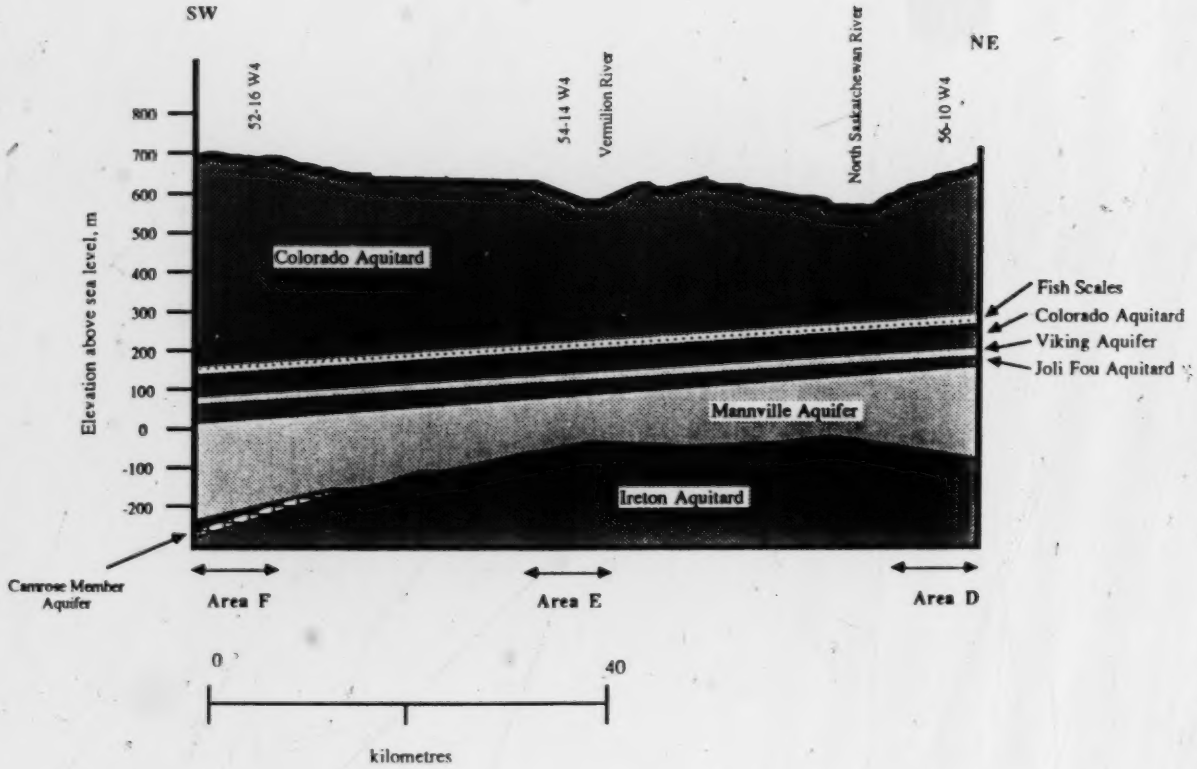

Fig. 5.4 Regional hydrostratigraphic section, northeast from Area F to Area D.

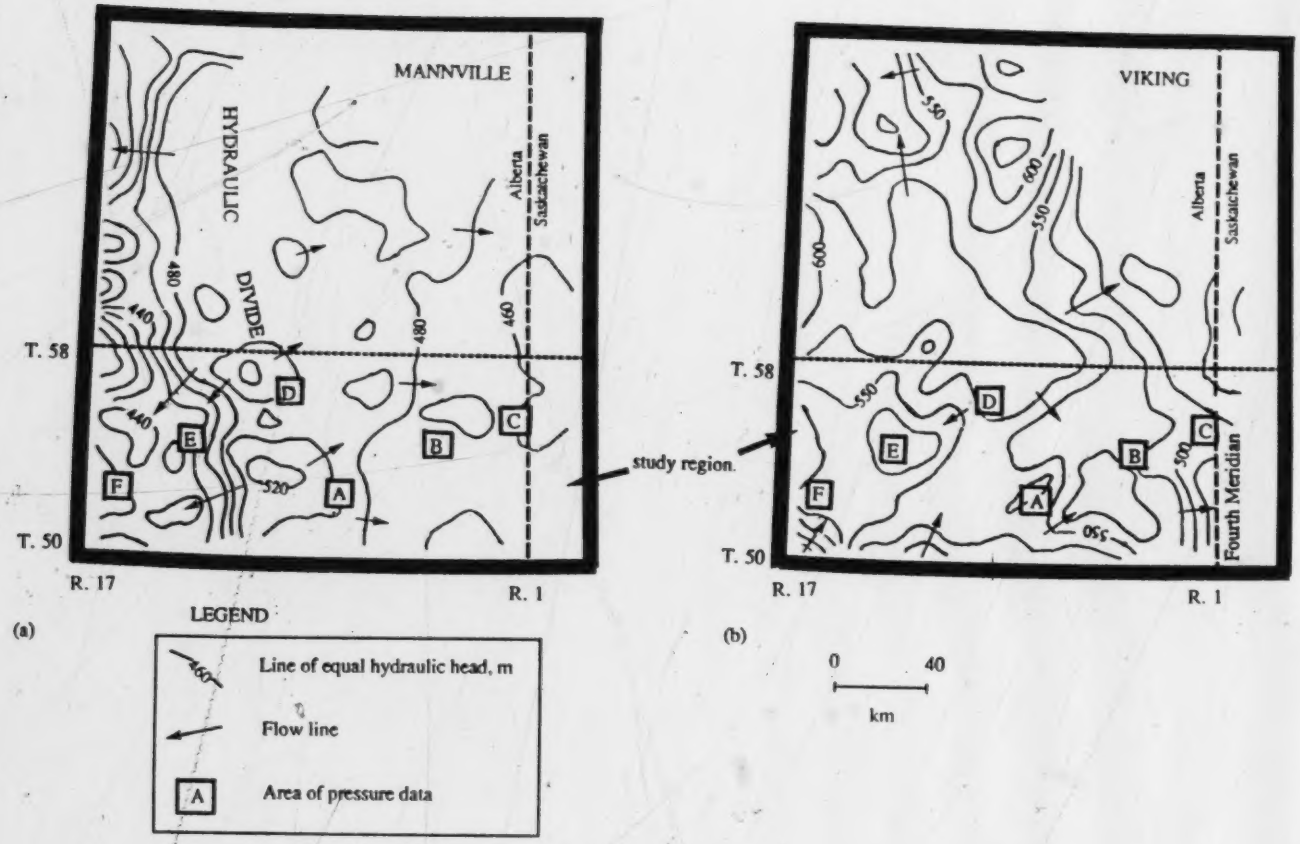

Fig. 5.5 Potentiometric surface maps of (a) the Mannville Aquifer, and (b) the Viking Aquifer [from Hitchon et al., 1989(b), Figure 42(c) and Figure 43(b)].

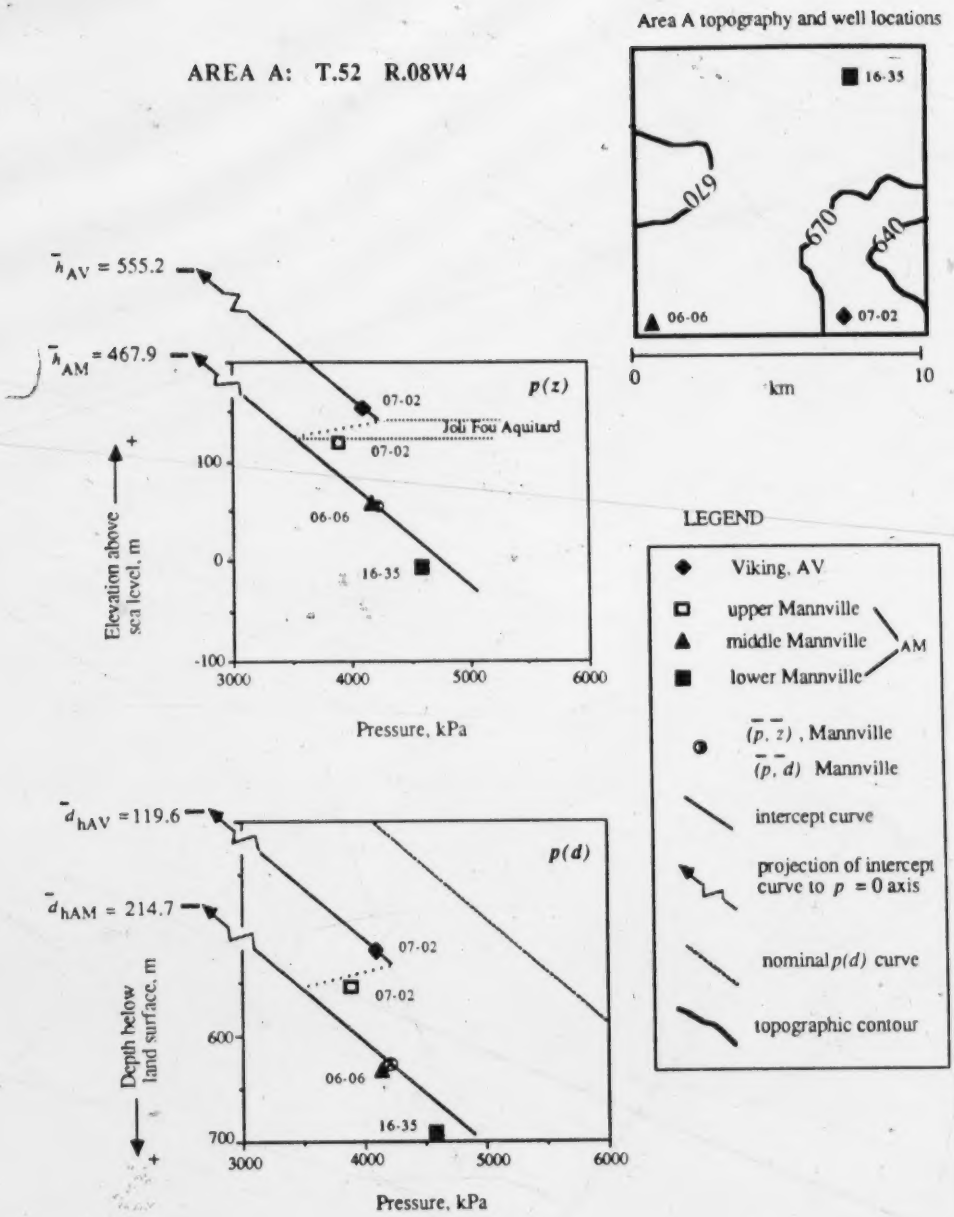

Fig. 5.6 Area A *p(d)-p(z)* pattern.

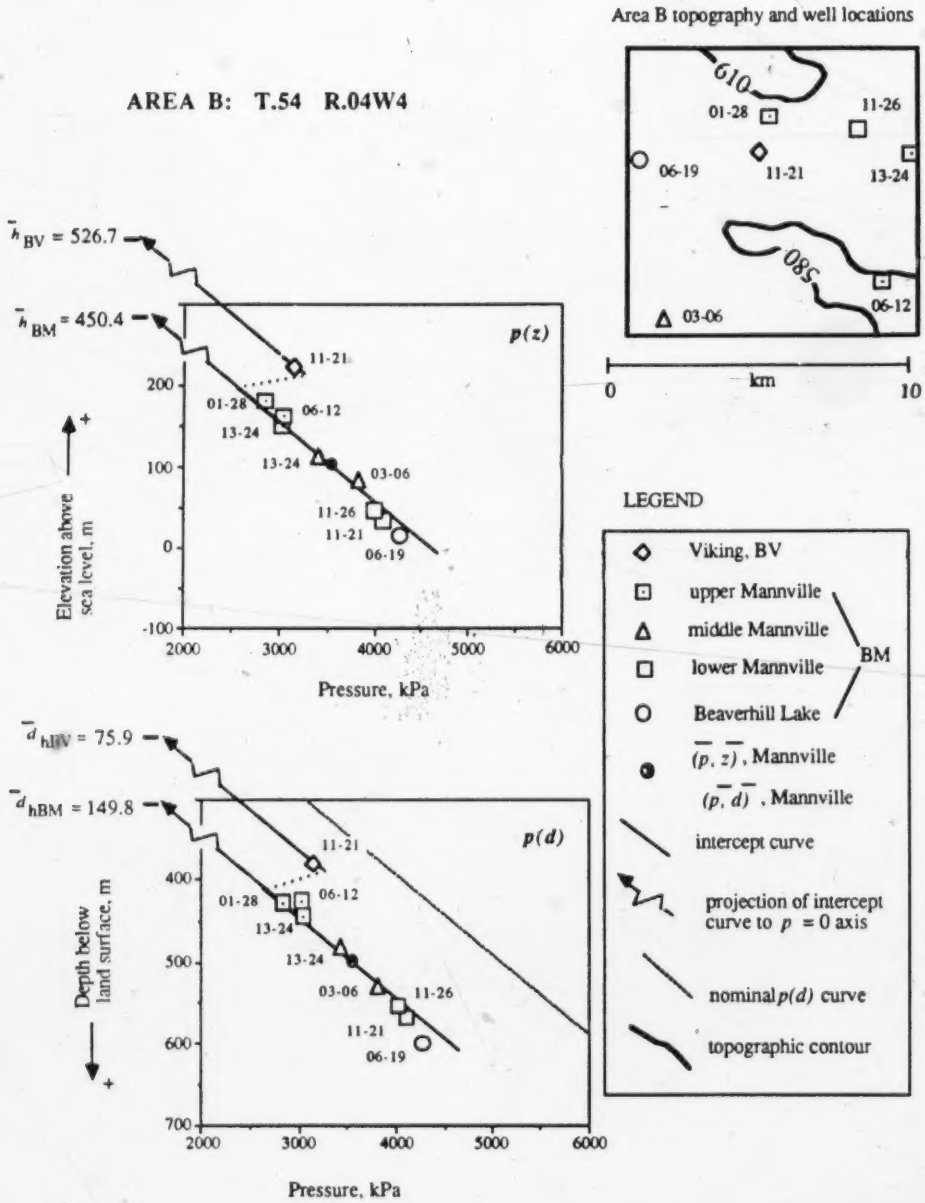

Fig. 5.7 Area B *p(d)-p(z)* pattern.

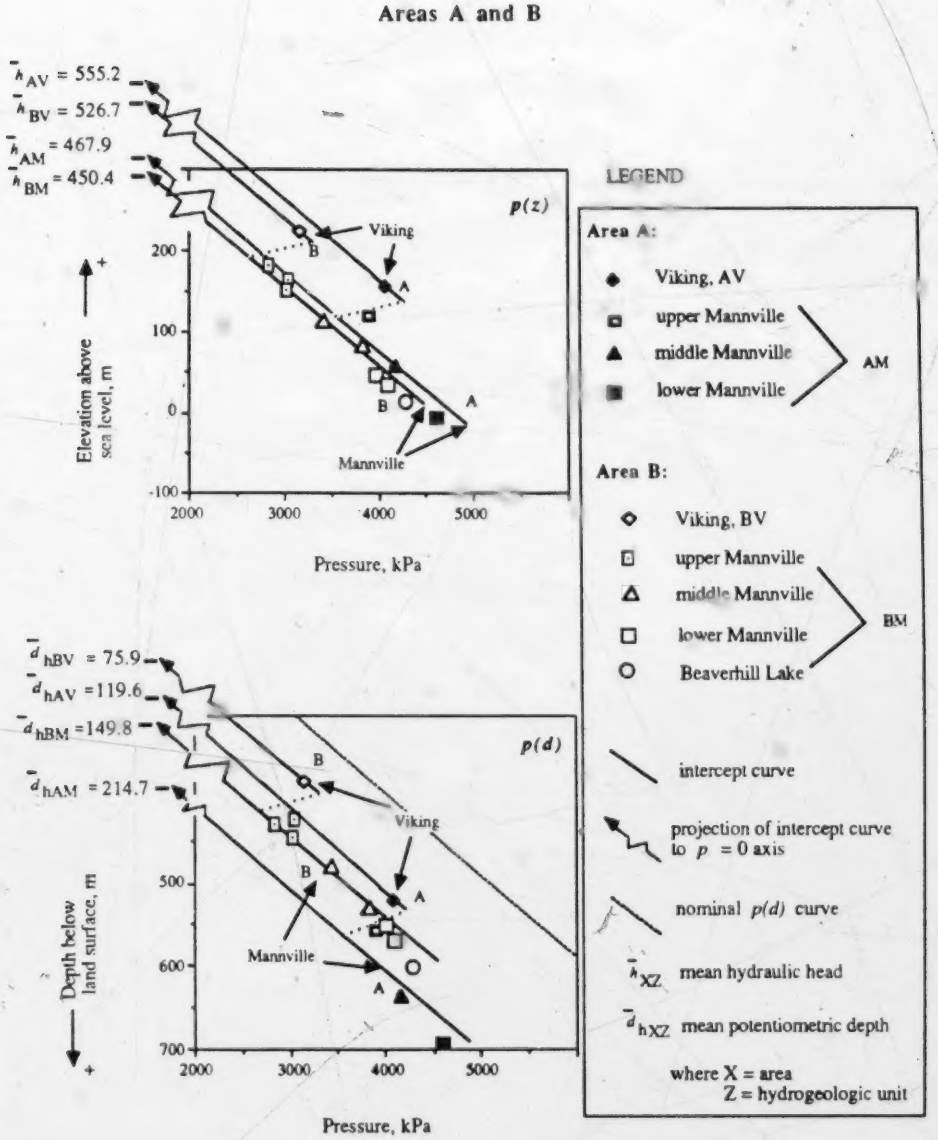

Fig. 5.8 Areas A and B *p(d)-p(z)* pattern.

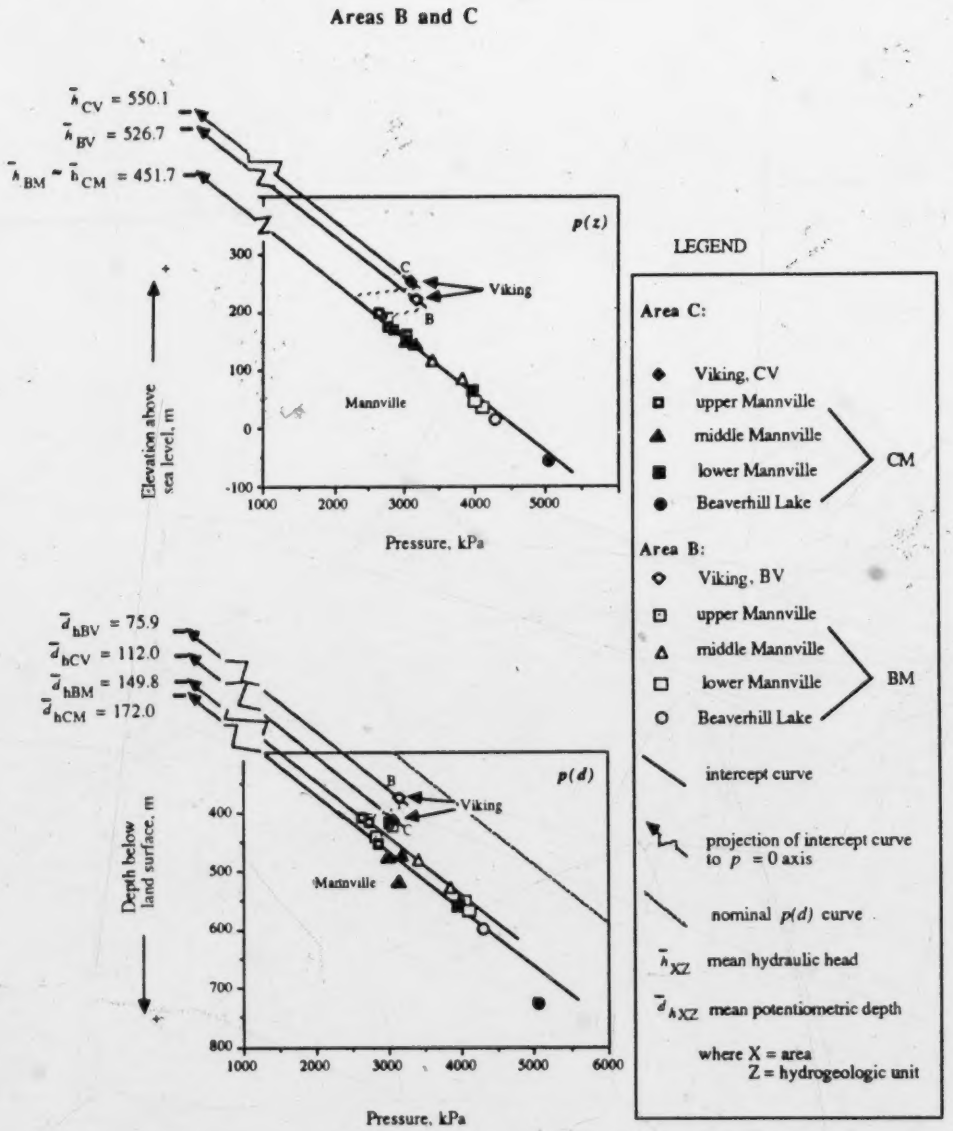

Fig. 5.9 Areas C and B *p(d)-p(z)* pattern.

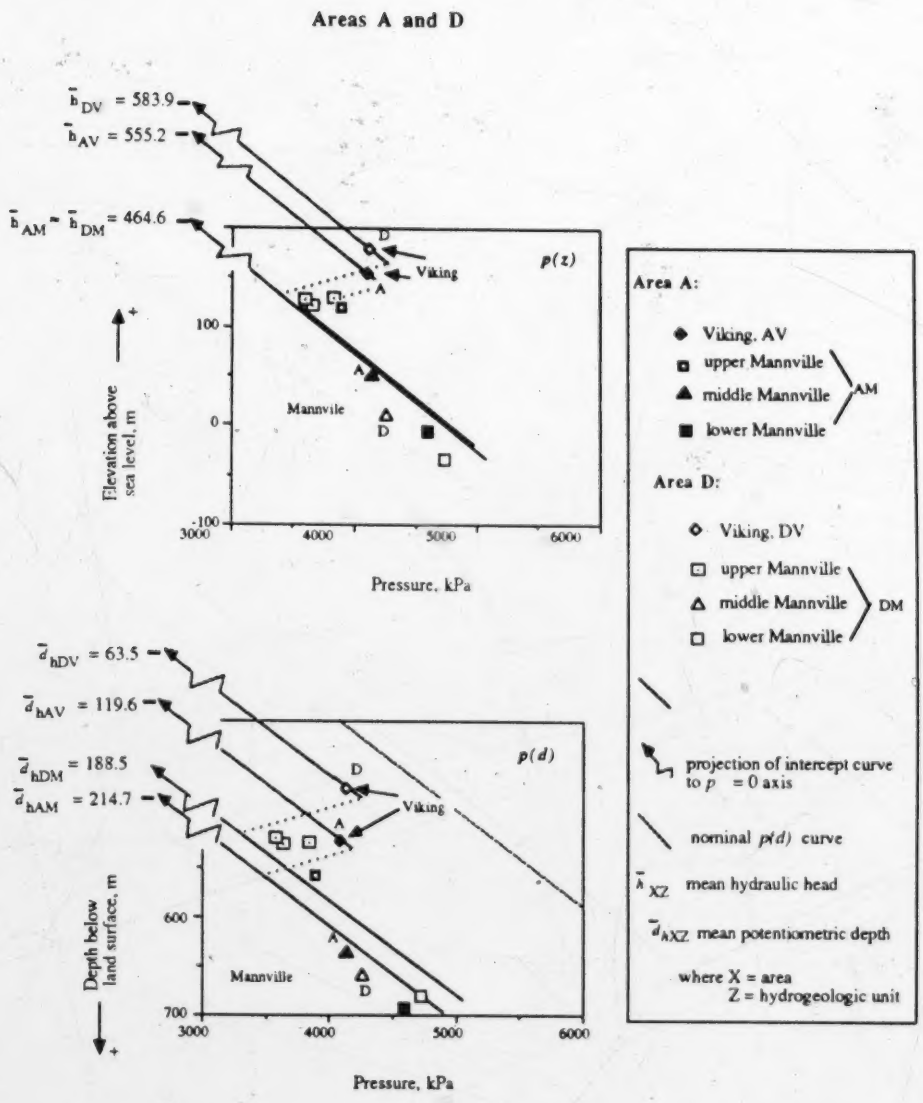

Fig. 5.10 Areas A and D *p(d)*-*p(z)* pattern.

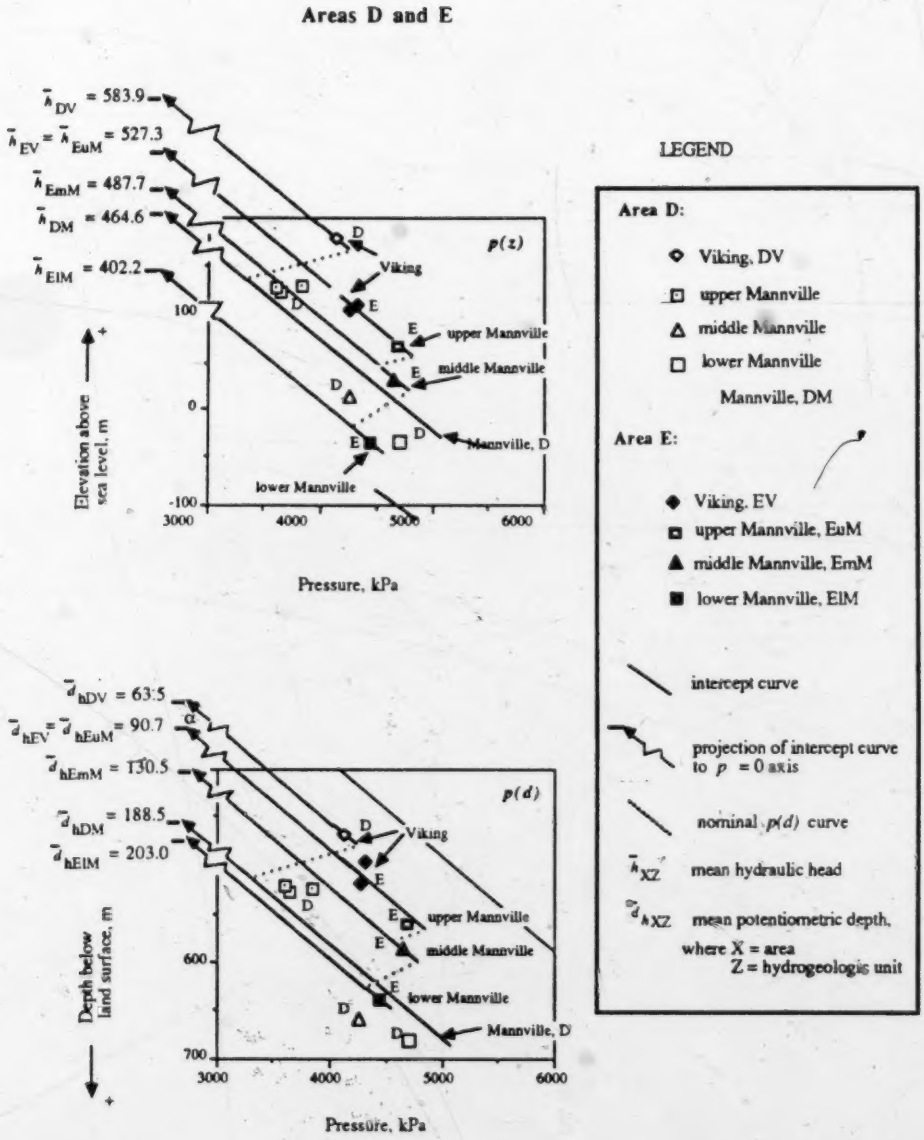

Fig. 5.11 Areas D and E *p(d)-p(z)* pattern.

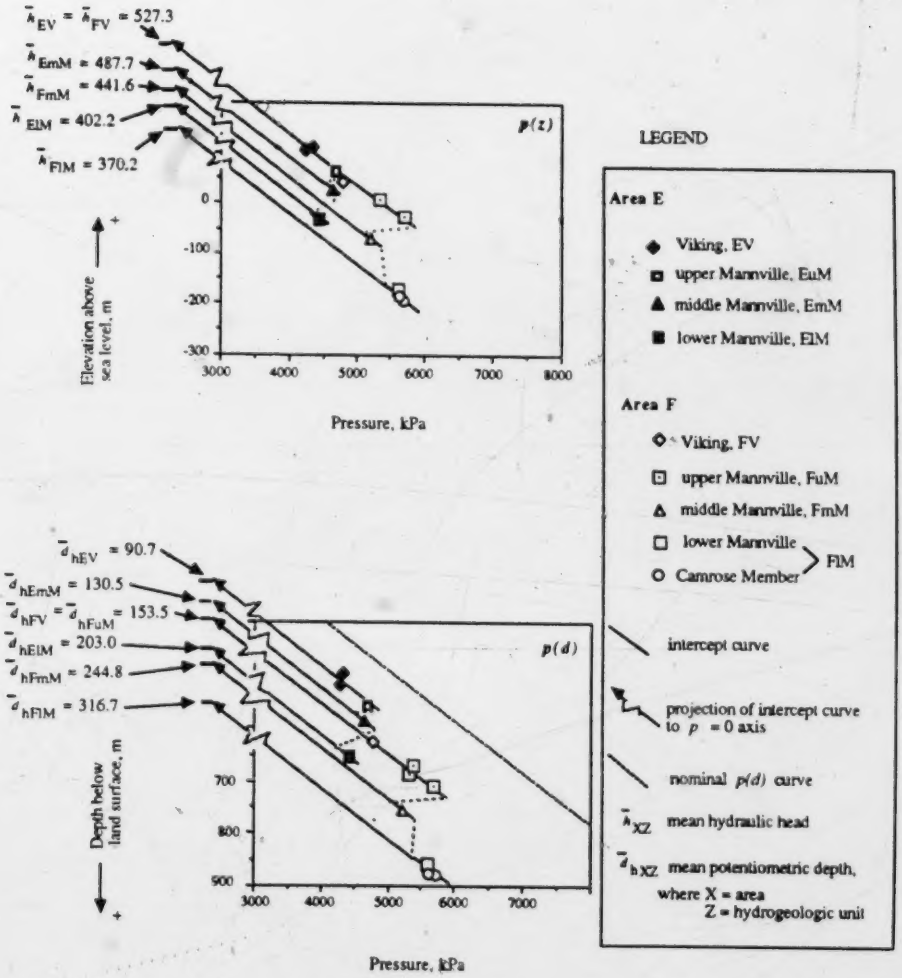

Fig. 5.12 Areas F and E *p(d)-p(z)* pattern.

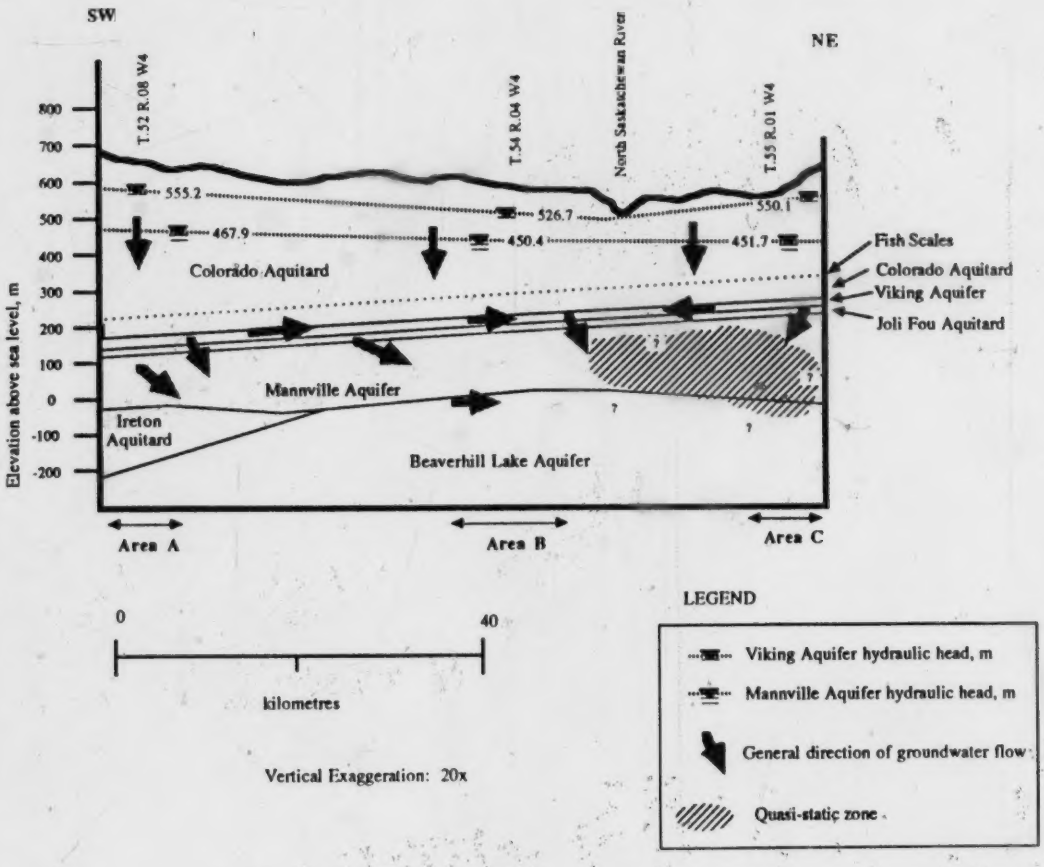

Fig. 5.13 Regional hydraulic section, northeast from Area A to Area C.

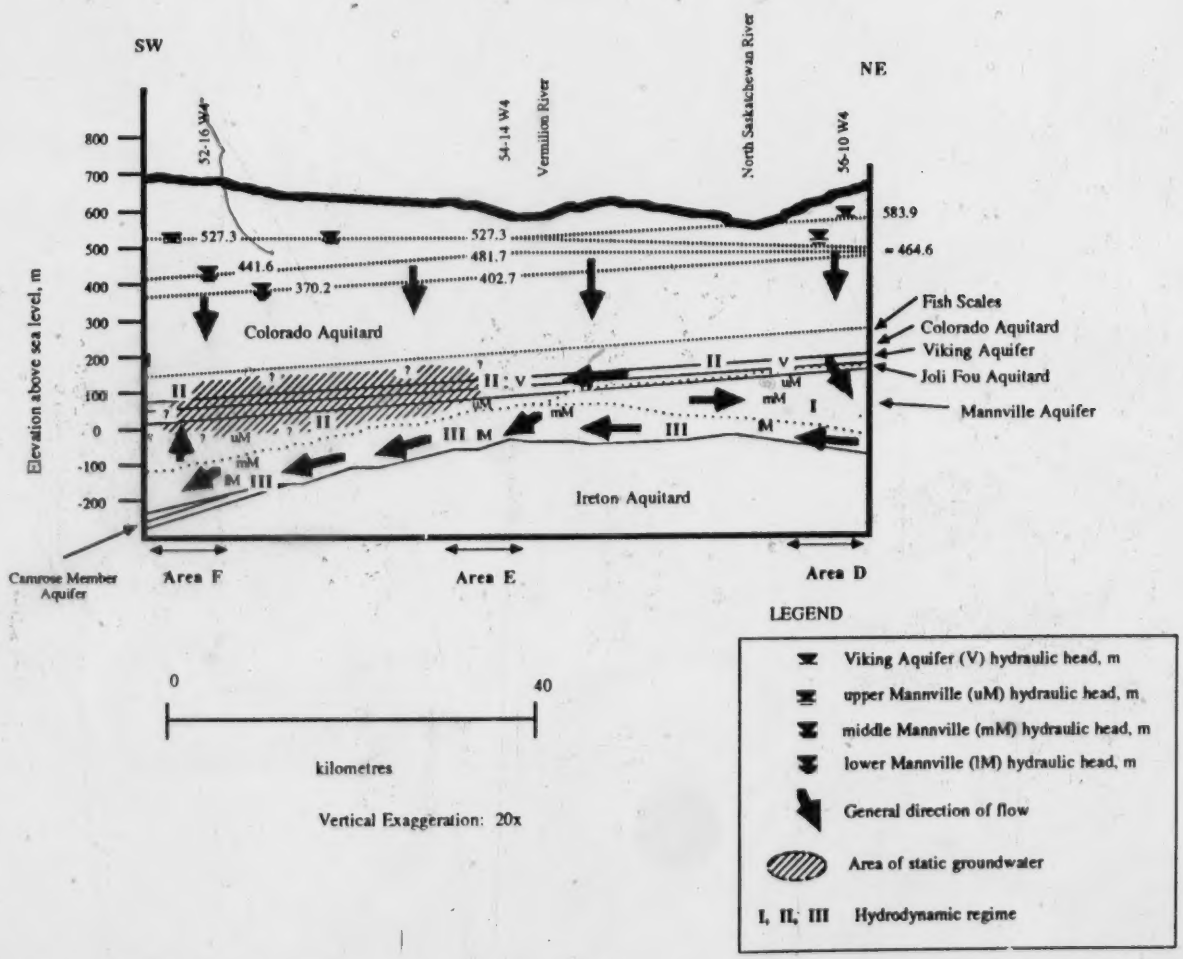

Fig. 5.14 Regional hydraulic section, northeast from Area F to Area D.

Table 5.1 - General Cretaceous-Devonian stratigraphy and hydrostratigraphy of east-central Alberta [after Hitchon et al., 1989(b), Table 1]

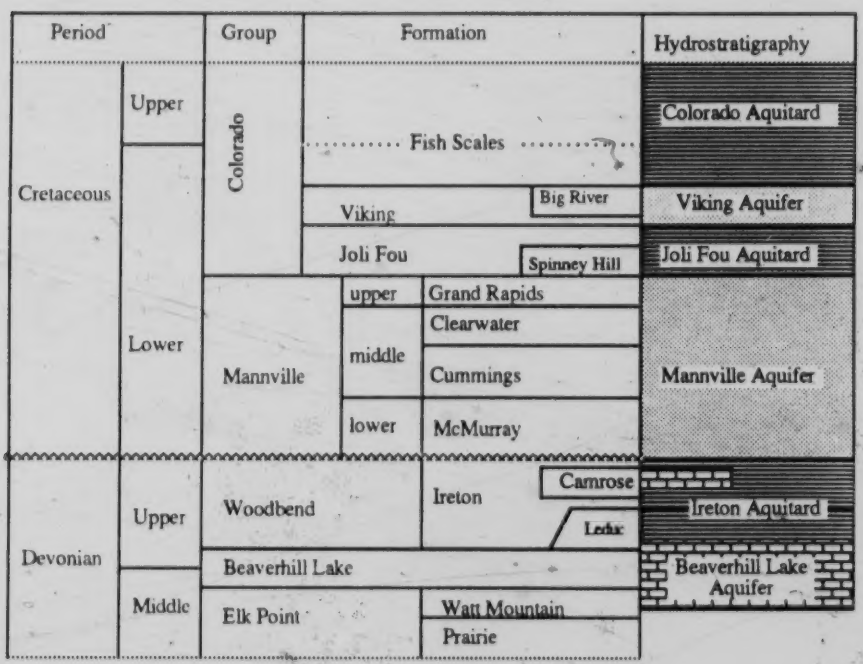

Table 5.2 - Representative values of hydraulic conductivity for strata in east and north central Alberta (compiled from Hitchon et al., 1989a, 1989b)

Hydrostratigraphic unit	Hydraulic conductivity (m/s)
Viking Aquifer	$3.4 \cdot 10^{-4}$ - $4.1 \cdot 10^{-7}$
Joli Fou Aquitard	$1.4 \cdot 10^{-10}$
Upper Mannville Aquifer	$1.0 \cdot 10^{-7}$ - $4.1 \cdot 10^{-7}$
Lower Mannville Aquifer	$6.7 \cdot 10^{-8}$ - $3.1 \cdot 10^{-7}$
Ireton Aquitard	$1.3 \cdot 10^{-8}$ - $1.7 \cdot 10^{-13}$
Camrose Member Aquifer	$2.5 \cdot 10^{-7}$
Beaverhill Lake Aquifer	$9.7 \cdot 10^{-8}$

6. SUMMARY AND CONCLUSIONS

The study addressed, both theoretically and practically, the combined use of *p(d)* and *p(z)* plots to analyze groundwater flow. After providing some theoretical background, the general properties of *p(d)* and *p(z)* plots, and the way each is non-unique, were outlined. Then the responses of theoretical *p(d)-p(z)* patterns to changes in the groundwater flow field were analyzed. Certain consistencies in the behavior of the *p(d)-p(z)* patterns became clear, and led to the definition of type *p(d)-p(z)* patterns. The type patterns reflect the scale and degree, if any, that a flow field is influenced by topography. Identification of topographic-influence is important, since it provides evidence of general hydraulic continuity. Once hydraulic continuity is evinced, groundwater flow can be reasonably inferred from the hydraulic head differences shown by a *p(d)-p(z)* pattern. And in hydrogeology, actual flow is usually too slow for observation; it must instead be inferred from hydraulic gradients. Finally, the *p(d)-p(z)* technique was applied to the investigation of lower Cretaceous hydrostratigraphy in east-central Alberta.

The *p(d) -p(z)* patterns were examined in terms of vertical and horizontal hydraulic head gradients. Two types of curves were defined: "gradient" and "intercept".

A gradient curve joins vertical pressures plotted either as *p(z)* or *p(d)*. It graphically represents the actual vertical pressure gradient $\partial p/\partial z = -\partial p/\partial d$. Relative to the groundwater's specific weight γ the slope of a gradient curve can be described as superhydrostatic, i.e., $\partial p/\partial d = -\partial p/\partial z > \gamma$, "hydrostatic", i.e., $\partial p/\partial d = -\partial p/\partial z = \gamma$,, or subhydrostatic, i.e., $\partial p/\partial d = -\partial p/\partial z < \gamma$. Gradient curves are used to infer vertical flow in isotropic media.

Intercept curves of elevation and depth were also defined. Intercept curves have hydrostatic slope γ. They are projected from a point of mean pressure-elevation or pressure-depth to a plot's $p = 0$ axis. On a *p(z)* plot, the $p = 0$ intercept gives the mean hydraulic head; on a *p(d)* plot, the intercept yields the mean potentiometric depth. Intercept curves are described according to their relative positions, and additionally in the case of *d*-intercept curves, according to their placement relative to nominal. Horizontal flow, in itself and in relation to topography, can be analyzed with intercept curves.

The theoretical analysis of Chapter 4 has shown the following:

1. The slope of a gradient curve depends on the sense and magnitude of the vertical hydraulic head gradient, i.e., the vertical groundwater driving force. A slope is superhydrostatic when the vertical component of force acts upward, hydrostatic when the force lacks a vertical component, and subhydrostatic when the force acts downward. The degree that a slope deviates from hydrostatic is proportional to the magnitude of the vertical hydraulic gradient.

2. For topography-driven flow, gradient curve slopes are increasingly subhydrostatic and superhydrostatic, respectively, toward the vertical hydraulic divides beneath recharge and discharge areas. With depth, the slopes tend to hydrostatic regardless of location within a basin.

3. The above-mentioned effects are enhanced when a shallow aquitard overlays a deep aquifer, since the flow is largely vertical in the aquitard and horizontal in the aquifer. A gradient curve in an aquitard is hydrostatic only at the areally-restricted hydraulic midline. A gradient curve in a deep aquifer will be essentially hydrostatic at all locations.

4. If vertically-measured pressures are unavailable, cross-formational flow can nevertheless be analyzed with intercept curves. A subhydrostatic *d*-intercept curve signifies a hydraulic head less than that at the overlying water table, and thus generally downward flow through a superjacent formation; one that is superhydrostatic means head in excess of that at the water table, and generally upward flow. Independently of topography, *z*-intercept curves from upper and lower strata reveal the vertical sense of flow, and indeed the magnitude of the vertical hydraulic gradient, across an intervening aquitard.

5. The use of intercept curves can be extended to two or three dimensions. The sense and magnitude of a horizontal hydraulic gradient is revealed by the relative positions and spacing, respectively, of *z*-intercepts. The degree that a horizontal hydraulic gradient coincides with the overlying topographic gradient is indicated with *d*-intercepts.

6. The spacing between *z*-intercept curves from equidistant areas is proportional to the magnitude of the intervening horizontal hydraulic gradient. Curves are overlain when the hydraulic gradient is zero, and increasingly spread as the horizontal hydraulic gradient increases.

7. The spacing between *d*-intercept curves from equidistant areas is inversely proportional to the degree of coincidence between the horizontal hydraulic gradient and the topographic gradient. The less the spacing, the greater is the coincidence, and vice versa.

8. Type *p(d)-p(z)* patterns were identified.

A Type I pattern, multiple *p(z)* curves and coincidental *p(d)* curves, signifies a horizontal hydraulic gradient equal to the topographic gradient, i.e., ideally unconfined conditions.

A Type II pattern, an exchange of curve positions from one plot to another, occurs uniquely when the hydraulic gradient has the same sense as the topographic gradient but is relatively subdued, i.e., likely topographic influence made possible by hydraulic continuity.

A Type III pattern, coincidental *p(z)* curves and multiple *p(d)* curves, indicates a zero horizontal hydraulic gradient beneath a sloping land surface. Depending on the scale of investigation, this pattern can signify either the potentiometric strike of an aquifer uninfluenced by the locally-overlying topography, or a static and regionally-confined condition, or a hydraulically-closed system.

The Types IV and V patterns both show a lack of positional exchange. A Type IV is observed when groundwater flow is against topography, a Type V when the motion is under a hydraulic gradient that exceeds the slope of the land. Depending on the scale of investigation, both types suggest either a dynamic but confined condition, or a source of potential other than gravity.

The field investigation of Chapter 5 has shown the following:

1. The flow directions inferred from the *p(d)-p(z)* method generally agreed with those obtained from previous studies. The existence of a major hydraulic divide in the lower Cretaceous strata was confirmed.

2. Three hydrodynamic zones are present. Hydrodynamic Zone I is northeast of the hydraulic divide, whereas Zones II and III are southwest of it.

3. Hydrodynamic Zone I comprises the Viking and Mannville Aquifers. The Viking Aquifer is regionally unconfined. Flow is downward from the Viking to the Mannville Aquifer under a steep vertical hydraulic gradient. A further head decline with depth is observed generally in the Mannville. In the northeast, a quasi-static zone occurs in the Mannville. Heavy oil sand deposits are associated with the zone. The hydraulic heads of Zone I are influenced by regional topography as well as by subcrop-discharge of Mannville waters.

4. Hydrodynamic Zone II includes the Viking and upper Mannville. The Viking heads decrease steeply toward a regional topographic low located in the southwest. Further to the southwest, beneath a regional topographic high, they become laterally constant and, at the same time, equal to the upper Mannville heads. Erosional rebound of the Colorado shales may influence the head distribution of Zone II.

5. Hydrodynamic Zone III comprises the middle and lower Mannville. Flow to the southwest is against the topography at any scale. Vertically, flow is downward from the middle to the lower Mannville. The motion may be influenced by the Rimbey-Meadowbrook reef trend, a postulated conduit for basinal flow.

Essentially, characterizing a groundwater flow field and identifying the mechanisms which influence it are three-dimensional problems. The *p(d)-p(z)* technique allows vertical and horizontal hydraulic gradients to be determined, and then analyzed in terms of their possible relation to topography. It thus seems that the combined use of *p(d)* and *p(z)* plots may prove to be a useful new technique for investigating groundwater flow.

7. REFERENCES

Bair, E.S., 1987a. Analysis of hydraulic gradients across the host rock at the proposed Texas Panhandle Nuclear Waste Reposition Site. Ground Water, v. 25 p. 440-447.

Bair, E.S., 1987b. Regional hydrodynamics of the proposed high-level nuclear waste repository sites in the Texas Panhandle. J. Hydrol. v.92 p. 149-172.

Bear, J., 1988. Dynamics of Fluids in Porous Media. Dover, New York, 764 p.

Beaumont, E. A., 1984. Retrogradational shelf sedimentation: Lower Cretaceous Viking Formation, central Alberta; *in* Tillman, R.W. and C.T. Siemans (Eds.), Siliciclastic Shelf Sediments. Tulsa, Society of Economic Paleontologists and Mineralogists, Special Publication 34, p.163-178.

Beer, F. P. and E. P. Johnston, 1977. Vector Mechanics for Engineers. McGraw-Hill, New York, 448 p.

Belitz, K. and J. D. Bredehoeft, 1989. Hydrodynamics of Denver Basin: explanation of subnormal fluid pressures. Amer. Assoc. Petrol. Geol. Bull., v. 72, p. 1334-1359.

Bradley, J.S., 1975. Abnormal formation pressure. Amer. Assoc. Petrol. Geol. Bull., v. 59, p. 957-973.

Bredehoeft, J. D. and B. B. Hanshaw, 1968. On the maintenance of anomalous fluid pressures: I. thick sedimentary sequences. Geol. Soc. Amer. Bull., v.79, p. 1097-1106.

Dahlberg, E. C., 1982. Applied Hydrodynamics in Petroleum Exploration., Springer-Verlag, New York, 161 p.

Domenico, P. A., 1972. Concepts and Models in Groundwater Hydrology. Prentice-Hall, New York, 405 p.

Domenico, P. A. and F. W. Schwartz, 1990. Physical and Chemical Hydrogeology. John Wiley and Sons, New York, 824 p.

Draper, N. P. and H. Smith, 1967. Applied Regression Analysis. Wiley, New York.

England, L. A. and R. A. Freeze, 1988. Finite element simulation of long-term transient regional groundwater flow. Ground Water, v. 26, p. 298-308.

Freeze, R. A., 1969. Theoretical Analysis of Regional Groundwater Flow. Scientific Series No. 3, Inland Waters Branch, Energy, Mines and Resources, Canada. Ottawa.

Freeze, R. A., and J. A. Cherry, 1979, Groundwater. Prentice Hall, Englewood Cliffs, New Jersey, 604 p.

Freeze, R. A., and P. A. Witherspoon, 1966. Theoretical analysis of regional groundwater flow. I, Analytical and numerical solutions to the mathematical model. Water Resour. Res., v.2, p. 641-656.

Freeze, R. A., and P. A. Witherspoon, 1967. Theoretical analysis of regional groundwater flow. II, Effect of water table configuration and subsurface permeability variations. Water Resour. Res., v.3, p.623-634.

Garven, G., 1989. A hydrogeological model for the formation of the giant oil sands deposits of the Western Canada Sedimentary Basin. Submitted to the American Journal of Science, August, 1987.

Hitchon, B. 1969. Fluid flow in the Western Canada Sedimentary Basin. 2. Effect of geology. Water Resour. Res. v.5 p. 460-469.

Hitchon, B., C. M. Sauveplane, S. Bachu, E. Koster and A. Lytviak, 1989a. Hydrogeology of the Swan Hills Area, Alberta: Evaluation for deep waste injection. Alberta Research Council Bulletin No. 58. Alberta Research Council, Alberta Geological Survey, Edmonton, Canada.

Hitchon, B., S. Bachu, C. M. Sauveplane, A. Ing, A. T. Lytviak and J. R. Underschultz, 1989b. Hydrogeological and geothermal regimes in the Phanerozoic succession, Cold Lake area, Alberta and Saskatchewan. Alberta Research Council Bulletin No. 59. Alberta Research Council, Alberta Geological Survey, Edmonton, Canada.

Holysh, S., 1989. Petroleum Related Geochemical Signatures and Regional Groundwater Flow, Chauvin Area, East-Central Alberta. Unpubl. M. Sc. Thesis. University of Alberta, Edmonton.

Horner, D. R., 1951. Pressure buildup in wells. Proc., 3rd World Petrol. Cong., The Hague, Sec. II, p. 503-523.

Hubbert, M. K., 1940. The theory of groundwater motion. J. Geol., v.48, p.785-944.

Hugo, K. 1990. Mechanisms of groundwater flow and oil migration associated with Leduc reefs. Can. Petrol. Geol. Bull., v. 38, p. 307-319.

Hunt, J. M., 1990. Generation and migration of petroleum from abnormally pressured fluid compartments. Amer. Assoc. Petrol. Geol. Bull., v.74, p. 1-12.

Johnston, R. H., 1986. Opus Handbook: Formation Waters of Alberta. Opus Petroleum Engineering Ltd., Calgary.

Kendall, M. G. and A. Stuart, 1965. The Advanced Theory of Statistics, v. 2. Hafner, New York, 678 p.

Kovács, G., 1978. General Report I, Hydrogeology of Great Sedimentary Basins. Proceedings of the Budapest Conference, May/June 1976. IAH-IAHS.

Le Breton, E. G., 1963. Groundwater Geology and Hydrology of East-Central Alberta. Research Council of Alberta, Bull. 13. Research Council of Alberta, Edmonton.

Lindley, D. V., 1947. Regression Lines and the Linear Functional Relationship. Supplement to the Journal of the Royal Statistical Society, v. 9, no. 2, series B., p.218-244.

Lusczynski, N. J., 1961. Head and flow of groundwater of variable density. J. Geophys. Res. v. 66, p. 4247-4256.

Mark, D. H. and M. Church, 1977. On the misuse of regression in earth sciences. Mathematical Geology, v. 9, p.63-74.

de Marsily, G., 1986. Quantitative Hydrogeology, Groundwater Hydrology for Engineers. Academic Press, San Diego, California, 440 p.

McDonald, M. G., and A. W. Harbaugh, 1988. A modular three dimensional finite difference groundwater flow model. U.S. Geol. Survey.

Neuzil, C. E. and D. W. Pollock, 1982. Erosional unloading and fluid pressures in hydraulically "tight" rocks. J. Geol., v. 91, p. 179-183.

Oberlander, P. L., 1989. Fluid density and gravitational variations in deep boreholes and their effect on fluid potential. Ground Water, v. 27 p. 341-350.

Orr, E. and C.W. Kreitler, 1985. Interpretation of pressure-depth data from confined underpressured aquifers exemplified by the Deep Basin Brine aquifer. Water Resour. Res., v. 21, p. 533-544.

Porter, J. W., R. A. Price and R. G. McCrossan, 1982. The Western Canada Sedimentary Basin. Phil. Trans. R. Soc. Lond. A v. 305, p. 169-172.

Putnam, P. E., 1982. Aspects of the petroleum geology of the Lloydminster heavy oil fields, Alberta and Saskatchewan. Bull. Can. Petrol. Geol., v. 30, p. 81-111.

Reid, H. W., 1986. Drillstem Test Interpretation Seminar Manual. H. W. Reid and Assoc. Ltd., Calgary, Alberta.

Remson, I., G. M. Hornberger and F.J. Molz, 1971. Numerical Methods in Subsurface Hydrology. Wiley Interscience, New York.

Sampson, R. J., 1975. Surface II Graphics System. Kansas Geological Survey Series on Spatial Analysis, No. 1. Lawrence, Kansas.

Senger, R. K. and G. E. Fogg, 1987. Regional underpressuring in deep brine aquifers, Palo Duro Basin, Texas. 1, Effects of hydrostratigraphy and topography. Water Resour. Res., v. 23, p. 1481.

Sharp, J. H., 1983. Permeability control on aquathermal pressure. Amer. Assoc. Petrol. Geol. Bull., v.67 p. 2057-2061.

Simpson, F., 1975. Marine lithofacies and biofacies of the Colorado Group (middle Albian to Santonian) in Saskatchewan; *in* The Cretaceous system in the western interior of North America, W. G. E. Caldwell (ed.), Geological Association of Canada Special Paper 13, p. 553-588.

Stoakes, F. A., 1980. Nature and control of shale basin fill and its effect on reef growth and termination: Upper Devonian Duvernay and Ireton formations of Alberta, Canada. Bull. Can. Petr. Geol., v. 28, p. 345-410.

Tóth, J., 1962. A theory of groundwater motion in small drainage basins in Alberta. J. Geophys. Res., v. 67, p. 4375-4387.

Tóth, J., 1963. A theoretical analysis of groundwater flow in small drainage basins. J. Geophys. Res., v. 68, p. 4795-44812.

Tóth, J., 1978. Gravity-induced cross-formational flow of formation fluids, Red Earth region, Alberta, Canada: Analysis, patterns and evolution. Water Resour. Res., v. 14 p. 805-843.

Tóth, J., 1979. Patterns of dynamic pressure increment of formation fluid flow in large drainage basins, exemplified by the Red Earth region. Bull. Can. Petrol. Geol., v. 27, p. 63-86.

Tóth, J., 1982. Reply to Kinji Magara including a discussion of the concept and phenomenon of the "tensiometric effect" in cross-formational gravity-driven flow systems of formation fluids. Bull. Can. Petrol. Geol., v. 29, p. 135-142.

Tóth, J., 1990. Hydraulic Continuity in Large Sedimentary Basins, *International Conference on Groundwater in Large Sedimentary Basins*, International Association of Hydrogeologists. July 8 - 10, 1991, Perth, Australia.

Tóth, J. and R. F. Millar, 1983. Possible effects of erosional changes of the topographic relief on pore pressures at depth. Water Resour. Res., v. 19, p. 1585-1597.

Tóth, J. and T. Corbet, 1986. Post-Paleocene evolution of groundwater flow systems and their relation to petroleum accumulations, Taber area, Southern Alberta. Bull. Can. Petrol. Geol., v. 34, p. 339-363.

Tóth, J. and K. Rakhit, 1988. Exploration for reservoir quality rock bodies by mapping and simulation of potentiometric surface anomalies. Bull. Can. Petrol. Geol., v. 36, p. 362-378.

Trescott, P. C., G. F. Pinder and S. P. Larson, 1976. Finite difference model for aquifer simulation in two dimensions with results of numerical experiments. U. S. Geol. Surv. Tech. Water Res. Invest., Book 7, Chap. C1, 116 p.

Wang, H. F., and M. P. Anderson, 1982. Introduction to Groundwater Modeling- Finite Difference and Finite Element Methods. W. H. Freeman, San Francisco, 237 p.

Williams, E. J., 1959. Regression Analysis. Wiley, New York.

Appendix A

Programs used for numerical simulation and sample output

```
Listing of BCF EC at 20 03 27 on MAR 27, 1991 for CC1@rMACC on UALTAMTS

     1                1                0
     2        0
     3                0            1 0
     4                8              1 (200F6 1)          -4
     5                9              1  (72F6 1)          -4
     6               10              1 (200E9 2)          -4

LIST $1B 6Q *PRINT* LPP=126
```

```
Listing of STP EC at 20 03 28 on MAR 27, 1991 for CC1@rMACC on UALTAMTS

     1              350                5
     2            1 0     1 0E-5            0    3 6E-07          1

 IST $1C 6Q *PRINT* LPP=126
```

```
Listing of $1C EC at 20 03 28 on MAR 27, 1991 for CC1@rMACC on UALTAMTS

     1                6
     2                1                1                0          0
     3                1                0                           0

LIST $RQ $ 1S1 *PRINT* LPP=126
```

Listing of SHD 5 LST at 20 03 26 on MAR 27, 1991 for EC1@RMACC on BALTAMIS

```
      1     C SHD 5 LST
      2     C This program assigns nodes at the upper boundary, as well as starting nodes  for basins of simple topography
      3     C
      4           IMPLICIT REAL*8(A-H)
      5           DIMENSION DELR(300),SHEAD(300,72)
      6           INTEGER NCOL,NROW
      7           NCOL=300
      8           NROW=72
      9     C
     10           READ(5,10) (DELR(J),J=1,NCOL)
     11        10 FORMAT(300F5 1)
     12     C
     13           SUM1=DELR(1)/2 0
     14           DO 20 J=2 NCOL
     15           SUM(J)=SUM(J-1)+(DELR(J-1)/2 0)+DELR(J)/2 0
     16        20 CONTINUE
     17           DO 30 I=1,NROW
     18                DO 40 J=1,NCOL
     19                   SHEAD(J,I)=-12 00E-2*SUM(J)+1200 00
     20        40      CONTINUE
     21        30 CONTINUE
     22     C
     23           DO 50 I=1,NROW
     24           WRITE(8,60) (SHEAD(J,I),J=1,NCOL)
     25        60 FORMAT(300F7 2)
     26        50 CONTINUE
     27           STOP
     28           END
```

LIST src 5 lst /PRINT= LPP=126

Listing of SRC 5 LST at 20 03 26 on MAR 27, 1991 for EC1@RMACC on BALTAMIS

```
      1     C******  SRC 5 LST
      2     C This program assigns row and column widths, where
      3     C           DELR(NCOL) is column width
      4     C           DELC(NROW) is row width
      5     C
      6           IMPLICIT REAL*8(A-H)
      7           DIMENSION DELR(300), DELC(72)
      8           INTEGER NCOL, NROW
      9           NCOL=300
     10           NROW=72
     11     C
     12     C Assign column widths (DELR)
     13     C
     14           DO 10 J=1,NCOL
     15           DELR(J)=100 0
     16        10 CONTINUE
     17     C
     18     C Assign row widths (DELC)
     19     C
     20           DO 30 I=1,27
     21           DELC(I)=30 0
     22        30 CONTINUE
     23           DO 35 I=28,39
     24           DELC(I)=10 0
     25        35 CONTINUE
     26           DO 40 I=40,48
     27           DELC(I)=30 0
     28        40 CONTINUE
     29           DO 50 I=49,59
     30           DELC(I)=10.0
     31        50 CONTINUE
     32           DO 60 I=61,72
     33           DELC(I)=30.0
     34        60 CONTINUE
     35     C
     36     C Write DELR and DELC so that they may be read by module MODBAS. (FMTINCFG 1)
     37     C
     38           WRITE(6,100) (DELR(J),J=1,NCOL)
     39       100 FORMAT(10GF8 1)
     40           CONTINUE
     41           WRITE(7,200) (DELC(I),I=1,NROW)
     42       200 FORMAT(72F8 1)
     43           STOP
     44           END
```

LIST src 5c lst /PRINT= LPP=126

Listing of TRN 2C LST at 20 03 28 on MAR 27, 1991 for CC1@+MACC on UALTAMTS

```
      1      C******* TRN 2C LST
      2      C*** A program that writes transmissivities along rows
      3      C
      4            IMPLICIT REAL*8(T)
      5            DIMENSION TRN(200,72)
      6            INTEGER NROW,NCOL
      7            NROW=72
      8            NCOL=200
      9      C
     10            DO 100 I=1,84
     11            DO 10 J=1,NCOL
     12            TRN(J,I)=20 00E-10
     13         10 CONTINUE
     14        100 CONTINUE
     15      C
     16            DO 200 I=85,NROW
     17            DO 20 J=1,NCOL
     18            TRN(J,I)=20 00E-07
     19         20 CONTINUE
     20        200 CONTINUE
     21      C
     22            DO 300 I=1,NROW
     23            WRITE(6,400) (TRN(J,I),J=1,NCOL)
     24        300 CONTINUE
     25        400 FORMAT(200E8 3)
     26            STOP
     27            END
```

```
LIST src $ dg *PRINT* LPP=126
```

Listing of SRF $ EC at 20 03 28 on MAR 27, 1991 for CC1@+MACC on UALTAMTS

```
      1      TITLE    'simple - 1.20 - mm32, no v.e., 2g'
      2      DEVI     1,'MACC'
      3      IQRY     12400,11,3,1,2,3,-1,0,0,0,'(3F12.3)'
      4      GRID     1,100,100,1,4,1,0
      5      ROUT     12,1,'(3F10.3)'
      6      POUT
      7      BLAN
      8      EXTR     0.20000 0,0,2000 0
      9      OCTA     1,2,,,4,11,35
     10      NEAR     2,0,,,
     11      CONT     0,0,,0,0
     12      CINT     2,,,,,0 05,0,1 5,
     13      LEVE     13,19,'(F5 0,13)'
     14      BOX      1000 0,0,1000 0,0,,,,,,
     15      BIIC     1,14 0,
     16      PERP
     17      STOP
```

```
LIST rog $ tst *PRINT* LPP=126
```

```
Listing of $OU $ DAT at 20-03-28 on MAR 27, 1991 for CC:[GMACC on UALTAMTS

     1          $   1
     2              0.00          0.00
     3          20000.00          0.00
     4          20000.00        800.00
     5              0.00       1200.00
     6              0.00          0.00
     7       1060  0  0
     8       1040  0  0
     9       1020  0  0
    10       1000  0  0
    11        980  0  0
    12        960  0  0
    13        940  0  0
    14        920  0  0
    15        900  0  0
    16        880  0  0
    17        860  0  0
    18        840  0  0
    19        820  0  0


LIST TOV $ DAT "PRINT" LPP=125
```

```
Listing of LEV $ DAT at 20-03-28 on MAR 27, 1991 for CC:[GMACC on UALTAMTS

     1       1180  0  0
     2       1160  0  0
     3       1140  0  0
     4       1120  0  0
     5       1100  0  0
     6       1080  0  0
     7       1060  0  0
     8       1040  0  0
     9       1020  0  0
    10       1000  0  0
    11        980  0  0
    12        960  0  0
    13        940  0  0
    14        920  0  0
    15        900  0  0
    16        880  0  0
    17        860  0  0
    18        840  0  0
    19        820  0  0


RELEASE "PRINT"
"PRINT"  explicit hold has been removed
$ SDISPLAY WARDS SOFTS
Invalid operand "SOFTS"

Usage     COPY  FROM: (Fdname1)    TO: (Fdname2):
          (Fdname1) and (Fdname2) may be arbitrary Fdnames
          containing at most one file-name pattern each


$ LOC OFF
"LOC"  does not exist


$SIC
```

```
Listing of REC $ LST d1 20:03:26 on MAR 27, 1991 for CC:dsMACC on WALTAMYS

      1     C REC $ LST
      2     C  A program that transfers x,d, p and h at x=50 0,10050.0 and 18550 0 m for analysis on the Macintosh
      3           IMPLICIT REAL*8(D-Z)
      4           CHARACTER*1 TAB
      5           DIMENSION DD(200,72),,HH(200,72),,XX(200,72),,PP(200,72),,ZZ(200),
     6           *ZZ(72)
      7           INTEGER NROW,NCOL
      8           TAB=CHAR(09)
      9           NROW=72
     10           NCOL=200
     11     C
     12     C Read data from _ grd
     13     C
     14           DO 10 I=1,NROW
     15           DO 10 J=1,NCOL
     16           READ(5,100) ZZ(J),ZZ(I),HH(J,I)
     17        10 CONTINUE
     18       100 FORMAT(3F20 2)
     19     C
     20     C Determine depths and pressures
     21     C
     22           DO 15 I=1,NROW
     23           DO 15 J=1,NCOL
     24           XX(J,I)=-0 00E-02*ZZ(J)*1200 00
     25           DD(J,I)=XX(J,I)-ZZ(I)
     26           PP(J,I)=(HH(J,I)-ZZ(I))*9 80665
     27        15 CONTINUE
     28     C
     29     C Rewrite.
     30     C
     31           DO 30 J=1,NCOL
     32           DO 30 I=1,NROW
     33           IF(ZZ(J) EQ 50 00 OR XX(J).EQ 10050 00.OR ZZ(J) EQ 18550 00) THEN
     34           WRITE(8,200) ZZ(J),TAB,ZZ(I),TAB,DD(J,I),TAB,PP(J,I),TAB,HH(J,I)
     35           ENDIF
     36        30 CONTINUE
     37       200 FORMAT(5(F8 2,A1))
     38           CONTINUE
     39           STOP
     40           END


LIST REC.$ dat /PRINT/ LPP=126
```

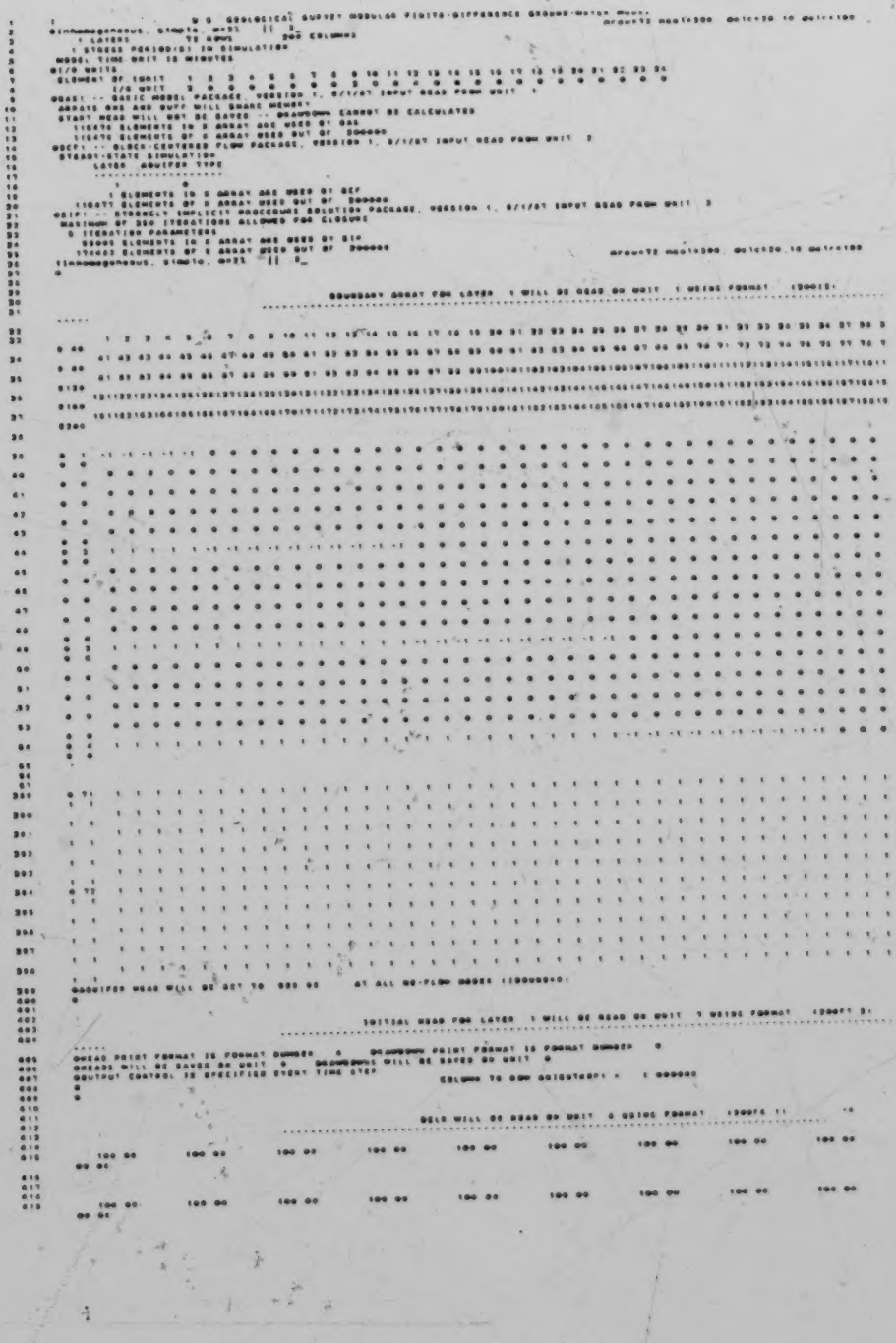

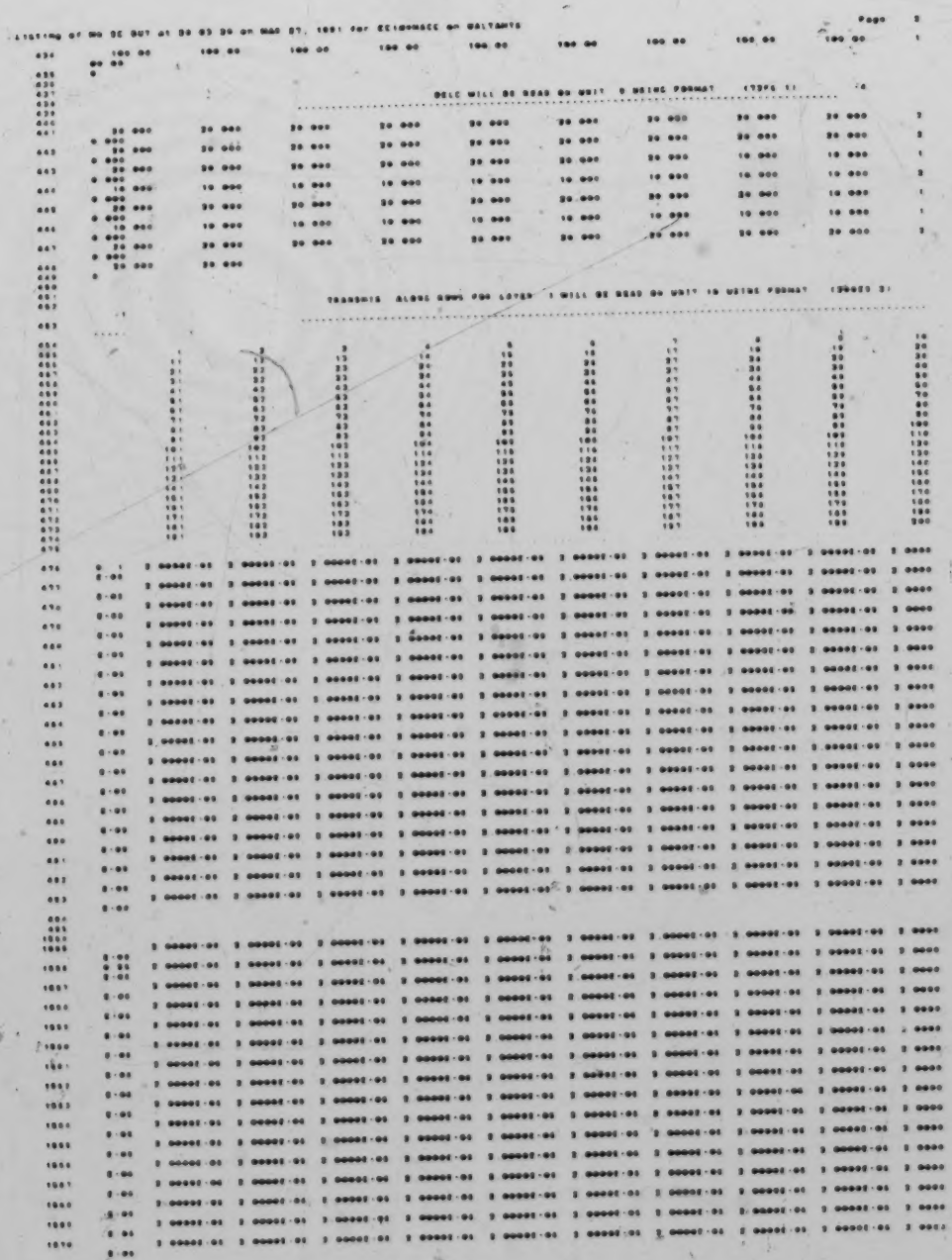

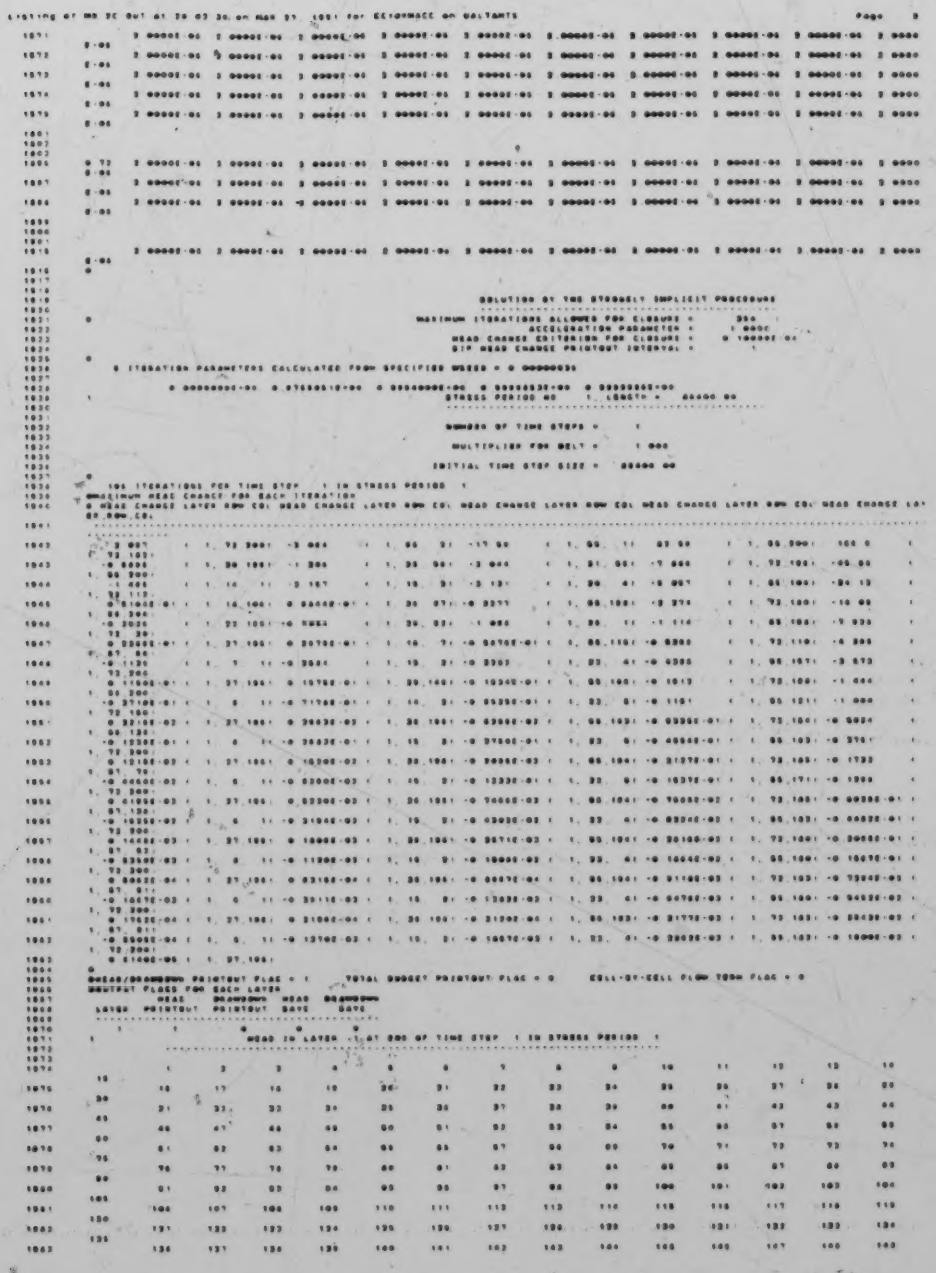

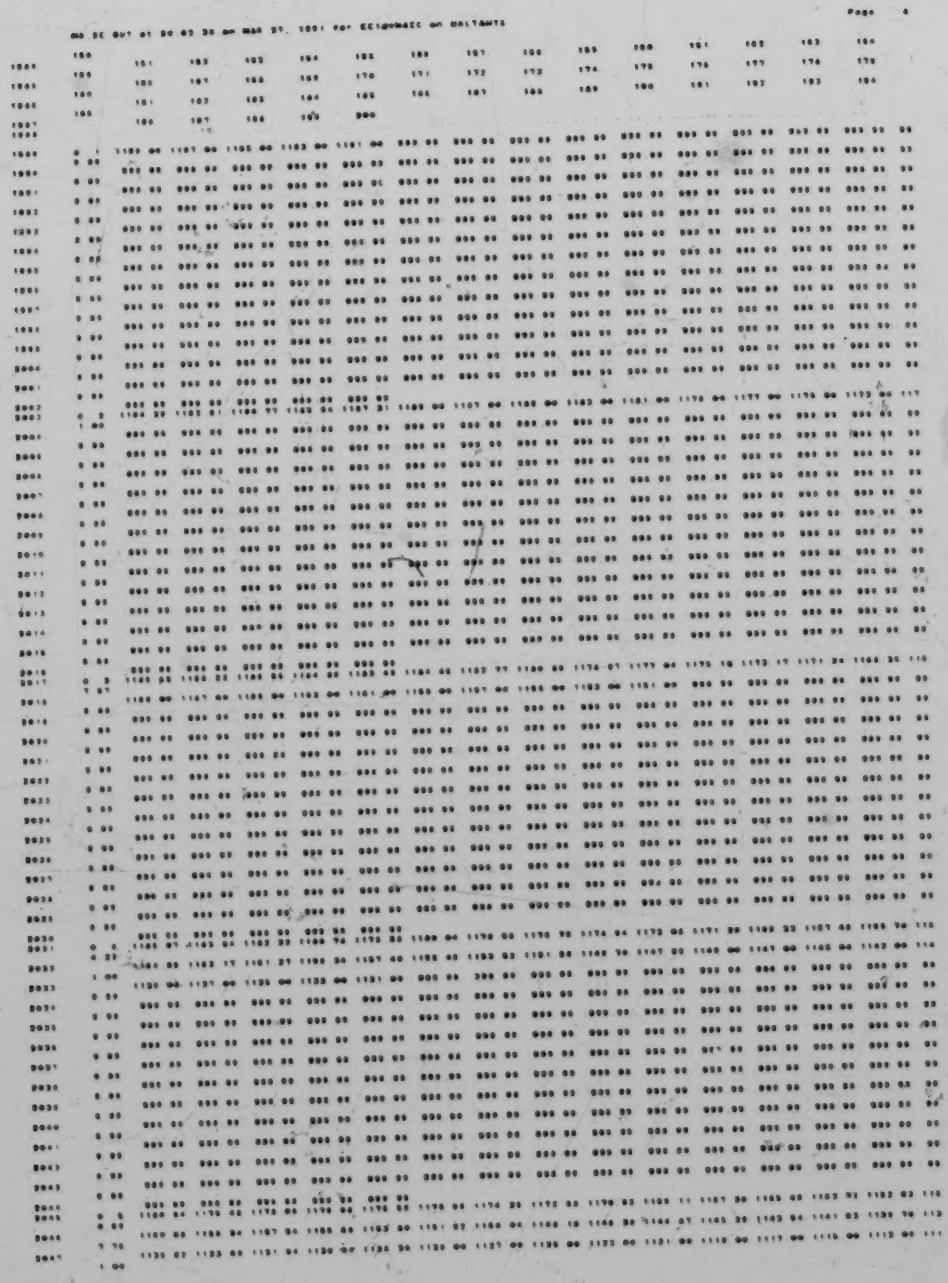

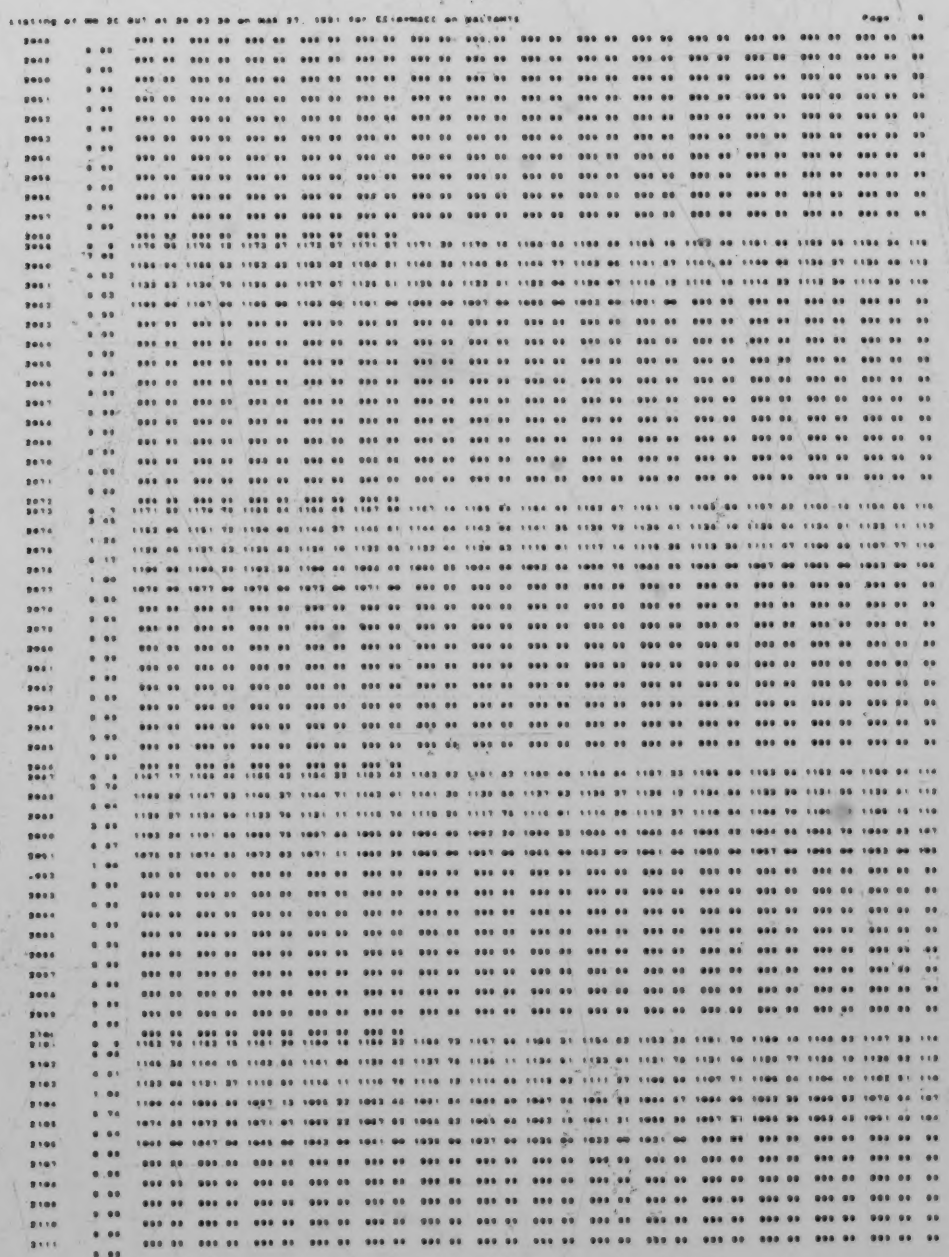

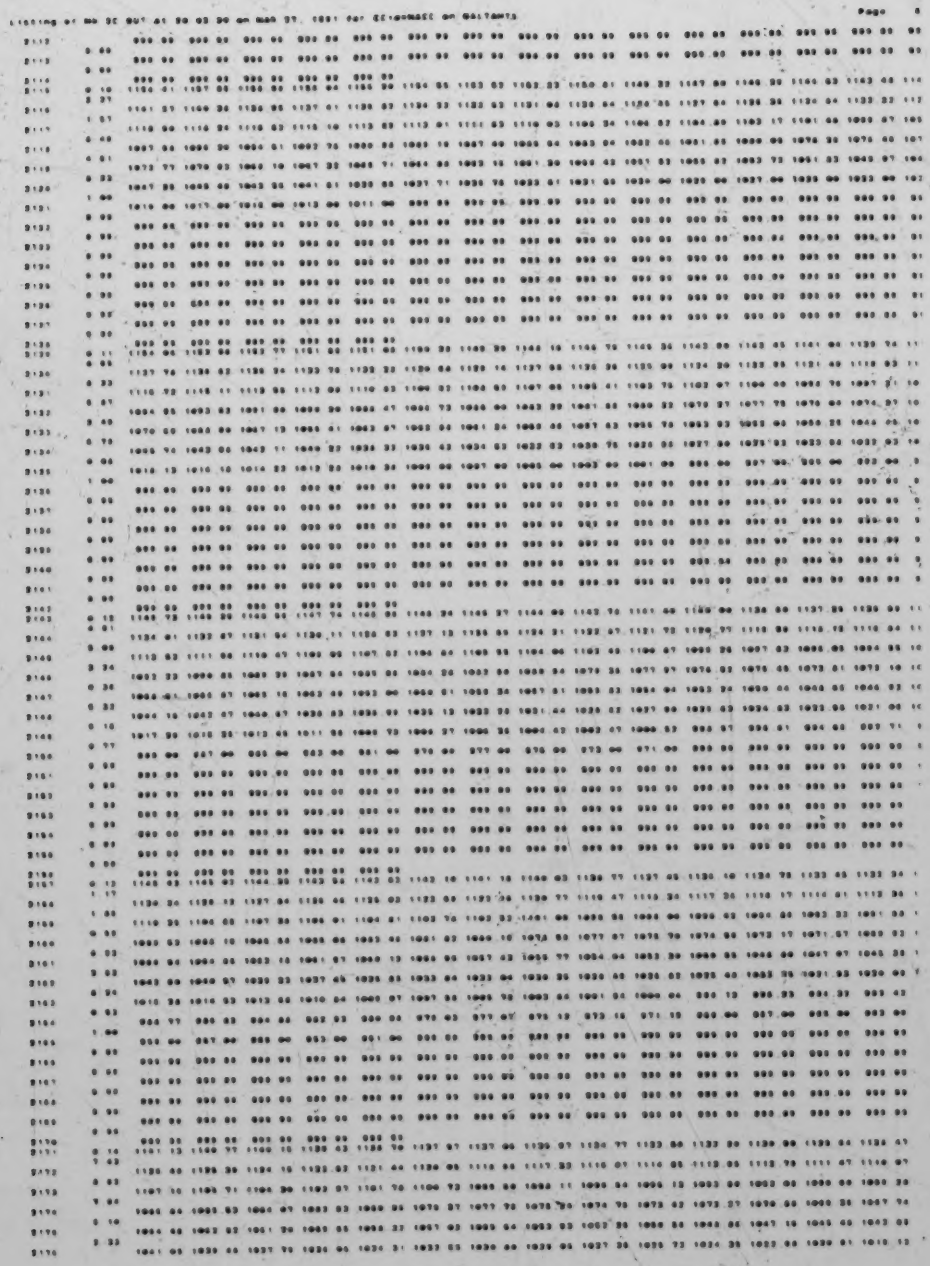

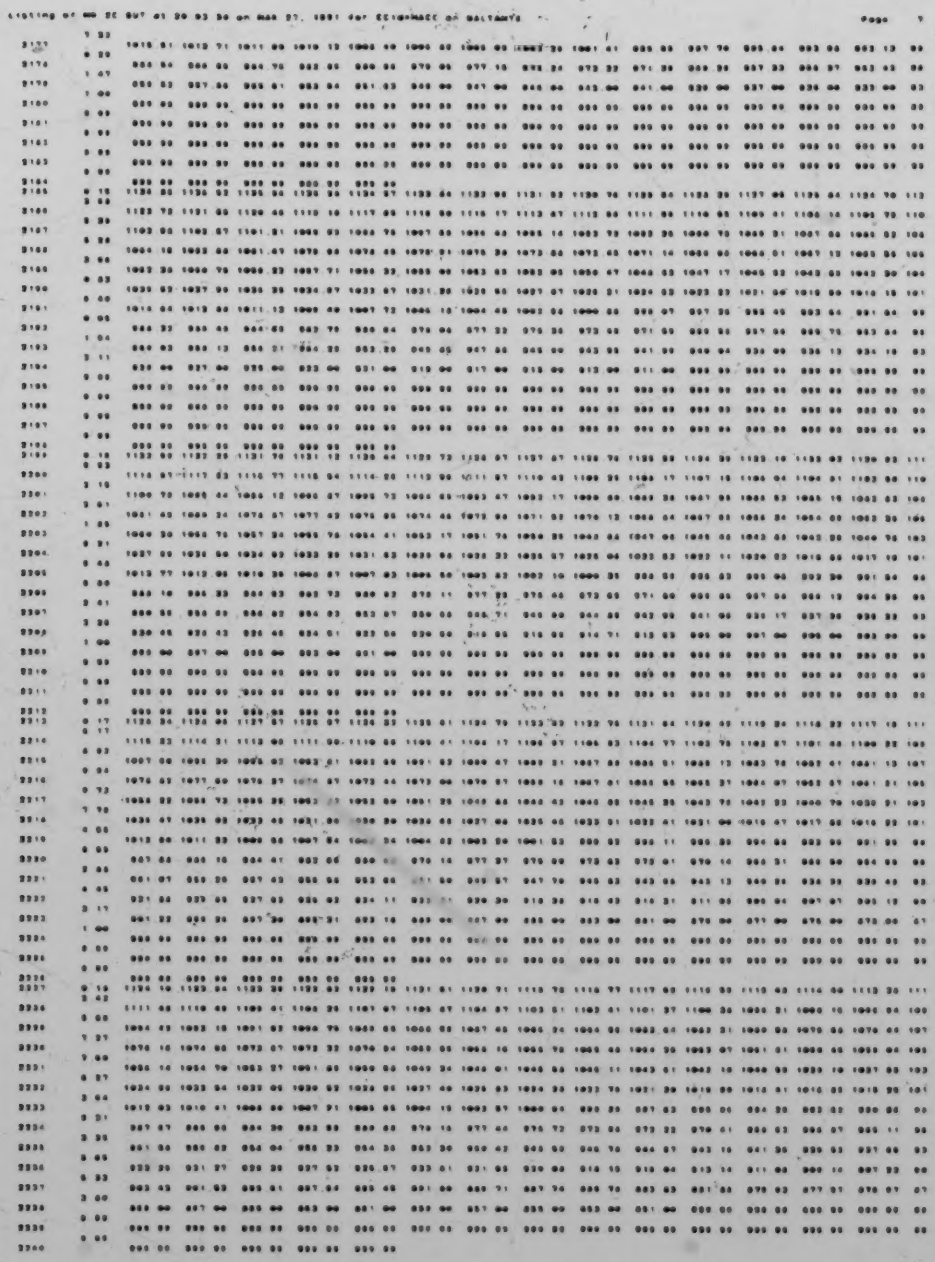

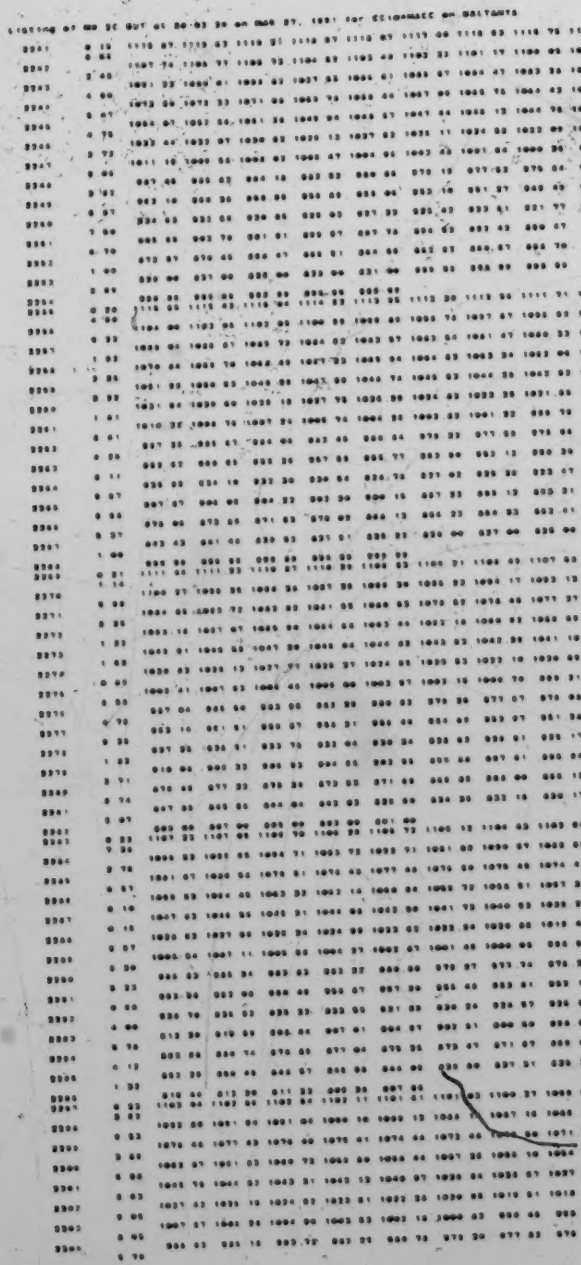

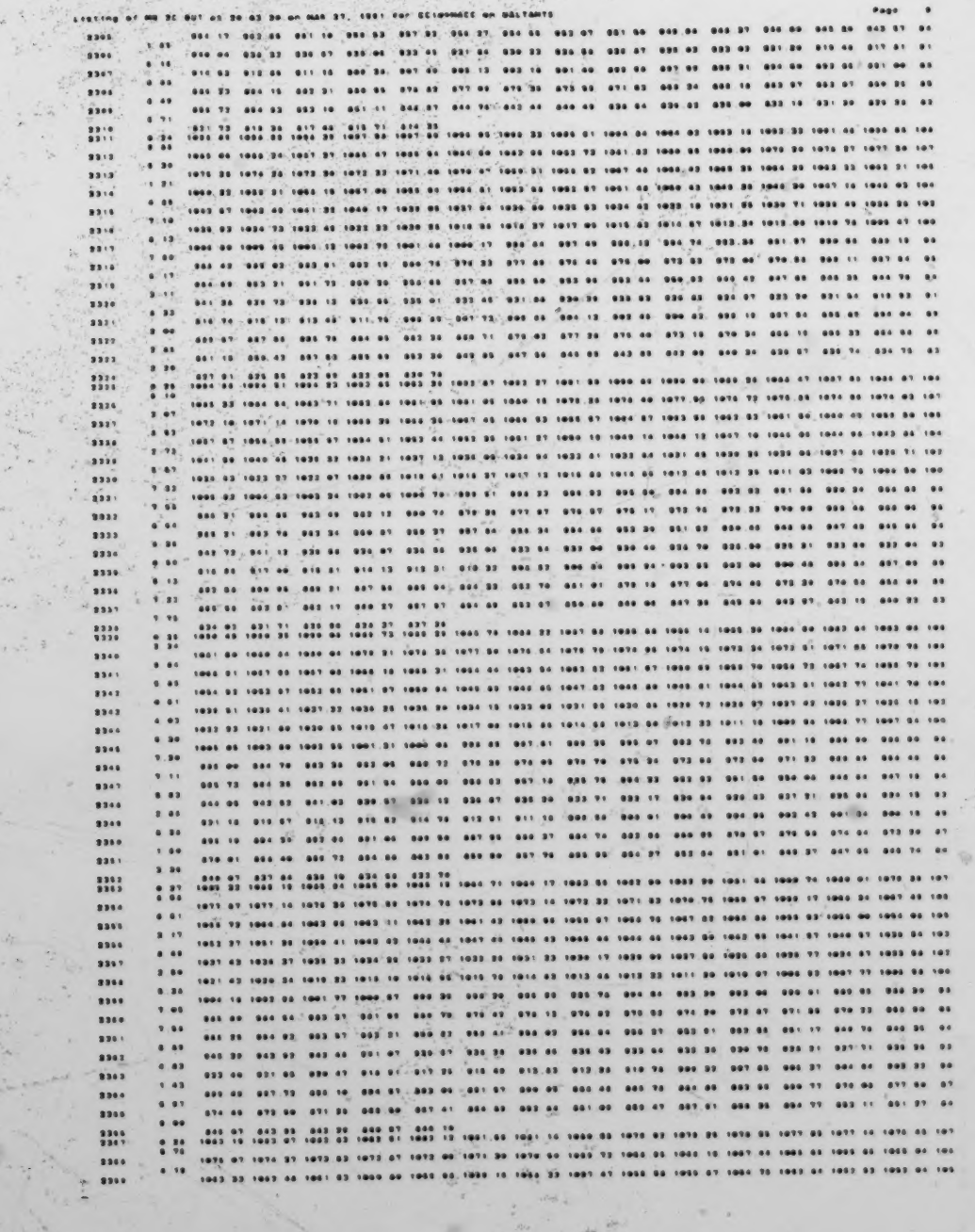

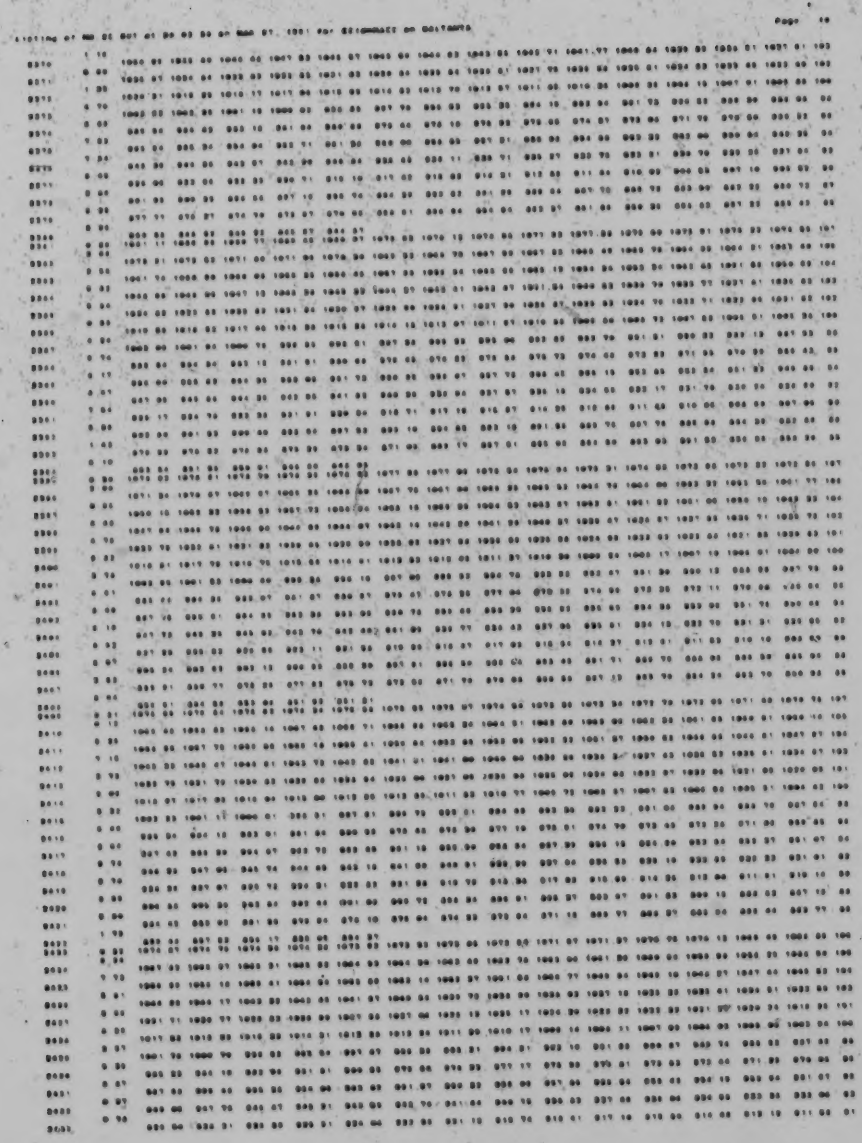

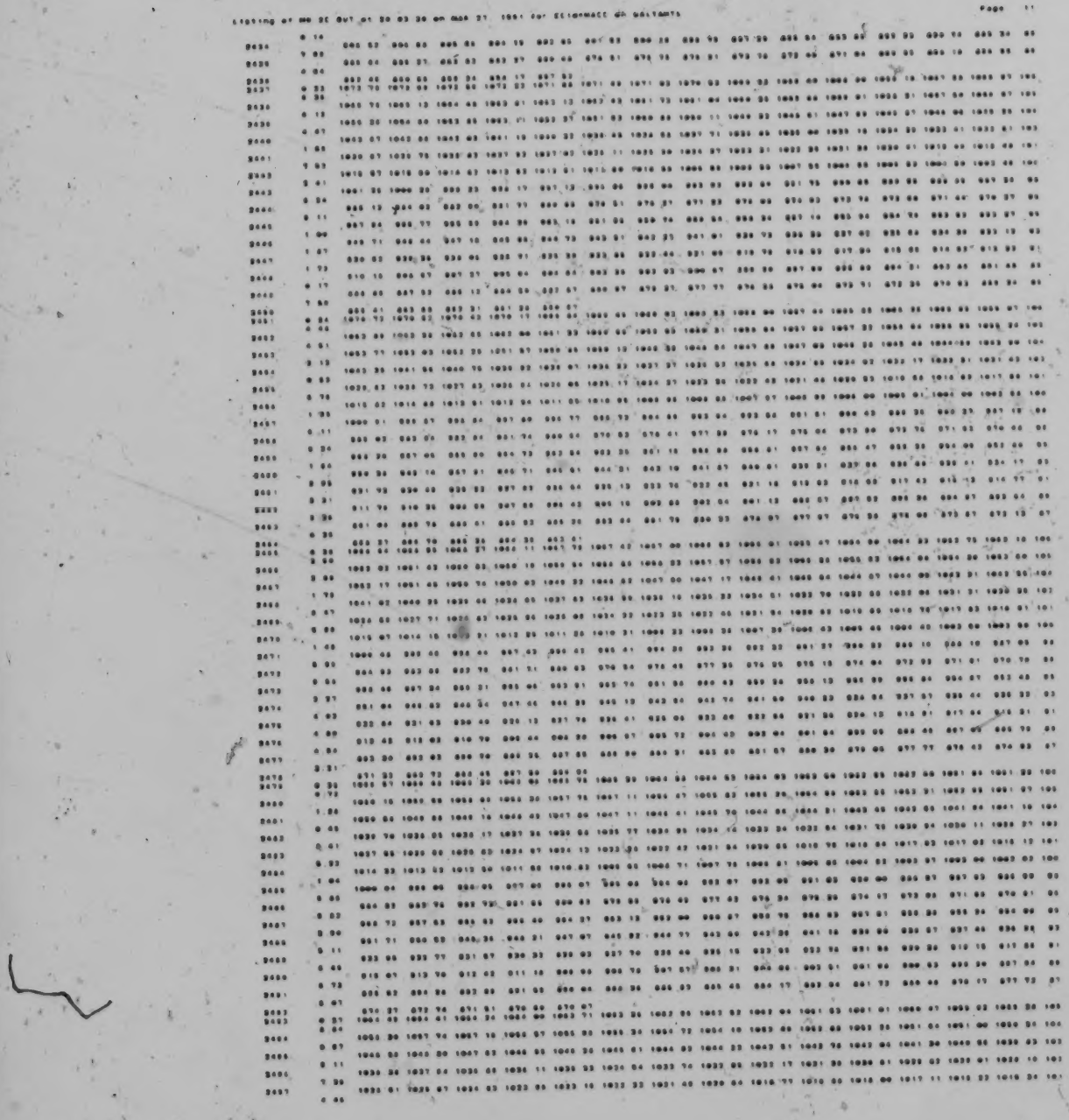

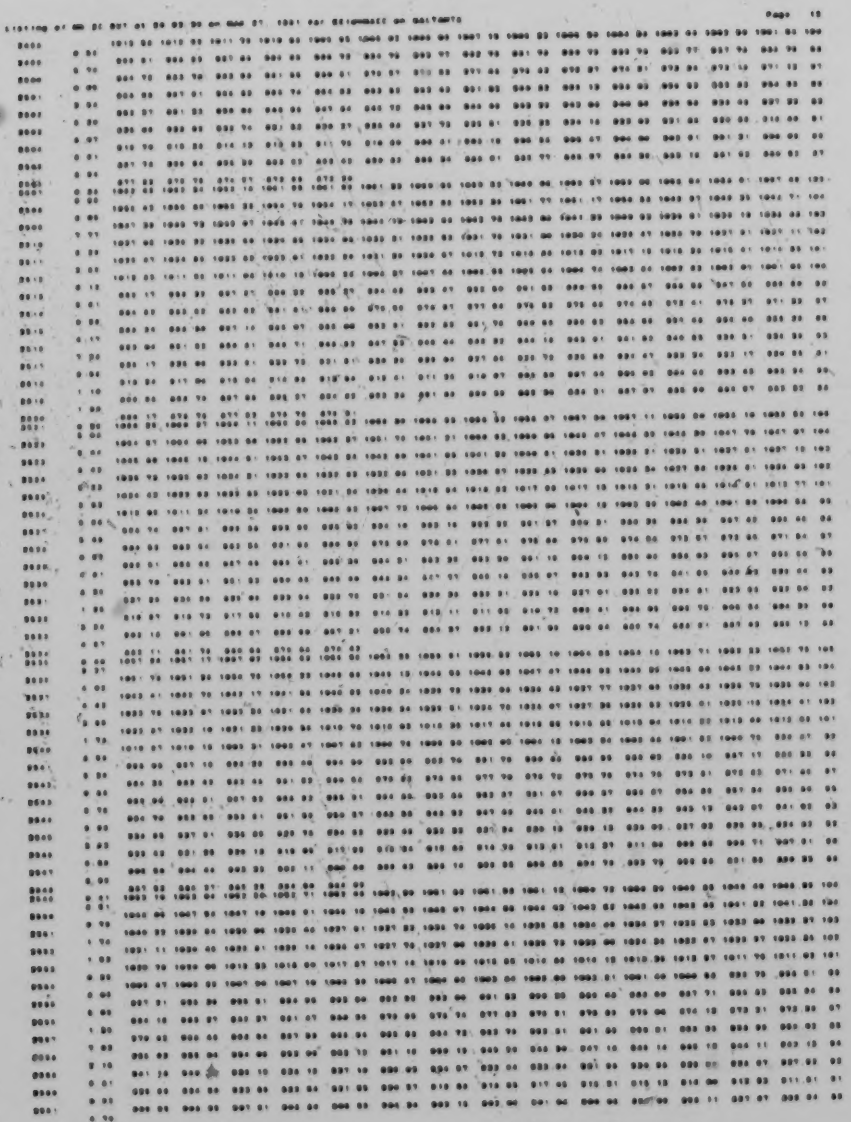

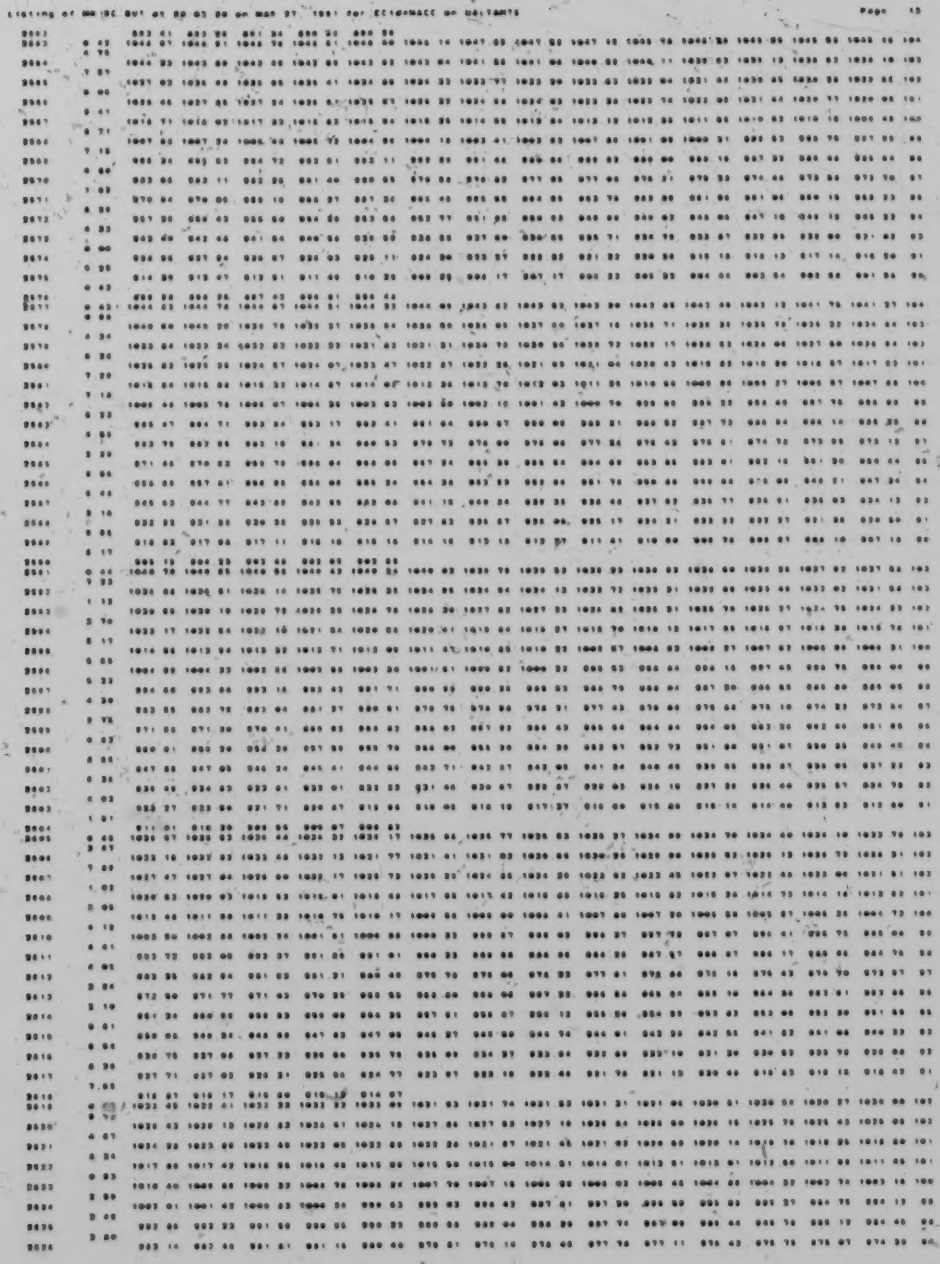

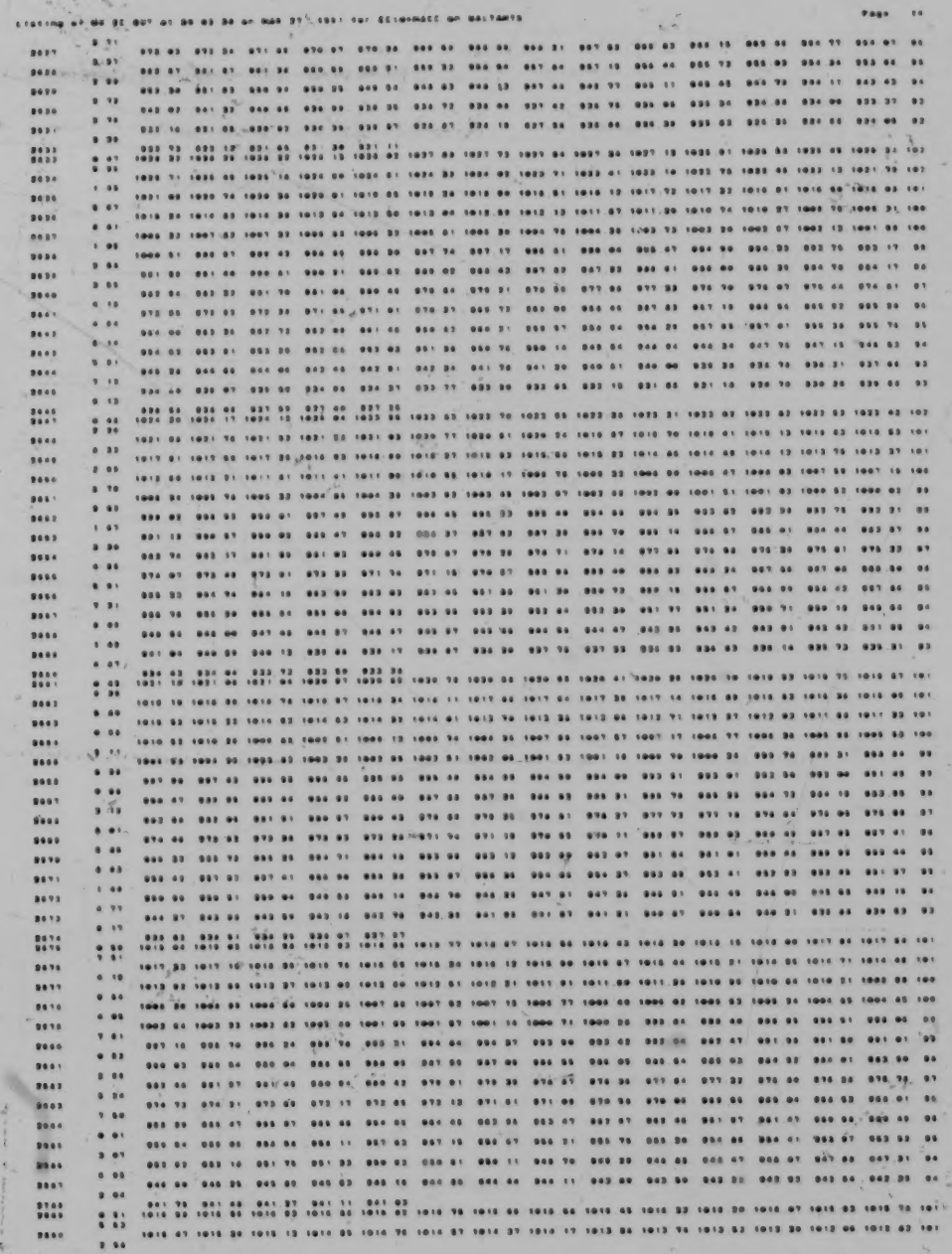

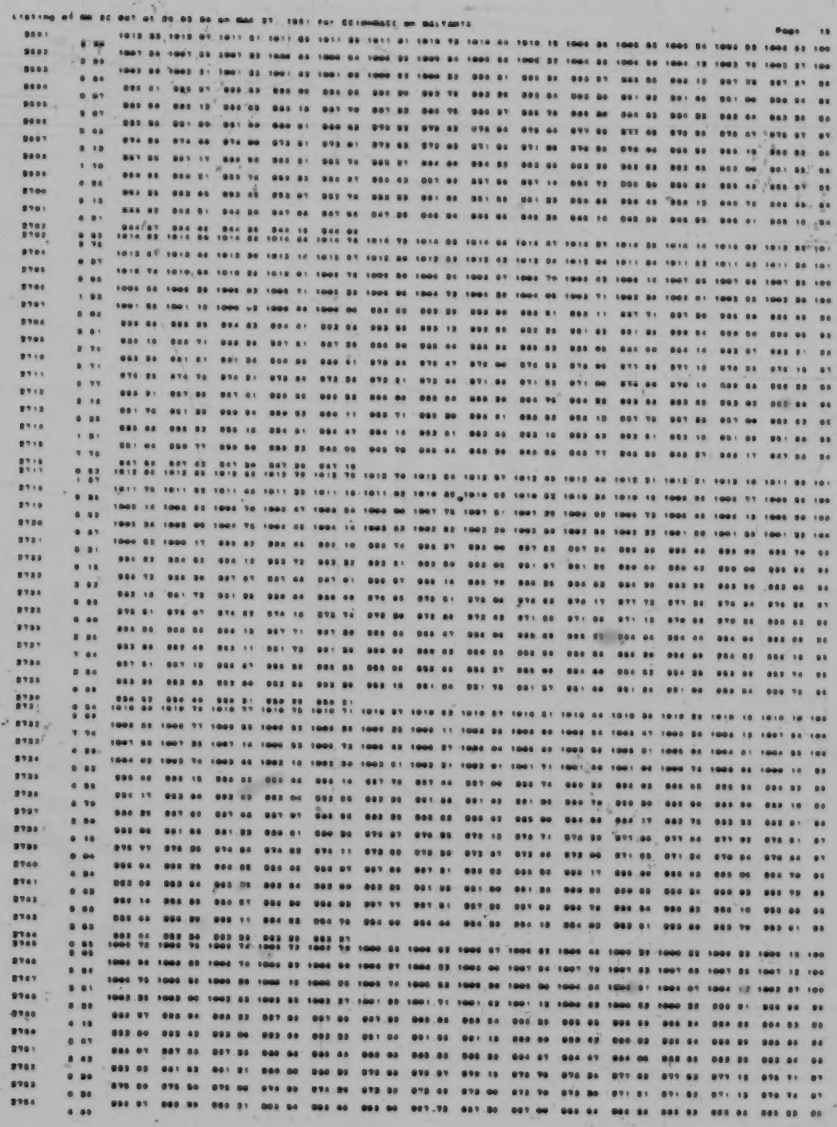

University of Alberta

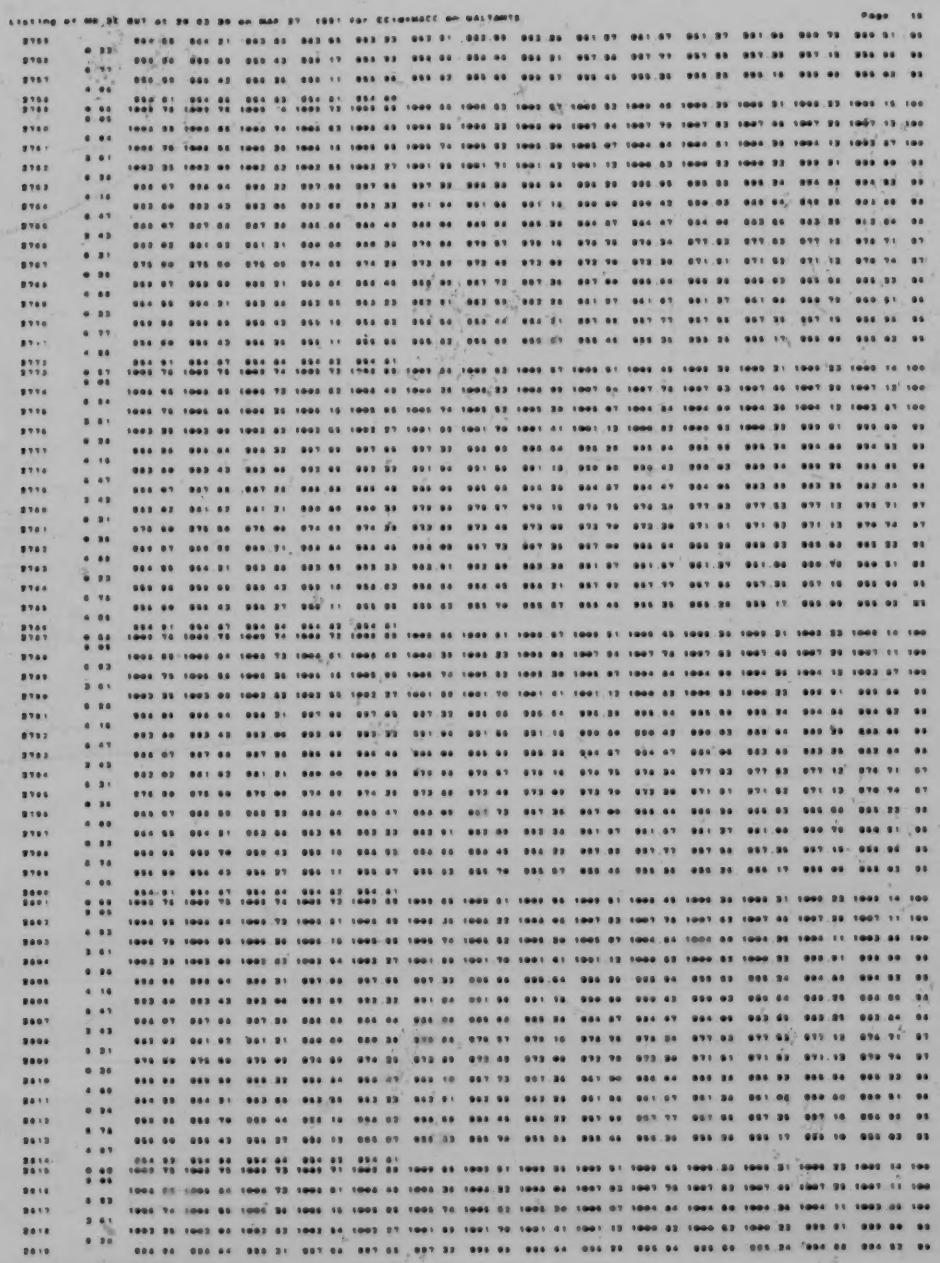

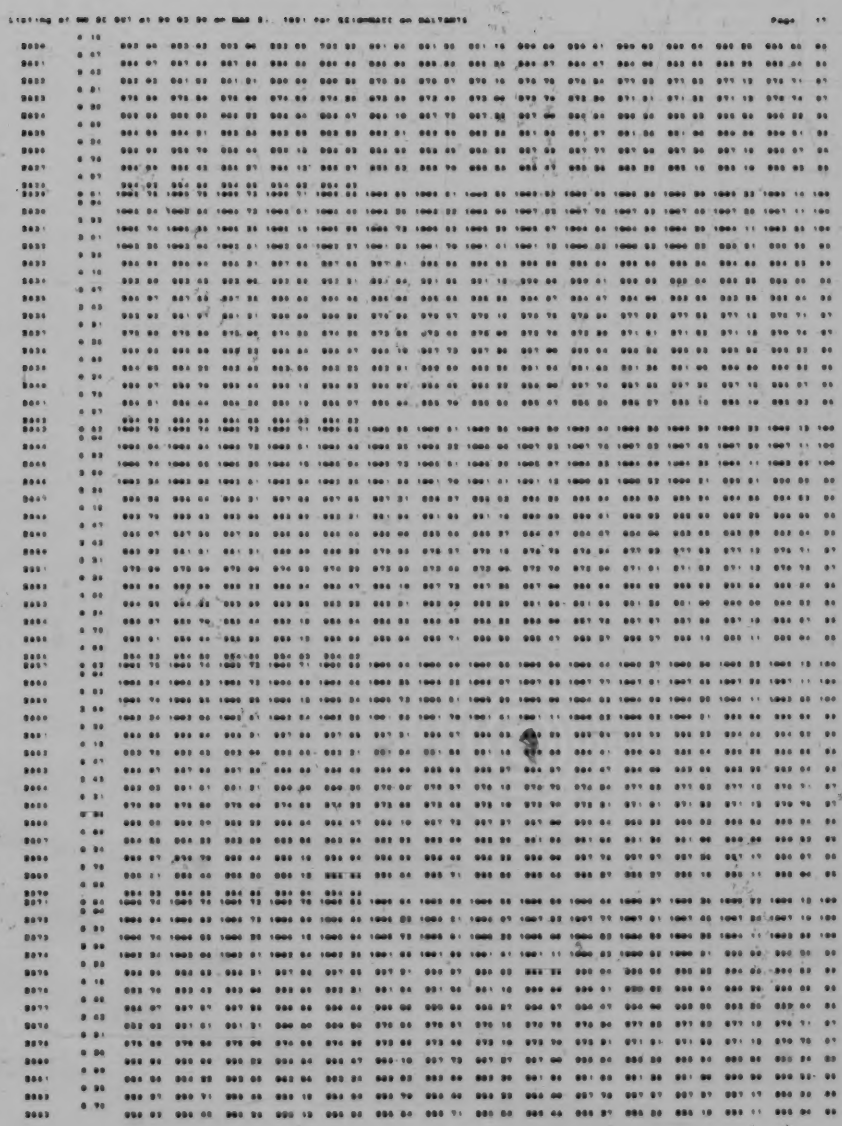

University of Alberta

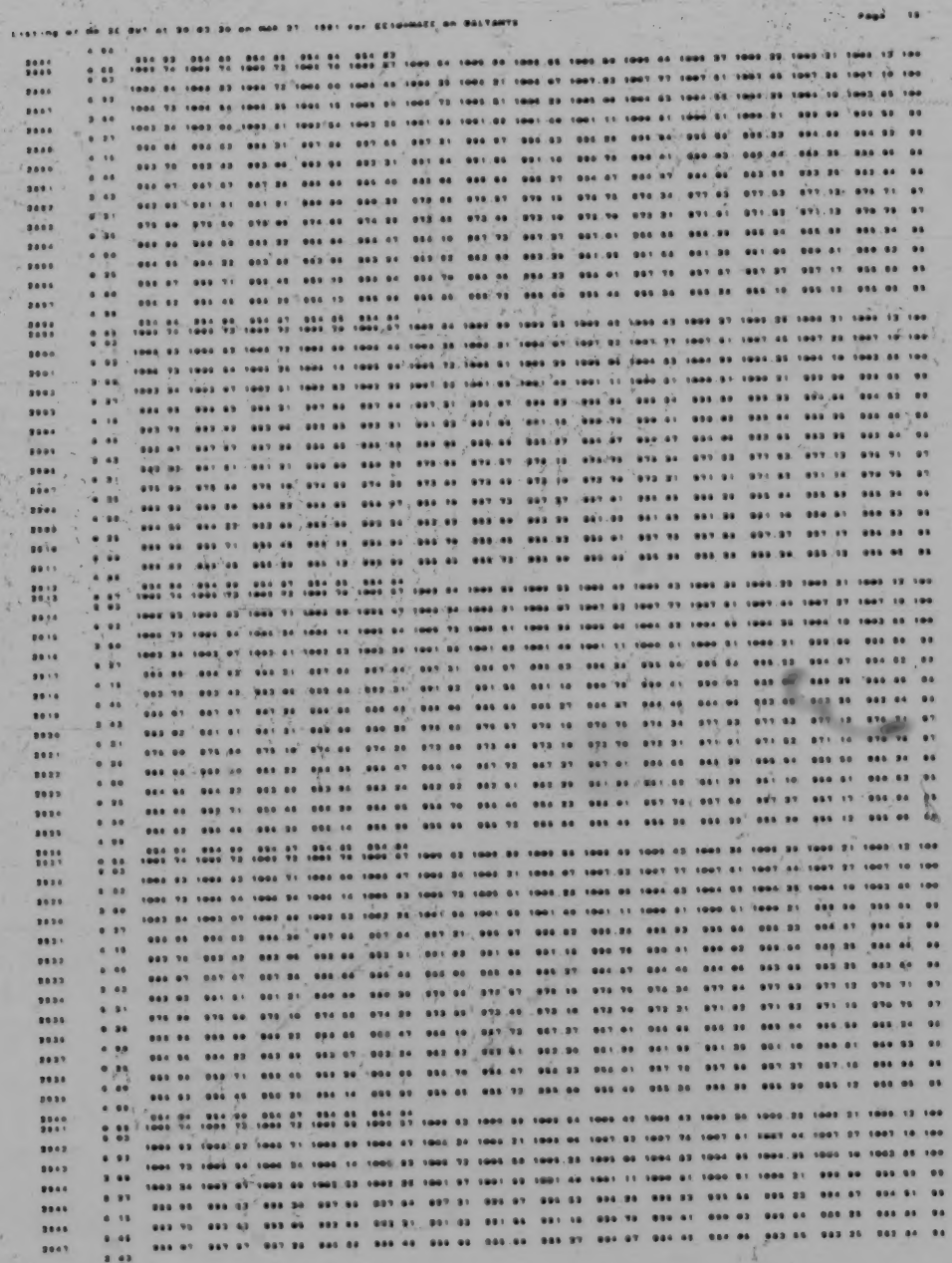

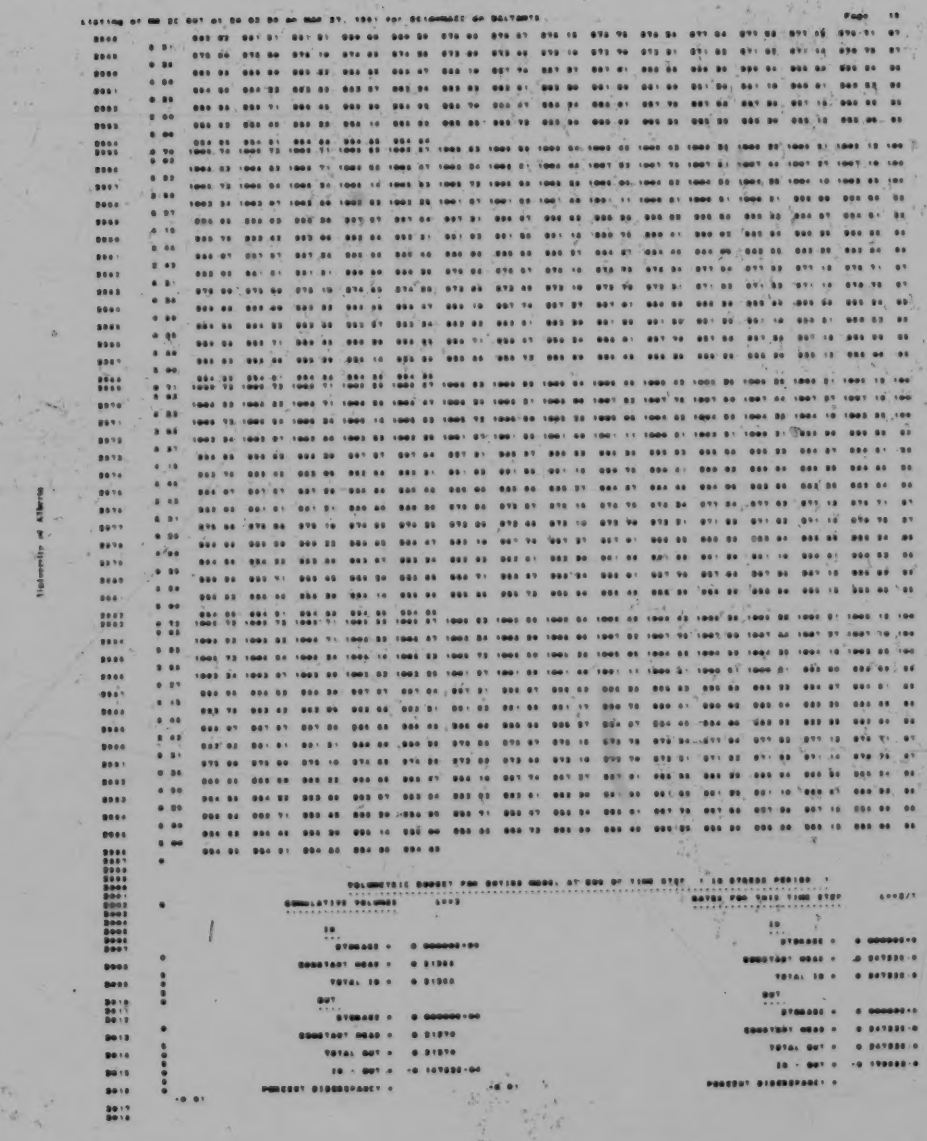

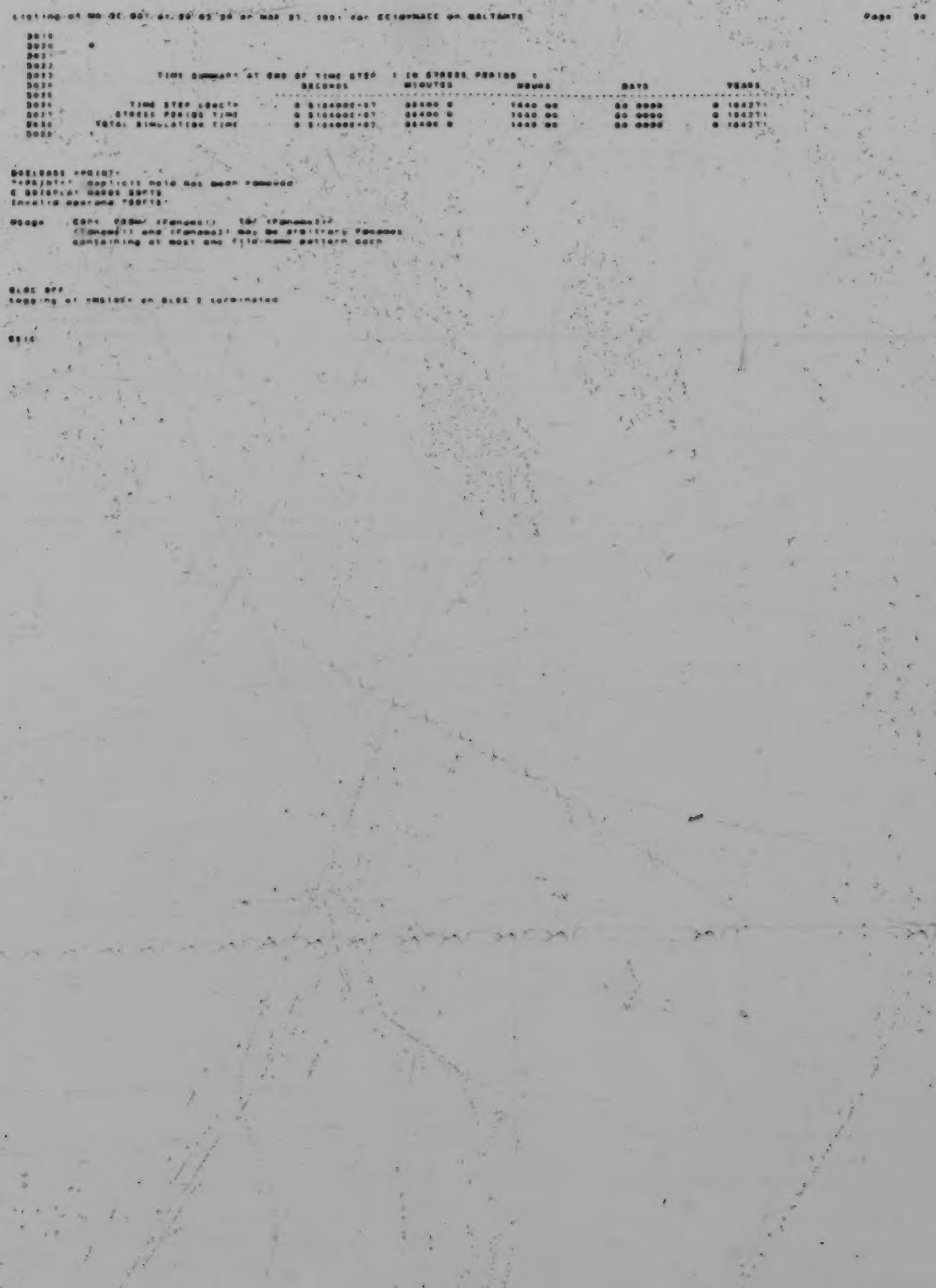

Appendix B

Drillstem test data used in field study

Drillstem Test Data

Location	Formation	KB Elevation, m	Depth, m	Elevation, m	Pressure, kPa	Hydraulic Head, m
Area A: T.52 R.08W4						
07 02	Viking	674.8	521.2	153.6	4095.6	555.2
07 02	upper Mannville	674.8	555.3	119.5	3881.9	500.1
06 06	middle Mannvile	687.3	634.3	53.0	4143.9	459.3
16 35	lower Mannville	685.7	692.0	-6.3	4594.2	444.2
Area B: T.54 R.04W4						
11 21	Viking	602.6	378.0	224.6	3081.0	526.7
06 12	upper Mannville	585.8	423.1	162.7	3040.7	460.8
13 24	upper Mannville	595.1	442.3	152.8	3025.0	449.4
01 28	upper Mannville	609.9	426.0	183.9	2841.0	462.5
03 06	middle Mannville	613.9	529.1	84.8	3819.8	459.3
13 24	middle Mannville	595.1	479.5	115.6	3425.0	451.4
11 21	lower Mannville	602.6	563.0	35.6	4088.0	436.4
11 26	lower Mannville	599.7	552.0	47.7	3998.5	439.8
06 19	Beaverhill Lake	613.3	597.7	15.6	4274.9	434.8
Area C: T.55 R.01W4						
06 31	Viking	662.0	412.9	249.1	3070.0	550.1
07 04	upper Mannville	604.1	413.0	191.1	2697.3	455.6
10 09	upper Mannville	625.8	449.9	175.9	2860.7	456.4
10 20	upper Mannville	590.1	409.7	180.4	2740.0	449.1
07 30	upper Mannville	588.0	386.2	201.8	2620.1	458.7
10 09	middle Mannville	625.8	471.4	152.5	3002.1	446.8
07 22	middle Mannville	616.9	470.9	146.0	3178.6	457.7
06 31	middle Mannville	662.0	518.0	144.0	3140.0	451.9
10 09	lower Mannville	625.8	559.6	66.2	3936.4	452.2
02 26	Beaverhill Lake	667.5	723.3	-55.8	5033.4	437.7

Drillstem Test Data

Location	Formation	KB Elevation, m	Depth, m	Elevation, m	Pressure, kPa	Hydraulic Head, m
Area D: T.56 R.01W4						
05 28	Viking	647.4	468.2	179.0	4129.4	583.9
06 18	upper Mannville	653.5	524.0	129.5	3829.5	505.0
05 28	upper Mannville	647.4	524.9	122.5	3636.4	479.0
07 28	upper Mannville	646.5	520.0	126.8	3588.2	478.6
10 36	middle Mannville	671.6	658.0	13.6	4264.7	431.8
06 32	lower Mannville	646.2	680.3	-34.1	4716.9	428.4
Area E: T.54 R.13W4						
11 12	Viking	624.5	518.2	106.3	4271.5	525.1
14 19	Viking	605.1	496.0	109.1	4314.8	532.2
11 12	upper Mannville	624.5	558.1	66.4	4675.6	524.8
06 28	middle Mannville	618.2	586.7	31.5	4653.0	487.7
14 19	lower Mannvile	605.2	631.9	-32.7	4435.4	402.2
Area F: T.52 R.16W4						
15 36	Viking	669.0	625.3	43.7	4770.0	511.4
11 19	upper Mannville	693.7	683.1	10.6	5311.4	531.4
07 08	upper Mannville	685.5	710.2	-24.6	5691.1	533.3
06 25	upper Mannville	674.5	666.9	7.6	5360.2	533.2
11 10	middle Mannville	686.4	755.9	-69.5	5212.6	441.6
13 09	lower Mannville	683.5	857.3	-173.8	5614.0	376.7
08 30	lower Mannville	691.4	873.0	-181.6	5633.0	370.7
11 10	Camrose	686.4	877.2	-190.8	5688.4	366.9
11 10	Camrose	686.4	876.0	-189.6	5674.6	366.8